University of Strathclyde

Department of Pure and Applied Chemistry

The Use of Contemporary Chemoproteomic Techniques in Antimalarial Target Identification

Thesis submitted to the University of Strathclyde in fulfilment of the requirements for the degree of Doctor of Philosophy

by

Jessie S. Tucker

2020

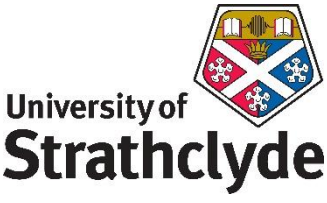

Author Declaration

This thesis is the result of the author's original research. It has been composed by the author and has not been previously submitted for an examination which has led to the award of a degree.

Signed: Date:

Abstract

Malaria remains a significant public health burden, with antimalarial resistance threatening the efficacy of current antimalarial medicines and resulting in an immense need to develop novel disease treatments. In our laboratories, an antimalarial quinazolinamine hit with a novel mechanism of action was identified in a phenotypic screen against the blood stage *Plasmodium falciparum* parasite. This thesis discloses the identification of the target proteins of this potential drug series, through use and analysis of contemporary chemoproteomic techniques for target identification.

The introductory chapter of this thesis provides: an overview of malaria biology; current antimalarial treatments and their limitations; and a discussion of contemporary chemoproteomic techniques for target identification. The nascent antimalarial quinazolinamine series is introduced, and the aim to identify the protein targets of this series is described.

Chapter 2 describes the synthesis of three chemical probes based on the quinazolinamine series. These probes incorporate an alkyne functional handle for immobilisation onto solid beads, which were used in affinity-based chemoproteomic experiments to affinity-capture protein targets in *Plasmodium falciparum* lysates. However, using this typical workflow, the appropriate target proteins were not successfully identified. As a result, attention was turned to the use of a photoaffinity labelling technique for target identification.

Chapter 3 describes the synthesis of photoreactive probes of the quinazolinamine series. These were used in an innovative photoaffinity labelling assay which was established for the first time in our laboratories, enabling the covalent capture of target proteins in live *P. falciparum* parasites. Two transporter proteins, *P. falciparum* apicomplexan amino acid transporter 2 (*Pf*ApiAT2) and *P. falciparum* equilibrative nucleoside transporter 1 (*Pf*ENT1) were captured as target proteins of the antimalarial quinazolinamine series. These proteins have both been reported as essential for parasite survival and have no known human homologues. Chapter 3 concludes with a discussion of their key features, and Chapter 4 provides an analysis and comparison of the techniques used in their identification.

Acknowledgements

I owe thanks to a significant number of people for the support that they have provided me throughout my PhD studies. Firstly, I would like to thank my supervisors, Craig Jamieson (University of Strathclyde) and Vipul Patel (GSK) for their commitment to my scientific education and growth, their enthusiasm, and their guidance. Craig, you have always been so encouraging, and have ensured that I am proud of my achievements and confident in my ability. Vipul, you have provided me with some excellent experiences through your ambitious attitude and willingness to let me take on the unknown. I am extremely grateful to you both. I would also like to thank my first-year supervisors, Natalie Theodoulou (GSK), for her support in setting me up in the GSK laboratories, and to Allan Watson (University of Strathclyde) for the guidance during the initial stages of my PhD.

There are many other people who have supported me over the past 3.5 years, even if I have not been able to explicitly name them here. However, I would like to express my thanks to my colleagues at GSK Tres Cantos, in particular Olalla Sanz, Maria Jesús Chaparro-Martín, Beatriz Cosme-Hernandez, and Esther Fernandez-Velando for their help in orchestrating my placement to Tres Cantos. Without this, I would not have been able to have such a constructive and unforgettable experience in the incredibly interesting P3 laboratories there. Special thanks have to go to Olalla, who spent a significant amount of time in the lab with me teaching me all about malaria cultures and their maintenance. Thanks also go to colleagues who provided day-to-day guidance and company during my placement: Felix Calderon, Jose Ignacio Martin Hernando, Jose Luis Llergo-Largo, Maria De Gracia Gomez-Lorenzo, Maria Jose Lafuente-Monasterio, Jorge Fernandez-Molina, Benigno Crespo, Blanca Huertas, Irene Molina, Sara Palomo Diaz, Sonia Moliner, and Lydia Mata Cantero.

I wish also to thank my colleagues at Cellzome, Sonja Ghidelli-Disse and Chris Eberl, both of whom have provided significant support and helped me grasp new and complex scientific concepts surrounding the field of chemoproteomics. Although I did not manage to meet face-to-face many of my Cellzome colleagues, many others also

helped with the pull down and mass spectrometry analysis of my results, and I thus extend my thanks to them.

Thanks go to many of my colleagues at GSK Stevenage, in particular Stephen Richards for assistance with NMR spectroscopy; to Blandine McKay and Catherine Alder for assistance with using the glovebox, light boxes, and high-throughput facilities; and to my coworkers in the lab who have helped me day-to-day, for which there are so many I cannot list them all here.

I would like to express my gratitude to Harry Kelly and William Kerr for giving me a place on the industrial PhD programme, without which I would not have been able to carry out this work, and to Andrea Malley and Abby Mullord for all the administrative support.

I would like to finish by thanking those co-workers and other PhD students who have become good friends of mine. These people have all made my time at GSK even more enjoyable, by providing laughs and entertainment throughout. In particular I would like to thank Nick Measom for all the dinners and movie nights where we put the world to rights, as well as Jonathan Taylor, Jack Coward, Andrew Baxter, Mike Clegg, Oli Turner, Brett Cosgrove, John Priestner, James Thompson, Sam Holman, Pete Clark, and Lucia Fusani. Lastly, I would like to thank Kike Bendito for always making me laugh and striving to keep me happy, and my family for the constant encouragement that has allowed me to get to this point.

Contents

Abbreviations

AAT1	Amino Acid Transporter 1
Ac	Acetate
ACT	Artemisinin Combination Therapies
ADA	Adenosine Deaminase
ADE2	Adenine Requiring Protein 2
ADME	Absorption Distribution Metabolism Excretion
ADP	Adenosine Diphosphate
AK	Adenosine Kinase
AMP	Adenosine Monophosphate
AP	Atovaquone-Proguanil
ApiAT2	Apicomplexan Amino Acid Transporter 2
ApiAT8	Apicomplexan Amino Acid Transporter 8
Arg	Arginine
Asn	Asparagine
Asp	Aspartic acid
ATP	Adenosine Triphosphate
ATP4	P-type Cation Translocating ATPase 4
BnBr	Benzyl Bromide
Boc	*tert*-Butyloxycarbonyl
Bpin	Bis(pinacolato)diboron
BSA	Bovine Serum Albumin
CAA	2-Chloroacetamide
CDPK5	Plant-Like Calcium Dependent Protein Kinase 5
CelTOS	Cell Traversal Protein for Ookinetes and Sporozoites
CFDA-SE	Carboxyfluorescein Diacetate Succinimidyl Ester
cGMP	Cyclic Guanosine Monophosphate
CID	Collision-Induced Dissociation
CN	Nitrile
Conc.	Concentration
CRT	Chloroquine Resistance Transporter
CSA	Camphorsulfonic Acid
CSP	Circumsporozoite Protein
CuAAC	Copper-catalysed Azide-Alkyne Cycloaddition
CuI	Copper(I) Iodide
Cyt*b*	Cytochrome *b*
DA	Diels-Alder
DAPI	4’,6-Diamidino-2-phenylindole
DBU	1,8-Diazabicyclo[5.4.0]undec-7-ene
DCC	*N*,*N*′-Dicyclohexylcarbodiimide
DCM	Dichloromethane
DHFR	Dihydrofolate Reductase
DHODH	Dihydroorotate Dehydrogenase
DHPS	Dihydropteroate Synthase
DIC	*N,N’*-Diisopropylcarbodiimide

DIPEA	*N*,*N*-Diisopropylethylamine
DMA	*N*,*N*-Dimethylacetamide
DMAP	4- *N*,*N*-Dimethylaminopyridine
DME	Dimethoxyethane
DMF	Dimethylformamide
DMSO	Dimethyl Sulfoxide
DNA	Deoxyribonucleic acid
Dppf	1,1'-Bis(diphenylphosphino)ferrocene
DTT	Dithiothreitol
EBA	Erythrocyte Binding Antigen
EBP2	Erythrocyte Binding Protein 2
EDC	1-Ethyl-3-(3-dimethylaminopropyl)carbodiimide
EDTA	Ethylenediaminetetraacetic Acid
EMP	Erythrocyte Membrane Protein
ENT1	Equilibrative Nucleoside Transporter 1
ESI	Electrospray Ionisation
eq.	Equivalents
EXP1	Exporter Protein 1
FACS	Fluorescence-Activated Cell Sorting
FDA	Food and Drug Administration
FUI1	Fluorouridine Transporter 1
FUrd	Fluorouridine
FV	Food Vacuole
G	Gibbs Free Energy
GAC	GTPase Associated Centre
Gln	Glutamine
Glu	Glutamic acid
GTP	Guanosine Triphosphate
h	Human
H%	%Hematocrit
HATU	1-[Bis(dimethylamino)methylene]-1*H*-1,2,3-triazolo[4,5-b]pyridinium 3-oxide hexafluorophosphate
HBSS	Hank's Balanced Salt Solution
HCD	High-Energy Collisional Dissociation
HEPES	4-(2-Hydroxyethyl)-1-piperazineethanesulfonic Acid
hERG	Human Ether-a-go-go
HGXPRT	Hypoxanthine Guanine Xanthine Phosphoribosyltransferase
His	Histidine
HKMT	Histone Lysine Methyltransferase
HOSA	Hydroxylamine-*O*-Sulfonic Acid
HpH	High pH (pH 10 – see **Chapter 5 – Experimental**)
HPLC	High Performance Liquid Chromatography
HRMS	High Resolution Mass Spectrometry
IC_{50}	Half Maximal Inhibitory Concentration
ID	Identification
iEDDA	Inverse Electron Demand Diels-Alder
IMP	Inosine 5'-Monophosphate
IP	Intellectual Property
IPA	*Iso*propyl Alcohol

IR	Infrared
iTRAQ	Isobaric Tags for Relative and Absolute Quantification
K_d	Dissociation Constant
LC	Liquid Chromatography
LDS	Lithium Dodecyl Sulfate
LE	Ligand Efficiency (given by the equation LE = ΔG/N = 1.37(pIC_{50}/N))
LED	Light Emitting Diode
LLE	Lipophilic Ligand Efficiency
Lys	Lysine
MC-2TM	Maurer's Cleft Two Transmembrane Protein
DMAP	Mass-Directed Auto Preparative
MDR1	Multidrug Resistance Protein 1
MeCN	Acetonitrile
Mer	Merozoite
MFR	Major Facilitator Superfamily-Related Transporter
MMV	Medicines for Malaria Venture
m.p.	Melting Point
mRNA	Messenger Ribonucleic Acid
MS	Mass Spectrometry/Mass Spectrum
MS-CETSA	Mass Spectrometry Coupled-Cellular Thermal Shift Assay
MSP	Merozoite Surface Protein
N	Heavy Atom Count or Nucleus, appropriately
NaHMDS	Sodium Bis(trimethylsilyl)amide
NAP	*N*'-(Acyloxy)phthalimide
NHS	*N*-Hydroxysuccinimde
NIS	*N*-Iodosuccinimide
NMR	Nuclear Magnetic Resonance
NPT	Novel Putative Transporter
OCT2	Organic Transporter 2
P%	%Parasitaemia
PAL	Photoaffinity Labelling
PBS	Phosphate-Buffered Saline
PC	Photocatalyst
Pd/C	Palladium on Carbon
PDX1	Pyidoxine Biosynthesis Protein 1
PEG	Polyethylene Glycol
Pf	*Plasmodium falciparum*
Pf_{3D7}	3D7 strain of *Plasmdium falciparum*
P. falc	*Plasmodium falciparum*
PFI	Property Forecast Index
Pgh-1	P-Glycoprotein Homologue 1
Ph	Phenyl
pIC_{50}	$-\log(IC_{50})$
PI4K	Phosphatidylinositol 4-Kinase
pK_a	Acid Dissociation Constant
PKG	cGMP-Dependent Protein Kinase
PLP	Perforin-Like Protein
PNP	Purine Nucleoside Phosphorylase

PTM	Post-Translational Modification
Pv	*Plasmodium vivax*
PV	Parasitophorous Vacuole
PVM	Parasitophorous Vacuole Membrane
pXC_{50}	$-\log(XC_{50})$
Py	Pyridine
PyBOP	Benzotriazol-1-yl-oxytripyrrolidinophosphonium hexafluorophosphate
R	Gas Constant
RBC	Red Blood Cell
RFID	Radio Frequency Identification
RH	Reticulocyte Binding Homologues
RNA	Ribonucleic Acid
RPMI 1640	Roswell Park Memorial Institute 1640 medium
R_t	Retention Time
RT	Room Temperature
RTS,S	Malaria vaccine, trade name Mosquirix
SAR	Structure-Activity Relationship
SCX	Strong Cation Exchange
SDS	Sodium Dodecyl Sulfate
Ser	Serine
SET	Single Electron Transfer
SILAC	Stable Isotope Labelling by Amino Acids in Cell Culture
S_N2	Substitution Nucleophilic Bimolecular
SP	Sulfadoxine-Pyrimethamine
SPECT1	Sporozoite Protein Essential for Cell Traversal 1
T	Temperature
TBME	*tert*-Butyl Methyl Ether
^{t}Bu	*tert*-Butyl
TCEP	Tris(2-carboxyethyl)phosphine
TCO	*trans*-Cyclooctene
TFA	Trifluoroacetic Acid
T. gondii	*Toxoplasma gondii*
THF	Tetrahydrofuran
THPTA	Tris(3-hydroxypropyltriazolylmethyl)amine
Thr	Threonine
TLC	Thin Layer Chromatography
TMD	Transmembrane Domain
TMT	Tandem Mass Tag
TRAP	Thrombosporin-Related Anonymous Protein
tRNA	Transfer Ribonucleic Acid
TVN	Tubovesicular Network
UIS4	Upregulated in Infective Sporozoites 4
UK	United Kingdom
USA	United States of America
UV	Ultraviolet
WHO	World Health Organisation
wt	weight
XC_{50}	Half Maximal Effective Concentration

Chapter 1 – Introduction

1.1 Malaria as a Widespread Infectious Disease

Malaria is a serious and life-threatening infectious disease caused by five parasitic protozoa of the *Plasmodium* type; *P. falciparum*; *P. vivax; P. ovale; P. malariae;* and *P. knowlesi*. The infection is transmitted to humans, the exclusive mammalian host of the infection, by the bites of the female *Anopheles* mosquito.[1,2]

Malaria is often classified as asymptomatic, uncomplicated, or severe (complicated). In asymptomatic malaria, the patient carries circulating parasites but displays no symptoms of the disease. Uncomplicated malaria manifests as a combination of symptoms that often include fever, chills, sweats, headaches, nausea, vomiting, aches, and digestive problems as a result of the synchronous infection and lysis of red blood cells. Severe malaria is diagnosed when infections are also complicated by serious organ failures or abnormalities in the sufferer's blood or metabolism due to parasite sequestration in vital tissues. This is characterised by potentially fatal symptoms such as cerebral malaria, anaemia, organ damage such as acute kidney injury, comas, and seizures.[3]

The World Health Organisation (WHO) estimated in their 2018 World Malaria Report that in 2017 there were 219 million cases of malaria worldwide, with 435,000 deaths.[4] The disease presents a threat across 97 different countries,[1] with transmission occuring in sub-Saharan Africa, South East Asia, the Eastern Mediterranean, Western Pacific, and the Americas. *P. falciparum* is the most lethal pathogenic form from which nearly half of the world's population is at risk, presenting a significant public health burden and a continuing need for effective treatments.[2]

1.2 The Malaria Lifecycle

The complex lifecycle of the malaria parasite involves multiple different stages within both human and mosquito hosts (Figure 1.1).

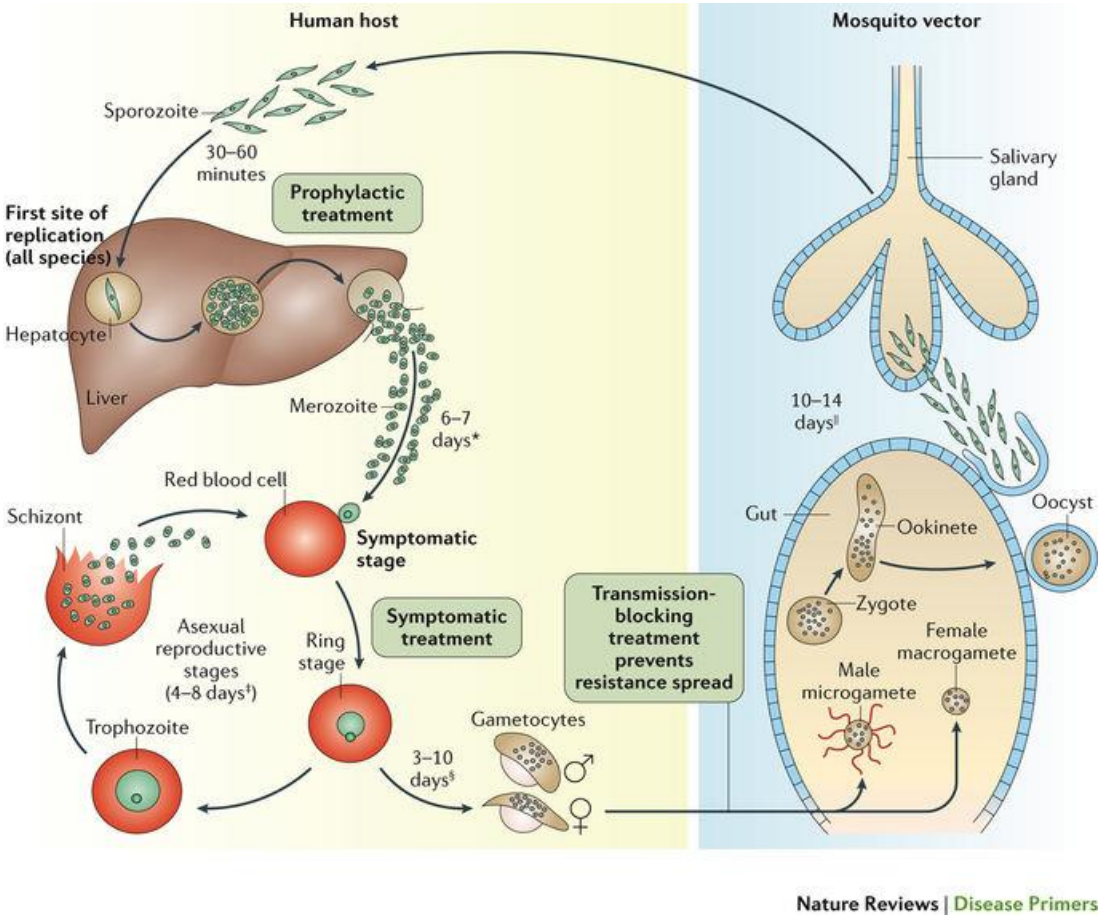

Figure 1.1. The malaria parasite lifecycle, reproduced from Philips *et al.*[2]

An infected female *Anopheles* mosquito transmits the disease to its human host during a blood meal in which the infective stage of the *Plasmodium* parasite, sporozoites, are injected into the host's dermis *via* the mosquito's anticoagulating saliva.[2,5] A few hundred sporozoites can be injected underneath the skin in a single mosquito bite. Shortly after, these highly motile sporozoites migrate in an apparently random fashion until they encounter a blood vessel and can enter the bloodstream.[5] Once within the blood circulation, these sporozoites travel towards the liver and invade and infect their target hepatocytes. In a process known as schizogony, a single sporozoite within its host hepatocyte undergoes multiple rounds of nuclear division over 2 to 10 days to

produce a hepatic schizont: a cell that, through schizogony, has divided to form up to 40,000 merozoite daughter cells. These merozoites are the form of the parasite capable of initiating a new cycle of sexual or asexual development. This process occurs with no obvious clinical symptoms, leading to the descriptor of 'the silent phase' of malaria development.[5] Prophylactic treatment for malaria concerns the disruption of this sporozoite phase. In cases of *P. vivax* and *P. ovale* infection, a dormant parasitic state known as a hypnozoite can form and exist in the liver for up to a number of years. This results in the potential for schizont development to take place after a latent period, leading to disease development much later than the mosquito bite event.

The merozoites that develop within hepatocytes are contained inside vesicles derived from the host cell membranes, known as merosomes, that allow intact exit from the liver by protecting from clearance mediated by Kupffer cells.[6] These merozoites are released into the bloodstream at the lung capillaries on rupture of the merosomes, thus initiating the symptomatic blood stage infection. In this stage, the free merozoites rapidly invade erythrocytes using multiple receptor-ligand interactions, attaching themselves to erythrocytes *via* surface proteins and penetrating the new host cell using motor and transmembrane proteins.[6,7] This occurs in as little as 60 seconds such that the parasite largely evades the host immune system response in the blood plasma. Simultaneous formation of a parasitophorous digestive vacuole within the host cell provides a hospitable environment for asexual reproduction. Once this infection is established, the parasite appears as an intracellular 'ring', and thus is known as a 'ring' stage parasite (Figure 1.2).

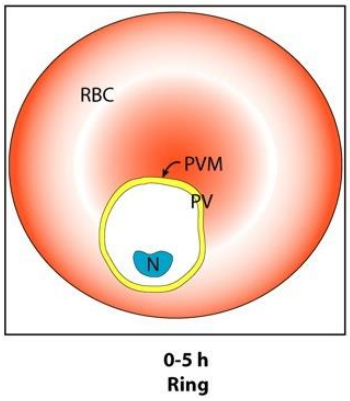

Figure 1.2. The intraerythrocytic structure of a ring stage malaria parasites, reproduced from Marti *et al*.[8] Once invasion is established, the parasite is surrounded by a parasitophorous vacuole (PV), with a parasitophorous vacuole membrane (PVM). The parasite grows within this membrane. N = nucleus, and RBC = red blood cell.

Subsequent rapid growth requires sustained sources of amino acids for protein synthesis, which are acquired by the parasite from the digestion of host cell haemoglobin.[2] The toxic haem side product as a result of this digestion is detoxified by haem polymerase and sequestered as the insoluble crystal, haemazoin, in an intra-parasitic compartment known as the food vacuole (FV). The ring stage parasite grows into a larger form known as a trophozoite, in which the proteins responsible for cell invasion are lost. Membrane structures known as tubovesicular networks (TVNs) are formed that protrude from the PVM and are thought to be involved in nutrient transport into and out of the parasite.[9] In addition, membrane-tethered Maurer's clefts are formed, with an elusive function but being reported as part of a protein transport system in the host cell cytosol.[10,11] Late-stage trophozoites can be identified by thousands of small structures ('knobs') on the surface of the host erythrocyte.[8] Further growth into a final stage schizont results in erythrocytic schizogony, in which the formation of multiple merozoites from one schizont occurs *via* nuclear division. Final destruction of the parasitophorous vacuole membrane and the host cell membrane leads to the release of these merozoites into the bloodstream and triggers the invasion of further red blood cells (Figure 1.3). This propagates the intra-erythrocytic stage of the parasite life cycle.[1,2]

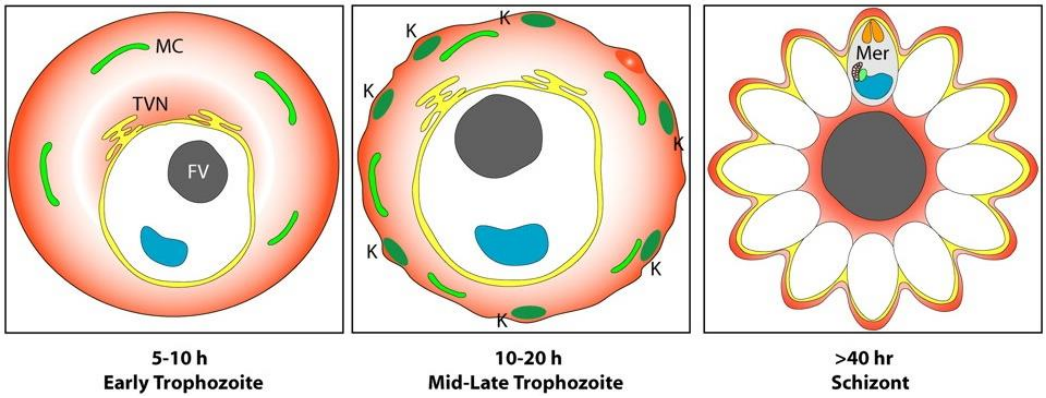

Figure 1.3. Trophozoite and schizont intraerythrocytic plasmodium parasite structures, reproduced from Marti *et al.*[8] MC = Maurer's cleft, TVN = tubovesicular network, K = knob, Mer = merozoite.

These *P. falciparum* intra-erythrocytic development stages can be observed in malaria cultures, as demonstrated by Radfar *et al*,[12] by use of an appropriate dye (Figure 1.4). The ring stage is observed between 6 and 22 hours, the trophozoite stage between 22 and 38 hours, and the schizont stage between 38 and 48 hours. Finally, merozoites released into the blood stream can be observed at 48 hours, just before further red blood cell invasion.

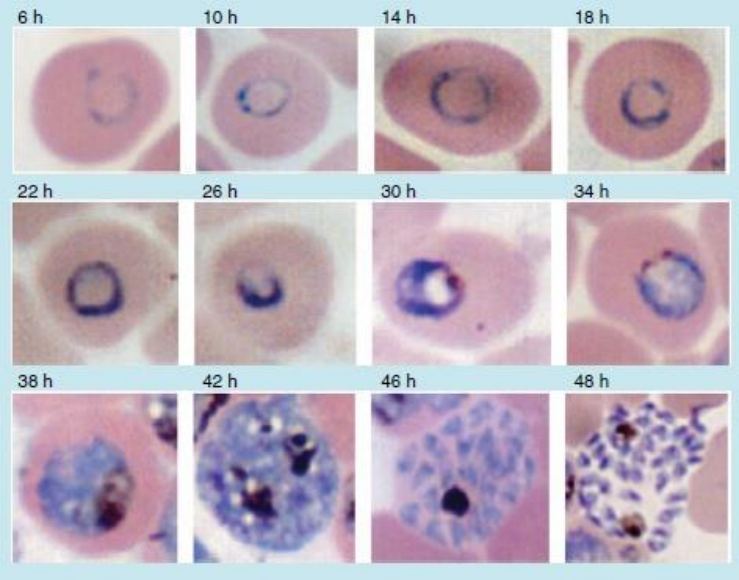

Figure 1.4. The intraerythrocytic blood stages of *P. falciparum* in culture, stained with Wright's dye, reproduced from Radfar *et al.*[12]

The manifestation of disease symptoms coincides with the rupture of red blood cells and the release of large amounts of endotoxins, occurring in a highly synchronous fashion in infections that result from a single infectious bite.[2] These endotoxins are understood to include complexes of haemozoin and parasite DNA that trigger a nucleotide-sensing receptor involved in the host immune response against pathogens.[2] In addition to this, the increase in rigidity of the infected erythrocytic membrane contributes to the obstruction of capillaries, which can lead to life-threatening disease symptoms when vital organs are affected, as seen in cases of severe malaria. The majority of drug treatments for malaria therefore target this intraerythrocytic, symptomatic stage of the infection.[2]

During the process of invasion and destruction of red blood cells by merozoites, a proportion of the protozoa undergo a developmental switch which commits them to sexual development. These parasites differentiate into sexual male and female gametocytes, which develop over 11 days within the host bone marrow in order to avoid splenic clearance. Once matured, these gametocytes emerge into the bloodstream and accumulate in the skin capillaries of the host. This makes them available for uptake in a blood meal for a feeding mosquito and leads to disease transmission.[1,2] Treatment therapies that target the gametocyte forms of the parasite are being increasingly investigated as a means to prevent disease transmission.[2]

The male gametocyte differentiates into eight microgametes in the midgut of the mosquito, whilst the female forms a single macrogamete.[13] These fuse to form a diploid zygote which elongates into a form known as an ookinete. This ookinete migrates across the mosquito midgut epithelium and becomes an oocyst, which settles in the midgut epithelium and undergoes schizogony cycles of replication and division to form sporozoites. On rupture of the oocyst, the formed sporozoites move from the abdomen of the mosquito to its salivary glands. After completion of this mosquito-based process, the insect is capable of transmitting the disease to another human host, thereby causing the spread of the infection amongst populations.[2]

1.3 The Functions of Major Protein Families Across the Parasite Lifecycle

Investigations into the proteome of the *Plasmodium falciparum* parasite provide an increased understanding of the protein families that facilitate the multiple changes that occur across the complex parasite lifecycle. This knowledge can be used to target specific lifecycle stages in the development of interventional therapies, with increased efficacy expected as a result.[14]

Protein expression changes considerably across the different parasitic stages.[14,15] Nearly half (49%) of the sporozoite proteins have been found to be unique to that stage. In contrast, trophozoites, merozoites, and gametocytes have been shown to have between 20% and 33% unique proteins. Only 152 proteins (6%) are common to the sporozoites, merozoites, trophozoites, and gametocytes, indicating the wide-ranging variability in the active proteome.[14]

The main function of the sporozoites, the parasitic form initially injected into the human host, is to evade the host immune system for long enough to successfully migrate to, and invade, hepatocytes. Accordingly, the main class of sporozoite proteins are cell surface and organelle proteins, with the parasite possessing an apex of complex machinery involved in host cell invasion.[14] Motility is facilitated by a combination of proteins that include the surface protein circumsporozoite protein (CSP), sporozoite-specific plasma-membrane spanning proteins of the thrombosponin-related anonymous protein (TRAP) family, actin and actin-binding proteins, and the motor protein myosin, amongst others.[16] The CSP protein is of particular significance because of its use in the RTS,S malaria vaccine, in which an antigen derived from CSP is used to activate the immune response.[17] Parasite invasion of hepatocytes is aided by the sporozoite protein essential for cell traversal 1 (SPECT1), perforin-like proteins (PLPs), and cell traversal protein for ookinetes and sporozoites (CelTOS), which function by forming pores in the host cell membrane.[18] Many other highly expressed proteins in the sporozoite parasite are associated with the rhoptry, an organelle in the apex of the parasite involved in facilitating the interaction between the host and

parasite, and micronemes, also located in the apical pole of the parasite and implicated in host-cell invasion (Figure 1.5).[14]

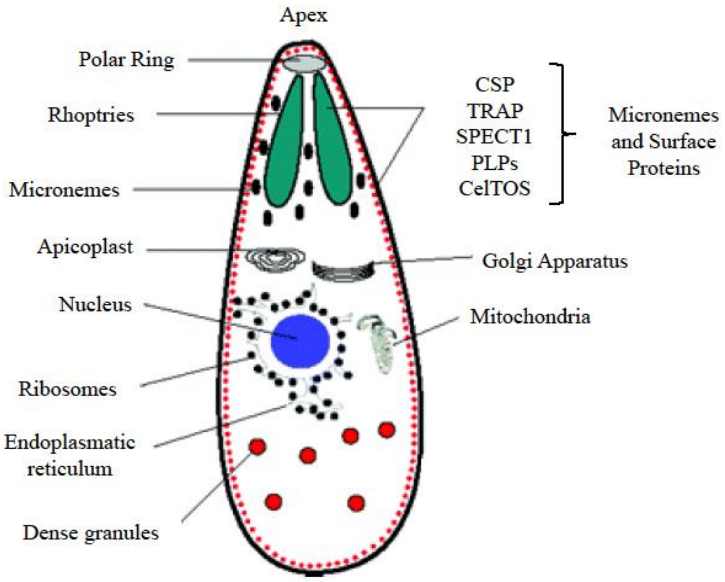

Figure 1.5. Structure of a sporozoite parasite, adapted and reproduced from Garcia *et al.*[19]

The merozoite parasites are involved in the evasion of the host immune response in the blood plasma, and the invasion and infection of erythrocytes. Therefore, there is some overlap observed between expressed proteins in this stage with those in the sporozoite stage, and the merozoite parasite has a similar internal structure. For example, an active actin-myosin motor in the apical organelles of the merozoite mediates cell recognition and invasion. In addition, the reticulocyte binding homologue (*Pf*RH) family has been reported in both sporozoites and merozoites, with an unknown exact role but the belief that they are components in the structure that links the erythrocyte and the actin-myosin motor in the invading parasite.[20] Indeed, the essential *Pf*RH5 protein is a leading blood stage vaccine candidate, as neutralisation of *P. falciparum* has been observed through antibody inteference of the *Pf*RH5 interaction with the host receptor, basigin.[21] Differences between the expressed proteome of the merozoites and sporozoites do exist, with the merozoites expressing erythrocyte-binding antigens (EBAs) such as EBA 175 and EBA 140 while the sporozoites do not, and the merozoites showing higher levels of expression of immune evasion proteins such as the merozoite surface proteins (MSPs), MSP1 and, MSP2.[14]

During the asexual intraerythrocytic stage of malaria parasite development, the parasite undergoes multiple rounds of DNA replication and nuclear division. Major protein classes are consequently involved in the facilitation of parasite growth through, for example, the transport of molecules in and out of the cell, or the digestion of cytoplasmic contents.[14] Across the ring, trophozoite, and schizont stages of the *P. falciparum* intraerythrocytic lifecycle, 2767 malarial proteins have been identified, representing 55% of the total proteome, with the remaining proteins being assumed to be expressed in alternative liver, sexual, or mosquito stages.[15] Differences in the expressed proteome between each of the intraerythrocytic ring, trophozoite and schizont stages are also observed, with 1832 proteins globally expressed across these three *P. falciparum* intraerythrocytic forms, but with 935 proteins showing significant changes in expression (Figure 1.6).[15]

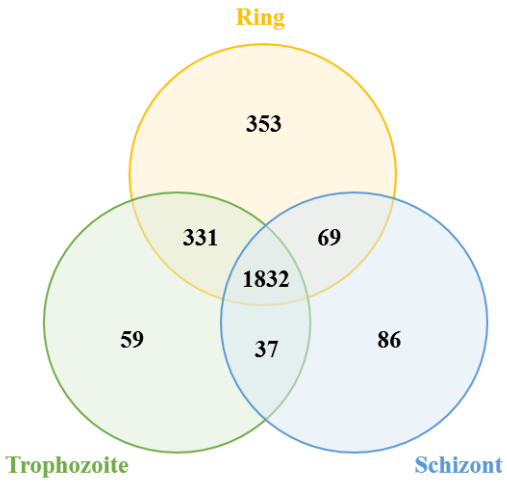

Figure 1.6. Venn diagram indicating the distribution of proteins identified over different stages of the intraerythrocytic lifecycle, adapted and reproduced from Pease *et al.*[15]

Proteins with increased expression in the early intraerthrocytic ring stage include those associated with metabolism such as ornithine aminotransferase and phosphoethanolamine *N*-methyltransferase, implicated in polyamine synthesis for the replication and survival of growing cells and in lipid biosynthesis, respectively.[22,23] Examples of proteins enriched in the trophozoite stage include the erythrocyte membrane proteins 2 and 3 (EMP2 and EMP3), which are exported by the parasite to the surface of the erythrocyte membrane, resulting in significant remodelling of the

host erythrocyte surface. This facilitates adhesion to endothelial cells, which leads to further binding with uninfected erythrocytes (through red blood cell sequestration) and thus aids the parasite to easily spread between erythrocyte hosts.[24] The Maurer's cleft two transmembrane protein (*Pf*MC-2TM) is also enriched in the trophozoite stage, and implicated in the transport of proteins secreted from the parasite to the erythrocyte surface.[11,15] Members of the plasmepin family (aspartic proteases), falcipain family (cysteine proteases), and falcilysin (a metallopeptidase) have all been clearly identified in trophozoites as proteins that aid in the digestion of haemoglobin to produce amino acids for parasite protein synthesis.[14] The late stage schizont forms of the intraerythrocytic stage of the *Plasmodium falciparum* parasite show increased expression of proteins such as myosin A, a motility protein critical for the red blood cell invasion that occurs just after schizont rupture.[15,25]

In addition, proteins associated with pathogenesis (the observable development of disease) are upregulated in the schizont stage in comparison to the ring and trophozoite stage, representing 7% of proteins identified in this stage in comparison to less than 1% for the average expression across all stages.[15] These proteins include the erythrocyte binding protein 2 (*Pf*EBP-2), with a role in erythrocyte invasion.[26] The coordinated rupture of schizonts and release of merozoites also involves a number of proteins from the kinase family, including plant-like calcium-dependent protein kinase *Pf*CDPK5, and cGMP-dependent protein kinase *Pf*PKG, both of which have been implicated in the signalling processes required to trigger parasite egress.[1,27,28] The observation that many parasitic protein kinases display significant structural and functional differences compared to their counterparts in their human hosts has incited discussion in the literature around the selective inhibition of this protein class for the treatment of malaria.[29]

The expressed proteome of the gametocyte parasites again varies significantly from the other parasitic stages due to their purpose of sexual reproduction. The gametocytes, particularly the female forms, show upregulation of proteins involved in translation and transcription, such as putative transcription or splicing factor-like proteins, and in messenger RNA processing, such as RNA-binding proteins.[14,30] Ribosomal proteins are largely represented in the female gametocytes, reflecting the need to accommodate

a sudden increase in protein synthesis during early zygote development.[14] The male gametocytes, however, are largely devoid of ribosomes and are terminally differentiated (showing cell cycle arrest with repression of transcription), with the primary task of producing motile microgametes in order to find and fuse with the female forms.[31]

The complex changes in expressed proteome across the malaria multi-stage lifecycle indicate that a comprehensive understanding of this biology could aid in the design of drugs or vaccines that target this disease.[14] In addition, this understanding could help overcome issues currently arising with the development of antimalarial resistance to important antimalarial drug classes currently on the market.[32]

1.4 Current Therapies for the Treatment of Malaria

The primary objective of malaria treatment is to cure the patient *via* rapid and full elimination of the *Plasmodium* parasite from the blood in order to prevent development of uncomplicated malaria to severe malaria and/or death, and to prevent chronic infection that leads to anaemia. A secondary objective of malaria treatment is to reduce the transmission of the disease to others in order to spare at-risk populations and prevent the emergence of antimicrobial resistance to medicines.[33] A number of antimalarial treatments have been developed over the past century, each with their own unique efficacies and resistance issues (Figure 1.7).

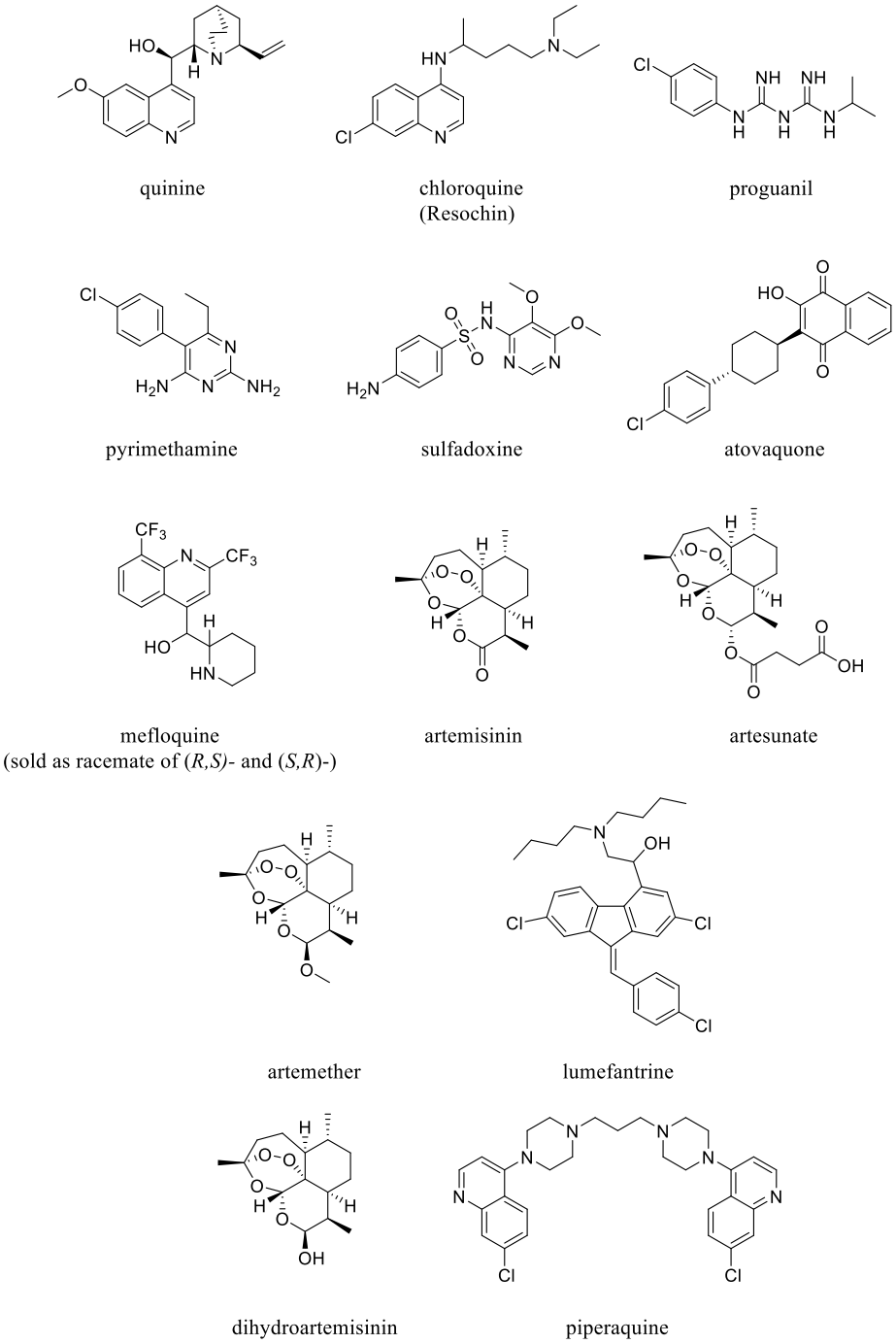

Figure 1.7. Structures of antimalarial drugs.

Antimalarial discovery and development has been intricately linked to significant historical events. The natural compound quinine, first isolated from the bark of the cinchona tree in 1820, was the favoured malaria treatment across the world throughout the 19th and 20th centuries as a result of its observed therapeutic effects when used to

treat intermittent fever. However, access to cinchona tree plantations during the First World War was limited, and led to the discovery of a synthetic quinine substitute by the German government that came to be known as chloroquine, belonging to a new class of antimalarial four-amino quinolines.[34] Chloroquine became one of the principal driving treatments for malaria in the WHO's 'global malaria eradication' campaign of the 1950s, as a result of its low cost and respectable safety profile, resulting in a notable reduction of malaria deaths.[35] However, antimicrobial resistance to both quinine and chloroquine has since been reported in both Asia and Africa with the emergence of resistant strains of the *P. falciparum* parasite.[35–37] By the 1980s, chloroquine resistance had contributed to the re-emergence and spread of the disease across Southeast Asia, South America, and Africa.

Another drug resulting from the antimalarial pipeline post-World War Two was proguanil, and after further study of its pharmacological class, pyrimethamine. However, resistence emerged rapidly after the introduction of both monotherapies as common treatments for malaria, with resistance to proguanil being observed within just a year. Other classes of antimalarial included the sulfones and sulfonamides, which were combined with proguanil or pyrimethamine in combination therapies in an attempt to overcome the resistance issues seen with the monotherapies.[34] The sulfadoxine-pyrimethamine (SP) combination therapy became a first-line treatment, along with the atovaquone-proguanil (AP) combination, currently commercially available as Malarone for the treatment and prevention of malaria. However, both therapies have been complicated with resistance issues in recent years.[38]

During the Vietnam War between 1955 and 1975, the United States of America (USA) developed an antimalarial for their troops that was curative with one dose against chloroquine-resistant parasites, known as mefloquine. Mefloquine was effective for 6 years before the emergence of mefloquine-resistant strains of the malaria parasite.[39] The North Vietnamese, also suffering major losses from chloroquine-resistant malaria infection amongst their army, requested help from the Chinese government to develop their own novel antimalarial. The Chinese government initiated a secret campaign to search for traditional Chinese herbal recipes that showed antimalarial activities.[40,41] These efforts resulted in the isolation of artemisinin, for which 100% inhibition of

rodent and monkey malaria was observed and for which half of the 2015 Nobel Prize in Physiology and Medicine was awarded to Professor Youyou Tu for her contributions to its discovery. Artemisinin and artemisinin derivatives rapidly clear parasite biomass by up to 10,000-fold every 48 h, working within the first 1 – 3 hours after administration. A drug with a longer half-life is required to destroy the remaining parasites and minimise the development of artemisinin resistance.[42] These Artemisinin Combination Therapies (ACTs) are the current first-line treatment for malaria, and are recommended for use by the World Health Organisation. They include artesunate-mefloquine, artemether-lumefantrine, and dihydroartemisinin-piperaquine combinations (Figure 1.7).[43,44] These drug treatments play an indispensable role in the current fight against malaria. However, their efficacy is now threatened by artemisinin resistance, defined in recent years as a parasite clearance half-life of greater than 5 hours following treatment by an ACT.[42] Artemisinin resistance was first reported in Cambodia in 2009, and has since spread to other parts of South East Asia including Thailand, Myanmar, and Vietnam, indicating a pressing need for development of the next generation of potent antimalarial therapies.[43] In addition to this, there are clear benefits to understanding the underlying biological mechanisms of action and resistance for novel antimalarial treatments, including the increased ability to control the spread of resistance.[35]

1.5 Modes of Action of Current Malaria Treatments and the Associated Parasitic Resistance Mechanisms

Many antimalarial drugs that target the intraerythrocytic parasite stages exhibit complex polypharmacology. Despite difficulties in the resultant deconvolution of their mechanisms of action, some insight into their mechanisms and their associated modes of resistance have been identified.[45] These are discussed in the following sections.

1. Quinine

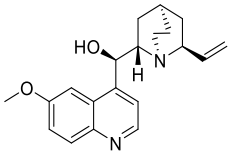

Figure 1.8. The structure of antimalarial compound quinine.

Quinine was the first-in-class quinoline used in antimalarial treatment, and remains the treatment of choice for uncomplicated malaria in pregnant women during their first trimester.[46] Its mechanism of action remains elusive as it has done for centuries since its discovery, although a recent study using a mass spectrometry coupled-cellular thermal shift assay (MS-CETSA) indicated that the compound binds to *P. falc* purine nucleoside phosphorylase (*Pf*PNP).[46] *Pf*PNP is an enzyme important for the salvage and recycling of purines, necessary due to the inability of the parasite to synthesise its own purine bases required for nucleic acid synthesis.[47,48] Due to the uncertainty in the complete mechanism of action of quinine, the mechanisms of resistance have also been difficult to uncover, and the reasons for quinine resistance remain unclear.[49]

2. Chloroquine

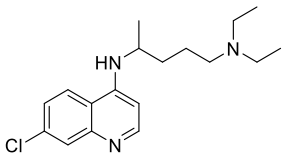

Figure 1.9. The structure of antimalarial compound chloroquine.

Despite being a member of the same class of quinolines, chloroquine appears to have a different mechanism of action to that of quinine.[46] The parasite grows by haemoglobin digestion that occurs during the intraerythrocytic stage of the parasite lifecycle. The associated side product, heme, is crystallised into hemozoin in order to reduce its toxic effects. Chloroquine caps hemozoin molecules to prevent further biocrystallisation of heme, thus leading to toxic heme build-up. This interferes with parasite detoxification processes.[50] Chloroquine efficacy is thought to be due to the

acid-base properties of the molecule. The three pK_a values of chloroquine are 4.0, 8.4, and 10.2, allowing the drug to accumulate as the di-protonated form in the acidic vacuole (pH ~ 5.4) where haemoglobin digestion takes place.[51,52]

The membrane of the digestive vacuole is impermeable to the positively charged chloroquine species *via* free diffusion. However, a point mutation in a gene leads to the subsequently named *P. falciparum* chloroquine resistance transporter (*Pf*CRT) protein being capable of interacting with the positively charged chloroquine. This leads to the transportation of chloroquine out of the digestive vacuole and results in parasitic resistance to the drug.[50]

3. Sulfadoxine-Pyrimethamine Combination Drug

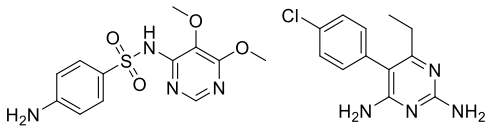

sulfadoxine pyrimethamine

Figure 1.10. The structures of antimalarial compounds sulfadoxine and pyrimethamine.

In a synergistic manner, the SP combination drug works by sulfadoxine binding to dihydropteroate synthase (DHPS), and pyrimethamine binding to dihydrofolate reductase (DHFR), both crucial enzymes in the folate biosynthesis pathway for DNA replication and cell division.[53,54]

Mutations in both enzymes lead to a reduced binding affinity for the drugs. These mutations include an alanine to glycine mutation in DHPS, and a serine to asparagine mutation in DHFR.[53,54]

4. Atovaquone-Proguanil Combination Drug

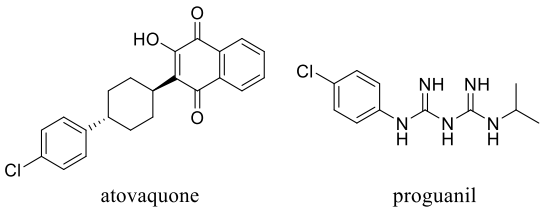

Figure 1.11. The structures of antimalarial compounds atovaquone and proguanil.

Atovaquone inhibits the cytochrome bc_1 complex, a subunit of the Cytochrome *b* (Cyt*b*) protein encoded by the mitochondrial genome of *P. falciparum*.[51] Cytochrome bc_1 is essential in the mitochondrial electron transport chain, and its inhibition leads to a decreased catalytic ability of various dehydrogenases present in the parasitic mitochondria. One of these is dihydroorotate dehydrogenase (DHODH), an enzyme that catalyses the pyrimidine biosynthetic pathway. Disruption of this process leads to parasitic death due to the inability of the *Plasmodium* parasite to salvage pyrimidines from the host cells and thus to synthesise new nucleic acids and proteins.[51] The addition of proguanil significantly decreases the concentration of atovaquone required to do this through suspected multiple mechanisms, including *via* a metabolite, cycloguanil, which is a known DHFR inhibitor.[38,55–57]

A point mutation in the mitochondrial Cyt*b* gene leads to a change in the atovaquone binding site, and a reduced binding affinity of atovaquone.[58] Additionally, point mutations in the DHFR enzyme are thought to contribute to proguanil resistance.[38]

5. Mefloquine

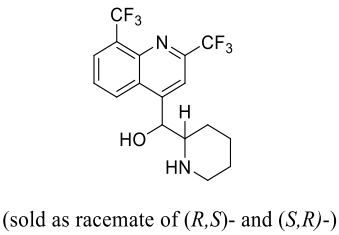

Figure 1.12. The structure of antimalarial compound, mefloquine.

Mefloquine inhibits parasite protein synthesis through direct binding to the cytoplasmic ribosome (*Pf*80S) *via* the GTPase associated centre (GAC) of the large ribosomal subunit, *Pf*60S.[59] This region is critical for translation, binding the translational GTPases and facilitating the elongation steps of protein synthesis by activating the translocation of the tranfer RNA (tRNA)-messenger RNA (mRNA) complex through the ribosome.[59] Interestingly, conflicting reports as to the more active enantiomer exist in the literature, and their properties appear to be *Plasmodium* strain-dependent.[60,61]

Mutations in the encoded drug transporter of *P. falciparum* multidrug resistance protein 1 (*Pf*MDR1***),*** Pgh-1, results in efflux of mefloquine from the cytoplasm to the parasitic food vacuole, where it is incapable of reaching its site of action.[59,62,63]

6. Artemisinin

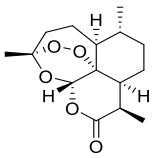

Figure 1.13. The structure of antimalarial compound artemisinin.

Artemisinins are fast-acting compounds displaying the highest parasite killing rates across all currently studied antimalarials.[51] These compounds are thought to act *via* multiple different mechanisms, a theory supported by the slow development of resistance. The endoperoxide component within artemisinin and its derivatives is crucial for their antimalarial properties. Iron-mediated reductive cleavage of the endoperoxide bond generates free radicals, with iron sourced from the heme species liberated in haemoglobin digestion.[64] These free radicals lead to eventual alkylation of parasitic proteins and biomolecules, causing oxidative stress and irreversible parasite damage through multiple different mechanisms.[65] Resistance mechanisms remain unclear although a mutation in the K13 gene has been observed to lead to an enhanced cell stress response, potentially indicating a mechanism of resistance.[65]

Due to the high lipophilicity of the natural product artemisinin, and thus low solubility and low bioavailability, semisynthetic derivatives of artemisinin are often used to

improve the pharmacokinetic properties of the drug. For example, artesunate is an artemisinin derivative with a much higher aqueous solubility and is a prodrug for the active metabolite, dihydroartemisinin, formed *via* esterase-catalysed hydrolysis (see Figure 1.11). Artesunate can be administered orally, but is also the only artemisinin derivative with sufficient water solubility to be administered intravenously.[66]

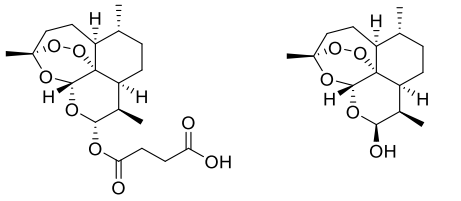

Figure 1.14. Structures of artemisinin derivatives.

1.6 Target Identification in Antimalarial Drug Discovery

1.6.1 The Drug Discovery Pipeline

Developing a new drug from an initial hypothesis to a marketed product often takes in excess of 12 years and can cost over £1 billion.[67,68] More often than not, the optimisation of a new medicine starts when a new biological target (such as a protein, enzyme, or gene) implicated in a specific disease becomes apparent through data mining, literature reports, or appropriate genetic data.[67,68] Selection of this target and further validation can progress to the lead discovery and lead optimisation stages of the drug discovery process, in which medicinal chemists work to design and synthesise drug-like small molecules through iterative cycles of designing and testing against appropriately developed assays.[67] Once a suitable development candidate has been identified, this molecule is selected and progressed onto preclinical and clinical development. During these development stages, clinical trials are used to demonstrate the efficacy, or lack of, of the designed drug molecule in human patients (Figure 1.15).

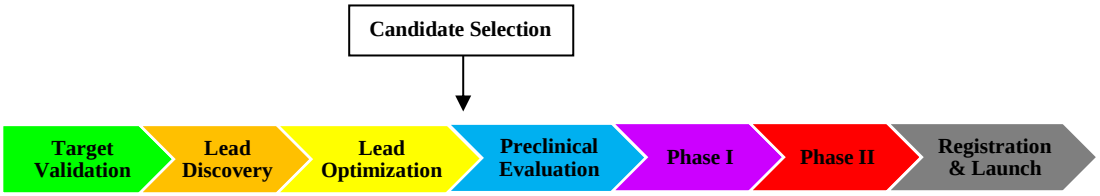

Figure 1.15. The drug discovery and drug development process.[69]

1.6.2 Target-Based *versus* Phenotypic Screening

Two broad approaches to initial screening for drug-like molecules in early stage drug discovery have dominated in recent years: target-based, and phenotypic screening. In the more common target-based screening, a protein target considered instrumental in a certain disease is selected and purified before exposure to potential drug molecules. A specific assay for the selected target is established, and binders or inhibitors of this protein are then optimised based on the output from this assay.[70] Phenotypic screening is considered a 'target-agnostic' approach, and involves the screening of thousands of molecules against a relevant biological system to look for a specific phenotype (an observable characteristic), without needing to rely on knowledge of the identity of the protein target or its role in disease at the initial screening stage.[71]

Phenotypic screening provides benefits over target-based methods due to a removal of restrictions on sampled biological space, thus increasing the chances of identifying first-in-class drugs with new modalities; the power to address the complexity of diseases that are poorly understood by the scientific community; the opportunity to identify drugs acting through multiple different pathways; and the fact that non-membrane permeable drugs are naturally eliminated from consideration.[71,72] However, phenotypic screening may often lead to slow progression of the drug candidate as a result of the empirical nature of subsequent drug optimisation programmes. Often significant resources and time will also be spent on the subsequent target identification and validation of the resultant drug molecule.[73] In target-based drug discovery, the mechanistic hypothesis often facilitates faster progress to clinical studies. However, this can be at the expense of traditional empirical evaluation and result in significant loss of time, money, and resources if the specific assay does not translate effectively to the clinic (Table 1.1).[70,73]

	Phenotypic Screening	Target-Based Screening
Advantages	• 'Target agnostic', allowing identification of new protein targets and first-in-class drugs. • Ability to address poorly understood diseases. • Potential to identify drugs with multiple mechanisms of action. • Non-permeable drugs eliminated from consideration.	• Clear mechanistic hypothesis. • Often more simple to execute when using one isolated protein. • Provides knowledge of a clear protein target.
Disadvantages	• Possible slow progression due to poor biological understanding. • Significant resources required for subsequent target identification and validation.	• High risk of poor translatability to the clinic.

Table 1.1. Advantages and disadvantages of phenotypic *versus* target-based screening.

Phenotypic screening has typically been the method of choice for antimalarial hit identification due to the dependence of global malaria eradication on finding drug therapies that have new modes of action, and that target all or multiple stages of the parasite lifecycle.[72] Target identification once these hits have been identified is desirable for faster progression and deeper understanding of the biological profile of the resultant drug compound, but can often be one of the most challenging and time consuming steps in the drug discovery pipeline. Indeed, in the literature, target identification has been likened to finding a needle in a haystack.[74] For *P. falciparum*, this is particularly true as a result of a high percentage of the genome lacking annotation (almost 50%), and the polypharmacology of many antimalarial compounds.[45,75]

Drugs often fail in the clinical development stages for two reasons; either they do not show the desired level of efficacy, or they are not safe.[67] As a result, in both target-based and phenotypic screening methods, there is a need to confirm the translational potential of the assay readout to the clinical disease indications. The target identification and validation stage at the beginning of the drug discovery process can therefore be one of the most important and impactful stages. Indeed, estimates suggest that 93% of drugs approved by the US Food and Drug Administration (FDA) have a defined target, and 82% have a defined mode of action.[45] These values demonstrate

that this knowledge is often central in medicinal chemistry programmes to improve selectivity, toxicity, and pharmacokinetic profiles; in clinical trials to understand patient reactions to new drugs; in aiding the selection of partner drugs; and in drug resistance surveillance.[45,67] This is particularly true in the area of antimalarial drug discovery in the face of developing antimalarial resistance. The inadequate knowledge amongst the scientific community about the modes of action of antimalarial drugs severely limits current efforts to tackle the disease, for which there are major implications for global eradication and control efforts, as well as huge risk to human health and life.[76] It is therefore of utmost importance to investigate the basic mechanisms through which antimalarial medicines function, and through which parasitic resistance to these medicines is generated, in order to design new drugs with novel modes of actions, and to make better use of drugs already in use.[77]

1.6.3 Strategies for Target Identification

A variety of target deconvolution strategies are routinely used throughout the pharmaceutical industry and include genetic approaches, computational inference, or biochemical methods. Often, a combination of multiple techniques is required to fully characterise on-target and off-target effects.[70]

Fundamental biological processes such as metabolism, transcription, translation, and signalling pathways, and their role in disease have been described in depth by their genetic sequences, and shown often to be conserved across different species.[78] As such, genetic manipulation and analysis has become commonplace for target identification in drug discovery. The process often entails the modulation of genetic markers for presumed targets, thus allowing the measurement of changes in sensitivity to small-molecules. Alternatively, resistant mutants can be compared to the drug-sensitive phenotype to analyse point changes in the genetic sequence and thus infer the relevant protein targets.[78] In antimalarial drug discovery, drug resistant strains are often evolved in the laboratory by applying a high and constant drug pressure to *P. falciparum* cultures. The parasite DNA can then be isolated and analysed to identify the genetic changes associated with the resistance and thus elucidate the potential mechanism of action of the drug being studied.[45] However, care must be taken when

assigning antimalarial modes of actions based on this method of resistance screening as a result of the possibility that resistance is confered *via* genes that are distinct from those of the molecular target. For example, mutations in the *Pf*MDR1 gene lead to resistance to mefloquine as a result of compound transport rather than mutations in the target *Pf*80S protein (see **Section 1.5 – Modes of Action of Current Malaria Treatments and the Associated Parasitic Resistance Mechanisms**).[45]

In silico target identification is made possible due to the large datasets that are routinely acquired and stored within the pharmaceutical industry leading to extensive possibilities for computational tools to analyse potential correlations, links, and inferences.[70,79] Using the assumption that compounds with the same mechanisms of action will exhibit similar behaviour across different biological assays (such as genetic assays, or small molecule screens), computational analysis of different datasets that probe different phenotypic effects can be used to infer the unknown mechanisms of action of new drug molecules from those of known ones.[70] Other structure-based methods, which rely on knowledge of the three-dimensional protein structure, can be used to predict the ligand binding of potential drug molecules to specific proteins. These methods are becoming increasingly utilised as a result of the increase in public access to large datasets relevant to drug discovery, but are limited in their application when searching for targets not previously known.[70,79]

Affinity chromatography as a biochemical method for target identification uses a small molecule of interest immobilised onto a stationary phase to capture its target proteins as the biological sample (e.g. a specific cell lysate) is passed through the matrix. Those proteins without substantial affinity for the bound small molecule pass directly through the column, whilst those that recognise it are slowed relative to their normal affinity constant. This subsequently allows the idenfication of those bound proteins, after their elution through a change in parameter such as pH or the small molecule in solution, and gel visualisation and excision.[80] Classically, these methods required large amounts of starting protein, extensive protein fractionation, and stringent wash conditions, and were typically poor at identifying weakly-bound proteins.[81] Recently, improved biochemical techniques based on a similar principle to that of affinity chromatography

have been optimised in order to overcome issues such as high background interactions and poor identification of weaker interactions.

Chemoproteomic techniques such as Stable Isotope Labeling by Amino acids in Cell culture (SILAC) often use affinity chromatography in combination with quantitative mass spectrometry to accurately identify protein interactions of small molecules.[81] SILAC involves the immobilisation of a small molecule onto beads, which are then incubated with both 'light' cell cultures, containing the natural isotope abundance forms, and 'heavy' cell cultures, containing ^{13}C and ^{15}N-bearing isotopes of arginine and lysine protein residues. Both types of peptides are observable by mass spectrometry, with characteristic mass shifts between the 'light' and 'heavy' forms of each protein peptide. Through addition of the free small molecule to one type of cell culture, the competitive binding between free and immobilised small molecule leads to a reduction in binding to the beads, which can be observed as a ratio other than 1:1 of the 'light' and 'heavy' isolated protein in the final mass spectrum, after digestion of the proteins captured by the beads. This technique allows for protein identification largely independent of protein abundance, and can provide information on the relative strength of binding to each protein based on the SILAC ratio (Figure 1.16).[81]

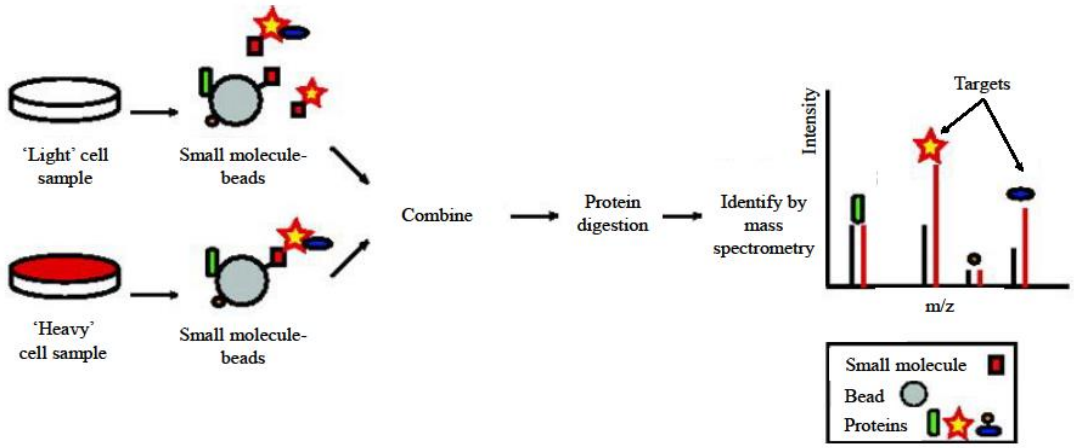

Figure 1.16. The SILAC approach to target identification, adapted from Ong *et al*.[81]

The use of mass spectrometry in the identification of proteins from a mixture enables target identification in drug discovery not only through the SILAC approach, but also through multiple other chemoproteomic techniques.[82] Two of these techniques are

discussed in further detail in the coming sections, and are key methods for the work outlined in this thesis as a result of the ability to apply expertise in chemistry to the largely biological challenge of target identification.

1.6.4 Chemoproteomic Techniques for Target Identification

Large catalogues of genetic data have been made available in recent years, including for several species of *Plasmodium* parasite.[14,15] As a result, the capabilities of biological experimentation have increased significantly, leading to an expansion in proteomic research looking for mechanistic insight into biological processes that underline disease.[83,84] Proteomics is a discipline that involves the identification and quantification of the proteins of a proteome, including expression, cellular localisation, interactions and post-translational modifications (PTMs). This is a substantial challenge, demonstrated by the fact that there are 100,000 possible protein forms encoded by the approximately 20,235 genes of the human genome.[83] Proteomics almost exclusively involves the use of liquid chromatography (LC) coupled to tandem mass spectrometry (MS/MS).[84] Significant advances in new technology for mass spectrometry and data analysis have driven the recent boom in proteomic research. In the past decade, these advances have been in resolution, mass accuracy, sensitivity, and scan rate of mass spectrometers: technology that is crucial for the deconvolution of complex protein mixtures.[83,85]

In the most widely used approach for protein identification, known as ‘bottom up’ or ‘shotgun’ protein analysis, after relevant purification, proteins are digested to a set of peptides using a protease.[83] Trypsin is the most commonly used protease, and specifically cleaves proteins at the carboxy-terminal of arginine and lysine residues, except when they occur after a proline residue. The specificity of this cleavage leads to a selection of peptides in the preferred mass range for sequencing (~20 residues).[86] Digesting the protein into a set of peptides also overcomes issues with direct identification of intact proteins, such as with solubility and viscosity.[86] The peptide mixture is then injected onto a high performance liquid chromatography (HPLC) column that is directly linked to the mass spectrometer. The peptides elute from the HPLC and flow through a narrow needle tip, where they are vaporised and ionised by

the effect of a strong electric potential difference between the needle and the inlet to the mass spectrometer. This process is known as electrospray ionisation.[85,87] Charged droplets in the form of a fine mist are resultantly created, with the application of a drying heat or gas used to evaporate the remaining solvent, leaving desolvated ions.[85] These ions enter the mass spectrometer where their flight paths are manipulated by an applied electric field. The mass-to-charge (*m/z*) ratio determines the amount of deflection of the ions as a result of the applied electric field, and the mass spectrometer generates a mass spectrum (MS1) with a signal intensity proportional to the number of ions collected at each value of the appropriate *m/z* scale (Figure 1.17).[86]

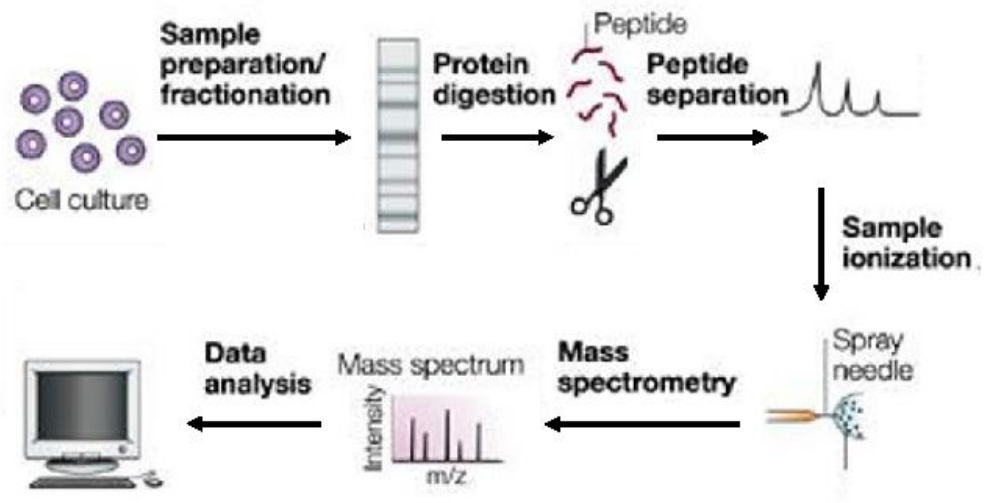

Figure 1.17. The mass spectrometry workflow used in proteomic research, reproduced from Steen *et al.*[86]

Having determined the *m/z* values and intensities of each of the peaks in the spectrum, the mass spectrometer proceeds to obtain further structural information about each of the most abundant identified peptides, giving the process the name of tandem mass spectrometry (or MS/MS). This involves two stages of mass spectrometry, with each of the most abundant identified peptides taken and fragmented a second time through collision-induced dissociation (CID), in which collisions with an inert gas (e.g. nitrogen, helium, or argon) cause fragmentation along the peptide backbone. A mass

spectrum of the resulting fragments (MS2) is generated to provide further detail in order to facilitate protein identification.[86]

Traditionally, in order to identify the amino acid sequence of a parent protein from the mass spectrum of its fragmented peptides, an analysis of the mass difference between neighbouring peaks in a series was carried out in order to identify the relevant and subsequent amino acid. Difficulties as a result of incomplete spectra and intervening peaks can frustrate this process, known as *de novo* sequencing. In modern day proteomics, this problem is overcome by instead comparing the output mass spectrum with a database of known spectra, or with theoretical mass spectra generated from *in silico* digestion of a protein database.[83,86] This is a powerful technique because whilst a peptide mass spectrum might not have sufficient information to unambiguously determine the complete amino acid sequence, it may still provide enough information to be able to match the spectrum to a unique peptide sequence in a database.[86] The extensive genetic databases mentioned previously therefore enable the use of mass spectrometry in these proteomic techniques.

The transformation of LCMS/MS data from qualitative to quantitative data can be performed *via* stable isotope labelling approaches, such as the SILAC approach previously discussed. Another common isotope labelling strategy involves the introduction of isotope-containing tags into proteins or digested peptides *via* chemical reactions. This has recently been expanded to allow for the simultaneous analysis of multiple different samples at once. Isobaric tags for relative and absolute quantification (iTRAQ) and tandem mass tags (TMT) are the most commonly used, and react specifically with primary amine groups on the digested peptide residues (for example, the *N*-termini of amino acids, or the side chains on lysine residues).[88,89] The tag design consists of three main functionalities: an amine reactive group, a mass differentiation group, and a mass reporter (Figure 1.18).[90,91]

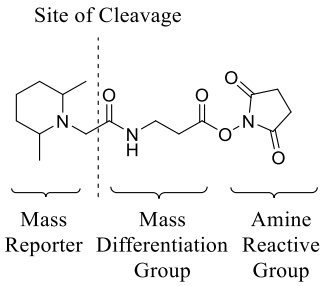

Figure 1.18. General structure of a tandem mass tag.

Different peptide samples are labelled with different isobaric tags *via* the protein reactive groups, and then mixed and analysed using LCMS/MS. The isobaric tags are chemically identical, thus identical peptides labelled with different tag variants will have the same mass and chromatographic profile and will coelute during LC separation (Figure 1.19).

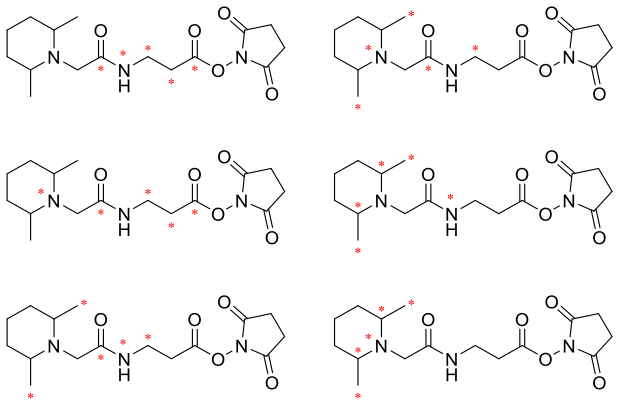

Figure 1.19. The 6 different TMT reagent structures from the Thermo Fisher TMTsixplex™ Isobaric Mass Tagging Kit (catalog #90064).[90] A red asterix indicates the isotopic form of the atom indicated. Each of the 6 TMT reagents have the same chemical structure and mass until CID leads to fragmentation at the position indicated in Figure 1.18, allowing differentiation between the different tags through analysis of the MS spectrum.

During the subsequent collision-induced dissociation step, the mass reporters are cleaved from the labelled peptides, leaving behind the mass differentiation groups. The cleaved mass reporter tags have different masses as a result of different isotopic make-up, which are observed in the MS/MS spectrum at low *m/z* values. The intensities of these mass reporter ions then provide the information needed to determine the relative

abundance of the peptides and proteins from each of the labelled samples.[89] This overall workflow is depicted in Figure 1.20.

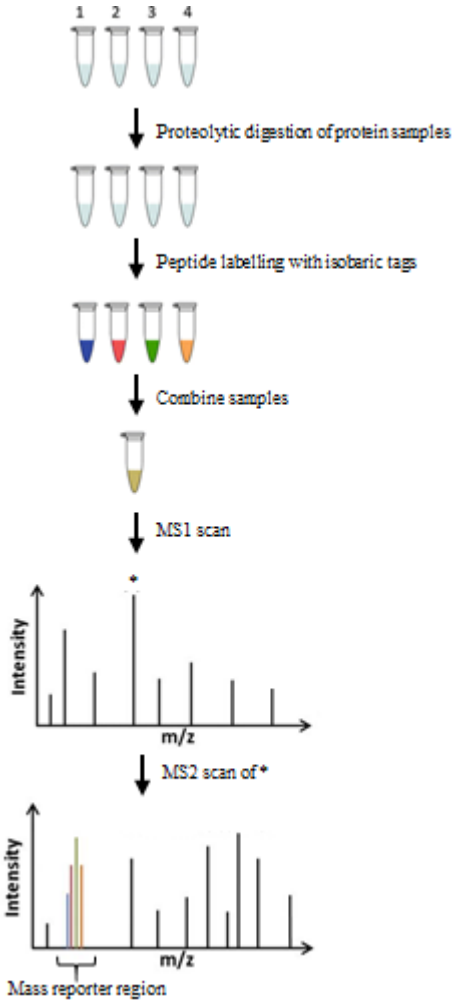

Figure 1.20. The workflow for a TMT labelling experiment for 4 protein samples, adapted from Xie *et al.* and Zhang *et al.*[89,90]

Chemical techniques in order to access appropriate protein mixtures to answer specific biological questions using LCMS/MS are becoming commonplace in the pharmaceutical industry. In particular, the field of chemoproteomics links the use of chemical synthesis of appropriate chemical probes with the field of proteomics in order to characterise the modes of action of small molecules and interpret their pharmacological effects.[82] The ways that these techniques can have, and have had, a major impact on our understanding of cellular molecular mechanisms are exemplified in the following sections.[82]

1.6.4.1 What is a Chemical Probe?

A chemical probe is a small molecule designed to modulate the function of a specific protein, thus allowing the user to investigate mechanistic questions about the role of the targeted protein in healthy and diseased cells and tissues.[92] Although the structures of chemical probes are often based on a drug with known phenotypic efficacy, their uses and characteristics vary (Table 1.2).[92,93]

Drugs	Chemical Probes
• Must be effective, and safe for human consumption. • May have undefined mode of action. • May have IP restrictions. • Must have human bioavailability. • High importance on appropriate physicochemical and pharmacological properties (potency, lipophilicity, permeability, toxicity).	• Ask a specific biological question. • Binds to its target with high affinity in an appropriate assay. • May require selectivity depending on the biological question being asked. • Drug-like properties such as bioavailability are not necessarily required. • Value can be enhanced by use of related inactive and active control compounds.

Table 1.2. The differences between drugs and chemical probes.[92]

1.6.4.2 Chemical Probes for Use in Affinity Capture Techniques

In affinity capture techniques for proteomic research, a chemical probe based on an analogue of a small molecule of interest is synthetically functionalised to incorporate a functional handle (such as an amine, carboxylic acid, alcohol, or alkyne) that is used for conjugation to a relevant solid support or resin *via* a linker such as an alkyl, polyethylene glycol (PEG), or amino acid chain.[94] In immobilised bead assays, this solid support often takes the form of agarose beads.[95] Different solid supports and resins are available incorporating diverse functional groups to allow various coupling methods for immobilisation. The choice of linker can depend on the experimental conditions. For example, alkyl chains are useful for modulating hydrophobicity and facilitating ease of entry into live cells or tissue, PEG chains are suitable for providing an increase in solubility for hydrophobic probes being manipulated in aqueous media, and amino acid linkers can be used to enhance specific binding to desired active sites of target proteins.[94] The immobilised compound is then incubated with cell extracts to

facilitate non-covalent affinity binding to target proteins. Purification followed by LCMS/MS is employed for the identification of captured proteins.[95]

Affinity capture techniques such as these immobilised bead assays have several associated risks. The fact that derivatised analogues of the compound of interest are employed, rather than the compound itself, can lead to changes in potency and selectivity as a result of structural alterations. Additionally, false positive protein identification is possible due to protein binding to solid supports or linkers. The presence of high abundance proteins, such as albumin or haemoglobin, may also obscure significant interactions even when they have low affinity for the chemical probe. Consequently, time consuming efforts must be made to validate each identified protein target.

One way to validate protein targets is to carry out parallel experiments in which active and inactive analogues of the chemical probe are used, thus allowing a comparison of mass spectrometric results. However, inactive analogues often require additional and extensive medicinal chemistry investigations, and this method can thus demand significant extra time and resources. An alternative method for target validation is to use competition-based experiments. Incubation of the immobilised probe in cell extract is carried out in the presence and absence of an excess of the free, unaltered, compound of interest. Identification of significant target proteins is possible through analysis of those proteins for which captured amounts using the immobilised probe are reduced in a dose-dependent fashion by increasing concentrations of the free compound.[95] In those samples in which there is a high concentration of competitor, there is stronger competition for the protein binding site between this competitor and the immobilised probe. This results in less of the target protein being captured by the immobilised probe, and thus less of the target protein is identified in the mass spectrum (Figure 1.21). For proteins captured by the immobilised probe due to non-specific binding, there is no dose-dependent competition on addition of the competitor compound. Amounts of ‘background’ proteins therefore remain roughly constant between samples, which again can be visualised in the mass spectrum.

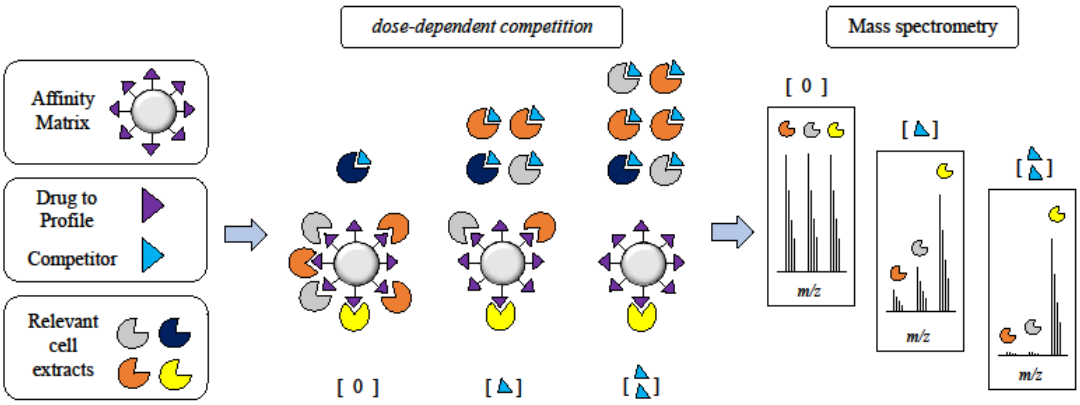

Figure 1.21. The immobilised bead assay workflow, with the compound of interest immobilised onto beads, indicated in purple, and the related free compound used in competition experiments indicated in blue. In this diagram, target proteins are shown in orange and grey, and proteins captured as a result of non-specific binding are shown in yellow. On addition of increasing concentration of competitor, the amounts of orange and grey protein captured by the immobilised probe decreases, as observed in the mass spectrum. The amount of captured background yellow protein remains constant.

Despite the challenges associated with immobilised bead assays for target identification, the technique has successfully been employed in antimalarial drug discovery. Cellzome identified *Plasmodium* phosphatidylinositol 4-kinase (*Pf*PI4K) as the target of antimalarial MMV390048 (Figure 1.22). Covalent immobilisation of a derivative of MMV390048, MMV666845, on Sepharose® beads was used to affinity capture potential protein targets from a *P. falciparum* blood-stage extract. Pull-down experiments were carried out both in the presence of and in the absence of excess drug MMV390048 in order to investigate which proteins were competitively inhibited. In a parallel experiment, an inactive analogue, MMV034137, was used in competition studies to analyse off-target effects. All compounds that were captured were quantified and identified through use of LCMS/MS. The drug MMV390048 was found to competitively bind only *Pf*PI4K, showing that this technique can be implemented successfully in the identification of novel targets for malaria.[96]

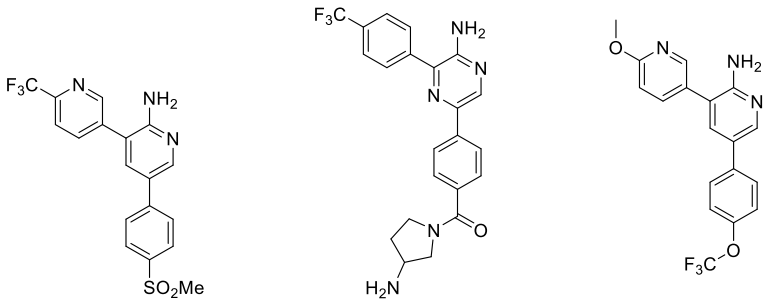

MMV390048 MMV666845 MMV034137

Figure 1.22. The structures of antimalarial MMV390048, the derivative used in the immobilised bead assay MMV666845, and the inactive analogue MMV034137.

Due to the intense interest in the kinase protein family in drug discovery, Cellzome have developed a similar capturing experiment in order to identify potential kinase targets of a compound whilst overcoming the risk that a derivitised chemical probe may not be compatible with all of the targets of its parent molecule.[97,98] This is achieved by the immobilisation of a selection of promiscuous adenosine triphosphate (ATP)-competitive kinase inhibitors onto what Cellzome have termed as 'kinobeads'. In combination, the immobilised promiscuous kinase inhibitors are capable of capturing a large portion of the kinome, as well as a defined set of other ATP- and purine-binding proteins such as chaperones, helicases, ATPases, motor proteins, transporters, and metabolic enzymes. The analysis of the effect of the competing 'free' ligand of interest on the binding of the immobilised kinase inhibitors to their known targets is monitored in order to identify specific kinase interactions (Figure 1.23). When the competing ligand binds to a kinase, this results in a reduction of binding of that kinase to the kinobeads, and thus there is a reduction in the amount of isolated protein kinase in the mass spectrum after digestion of those proteins bound to the beads. In the case of MMV390048, *Pf*PI4K was the only *P. falciparum* protein that was competitively inhibited on addition of the free drug to the relevant malarial cell extract in a kinobead assay, providing further evidence of the utility of these chemoproteomic techniques in the confirmation of novel antimalarial targets.[96]

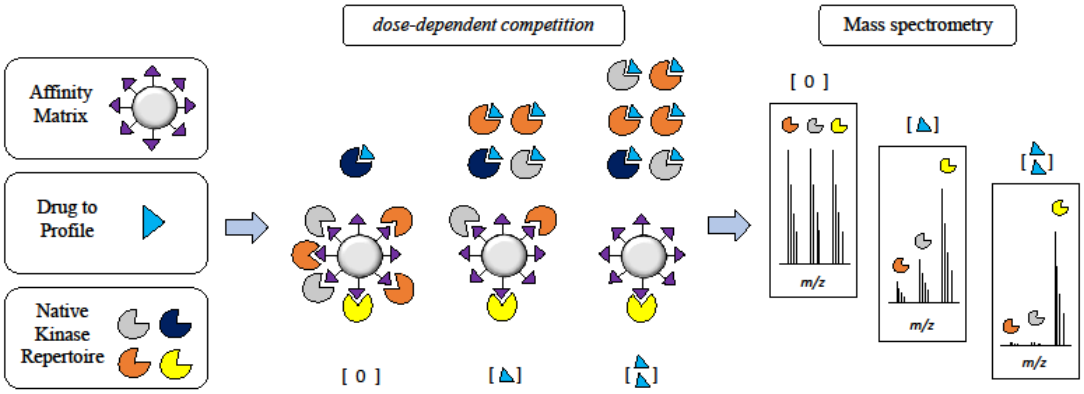

Figure 1.23. Kinobead assay workflow, as developed by Cellzome, with promiscuous kinase inhibitors indicated in purple and the compound of interest used in competition experiments indicated in blue. The promiscuous kinase inhibitors are immobilised onto an affinity matrix to form a kinobead, which is then incubated in the relevant cell extracts. Addition of the drug to profile will result in competition between the immobilised kinase inhibitors and this drug unit. This results in a reduction in binding to the kinobeads of protein kinases targeted by the drug unit, which is observed in the mass spectrum after digestion of the bead-bound proteins. In this diagram, the orange and grey proteins are the kinase proteins inhibited by the drug to profile, while the yellow protein is a kinase not inhibited by the drug to profile. Thus the amount of orange and grey protein isolated is reduced on addition of increasing concentration of drug unit, whilst the amount of isolated yellow protein remains constant.

1.6.4.3 Chemical Probes for Use in Photoaffinity Labelling

Photoaffinity labelling (PAL) is a powerful chemoproteomic method for target identification, using a chemical probe to covalently bind to its target on irradiation with light.[99] A photoaffinity probe is designed to incorporate three separate functionalities: an affinity unit, in the form of the drug that is being profiled, that facilitates reversible binding to target proteins; a photoreactive group (such as a diazirine, benzophenone, or phenylazide) that allows for photo-inducible permanent binding to these protein targets; and a functional handle (such as an alkyne, azide, or *trans*-cyclooctene moiety) for use in detection and purification of the final probe-protein complex (Figure 1.24). The photoreactive group and functional handle can be directly incorporated into the reversible binding affinity unit or can be placed on a linker.

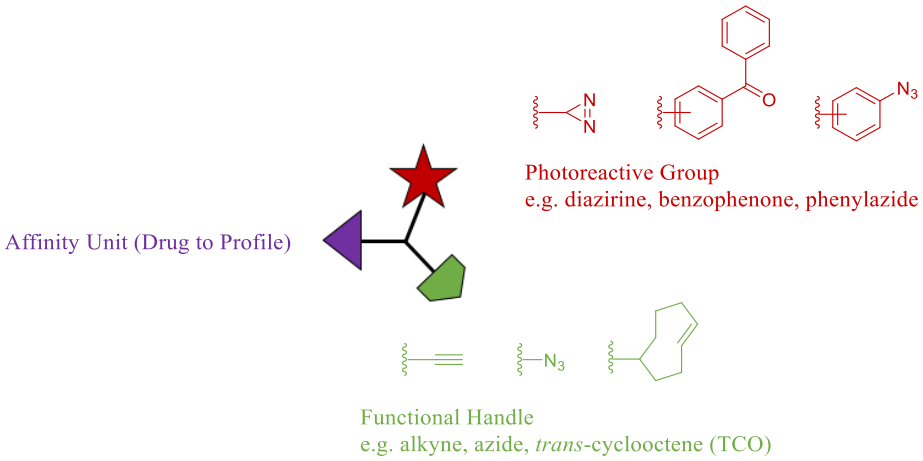

Figure 1.24. The general structure of a photoaffinity probe.

In photoaffinity labelling experiments for target identification, the PAL probe of interest is initially incubated with the relevant cell extract, or whole cells, to allow for reversible binding between the affinity unit and relevant target protein (Figure 1.25, part 2). For differentiation between background and proteins of interest, increasing concentrations of competitor (the unaltered parent drug) are added to successive samples to enable a dose-response analysis, similar to the competition experiments conducted for affinity based chemoproteomic techniques previously discussed (see **Section 1.6.4.3 – Chemical Probes for Use in Affinity Capture Techniques**). Irradiation with UV light of an appropriate wavelength for activation of the photoreactive group triggers the formation of the desired reactive intermediate, which rapidly reacts with nearby proteins or molecules through a variety of possible bond insertion and rearrangement mechanisms. Nearby target proteins are captured by the formation of a strong covalent bond as a result (Figure 1.25, part 3).

If using whole cell samples, cell lysis releases the captured protein-probe complex allowing for protein purification and isolation. This is typically carried out using biotin-derivatised reporter tags. For example, an alkyne functional handle undergoes facile click reactions with azide-derivatised biotin compounds (Figure 1.25, part 4). The almost irreversible binding of biotin to avidin (or streptavidin) occurs with high specificity and affinity (K_d = ~10^{-15} M), being one of the strongest naturally-occurring non-covalent interactions known.[100–102] This is exploited for use in affinity

purification, in which the biotinylated probe-protein complex is immobilised onto a solid support *via* its interaction with avidin, and non-captured proteins are removed with buffer washes. Harsh washes are compatible with the strong probe-protein covalent binding and biotin-avidin interaction, thus allowing maximum reduction in background noise. Immobilised captured proteins are then proteolytically digested into multiple peptide fragments, which are sequenced using LCMS/MS for identification (Figure 1.25, part 6).[99]

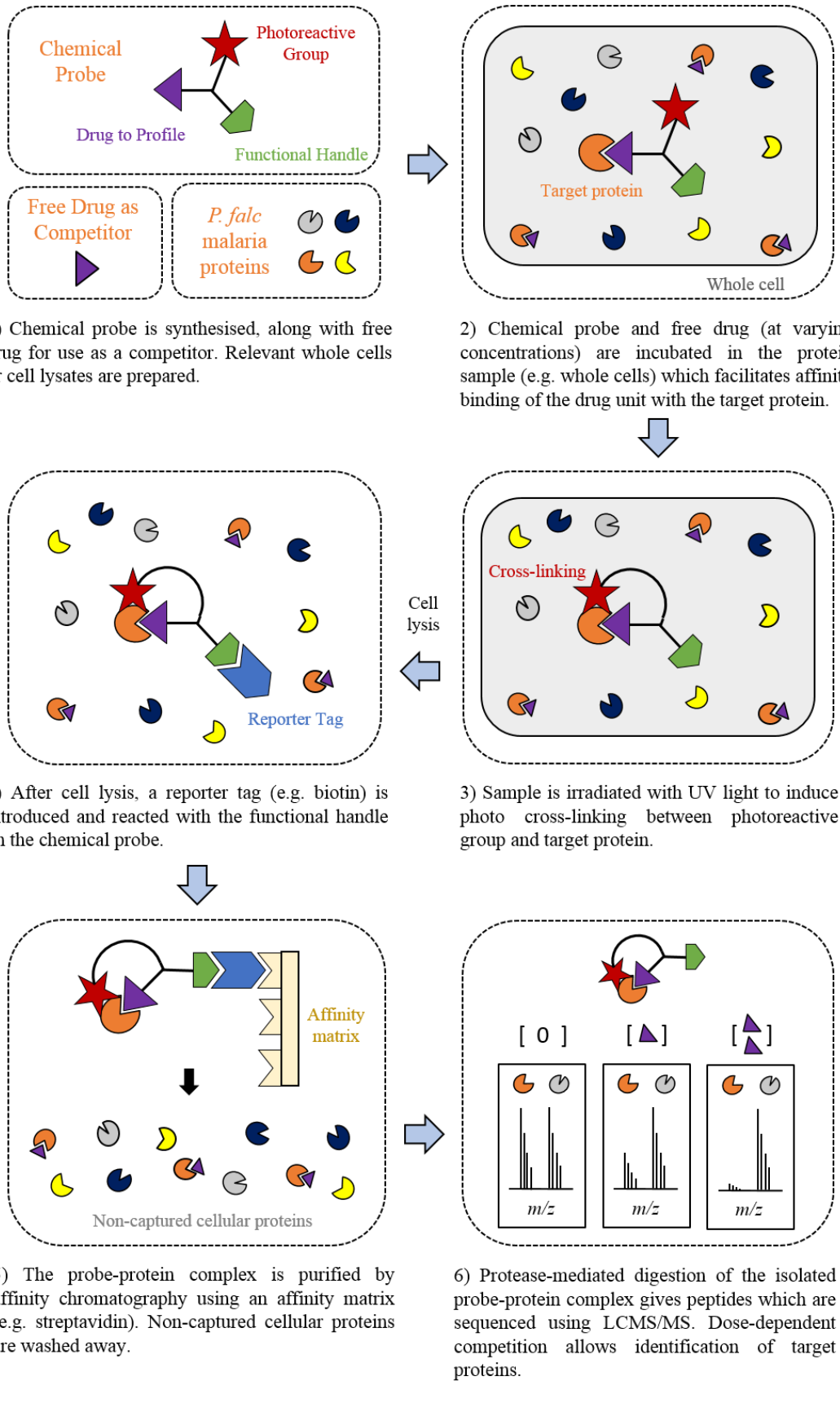

1) Chemical probe is synthesised, along with free drug for use as a competitor. Relevant whole cells or cell lysates are prepared.

2) Chemical probe and free drug (at varying concentrations) are incubated in the protein sample (e.g. whole cells) which facilitates affinity binding of the drug unit with the target protein.

3) Sample is irradiated with UV light to induce photo cross-linking between photoreactive group and target protein.

4) After cell lysis, a reporter tag (e.g. biotin) is introduced and reacted with the functional handle on the chemical probe.

5) The probe-protein complex is purified by affinity chromatography using an affinity matrix (e.g. streptavidin). Non-captured cellular proteins are washed away.

6) Protease-mediated digestion of the isolated probe-protein complex gives peptides which are sequenced using LCMS/MS. Dose-dependent competition allows identification of target proteins.

Figure 1.25. Photoaffinity labelling workflow.

Compelling advantages of photoaffinity techniques over affinity capture techniques such as the immobilised bead assay include the ability to carry out experimentation using live cells, providing a more realistic representation of the disease setting under investigation. In addition, the formation of a strong probe-protein covalent bond increases the probability of more effective capture, and allows for harsher conditions during purification. However, designing an appropriate photoaffinity probe can be a substantial task. Factors to be taken into account include the identification of a suitable site for incorporation of the photoreactive group and functional handle, cell permeability variations on addition of long linkers, and reductions in potency as a result of additional steric bulk.[99] In addition to this, the choice of photoreactive group and functional handle has an impact on the experimental workflow.

Common photoreactive groups used in chemoproteomic research include benzophenones, aryl azides, and diazirines, with the associated photochemically generated reactive species being diradicals, nitrenes, and carbenes, respectively (Scheme 1.1).[99,103]

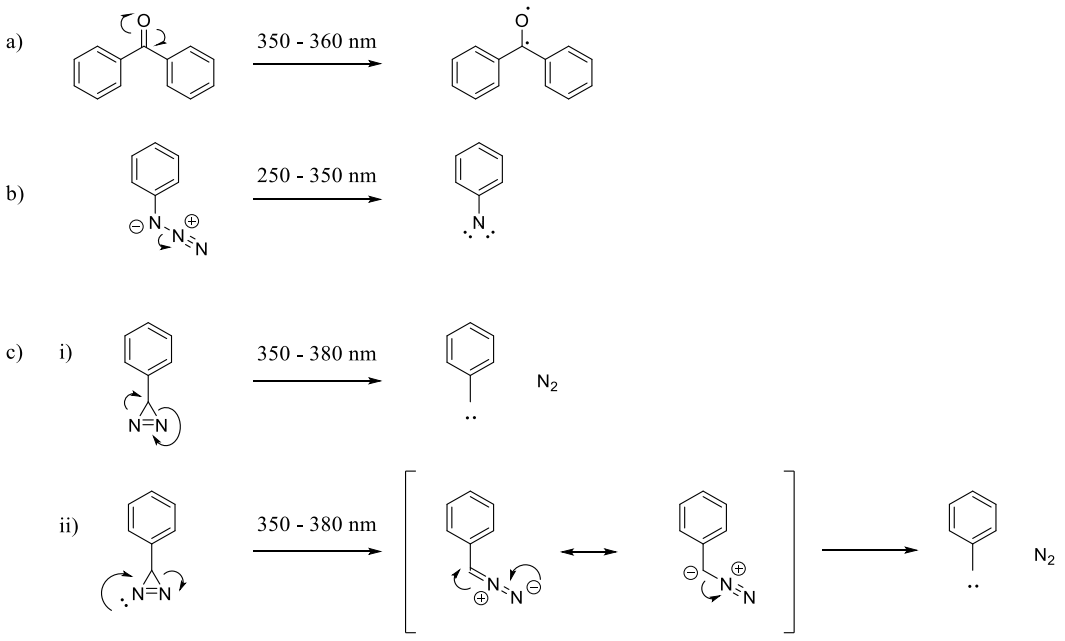

Scheme 1.1. a) Benzophenones form reactive diradicalson irradiation with light; b) Aryl azides form reactive nitrenes; c) Diazirines form reactive carbenes.

Benzophenones are a prominent photoreactive group in photoaffinity labelling research due to their inertness to solvents, facile preparation, and commercial

availability.[99,104] Benzophenones form a reactive diradical on UV irradiation with light of relatively long wavelength (350 – 360 nm), thus minimising the risk of damage to nearby biomolecules. The triplet diradical is known to be effective in hydrogen abstraction following a sequential abstraction-recombination mechanism, although this species can also undergo addition reactions or quenching with water (Scheme 1.2).[104] In addition, benzophenones are able to return to their ground state should they not covalently link with a nearby molecule, thus being available for activation in further photolysis. This multiple-activation characteristic often results in higher crosslinking yields to the intended protein targets when compared to alternative photoreactive groups, for which there is irreversible breakdown on UV irradiation.[105] However, the higher steric bulk of benzophenones and comparatively longer time periods of irradiation required can often lead to non-specific labelling.[99]

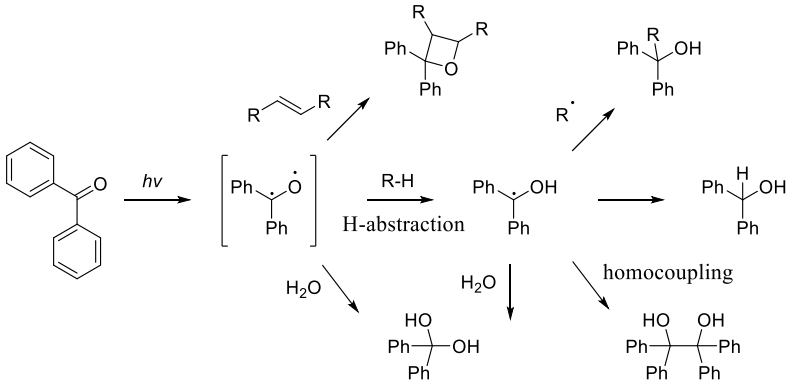

Scheme 1.2. Formation of a diradical from a benzophenone, and the subsequent possible abstraction and addition mechanisms.[106]

Aryl azides are also a commonly used photoreactive group in photoaffinity probes, and are preferred over their alkyl azide counterparts due to their increased stability and superior photophysical properties.[99,104,107] For example, a bis-azide-tagged chemical probe allows selective activation of an aryl azide under light irradiation, leaving a benzyl azide intact and available for further chemical transformations.[108] Aryl azides are useful photoreactive agents due to their ease of synthesis and commercial availability. The azide moiety itself is small, and can therefore be easily incorporated into aryl-containing molecules with minimal additional steric bulk. However, susbtituents *ortho*- to the azide group are generally avoided due to potential intramolecular cyclisations on photolysis, thus limiting this approach to PAL probe

design.[99] The relatively short wavelengths (250 – 350 nm) required to activate azides to give their nitrene derivatives can damage nearby biomolecules, which often absorb in the 200 – 280 nm region. An excess in absorption of light by proteins can lead to degradative chemical transformations and a subsequent reduction in efficient target labelling. Nitrenes generated from azides are able to insert non-specifically into C-H and N-H bonds, or undergo addition reactions with double bonds.[105] However, in comparison to carbenes, nitrenes exhibit lower reactivity, and can also undergo rearrangements to form undesired side products such as azirines and ketenimines, and even amines as a result of reduction by thiols (Scheme 1.3).[99,109,110]

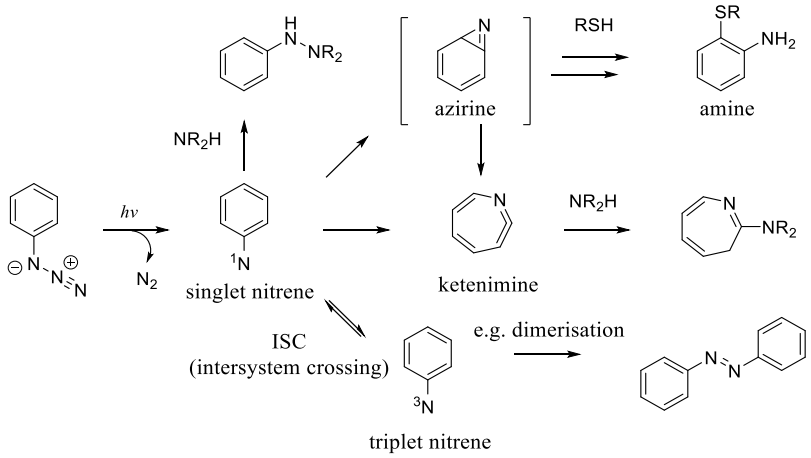

Scheme 1.3. Formation of a nitrene from phenyl azide and the subsequent possible bond insertion and rearrangement mechanisms.[109,110]

Similarly to aryl azides, diazirines decompose to highly reactive intermediates (in this case, carbenes) on irradiation with UV light, with loss of nitrogen and subsequent rapid insertion into nearby C-H, N-H, S-H or O-H bonds (Scheme 1.4). They require a high wavelength for activation (350 – 380 nm), resulting in minimal damage to biomolecules. The carbene formed is highly reactive, with a short half-life, allowing for rapid cross-linking and minimal non-specific binding. However, this high reactivity comes with associated risks such as rapid quenching by water resulting in reduced cross-linking yields.[99] Diazirines have generally superceded aryl azides as the preferred photoreactive reagent as a result of their high stability towards temperature, nucleophiles, acidic and basic conditions, and oxidising and reducing agents, as well

as their small size contributing minimal steric bulk, which can impact the overall properties of the probe compound.[103]

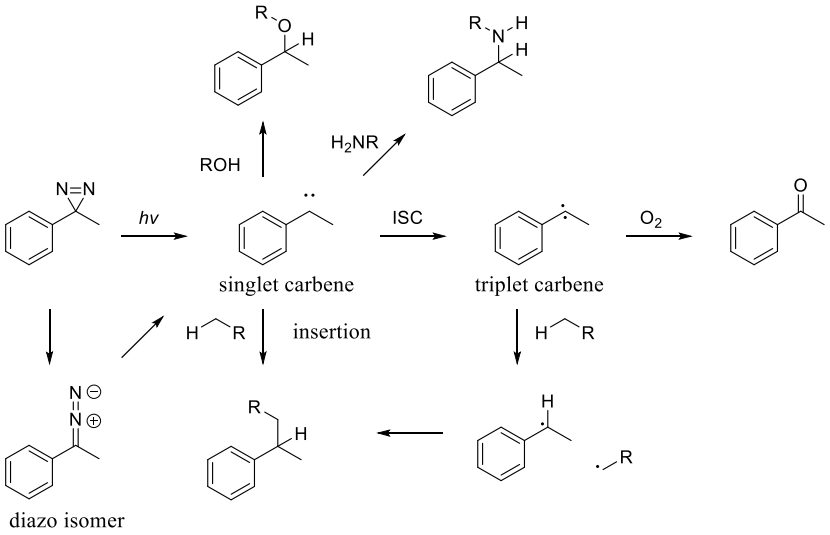

Scheme 1.4. Formation of a carbene from an aryl diazirine and subsequent possible bond insertion mechanisms.[99]

Diazirines can be classified as either aryl or alkyl diazirines, depending on whether the diazirine functional group is directly attached to an aromatic ring or an aliphatic chain, respectively.[103] Aryl diazirines exhibit superior photophysical properties compared with their alkyl relatives, with higher yields of carbene formation and increased stability.[103,111] Aryl diazirines are also less likely to undergo rapid isomerisation on irradiation of UV light into the corresponding diazo isomers.[103] The resulting diazo isomers have much longer lifetimes than carbenes, and can diffuse from the initial site of generation and contribute to non-specific binding.[111] In addition, the diazo compound generated is highly sensitive to protonation and subsequent attack by nucleophilic amino acid residues.[112] In attempts to overcome these issues, it has been reported that the introduction of a trifluoromethyl group adjacent to a diazirine has profound effects (Figure 1.26).[112]

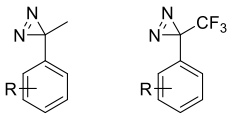

Figure 1.26. Chemical structures of methylphenyl diazirine and the trifluoromethyl relative.

The electron-withdrawing nature of the trifluoromethyl group stabilises the undesired diazo isomer to such an effect that it can be considered unreactive under physiological conditions, thus reducing the amount of non-specific crosslinking.[113] The presence of adjacent C-F bonds in the place of C-H bonds also reduces the tendency of the generated carbene to undergo 1,2-hydrogen shift rearrangements.[114] Despite the strong advantages of aryl diazirines over alkyl diazirines, alkyl diazirines are often the preferred choice due to their extremely compact size, which enables accommodation within the binding site of target proteins, as well as minimises changes in physicochemical properties.[103,114]

The functional handle (e.g. alkyne, azide, or TCO) in a PAL probe facilitates the introduction of a reporter tag (e.g. biotin) for purification. Alternatively, this reporter tag can be incorporated directly into the synthesised probe, although this has been known to significantly reduce bioactivities due to poor cell permeabilities, especially in the use of biotin.[107] Azides and alkynes are popular functional handles due to their small size and bioorthogonality.[115] Reporter tags can be introduced *via* copper-catalysed azide-alkyne cycloaddition (CuAAC) reactions. However, the cytotoxicity issues of copper means this method is not compatible with live cells.[107,116] TCO handles provide a solution to this, and can undergo rapid, strain-promoted, inverse electron demand Diels-Alder (iEDDA) reactions with tetrazine derivatives under copper-free conditions, making them suitable for use in PAL experiments using whole cells (Scheme 1.5).[107,115,117] The release of strain energy to facilitate chemical reactions is a fundamental method for the enhancement of reaction rate, and the *trans*-cyclooctene moiety reacts with a rate ten million times faster than the corresponding *cis* isomer, as a result of the additional strain that the *trans* alkene introduces into the cyclooctene ring.[118–121]

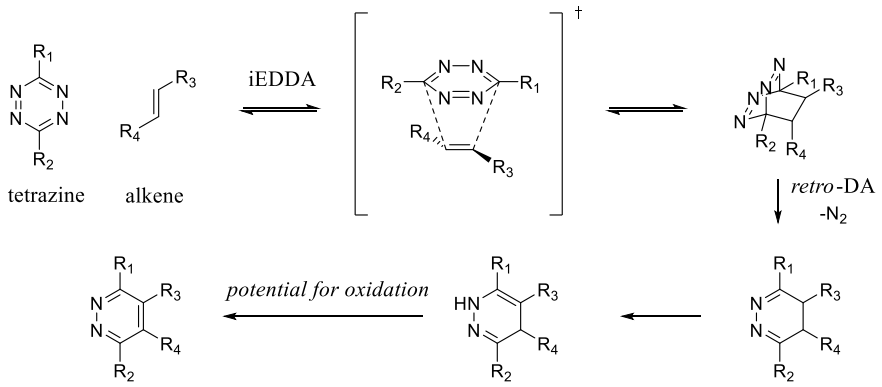

Scheme 1.5. Inverse-electron demand Diels-Alder (iEDDA) reaction between tetrazine and trans-cyclooctene. The iEDDA occurs followed by a retro-Diels Alder (DA) to lose nitrogen and afford a 4,5-dihydropyridazine. A subsequent 1,3-prototopic isomerisation leads to the 1,4-dihydro-isomer, a process which has been confirmed by ^{1}H-NMR. Oxidation to the pyridazine compound may then occur depending on the presence of oxidation conditions.[116]

Photoaffinity probes have been successfully implemented in target identification studies for multiple different cell types and extracts across multiple disease areas.[99] For example, studies have been carried out using PAL techniques in mitochondrial extracts to identify targets for diabetes treatments,[122] as well as in different cancer cells such as those of colon cancer,[123] and liver cancer.[124] However, there exists a limited selection of photoaffinity labelling experiments for target identification in antimalarial drug discovery.

The first and, to the best of our knowledge, the only published report describing photoaffinity capture of a transmembrane protein-drug interaction in live and intact malaria parasites successfully identified the *P. falciparum* Multidrug Resistance Protein 1 (*Pf*MDR1) as a target protein of a novel antimalarial chemotype (Figure 1.27).[125]

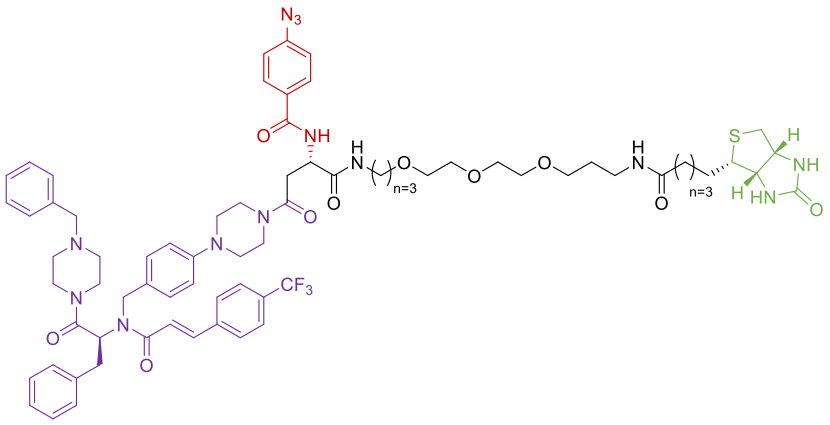

Figure 1.27. Photoaffinity probe, ACT-460953, based on the potent class of antimalarial compound represented in purple, with aryl azide photoreactive group in red and biotin functional handle in green.[125]

The authors ensured that the probe compound, ACT-460953, retained the biological characteristics of the parent molecule in terms of high potency against all asexual intraerythrocytic stages of the *P. falciparum* parasite. Incubation with blood stage parasite cultures and irradiation, followed by pull down experiments and mass spectrometry analysis identified *Pf*MDR1 as the primary target of this nascent series of antimalarials.

Despite this successful example of photoaffinity labelling for antimalarial target identification, to the best of our knowledge there are only a further 6 literature studies dedicated to the elucidation of modes of actions of antimalarials using photoaffinity probes.[126–131] Therefore PAL has yet to become commonplace in this area of drug discovery, despite its considerable advantages over other techniques, such as affinity based methods.[132]

1.7 The Identification of a Series of Antimalarial Quinazolinamines with a Novel Mode of Action

GlaxoSmithKline (GSK) carries out research and development at a site in Tres Cantos, Spain, that is dedicated to finding cures for diseases associated with the developing world such as chagas disease, tuburculosis, and malaria. The centre aims to find treatments for neglected tropical diseases that disproportionally affect those living in poverty, and aims

to do this by bringing together scientists and researchers into Public Private Partnerships that fund or co-fund coordinated drug discovery projects.

As an attempt to identify novel chemical starting points for new antimalarial drugs, colleagues at GSK Tres Cantos performed a high-throughput, phenotypic screen of 1,986,056 compounds from GSK's screening collection in order to test for inhibition of the intraerythrocytic cycle of *P. falciparum* (using the 3D7 strain of the *P. falc* parasite).[133] This screen identified a class of quinazolinamines as having a robust antimalarial profile, with follow up experiments indicating a novel mode of action not associated with any other known antimalarials. Prominence was given to this series as a result of these qualities, due to the opportunity to overcome pre-existing resistance mechanisms.

Quinazolinamine (**1**) was identified as the hit compound, with high whole cell activity (Pf_{3D7} IC_{50} of 0.06 μM) and ligand efficiency (LE of 0.41). The ligand efficiency (LE) is a measure of the potency of a drug per non-hydrogen atom it consists of, given by the equation:

$$LE = \frac{\Delta G}{N} = \frac{-RTln(K_d)}{N} = \frac{1.37 \times pIC_{50}}{N}$$

Where ΔG is the Gibbs free energy of binding, N is the heavy atom count (number of non-hydrogen atoms in the molecule), R is the gas constant, T is the temperature, and K_d is the kinetic dissociation constant. An LE value of 0.3 $kcalmol^{-1}$/heavy atom is considered a reasonable level of efficiency and is the target in many lead optimisation studies.[134] Although quinazolinamine (**1**) had the desired high potency and LE, its physicochemical and safety profile was sub-optimal (Table 1.3). Initial hit-to-lead efforts for the antimalarial quinazolinamine series were concentrated on maintaining potency whilst decreasing the undesirable hERG inhibition (corresponding to increased risk of cardiac arrhythmia),[135,136] and improving physicochemical properties through reducing lipophilicity. Lipophilicity is a property that has profound effects on absorption, distribution, metabolism, and excretion (ADME) of the compound in question.[137] The Property Forecast Index (PFI) is a lipophilicity measure that combines chromatographically determined lipophilicity and the number of aromatic rings within a molecule.[138] A PFI value of less than 7 is considered desirable for novel drugs due

to an associated reduction in attrition in clinical trials. For quinazolinamine (**1**), the PFI was an undesirable 7.9. After some limited SAR studies, quinazolinamine (**2**) was identified as a potential lead molecule with satisfactory *in vitro* and *in vivo* potency (Pf_{3D7} IC_{50} of 0.40 µM), a scalable synthesis, no ADME liabilities identified, and improved physicochemical properties (a PFI of 7.1) (Table 1.2). SAR studies are ongoing elsewhere in our laboratories to find further improvements for human ether-a-go-go-related gene (hERG) off-target activity, to enhance potency, and to tune the physicochemical properties.[139]

	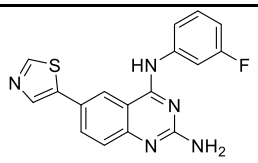	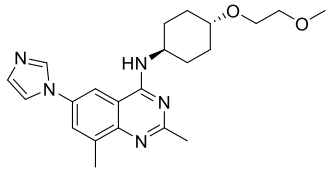
Number	**1**	**2**
Pf_{3D7} IC_{50} (µM)	0.06	0.40
pIC_{50}	7.2	6.4
LE	0.41	0.30
PFI	7.9	7.1
hERG pIC_{50}	5.5	5.1

Table 1.3. Potency and physicochemical properties of hit (1) and lead (2).

Due to interest in the novel mode of action of this antimalarial quinazolinamine series, a number of previous studies carried out at Tres Cantos used specific drug resistant *P. falciparum* strains to determine whether the quinazolinamine series inhibited a number of known protein targets and pathways. These included the bc_1 complex (as per atovaquone), *P. falciparum* P-type cation translocating ATPase '*Pf*ATP4' (implicated in Na^+ ion transport systems and proving a promising target in early drug discovery),[140] dihyrdoorotate dehyrdogenase (DHODH, an enzyme indirectly affected by the inhibition of the bc_1 complex by atovaquone),[141] the folate biosynthetic pathway (as per the sulfadoxine-pyrimethamine combination), and *Pf*PI4K (as per MMV390048).

Potency of the quinazolinamine series was retained against each of these strains, indicating that the mode of action of these quinazolinamines was not related to inhibition of any of these pathways.[142–144] Of note was the finding that the

quinazolinamines are inhibitors of the heme polymerisation process *in vitro*, with an IC_{50} similar to that of chloroquine, a known β-haematin inhibitor.[145,146] However, the quinazolinamines maintained their potency when tested against chloroquine-resistance strains (W2, V1/S, and Dd2), suggesting their mode of action may also involve alternative *Plasmodium* targets.[147] In further investigations, a representative selection of 8 quinazolinamines were tested in a *P. falciparum* kinobead assay at Cellzome to screen for inhibition of malarial kinases present in *P. falciparum* lysates. Results indicated that the quinazolinamines did not target any kinases in these extracts. When the quinazolinamines were screened in a further kinobead assay against 272 human protein kinases, none were inhibited significantly, thereby providing confidence of a potentially non-toxic drug profile.

Since the publication of the initial antimalarial quinazolinamine hit,[133] there has been some speculation in the literature as to the mechanism of action of these compounds. Researchers have noted that the quinazolinamine, BIX01294, is a potent human histone lysine methyltransferase (HKMT) inhibitor (Figure 1.28). These enzymes are vital in epigenetic regulation, due to their role of transfering methyl groups onto histones.[148] Due to the sequence homology of the human HKMT and the *P. falciparum* HKMT, and the SAR that tracks from the human inhibition to the *Pf*HKMT inhibition for this quinazolinamine series, the authors suggest that the quinazolinamine scaffold may also be targeting this enzyme in *Plasmodium* parasites.[148–150] This is experimentally demonstrated by reduced *P. falciparum* histone lysine methylation in a dose dependent manner on treatment with the compound BIX01294. However, this still remains a hypothesis, with a lack of unambiguous evidence of this targeted inhibition.

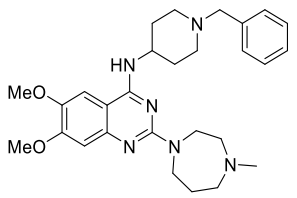

BIX01294

Figure 1.28. Structure of BIX01294, a human HKMT inhibitor that also shows antimalarial properties.

Another literature report has attempted the photoaffinity-based capture of target proteins of this diaminoquinazoline series by designing and using a probe based on the BIX01294 structure (Figure 1.29), with the diazirine moiety used as the photoreactive group.[128]

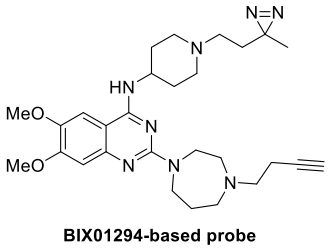

Figure 1.29. The photoaffinity probe designed and used in the literature based on antimalarial diaminoquinazoline, BIX01294.[128]

In this study, 205 proteins were captured and identified by the probe from *Plasmodium falciparum* lysates, of which 104 were significantly enriched by the probe in comparison to a DMSO control. Of these, a number were identified as essential for parasite survival, however none of the previously highlighted *Pf*HKMT proteins were identified as potential targets. The authors suggest either that the lysates used in their study may be inappropriate for identification of *Pf*HKMT targets, or that these enzymes are not in fact the major targets of the diaminoquinazoline series.

The use of lysates in these literature experiments reduces the number of proteins available for capture in their natural conformational state when compared to whole cell samples, thus limiting this approach to true target identification. Limitations of this study also include the lack of competition experiments or use of an inactive control compound to provide a more stringent differentiation between background captured proteins and those of significance. The authors recognise that the series may be exhibiting polypharmacology, similar to the previously discussed established antimalarial, artemisinin, and that further work is required to interrogate the true target proteins of the antimalarial quinazoline series.[128]

As previously highlighted in **Section 1.6.2 – Target-Based *versus* Phenotypic Screening**, understanding the mode of action of novel antimalarial drugs can provide invaluable information to help understand resistance profiles and mechanisms, as well

as provide useful information for the optimisation of medicinal chemistry programmes. As a result, and due to the limited literature discussion surrounding the topic, there is a desire to further understand the mode of action of these emerging antimalarial quinazolinamines.

1.8 Project Aims

This research uses the opportunity to design, implement, and leverage modern chemoproteomic techniques at GSK, as outlined in **Section 1.6.4 – Chemoproteomic Techniques for Target Identification**, to determine the cognate target proteins of the novel antimalarial quinazolinamine series represented by parent compound (**2**) (Figure 1.30). Methods will improve on those reported in the literature by using whole cells where possible, and carrying out stringent competition experiments in order to differentiate between targets of significance and proteins captured due to non-specific binding. Information regarding the mechanism of action of this series is anticipated to contribute to the pressing need for mechanistic understanding of antimalarial compounds, and thus facilitate the discovery of new malaria medicines. Although strong collaborations exist between medicinal chemists and biologists working in malaria drug discovery in our laboratories, it is seen as beneficial to further strengthen these ties through the development of chemoproteomic techniques, in which extensive knowledge coupled with practical skill in areas of both chemistry and biology can be exploited and the two fields can be even better integrated for the advancement of malaria drug discovery.

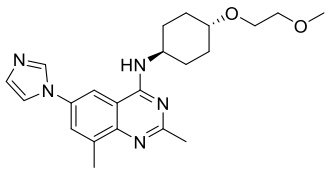

2

Figure 1.30. Antimalarial quinazolinamine (2), representing the quinazolinamine series for which target identification studies are described in this thesis.

This will be addressed *via* the aims and methods outlined below:

1. Design and synthesise appropriate chemical probes with suitable biological properties for use in affinity-based immobilised bead assays for the affinity-capture of protein targets in *P. falciparum* lysates. Should the results obtained from these experiments be inconclusive, proceed to aim 2).
2. Design and synthesise appropriate photoaffinity probes with suitable biological properties for use in photoaffinity labelling experiments for the covalent capture of protein targets in live *P. falciparum* parasites.
3. Establish a new photoaffinity labelling assay and assess the workflow and parameters in order to determine the future applicability of this chemoproteomic platform in our laboratories.
4. Provide a comprehensive account of protein targets captured for the quinazolinamine series in order to contribute valuable scientific knowledge and understanding of the novel mechanism of action exhibited by parent compound (**2**).

Taken as a whole, the objectives outlined here will not only provide specific insight into the emerging antimalarial quinazolinamine series, but will also potentially enable a new workflow for chemoproteomic approaches in the antimalarial therapy area in our laboratories.

Chapter 2 – Results and Discussion: The Immobilised Bead Assay for Target Identification of Novel Quinazolinamine Antimalarial Compounds

2.1 The Design and Synthesis of Appropriate Quinazolinamine Chemical Probes for Use in Immobilised Bead Assays

The design of appropriate chemical probes for use in immobilised bead assays must take into account the identity of the functional handle, the length and chemical properties of any linkers used, and the vector at which these groups preside. In the case of the quinazolinamine series, an alkyne functional handle was selected due to its high stability under the experimental conditions required to synthesise the compounds, and its fast and efficient reactivity in click reactions for immobilisation onto azide-derivatised beads, as previously discussed in **Section 1.6.4 – Chemoproteomic Techniques for Target Identification**.

An optimal substitution vector was initially unknown as a result of the lack of knowledge of the target protein and binding site of the series. Three different vectors were chosen for the design of three different chemical probes as a starting point for the development of an appropriate molecule for immobilised bead assays (Figure 2.1). These vectors were chosen based on limited SAR data that indicated changes in these regions could be tolerated. The pyrazole and imidazole group were seen to be interchangeable, as discussed in **Section 2.1.2 – The Chemical Strategy for the Synthesis of Chemical Probe (3)**.

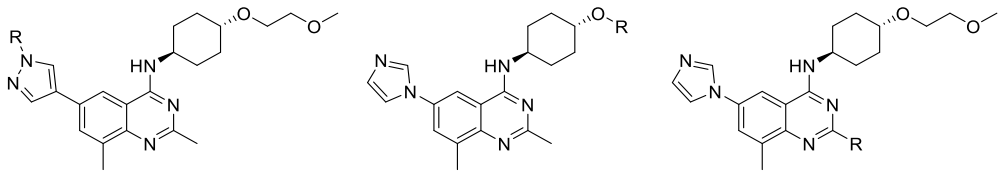

Figure 2.1. Target probe compounds based on lead compound (2), where R is the appropriate alkyne linker.

Although it was recognised that linker length can have a profound effect on the properties of a chemical probe, the ideal linker length was unknown at the outset of these studies.[151] Initially, a linker length of 6 atoms was selected, including the alkyne carbons. This was expected to be long enough to avoid major steric or electronic clashes in the binding pocket on reaction with the azido-derivatised bead, whilst still being short enough so as to minimise the changes in physicochemical properties of the drug, which could affect off-target binding. A linker length of 6 atoms also enables the use of a PEG chain consisting of 1 ether linking unit. Both PEG and alkyl linkers were deemed appropriate for attachment of this alkyne functional handle to the quinazolinamine core due to their ubiquitous use as linkers in chemoproteomic techniques.[152] However, a PEG chain was considered the superior linker due to its high solubility in aqueous media, facilitated by hydrogen bond formation between the polymer oxygens and water molecules.[153] This reduces the increase in lipophilicity on addition of the linker to compound (**2**) when compared to the equivalent alkyl chain. This comparison is demonstrated in Table 2.1, taking into account the experimental PFI of parent compound (**2**) as 7.1 (see **Section 1.7 – The Identification of a Series of Antimalarial Quinazolinamines with a Novel Mode of Action**). Minimising the change in physicochemical properties on the derivatisation of the parent compound (**2**) was envisaged to reduce non-specific binding during the affinity-based assay.

Number	Probe Design	Calculated PFI
3	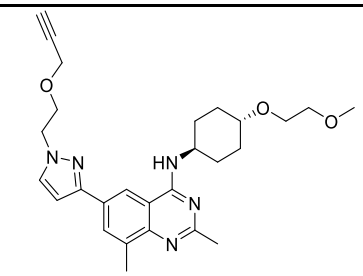	8.9 (experimental PFI = 8.0)
4	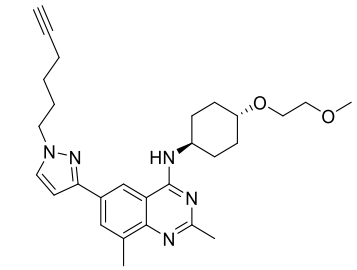	9.7
5	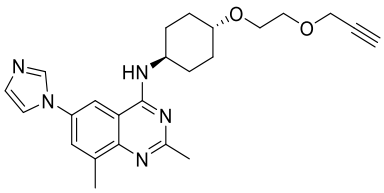	7.8
6	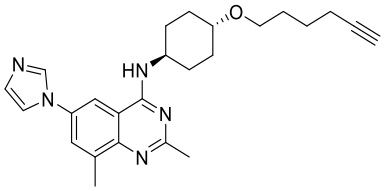	9.1
7	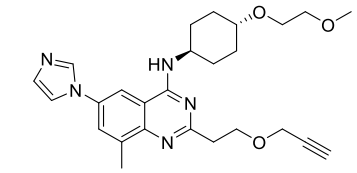	7.6
8	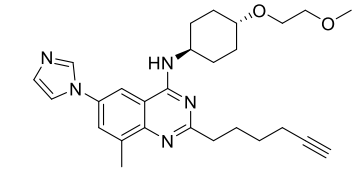	9.1

Table 2.1. A comparison of the lipophilicity, measured by calculated PFI, of probe compounds based on parent compound (2) with an incorporated PEG or alkyl linker. Use of PEG linkers is predicted to increase the lipophilicity of parent (2) (PFI = 7.1) by a reduced amount compared to addition of an alkyl linker.

It was recognised in this design stage that alternative chain compositions, as well as lengths, or vectors may be necessary if potency or synthetic tractability was found to be suboptimal, and this possibility was to be addressed if and when these issues were

faced. Indeed, it was expected that addition of the alkyne linker at at least one vector would result in a steric or electronic clash and thus a reduction in potency. Along with these initial chemical probes, the lead compound (**2**) was synthesised for use as the competitor in the relevant immobilised bead experiments.

2.1.1 Synthesis of Lead Compound (2) for Use as a Competitor

As stated above, lead compound (**2**) was synthesised for use as the competitor in both immobilised bead and photoaffinity labelling experiments, in order to allow the observation of a dose-dependent reduction in binding to the target protein(s) and thus to differentiate between background and proteins of significance (Scheme 2.1).

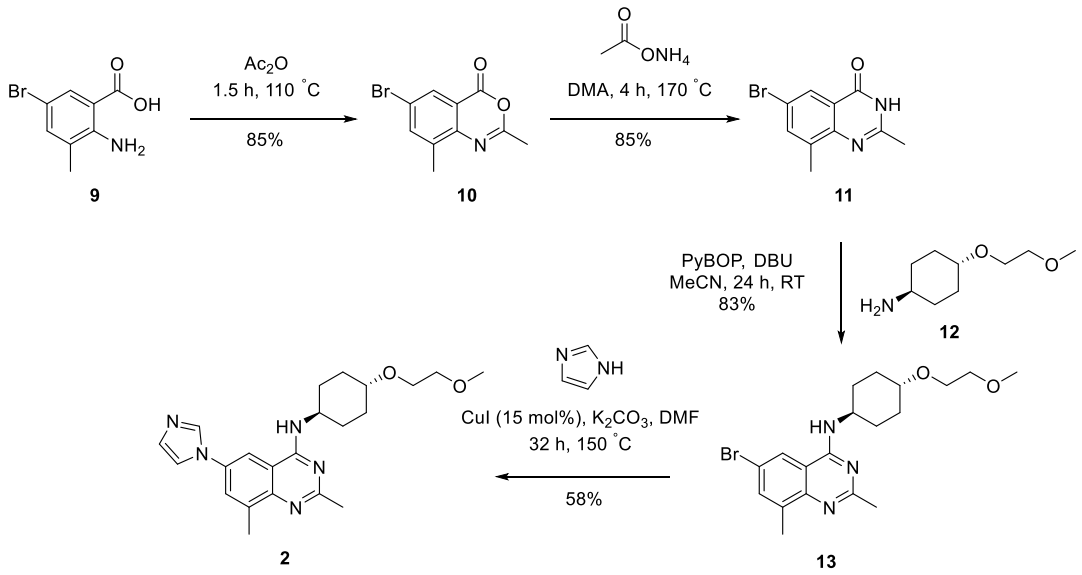

Scheme 2.1 Synthetic route towards competitor compound (2).

The quinazolinamine core was constructed by initial cyclisation of commercially available bromoaminobenzoic acid (**9**) with neat acetic anhydride followed by reaction with ammonium acetate to give quinazolinone (**11**). Both steps proceeded in the high yield of 85%, without the need for chromatographic purification. PyBOP-mediated coupling with amine (**12**) afforded the quinazolinamine (**13**) in 83% yield.[154] Final Ullmann coupling with imidazole was carried out to afford the competitor compound (**2**) in an acceptable 58% yield, and in a 35% overall yield over the 4 synthetic steps.

The requisite cyclohexylamine derivative (**12**) was accessed by a three step synthesis, using a protecting group strategy (Scheme 2.2).

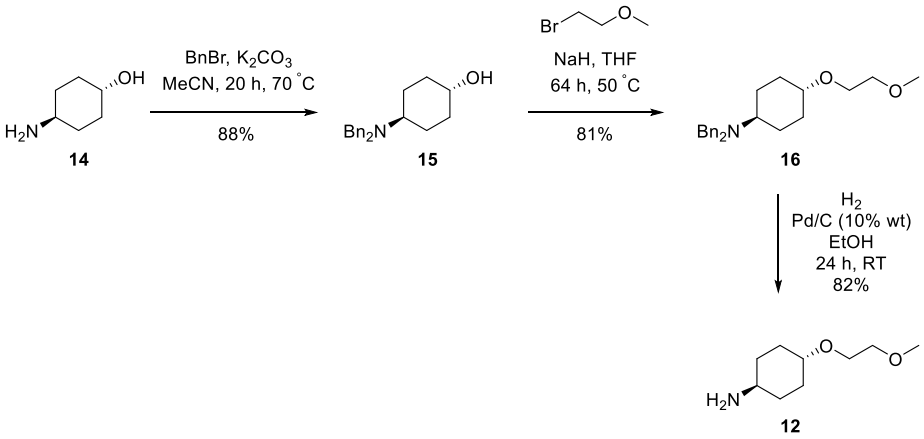

Scheme 2.2. Synthesis of cyclohexanamine intermediate (12).

The mesomer, *trans*-aminocyclohexanol (**14**), was dibenzyl protected to afford intermediate (**15**) in 88% yield. The free alcohol in intermediate (**15**) was then alkylated using 1-bromo-2-methoxyethane to afford intermediate (**16**), which was subsequently benzyl-deprotected through hydrogenation over palladium on carbon to afford target amine (**12**) in 82% yield. The final fragment (**12**) was accessed in a satisfactory 57% yield over three steps, with the synthesis being easily executed on large scale (~ 10 g) to provide a suitable batch of compound for use in the syntheses of multiple target chemical probes, described in the coming sections.

2.1.2 The Chemical Strategy for Synthesis of Chemical Probe (3)

It was envisaged that the synthetic method for accessing competitor compound (**2**) could be used as a basis to which appropriate alterations could allow access to each target chemical probe. Desirable characteristics of the initial synthetic strategy for the synthesis of chemical probes for use in the immobilised bead assay included utilising as few steps as possible, convergency, and yields high enough to afford at least 20 mg of final compound.

Quinazolinamine chemical probe (**3**) was the first compound targeted for synthesis with the incorporation of a PEG linker on the pyrazole fragment (Figure 2.2). In order

for this alkylation to be synthetically tractable, a pyrazole fragment at the C-6 position was used in place of the imidazole present in the lead compound (first mentioned in **Section 2.1 – The Design and Synthesis of Appropriate Quinazolinamine Chemical Probes for Use in Immobilised Bead Assays**). The precursor pyrazole compound (**17**) was assessed for potency in the *P. falciparum* whole cell assay before it was alkylated. Pleasingly, potency was essentially retained on replacing the imidazole with the pyrazole fragment, and thus it was deemed a suitable isostere.

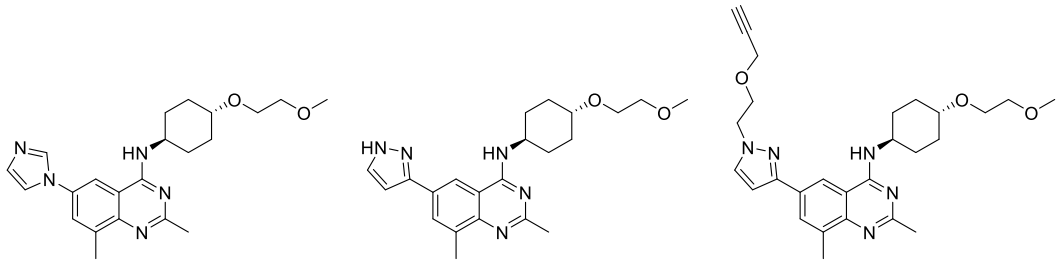

Figure 2.2. A comparison of competitor compound (2), the pyrazole relative (17), and the target chemical probe (3).

In order to design convergency into the synthesis of target probe (**3**), initial ideas focussed on central disconnections to allow the construction of the molecule from large fragments (Scheme 2.3).

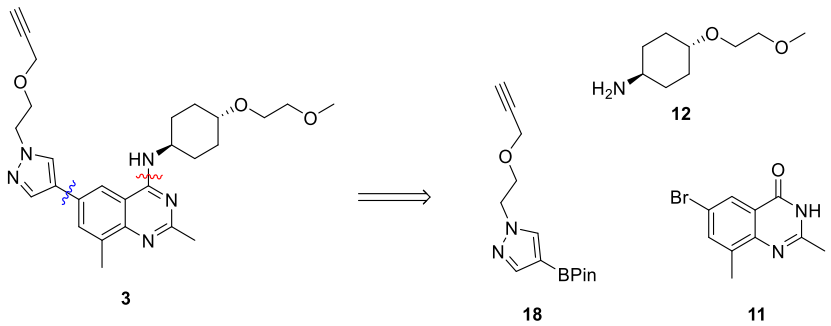

Scheme 2.3. Initial disconnection strategy for the synthesis of chemical probe (3).

The forward synthetic route was envisaged to follow the 4 step synthesis demonstrated in Scheme 2.4, with convergency incorporated *via* the separate synthesis of fragments (**12**) and (**18**).

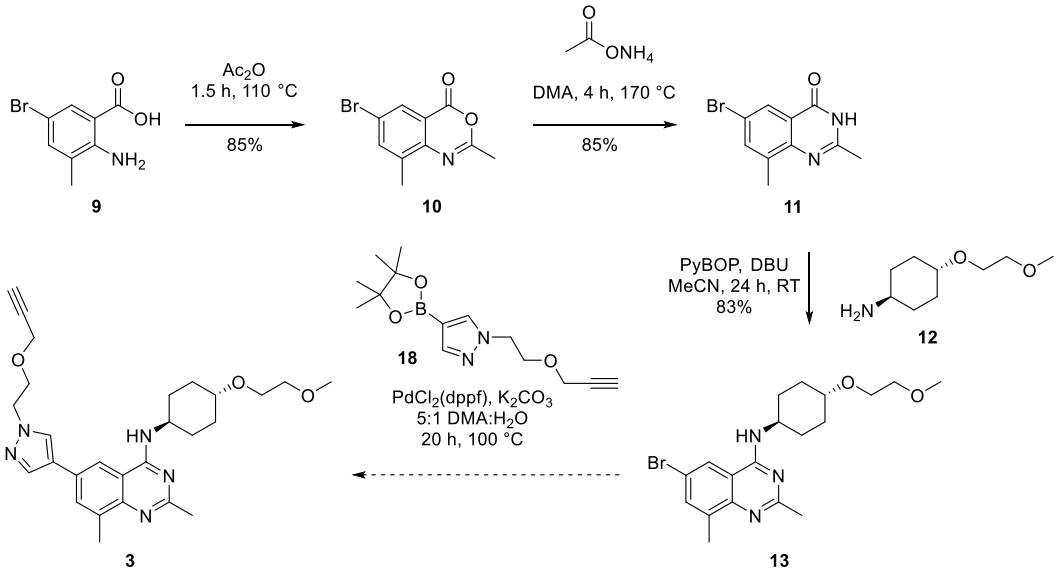

Scheme 2.4. Convergent synthetic route towards target chemical probe (3).

Amine (**12**) and quinazolinone (**11**) were synthesised as described in **Section 2.1.1 – Synthesis of Lead Compound (2) for Use as a Competitor**. Attempts at synthesising the fragment (**18**) involved the alkylation of pyrazole (**19**) (Scheme 2.5).

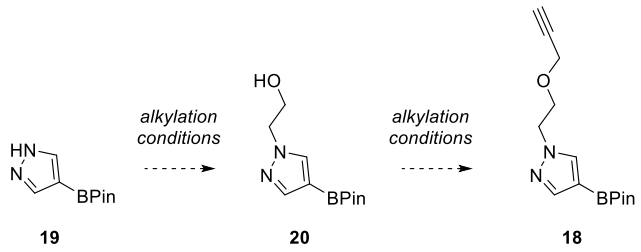

Scheme 2.5. Proposed synthesis for pyrazole fragment (18).

The initial alkylation of pyrazole (**19**) was attempted using chloroethanol and Cs_2CO_3 in DMF, and heating to 170 °C in order to facilitate the desired S_N2 reaction. However, after 18 h, no conversion to product was observed by LCMS analysis, with only small conversion to the boronic acid seen. In order to address this, further evaluation of the literature yielded alternative conditions which were each tested and analysed by LCMS (Table 2.2).

19 **20**

Entry	Reagents and Conditions	Outcome (determined by LCMS analysis)
1	Pyrazole (**19**) (1 eq.), chloroethanol (1.1 eq), Cs_2CO_3 (1 eq.), 170 °C, DMF, 18 h	No reaction
2	Pyrazole (**19**) (1 eq.), chloroethanol (1.1 eq), 1 M in THF NaHMDS (1 eq.), 100 °C, THF, 22 h[155]	12% product
3	Pyrazole (**19**) (1 eq.), chloroethanol (1.1 eq), Cs_2CO_3 (1 eq.), 100 °C, DMSO, 22 h[156]	23% product
4	Pyrazole (**19**) (1 eq.), chloroethanol (1.1 eq), NaO^{t}Bu (1 eq.), 100 °C, DMF, 22 h[157]	27% product
5	Pyrazole (**19**) (1 eq.), chloroethanol (1.1 eq), NaO^{t}Bu (1.5 eq.), 120 °C, DMF, 1 h	15% product
6	Pyrazole (**19**) (1 eq.), chloroethanol (10 eq), NaO^{t}Bu (1.5 eq.), 120 °C, DMF, 8 h	35% product
7	Pyrazole (**19**) (1 eq.), bromoethanol (10 eq), NaO^{t}Bu (1.5 eq.), 120 °C, DMF, 2 h	Degradation
8	Pyrazole (**19**) (1 eq.), bromoethanol (5 eq), NaO^{t}Bu (1.1 eq.), 100 °C, DMF, 5 h	32% product

Table 2.2. Conditions attempted for the alkylation of pyrazole (19), and reaction outcomes associated with each.

In Table 2.2, entries 2 – 4 indicate conditions used in literature examples for the alkylation of pyrazole fragments, which were adapted for alkylation of pyrazole (**19**) using chloroethanol.[155–157] Conversion to product, as observed by LCMS analysis, was low for each attempt. The highest percentage of conversion observed was 27% for conditions in entry 4. This was taken as a starting point for investigations into whether slight alterations could improve conversion yields. Increasing the stoichiometry of NaO^{t}Bu base from 1 eq. to 1.5 eq., and increasing the temperature to 120 °C from 100 °C, showed a slightly lower conversion of 15% when the reaction was carried out in a microwave for 1 h (entry 5). Attempting to improve conversion by increasing the number of equivalents of the chloroethanol electrophile from 1 eq. to 10 eq. and heating for 8 h showed only a slight improvement in conversion in comparison to

entries 4 and 5 (entry 6). Replacing chloroethanol with the more reactive bromoethanol showed complete degradation of the reaction mixture after only 2 h (entry 7). By reducing the stoichiometry of bromoethanol to 5 eq., and the temperature to 100 °C, 45% conversion to product and 34% remaining starting material was seen after 3 h of heating. However, after a further 2 h, significant degradation of the reaction mixture was observed, with only 32% product and 11% remaining starting material observed by LCMS (entry 8).

Following a reevaluation of the viability of this convergent route, it was decided that building fragment (**18**) using this method was unlikely to afford product in high yield. The attempts were abandoned as a result of promising results observed for a more linear synthesis in which the alkylated pyrazole fragment was built once the pyrazole group had been installed on the core (Scheme 2.6). Although this sacrificed the desirable convergent synthesis as first described in the disconnection strategy, the linear approach was considered practical in order to access chemical probe (**3**) in a timely manner.

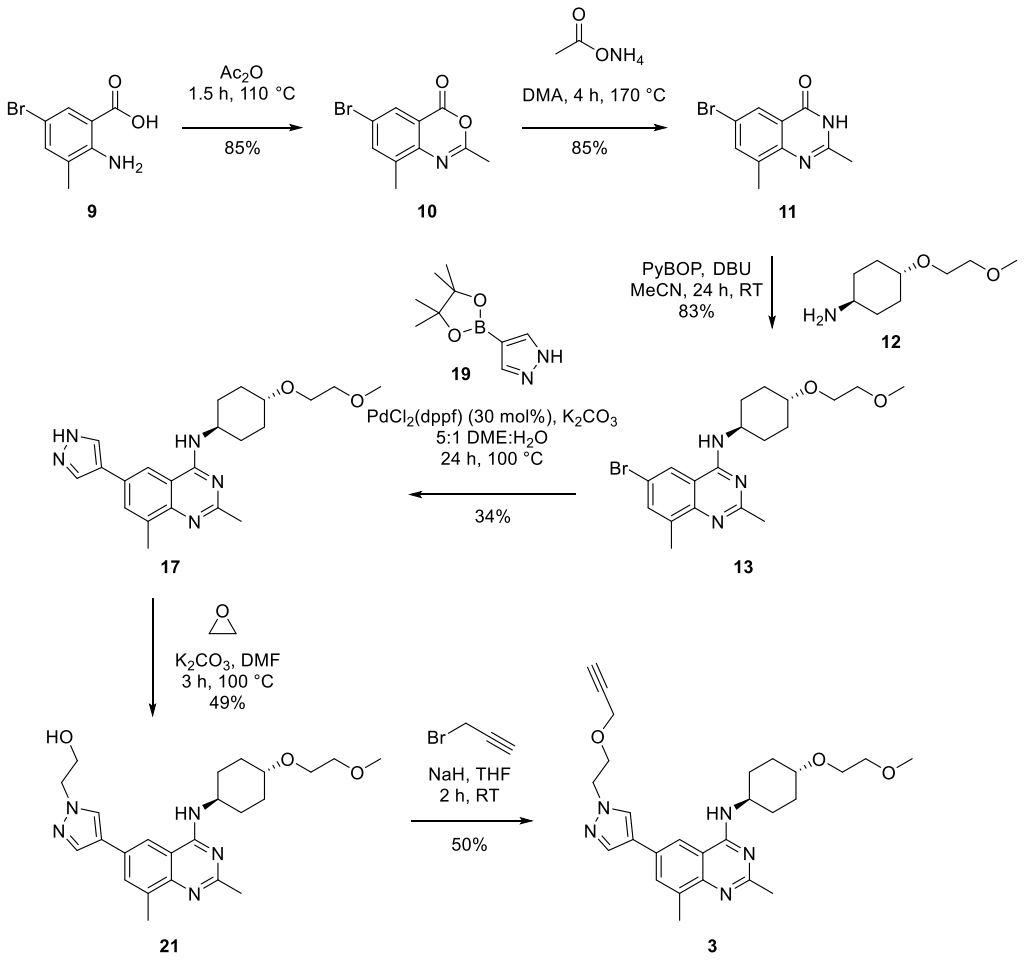

Scheme 2.6. Linear approach to the synthesis of chemical probe (3).

The initial 3 steps to access chemical probe (**3**) followed the same procedure as that for competitor compound (**2**). After PyBOP-mediated coupling of quinazolinone (**11**) and amine (**12**), intermediate (**13**) was coupled with pyrazole (**19**) using $PdCl_2$(dppf) and K_2CO_3 in a Suzuki-Miyaura coupling to afford (**17**) in a relatively low isolated yield of 34%. Due to the bespoke nature of the synthesis, optimisation of this step was not considered a priority at this stage. The free NH on the newly installed pyrazole in intermediate (**17**) was then successfully alkylated with ethylene oxide in the first step towards growing the linker chain off the quinazolinamine core, occuring in a 49% yield. The final alkylation step towards target probe (**3**) was performed using propargyl bromide and NaH at room temperature. These alkylation yields, although suboptimal, were considered acceptable considering the previously noted difficulties in the alkylation of pyrazole fragment (**19**). The final compound was isolated in a 50% yield,

affording 65 mg of the target probe (**3**) through a 6-step synthesis and with an overall yield of 5%. Despite the compromise taken in the convergency of the synthetic route, the final synthesis allowed access to a relatively high amount of compound when taking into account the quantity needed for immobilised bead experiments (1 − 5 mg being required).

2.1.3 The Chemical Strategy for Synthesis of Chemical Probe (34)

The initial target chemical probe (**5**) was designed to incorporate the desired alkyne functional handle at the C-4 position of the quinazolinamine core, with the PEG linker already included in the lead compound upon which the probe was designed (Figure 2.3).

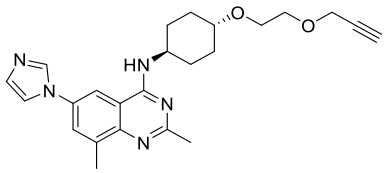

Figure 2.3. Target chemical probe (5) with alkyne functional handle protruding from the C-4 position of the quinazolinamine core.

With similar goals as described for the synthesis of chemical probe (**3**), the synthesis of desired chemical probe (**5**) was designed with convergency as demonstrated in the retrosynthetic analysis in Scheme 2.7.

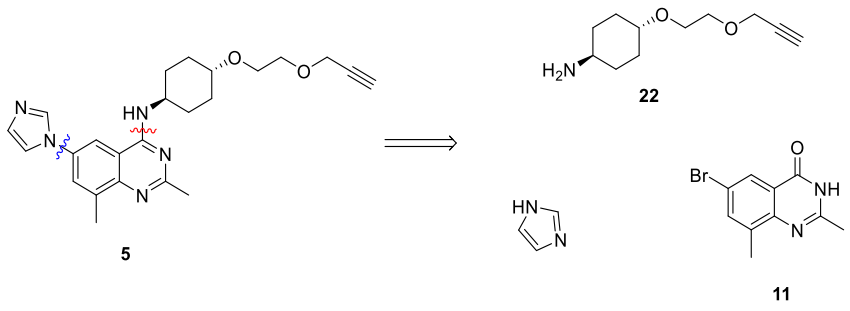

Scheme 2.7. Retrosynthetic analysis for the convergent synthesis of target chemical probe (5).

Fragment (**11**) was synthesised in 2 steps as described in **Section 2.1.1 – Synthesis of Lead Compound (2) for Use as a Competitor**. The preparation of amine (**22**) was therefore the final fragment required before the complete synthesis of chemical probe (**5**) could be executed. As per the synthesis of similar fragment (**12**) in **Section 2.1.1 – Synthesis of Lead Compound (2) for Use as a Competitor**, a protecting group strategy for the synthesis of fragment (**22**) was predicted to be suitable, albeit avoiding the benzyl protecting group. This was as a result of the newly incorporated alkyne in fragment (**22**) which was at risk of being hydrogenated under the traditional benzyl-deprotection conditions of hydrogen gas over palladium. The phthalimide amine protecting group was considered a suitable protecting group replacement in the synthesis of fragment (**22**) due to the ability to block both alkylation positions on the free amine of cyclohexylamine (**14**), and due to deprotection conditions that utilise hydrazine which, although toxic, would avoid the issues of hydrogenation of the alkyne. The synthesis of fragment (**22**) therefore followed the route as outlined in Scheme 2.8.

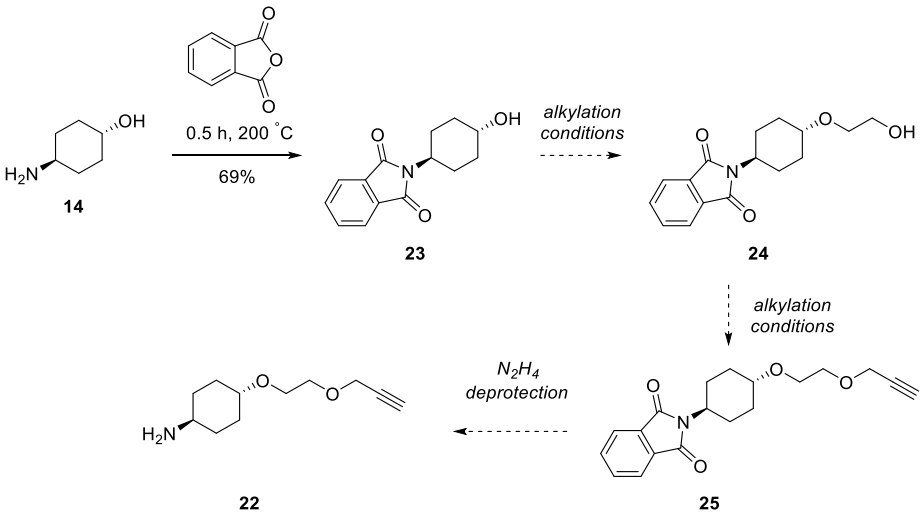

Scheme 2.8. Proposed synthetic route towards desired fragment (22) for use in the synthesis of target chemical probe (5).

Protection of cyclohexylamine (**14**) was successfully carried out with phthalic anhydride by heating to gentle boiling at 200 °C for 30 minutes, yielding desired protected amine (**23**) in a 69% yield following filtration after cooling.[158] In a first attempt for the subsequent alkylation of cyclohexanol (**23**), the same conditions for the

successful alkylation of the pyrazole fragment in compound (**17**) were tested (entry 1, Table 2.3). These conditions consisted of oxirane and K_2CO_3 in DMF at 100 °C. However, after 24 h of stirring at this temperature, no product was observed by LCMS analysis and significant starting material remained. This result indicated that the oxirane reagent was insufficiently electrophilic to facilitate the desired S_N2 reaction with the cyclohexanol fragment (**23**). In addition, the use of K_2CO_3 as a base was determined to be inadequate for facilitating the reaction by the *in situ* formation of the alkoxide species. As a result, further investigations into appropriate alkylation conditions were conducted (Table 2.3).

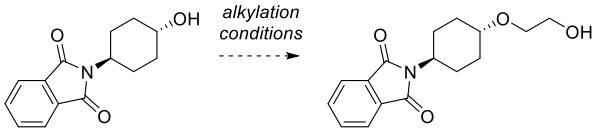

23 **24**

Entry	Reagents and Conditions	Outcome (determined by LCMS analysis)
1	2.5 M in THF oxirane, K_2CO_3, 100 °C, DMF, 24 h	No product
2	2.5 M in THF oxirane, 60% NaH in mineral oil, 100 °C, DMF, 24 h	No product
3	Bromoethanol, K_2CO_3, 100 °C, DMF, 24 h	No product
4	Bromoethanol, 60% NaH in mineral oil, 100 °C, DMF, 24 h	No product
5	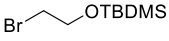 , 60% NaH in mineral oil, RT, DMF, 18 h	2% product
6	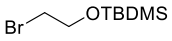 , 1 M in THF potassium bis(trimethylsilyl)amide, RT, THF, 18 h	8% product
7	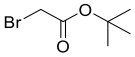 , 1 M in THF lithium bis(trimethylsilyl)amide, RT, THF, 18 h	Degradation
8	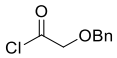 , triethylamine, DMAP, 0 °C, DCM, 6 h	No product

Table 2.3. Attempted reaction conditions for the alkylation of cyclohexanol fragment (23).

The use of NaH was investigated as a stronger base than K_2CO_3 in order to facilitate the reaction by the *in situ* formation of the alkoxide and therefore increase the nucleophilicity of cyclohexanol fragment (**23**) (entry 2). However, no product was

observed by LCMS analysis and significant starting material persisted. The use of bromoethanol as an alternative electrophile was examined under both K_2CO_3 and NaH conditions (entries 3 and 4) but again no product was observed. Using the stronger NaH base and *tert*-butyldimethylsilyl protected bromoethanol showed minimal conversion to product by LCMS after stirring for 18 h (entry 5). A slight variation of these conditions was achieved in a subsequent attempt by replacing the base with potassium bis(trimethylsilyl)amide, known for its use in the synthesis of poly(ethylene) oxide chains.[159] However, the quantity of product observed by LCMS only reached 8% under these conditions, with significant degradation of the reaction mixture also observed (entry 6). By using the highly electrophilic *tert*-butyl bromoacetate reagent and a similar lithium bis(trimethylsilyl)amide base, degradation was also observed and no product formation seen (entry 7). A final attempt at alkylation using the acid chloride in entry 8 also yielded no product despite stirring for 6 h. Despite the promising observation of a small quantity of product formation in entries 5 and 6, it was decided that full optimisation of this reaction was not time efficient, especially due to the high levels of degradation observed, often including evidence of phthalimide ring opening.

Considering the success of the synthesis for chemical probe (**3**) described in **Section 2.1.2 – The Chemical Strategy for Synthesis of Chemical Probe (3)** despite the sacrifice in convergency, a similar approach was attempted for the synthesis of target chemical probe (**5**). This entailed the attempted alkylation of the cyclohexyl fragment in compound (**26**) after installation on the quinazolinone core (Scheme 2.9).

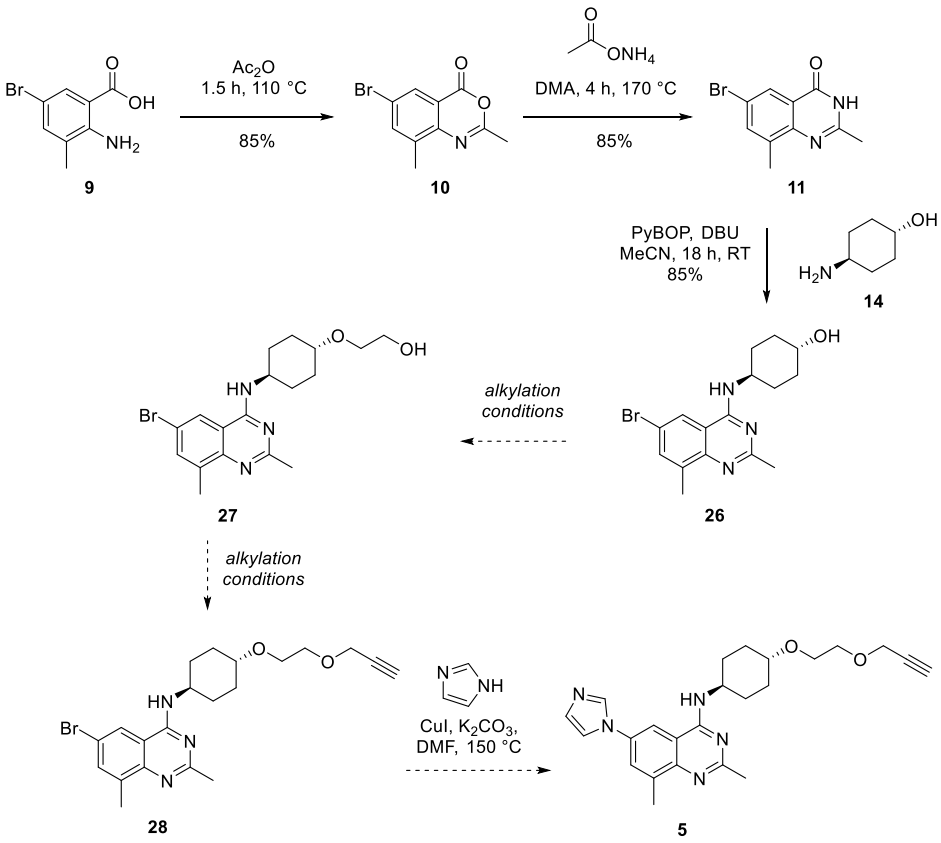

Scheme 2.9. Alternative synthesis of target chemical probe (5) in which alkylation of the cycohexanol fragment occurs in a linear fashion.

Again, it was envisaged that this route could yield final product in a timely manner and overcome issues of phthalimide ring opening as observed in alkylation attempts of the phthalimide protected fragment (**23**). However, alkylation attempts using electrophilic partners of oxirane and bromoethanol with alcohol (**26**) showed similar results to those previously observed. Similar persistance of starting material was observed by LCMS analysis, and alkylation attempts of intermediate (**26**) were abandoned whilst a reevaluation of the synthetic route to access chemical probe (**5**) was carried out.

On additional mining of the available SAR data for the quinazolinamine series,[160] it was observed that an amide linker on the cyclohexane moiety at the C-4 position is tolerated in compound (**29**), which had an IC_{50} value of 0.06 µM (Figure 2.4).

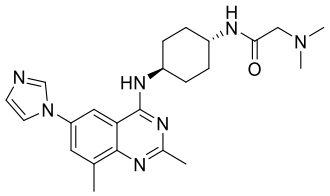

29
IC_{50} (μM) 0.06

Figure 2.4. Compound (29), with an amide linker at the C-4 position, and an IC_{50} value of 0.06 μM indicating the amide linker is tolerated.

In light of this data, it was envisaged that a similar amide linker could be used in the synthesis of a target chemical probe with its alkyne linker at the C-4 position. A model compound (**30**) was synthesised to test this hypothesis, also incorporating a long alkyl chain to assess its utility as a linker (Figure 2.5).

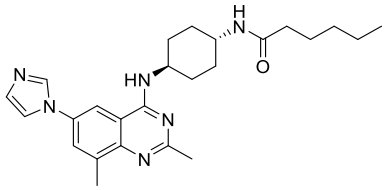

30

Figure 2.5. Test compound (30), designed in order to test the hypothesis that an amide linker and alkyl chain at the C-4 position on the cyclohexyl ring would be tolerated in a related chemical probe.

A synthesis was devised for compound (**30**) as described in Scheme 2.10.

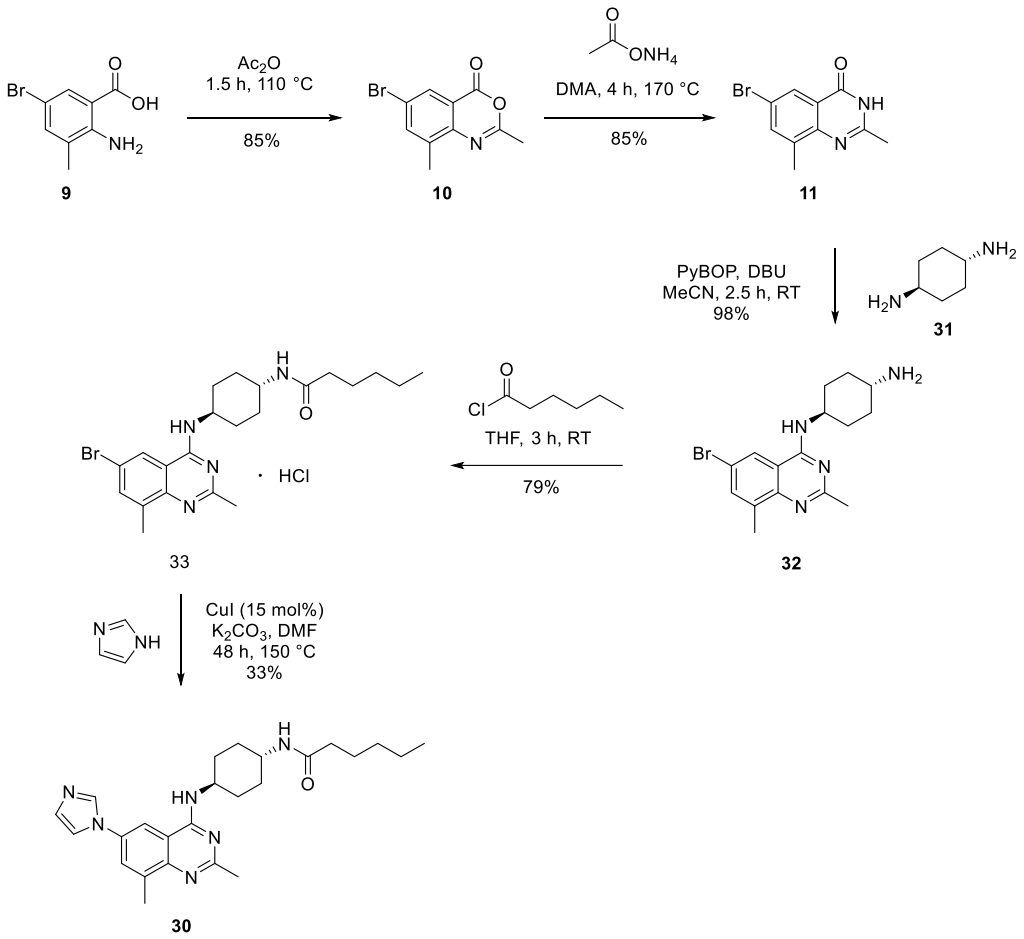

Scheme 2.10. Chemical synthesis for target compound (30).

As per chemical probe (**3**), the first two steps of the synthesis to access chemical probe (**34**) followed the established acetic anhydride-mediated cyclisation of aminobenzoic acid (**9**) followed by quinazolinone (**11**) formation through heating with ammonium acetate. By using commercially available *trans*-1,4-diaminocyclohexane in the subsequent PyBOP-mediated coupling reaction, the requirement for a separate synthesis using protecting group strategies was eliminated. This PyBOP coupling proceeded in a high 98% yield, affording amine (**32**) which was used to incorporate the alkyl chain *via* reaction with hexanoyl chloride, affording compound (**33**) as the chloride salt in a 79% yield. Lastly, Ullman coupling with imidazole afforded the target compound (**30**) in a 33% yield. This final compound was evaluated in the *P. falciparum* whole cell assay and shown to have an IC_{50} value of 0.44 µM, indicating that the amide linker and alkyl chain did not negatively impact the potency of the compound. This was a promising result, providing an alternative means for

incorporation of an alkyne linker onto the quinazolinamine core at this position, and providing evidence that an alkyl chain is tolerated. As a result of this, chemical probe (**5**) was redesigned to give chemical probe (**34**) in order to improve the synthetic tractability by using established chemistry to access a chemical probe with alkyne linker at the C-4 position in a timely manner (Figure 2.6). The alkyl linker in probe (**34**) has successfully been implemented in chemical probes in the literature, enhancing our confidence in the use of this linker.[152,161–163] In addition, amide-derived chemical probe (**34**) has a predicted PFI of 8.1, which is closer to that of the parent compound (**2**) (PFI = 7.1) than the equivalent ether alkyl compound (**6**) (PFI = 9.1) (first discussed in **Section 2.1 – The Design and Synthesis of Appropriate Quinazolinamine Chemical Probes for Use in Immobilised Bead Assays**). The alkyl ether compound (**6**) was not selected for synthesis due to predicted difficulties in its synthesis as seen for chemical probe (**5**).

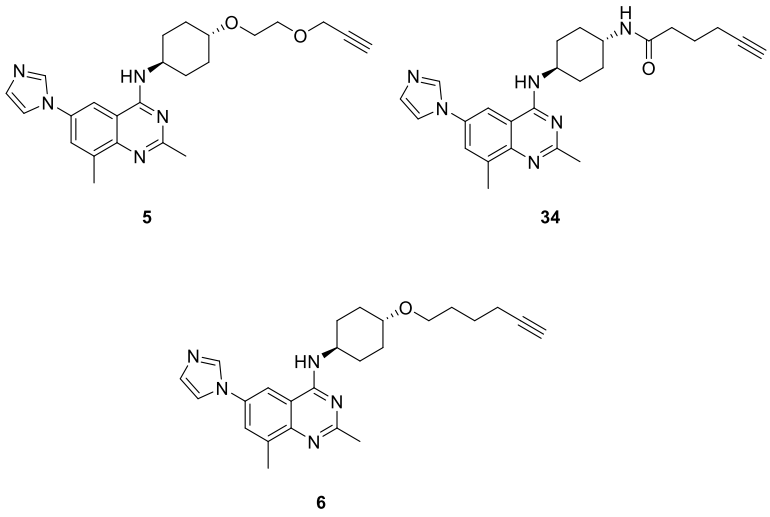

Figure 2.6. Initial target chemical probe (5) and newly designed target chemical probe (34).

The amide-containing chemical probe (**34**) was synthesised as described in Scheme 2.11.

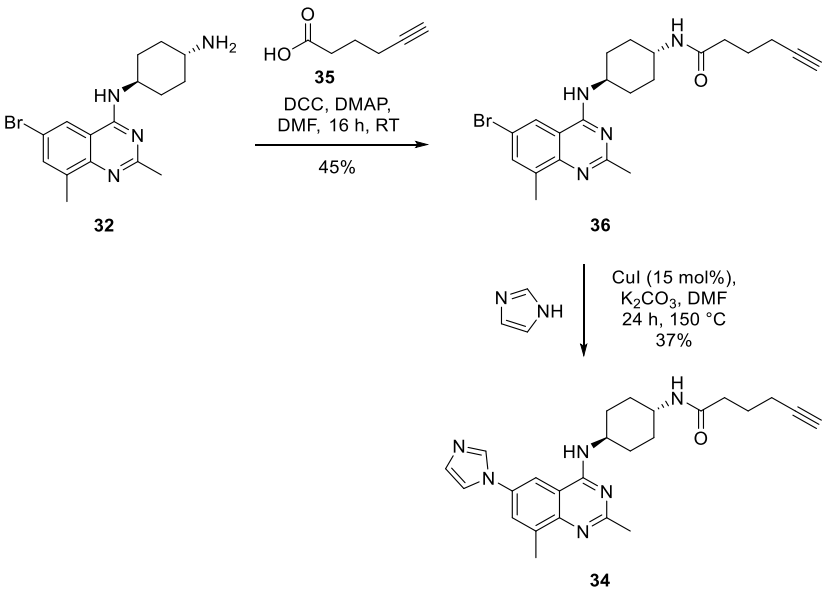

Scheme 2.11. Synthesis of target chemical probe (34).

Alkyne (**36**) was accessed *via* the amide coupling reaction between amine (**32**) and hexynoic acid (**35**). Final installation of imidazole occurred *via* Ullman coupling in a low 37% yield. This low yield was thought to be a result of the potential coordination of the copper catalyst to the newly installed amide thus rendering it ineffective. This could be through making the catalyst less available for oxidative addition into the carbon-iodine bond required in Ullman couplings. Although the yield of the reaction was disappointing, the synthesis furnished sufficient quantities for use in immobilised bead assays. Despite difficulties in initial attempts at synthesis of an appropriate chemical probe, the final desired probe (**34**) was accessed *via* a 5-step synthesis with a 12% overall yield. This was considered a success, with SAR data providing evidence that despite a change in the structure of the alkyne linker, the chemical probe should retain its potency.

2.1.4 The Chemical Strategy for Synthesis of Chemical Probe (51)

A third and final chemical probe was synthesised for use in immobilised bead assays before potency data became available. Similar to the previous chemical probes, the initial design included an ether-based linker in order to incorporate the alkyne

functional handle. Chemical probe (**7**) was designed with this linker extending from the C-2 position of the quinazolinamine core (Figure 2.7).

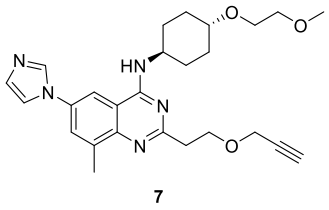

Figure 2.7. Target chemical probe (7) with alkyne linker protruding from the C-2 position of the quinazolinamine core.

An initial retrosynthetic analysis is described in Scheme 2.12.

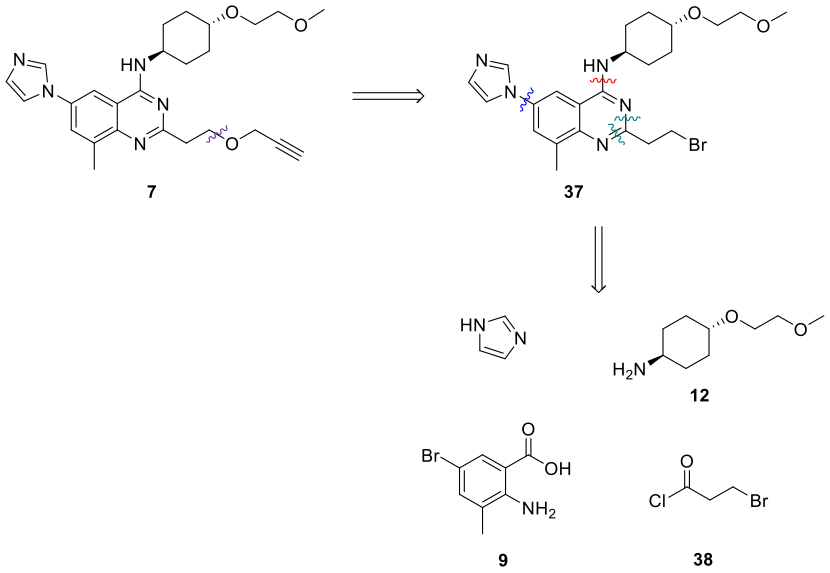

Scheme 2.12. Initial retrosynthetic analysis for the synthesis of target chemical probe (7).

The forward synthesis involved the installation of an ether on the target side chain *via* an S_N2 reaction between alkyl bromide (**37**) and propargyl alcohol. In the initial steps of the synthesis, this required the incorporation of the alkyl bromide chain into the quinazolinamine core (Scheme 2.13).

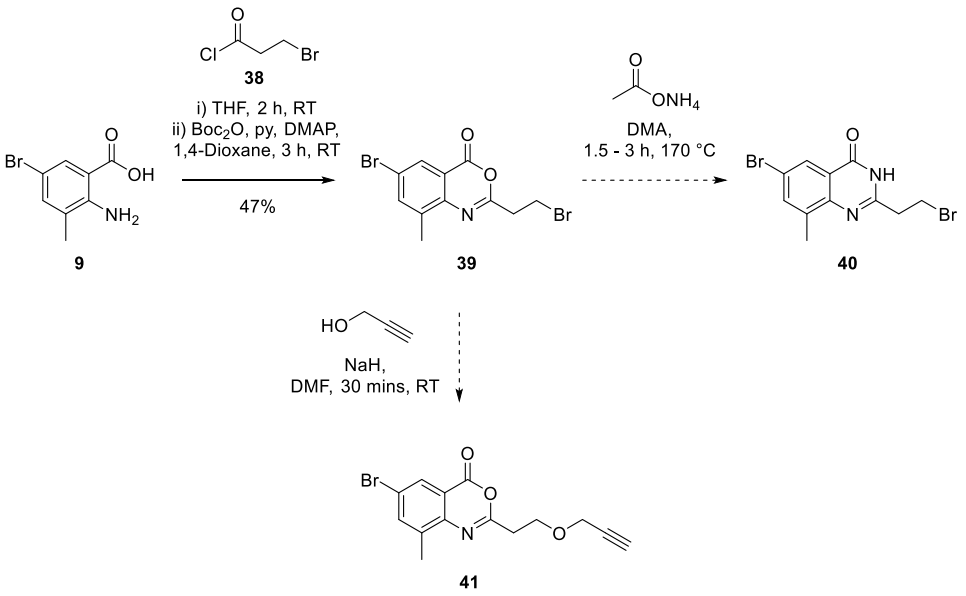

Scheme 2.13. Forward synthetic steps towards the synthesis of target chemical probe (7) *via* the synthesis described by retrosynthetic route a).

Initial reaction between aminobenzoic acid (**9**) and acid chloride (**38**), followed by Boc_2O-mediated cyclisation yielded the desired bromide-functionalised intermediate (**39**). However this appeared to be unstable and LCMS analysis suggested formation of alkene (**42**) on standing, consistent with bromide elimination (Figure 2.8). On application of the established ammonium acetate conditions for attempted transformation to the quinazolinone (**40**), no desired product was identified by LCMS analysis. Instead, conversion to the alkene side product (**42**) was again observed by LCMS analysis. This was, perhaps, unsurprising considering the high temperature required for the desired transformation and the alkene product being mesomerically stabilised across the molecule's core.

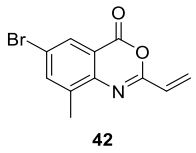

Figure 2.8. Undesired side product (42) indicating bromide elimination.

In order to assess the potential merit of synthetic route (a) in accessing the desired ether-containing linker, bromide intermediate (**39**) was reacted with propargyl alcohol

(previously deprotonated using NaH) in an attempt to carry out the required S_N2 reaction at an early stage in the synthesis *via* a Williamson-type ether synthesis. This was considered a potential method to overcome the instability of the alkyl bromide moiety. However, after stirring for 30 minutes at room temperature, 52% of the eliminated side product (**42**) was observed by LCMS analysis with only 19% desired product. As a result, synthetic route (a) was not considered a viable approach towards target probe (**7**) due to the ease of elimination of the bromide ion.

A promising organocatalysed, photoredox-mediated Minisci reaction was identified as an alternative potential method to funtionalise the quinazolinamine core at the C-2 position (Scheme 2.14).[164,165] The authors suggest that the mild conditions developed provide high functional group tolerance and thus the transformation can be used in late stage functionalisation of complex scaffolds.

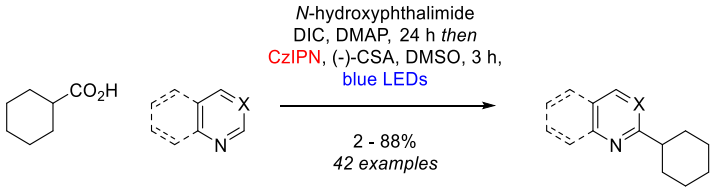

Scheme 2.14. Organocatalysed, visible-light photoredox-mediated Minisci reaction identified in the literature as a potential transformation for functionalisation at the C-2 position of the quinazolinamine core.[165] The photocatalyst CzIPN is indicated in red.

A retrosynthetic analysis that incorporated this photoredox reaction was devised (Scheme 2.15).

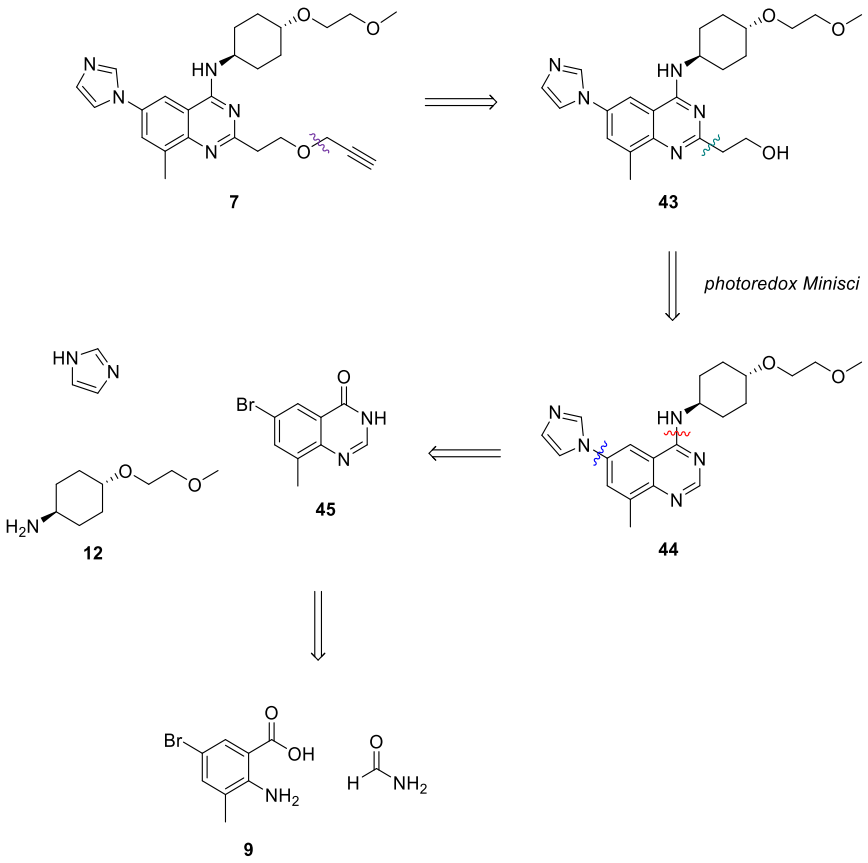

Scheme 2.15. Second retrosynthetic analysis for the synthesis of target chemical probe (7) incorporating a Minisci-type photoredox reaction.

The forward synthesis is detailed in Scheme 2.16, with the synthesis of intermediate (**44**) following similar steps as previously used for the construction of the quinazolinamine core.

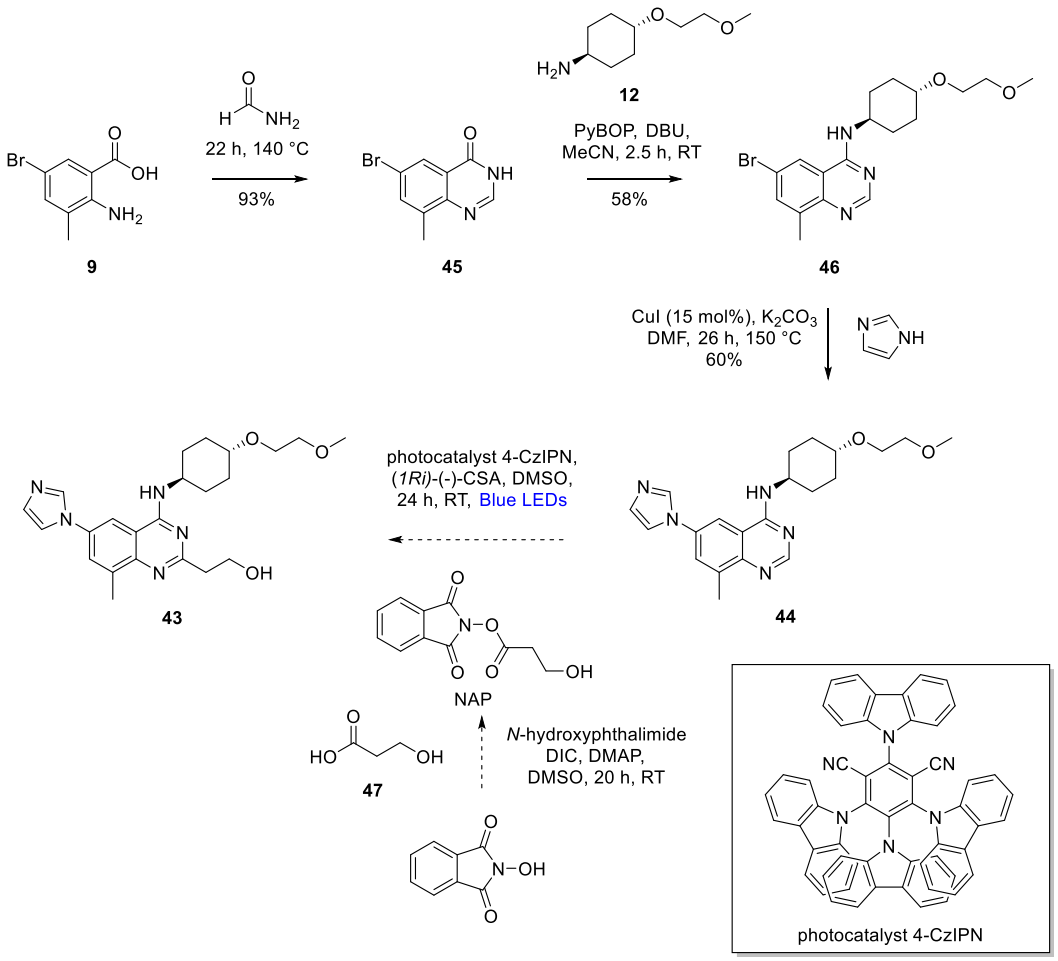

Scheme 2.16. Forward synthetic steps towards the synthesis of target chemical probe (7) *via* a Minisci-type photoredox reaction identified in the literature.[165]

Initial cyclisation of amino benzoic acid (**9**) using formamide afforded quinazolinone (**45**) directly in a high 93% yield. Subsequent PyBOP-mediated amide coupling between amine (**12**) and quinazolinone (**45**) allowed access to the quinazolinamine (**46**), which was reacted in an Ullmann coupling reaction with imidazole to afford the desired intermediate (**44**) in a satisfactory 60% yield. Intermediate (**44**) was used as the substrate for functionalisation at the C-2 position in the photoredox Minisci-type reaction. In a hypothesis put forward by the authors, the reaction is proposed to proceed *via* the *in situ* formation of an activated *N*-(acyloxy)phthalimide (NAP). The NAP then proceeds to oxidatively quench the excited photocatalyst (CzIPN) *via* single-electron transfer (SET), leading to reductive fragmentation to form the alkyl radical. This radical attacks a protonated heteroarene to afford the alkylated pyridine adduct which on deprotonation yields the tertiary radical. Single electron transfer with the oxidised

photocatalyst affords the protonated desired product and regenerates the photocatalyst to propagate the catalytic cycle (Scheme 2.17).

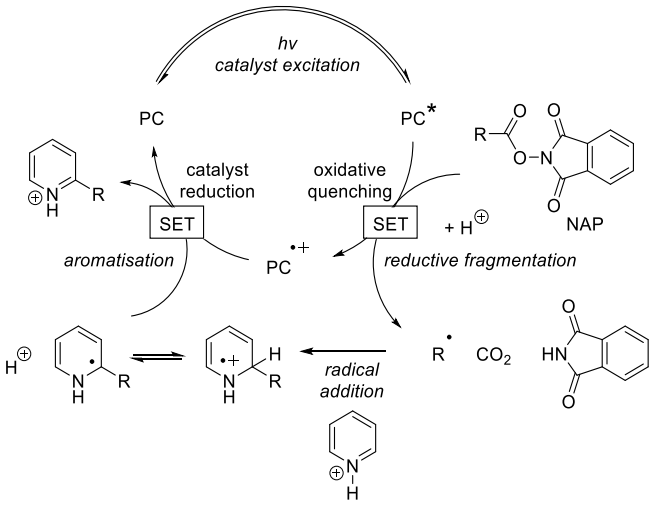

Scheme 2.17. Photocatalytic cycle for the photoredox-mediated Minisci reaction, proposed by Sherwood *et al.*[165] PC indicates the photocatalyst, and SET indicates single electron transfer.

Attempts to form the target free alcohol (**43**) directly, as per previous Scheme 2.16, yielded only 4% conversion by LCMS analysis and significant remaining starting material after 24 hours. The reaction scope as exemplified in the literature did not include a carboxylic acid substrate with a free alcohol moiety, and as such it was thought that the free alcohol in (**47**) may be the factor that was hindering reaction progression. A successful example in the paper was identified that used a benzyl protected alcohol (Scheme 2.18).[165]

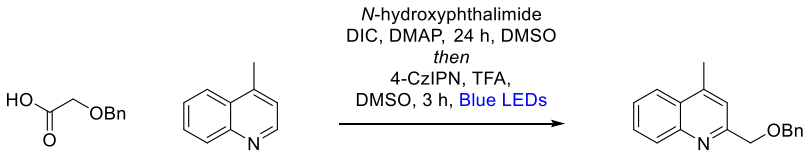

Scheme 2.18. Literature example of the photocatalysed Minisci reaction using a benzyl protected carboxylic acid starting material.[165]

Accordingly, a benzyl protected alcohol (**49**) was synthesised for use (Scheme 2.19).

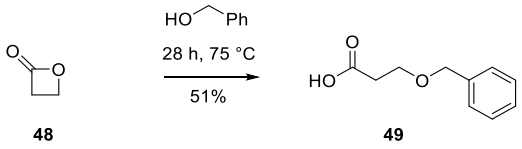

Scheme 2.19. Synthesis of ether (49) for use in the photoredox Minisci reaction for attempted synthesis of chemical probe (7).[166]

Benzyl protected alcohol (**49**) was used in the required Minisci reaction using the quinazolinamine (**44**) substrate (Scheme 2.20).

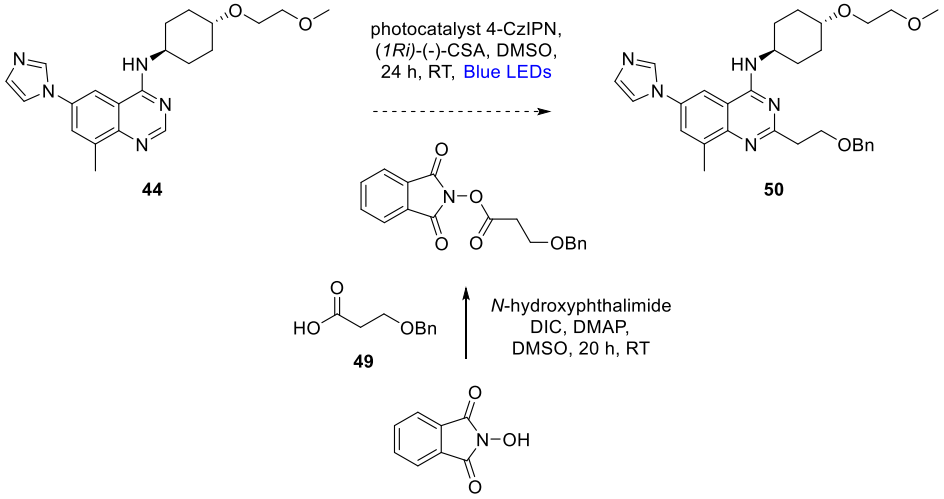

Scheme 2.20. Attempted photoredox reaction to access benzyl protected alcohol (50).

Despite the use of the benzyl protected alcohol (**49**), only 2% of the desired product (**50**) was observed by LCMS analysis, again with persistent starting material (**44**) being the major peak observed. It was decided that these conditions were therefore not applicable to the quinazolinamine (**44**) substrate. Due to time constraints, an alternative method for accessing a C-2 alkyne-functionalised chemical probe was pursued.

Given that an alkyl chain on the quinazolinamine core could be accommodated for previous chemical probe (**34**), the corresponding alkyl chain variant was chosen for synthesis as a replacement. Chemical probe (**51**) was envisaged to allow a shorter synthesis and efficient access to a desired probe with alkyne handle at the C-2 position (Figure 2.9). The shortened chain length was chosen due to commercial availability of

the requisite starting materials (as identified during the retrosynthetic analysis below), and a negligible change in calculated PFI (9.12 for the 6 atom chain, and 9.07 for the 5 atom chain).

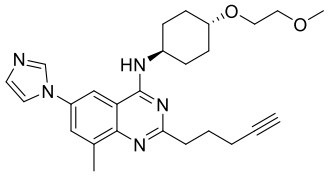

Figure 2.9. Target chemical probe (51) with alkyne functionalisation off the C-2 position *via* an alkyl linker.

A retrosynthetic analysis was performed, and accordingly an appropriate synthesis was designed based on well-documented chemical strategies for the synthesis of at least 20 mg of final target compound (**51**) (Scheme 2.21).

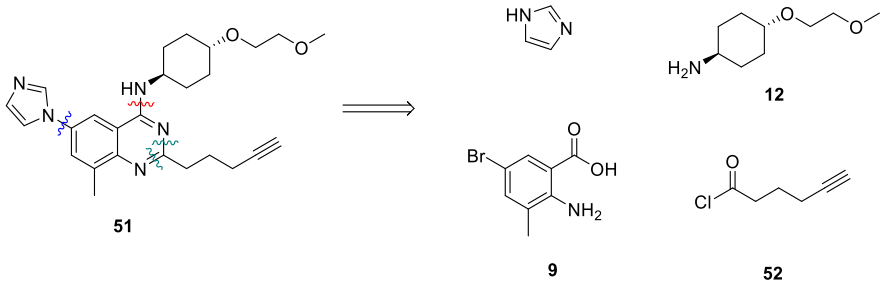

Scheme 2.21. Retrosythetic analysis for target chemical probe (51).

The forward synthesis for target chemical probe (**51**) is described in Scheme 2.22.

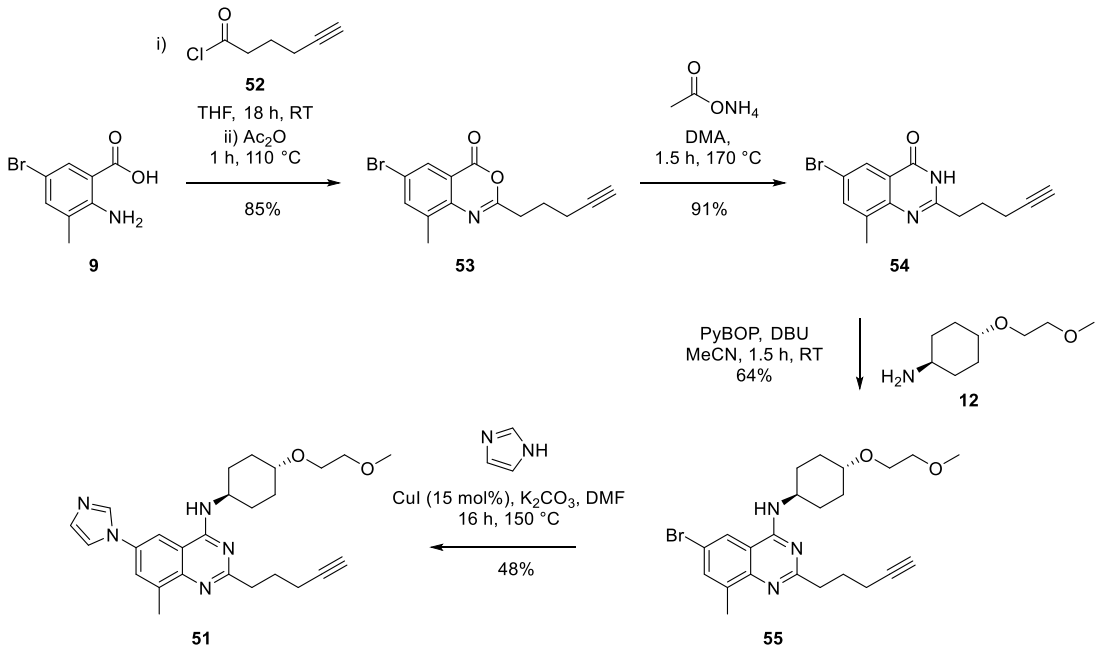

Scheme 2.22. Synthetic route towards target chemical probe (51).

Reaction between aminobenzoic acid (**9**) and commercially available acid chloride (**52**) followed by acetic anhydride-mediated cyclisation afforded alkyne (**53**) in a high 85% yield over the two steps. Subsequent reaction with ammonium acetate led to quinazolinone (**54**), to which amine (**12**) was coupled using PyBOP. Due to the absence of the amide moiety that was previously proposed to have a detrimental effect on Ullman coupling yield in the synthesis of chemical probe (**34**) as a result of its potential for coordinating the copper catalyst, the same Ullman coupling conditions were used in this synthesis with higher yields expected. This final Ullman coupling afforded the target compound (**51**) in 48% yield and was noted that this provided an improvement in yield from 37%, but still low overall. This may indicate that the absence of the amide moiety slightly improved the coupling efficiency, but that there are also other factors having a detrimental effect on yield. Again, due to the bespoke nature of this synthesis the reaction was not optimised, but strategies to improve this yield were considered in the syntheses of photoaffinity probes described in coming sections. The target chemical probe (**51**) was accessed in an overall yield of 24% over 5 steps, producing 98 mg of desired material. The synthesis was relatively efficient and the target of synthesising 20 mg of material was exceeded. Chemical probe (**51**),

along with the two previously discussed chemical probes, were then submitted to the *P. falciparum* whole cell assay for an assessment of antimalarial potency.

2.2 Potency Considerations for Chemical Probes (3), (34), and (51)

In order for chemical probes (**3**), (**34**), and (**51**) to be suitable for use in immobilised bead assays, their potencies against *P. falciparum* were required to be of a satisfactory level (pIC_{50} >6) as decided in our laboratories.[167] Low potencies would have suggested a steric or electronic clash in the binding pockets of any target proteins as a result of the newly incorporated linker and functional handle. This would have diminished the utility of the relevant compound as a chemical probe due to the associated difficulties in isolating the appropriate target protein(s) due to inefficient probe-protein binding.

The *in vitro* activities of the three chemical probes were measured through use of a [^{3}H]-hypoxanthine incorporation assay, in which the parasitic incorporation of radioactive [^{3}H]-hypoxanthine is proportional to parasite growth and is measured after 24 h of incubation with the relevant drug compound (see **Chapter 5 – Experimental**).[168] The resultant IC_{50} values provide quantitative values for the inhibition of parasite growth, normalised by assuming 100% parasite growth inhibition for a potent antimalarial control (artesunate), and 0% parasite growth inhibition for a DMSO control. This assay indicated that all three chemical probes were shown to have pIC_{50} values of greater than 6 (Table 2.4). This was surprising, as it was thought that addition of the alkyne linker would have a detrimental effect on potency at at least one of the three vectors (as discussed in **Section 2.1 – The Design and Synthesis of Appropriate Quinazolinamine Chemical Probes for Use in Immobilised Bead Assays**). These results may again hint towards the polypharmacology of the antimalarial quinazolinamine series, and the potential binding of the drug molecule to multiple protein targets or binding sites, resulting in the efficacies observed in the parasite whole cell assay. It was thus decided that all three probes should be used in the immobilised bead assay in an effort to identify the target protein(s) of quinazolinamine antimalarials.

Number	Structure	IC_{50} (μM)	pIC_{50}	Experimental PFI	LLE
3	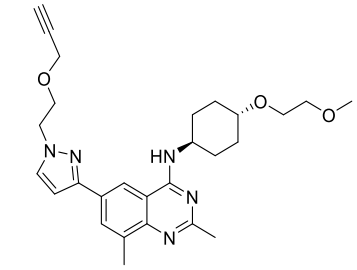	0.57	6.2	8.0	2.5
34	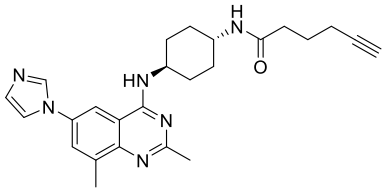	0.41	6.4	7.0	3.0
51	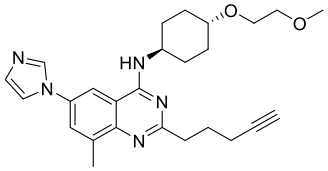	0.13	6.9	8.8	2.7

Table 2.4. Potency data for immobilised bead chemical probes as measured in a *P. falciparum* [^{3}H]-hypoxanthine incorporation assay (n = 2). LLE is the lipophilic ligand efficiency,

Of note was the surprisingly high potency observed for probe (**51**), with an IC_{50} over three times more potent than probe (**34**) and four times more potent than probe (**3**). It was thought that this could be due to the higher lipophilicity of probe (**51**), as demonstrated through PFI measurements, providing physicochemical charactistics that contribute to improved potency through improved partitioning into the compartment of its protein target. Indeed, an analysis of the lipophilic ligand efficiency (LLE) for each of the three probes showed that probe (**51**) had an LLE similar to that of probes (**3**) and (**34**) (Table 2.4). LLE allows the normalisation of potency with respect to changes in lipophilicity, and is calculated using the following equation:[169]

$$LLE = pIC_{50} - logD_{7.4}$$

Where $D_{7.4}$ is a measure of lipophilicity and is the distribution coefficient at a physiological pH of 7.4. This is the ratio of the sum of the concentrations of all forms of the compound (ionised and non-ionised) dispersed in a mixture of *n*-octan-1-ol and water, after it has been shaken and left to equilibrate:[134]

$$D_{7.4} = \frac{concentration\ in\ octanol\ at\ pH\ 7.4}{concentration\ in\ water\ pH\ 7.4} = \frac{[solute]_{octanol\ at\ pH\ 7.4}}{[solute]_{water\ at\ pH\ 7.4}}$$

The similar LLE values for probes (**3**), (**34**), and (**51**) indicate that the increase in potency of probe (**51**) is therefore likely to be attributed to its increase in lipophilicity.

2.3 The Immobilised Bead Assay for Target Identification of Antimalarial Quinazolinamines

All three synthesised probes were supplied to Cellzome along with the lead compound (**2**) to act as the competitor. Each chemical probe was separately investigated in immobilised bead assays, according to the standard protocols used by colleagues at Cellzome (see **Chapter 5 - Experimental**).

In brief, each probe was immobilised onto solid NHS-activated Sepharose® beads, which are commercially available activated agarose matrices. These had been derivatised with an azide functionality for use in the regioselective copper-catalysed azide-alkyne cycloaddition (CuAAC) reaction (Scheme 2.23).[170–172]

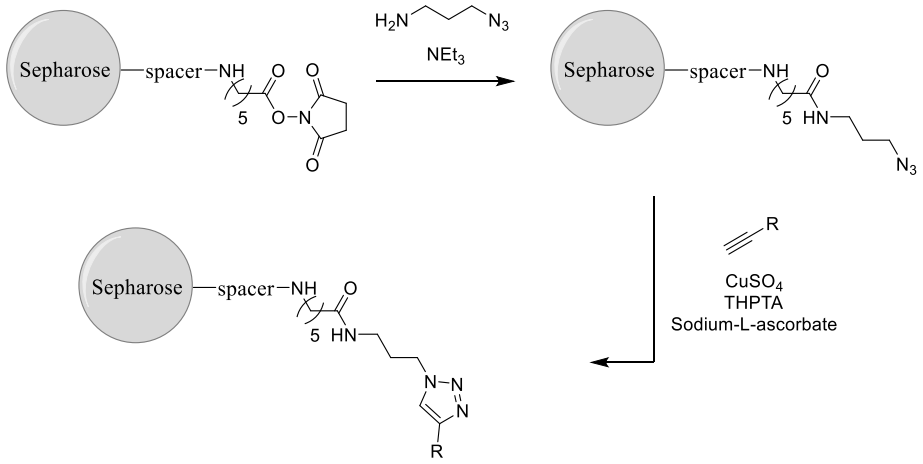

Scheme 2.23. Immobilisation of probes onto solid Sepharose beads, where R is the remaining structure of probe (3), (34), or (51).

The solid beads were then incubated in *P. falciparum* cell lysate, along with increasing concentrations of the parent competitor compound (**2**) in successive samples, to allow for affinity binding with the target protein binding site. The bead-containing samples

were then washed with buffer solution to remove unbound proteins and residual lysate, and the bound proteins were eluted by addition of appropriate enhanced buffer followed by incubation at heightened temperature. These bound proteins were subsequently analysed by enzymatic digestion followed by analysis by LCMS/MS.

Despite following this robust experimental procedure, only one potential target was identified with only weak competition observed. Previous experience of colleagues at Cellzome suggested this low return of competed proteins may be because of the high concentration of detergent used in the parasite lysis buffer (0.8% IGEPAL CA-630) for the preparation of the *P. falciparum* lysate as per the standard procedures.[167] On occasion, this has been seen to mask meaningful results. As a result, the experiment was repeated using a lower detergent concentration in the parasite lysis buffer (0.02% IGEPAL CA-630). However, results from this repeat assay yielded no target proteins that were competitively inhibited by the competitor compound (**2**), and the previously identified target was not detected for a second time. This indicates that there is a high probability that the initially identified protein was in fact an artefact, and thus not a protein of significance.

Due to the complex nature of the assay it is difficult to determine where the potential shortcomings of the experiment originate. However, the failure to identify a target protein could be due to a number of reasons such as low abundance or expression of the protein, or an unfavourable conformation of the target protein making it inaccessible to either the probe or parent compound under the experimental conditions used. This is possible due to the whole cell potency being measured using live *P. falciparum* parasite cultures unlike the immobilised bead assay, which used lysates. A reduction in potency of the compound once immobilised onto solid beads could also impact isolation of the target protein, or a change in the mechanism of action between the chemical probe and parent compound leading to no dose-dependent competition being observed. Without extensive further studies it is unrealistic to think that the true reason for the failure in identifying a target compound can be determined.

The lack of a definitive target protein from this assay provided added impetus to establish a photoaffinity labelling technique suitable for use in live parasites for target identification of this series. This approach gives rise to a strong covalent bond formed

between probe and protein, which may provide an improved method for the isolation of target proteins. Full attention, therefore, turned to the design and implementation of a new cellular assay for photoaffinity labelling at GSK Tres Cantos in Spain.

2.4 Chapter 2 Conclusions

In conclusion, in order to better understand the mode of action of promising antimalarial compound (**2**) (Table 2.5), three chemical probes incorporating an alkyne functional handle onto the core quinazolinamine at three different vectors have been successfully synthesised for use in affinity-based proteomic experiments. Each chemical probe required a bespoke synthesis, and significant quantities of product were accessed that exceeded initial targets (Figure 2.10).

	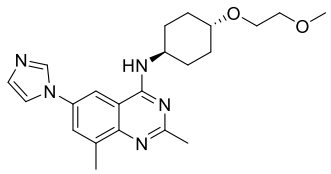
Number	**2**
Pf_{3D7} IC_{50} (µM)	0.40
pIC_{50}	6.4
LE	0.30
PFI	7.1
hERG IC_{50} (µM)	5.1

Table 2.5. Properties of promising antimalarial compound (2).

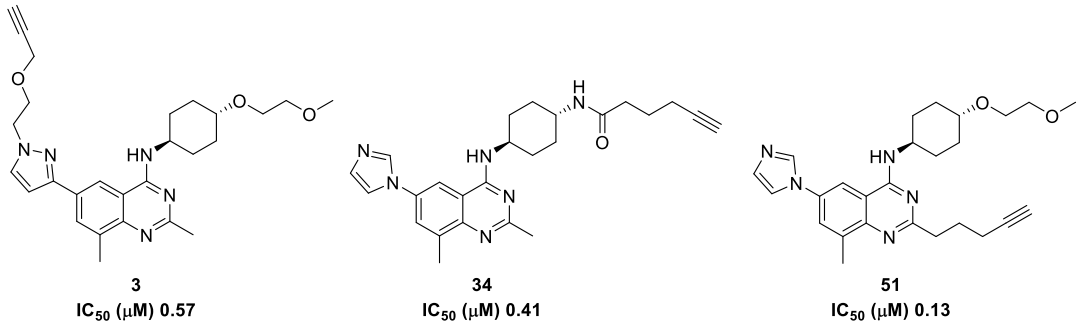

Figure 2.10. Synthesised chemical probes (3), (34), and (51) for use in immobilised bead assays for target identification studies of parent compound (2).

All three chemical probes (**3**), (**34**), and (**51**) were tested for potency in a *P. falciparum* whole cell [^{3}H]-hypoxanthine incorporation assay, and showed IC_{50} values of 0.57 µM, 0.41 µM, and 0.13 µM, respectively. These favourable results drove the decision to use all three chemical probes in the immobilised bead assay for target identification. Taking into account results from competition experiments with the parent compound (**2**), one potential target protein was identified, however, this result was not verified in subsequent repeats of the assay protocol.

The reasons for the lack of captured proteins that were competitively inhibited by the parent compound (**2**) remains unclear. Due to the large number of variables in these experiments, extensive further investigations would be required in order to fully understand the issues associated with identifying the corresponding protein targets. As a result, efforts subsequently focussed on the development of a photoaffinity labelling approach to target identification in live *P. falciparum* parasites.

2.5 Chapter 2 Future Work

Future work on the immobilised bead method for target identification of the antimalarial series represented by quinazolinamine (**2**) could include investigations into potential reasons for the lack of identifiable target proteins, and attempts to overcome these. An initial step could include the synthesis of compounds (**56**) – (**58**), for investigations into whether the click reaction between the alkyne chemical probe

and azide-derivatised solid bead to form a triazole results in a loss of potency (Figure 2.11).

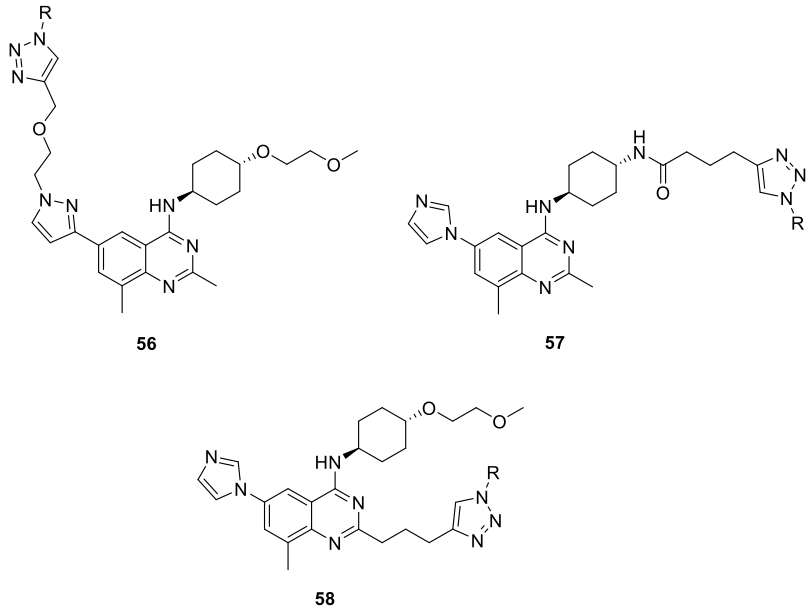

Figure 2.11. Proposed compounds for synthesis and testing in the whole cell *P. falciparum* assay, to investigate whether the click reaction to form a triazole results in loss of potency of the chemical probe. R indicates a the alkyl chain that mimics the chain on the solid beads used in immobilised bead experiments.

Should these chemical probes prove to have depleted potency in the whole cell assay (if permeability is also established as sufficient), it may suggest that the introduction of the triazole hinders probe-protein binding. As a result, further avenues for investigation could include the alteration of the linker length incorporated into each chemical probe. Syntheses could be optimised in order to allow for the synthesis of a number of different chemical probes containing differing linker lengths, of both PEG and alkyl varieties. An appropriate hypothesis could be that a longer linker length that leads to the resultant triazole moiety being held further out from the protein binding pocket thus may allow for better capture of target proteins due to reduced steric or electronic hinderance. In addition to this, the position of the alkyne linker could be varied further and different vectors investigated, as well as the click chemistry itself. For example, the strain-promoted inverse electron demand Diels Alder reaction between a *trans*-cyclooctene and a tetrazine could be implemented (first discussed in **Section 1.6.4 – Chemoproteomic Techniques for Target Identification**).

Chapter 3 – Results and Discussion: Photoaffinity Labelling for Target Identification of Novel Quinazolinamine Antimalarial Compounds

3.1 The Design and Synthesis of Appropriate Photoaffinity Chemical Probes

The design of appropriate photoaffinity probes must consider the identity of the functional handle, linker, and photoreactive group, as well as the vectors at which these groups reside. Unlike the immobilisead bead probes, for which an alkyne functional handle was deemed suitable, a *trans*-cyclooctene functional handle was selected for incorporation into photoaffinity probes. This was due to the potential requirement for click reactions to be carried out within live erythrocytes and *P. falciparum* parasites, leading to a preference for the copper-free, strain promoted, inverse electron demand Diels-Alder reaction (see **Section 1.6.4.3 – Chemical Probes for Use in Photoaffinity Labelling**).

In addition to the previously discussed benefit of high aqueous solubility of PEG chains, further considerations were also taken into account when reflecting on the use of these linkers in photoaffinity probes for experiments with live malaria parasites. PEG chains are ubiquitously used in drug discovery due to their low binding with blood plasma proteins.[153] This results in low intrinsic toxicity to cells as well as an increase in blood residence time,[173,174] and therefore circulation time, as a result of slower recognition and clearance by the immune system.[174–176] These characteristics are desirable in the application of many treatments as they result in reduced necessary dose as well as reduced toxicity. These qualities were also deemed desirable when designing a photoaffinity probe for use in malaria target identification. It was proposed that the PEG linker would not contribute significant background noise in pull-down experiments due to its lower binding to blood proteins, for which there is an excess in

malaria cultures (for example, from the Albumax solution containing bovine serum albumin required for continuous parasite cultures – see **Section 3.4.1 – The Determination of Required Parasitaemia and Culture Volumes for Isolation of Sufficient Parasite Protein**).[177] Therefore, in the synthesis of these PAL probes, there was a strong preference for a PEG chain over an alkyl chain, unlike in the design of the immobilised bead probes previously discussed.

A diazirine moiety was selected as the photoreactive group to be used in the target photoaffinity probes as a result of its high stability, small size leading to minimal steric bulk, and the fast reactivity of the carbene intermediate formed on irradiation (see **Section 1.6.4.3 – Chemical Probes for Use in Photoaffinity Labelling**). A photoreactive linker (**59**) previously used in successful photoaffinity labelling experiments in other projects of interest in our laboratories was identified (Figure 3.1).[178] Linker (**59**) was selected due to its desired diazirine photoreactive group, PEG chain, and a Boc-protected amine to which a TCO handle could be coupled after Boc-deprotection.

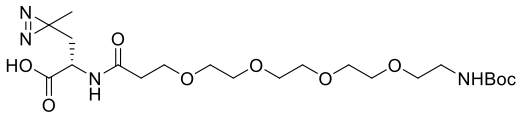

59

Figure 3.1. Photoreactive linker (59) as identified from previous efforts in our laboratories.

L-photo-leucine (**61**) was originally synthesised in the literature for incorporation into proteins *via* natural mammalian translation mechanisms, in order to study protein-protein interactions. The similarity of the compound to the naturally occurring amino acid leucine enables evasion of the stringent identity control mechanisms present in cellular protein synthesis.[179,180] However, the compound was also considered suitable for application in this current study, and thus was used in the synthesis of the appropriate photoreactive linker due to its commercial availability. The linker (**59**) was synthesised *via* formation of the activated *N*-hydroxylsuccinimide ester of PEG linker (**60**) followed by reaction with *L*-photo-leucine, the commercially available diazirine-functionalised amino acid (**61**), in a 51% yield over the two steps (Scheme 3.1).

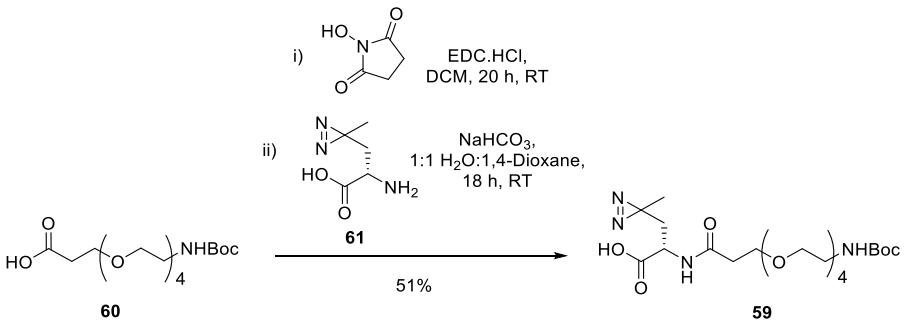

Scheme 3.1. Synthesis of photoreactive linker (59).

The synthetic procedure for incorporation of photoreactive diazirine linker (**59**) into potential drug compounds was envisaged to be carried out *via* first functionalising the compound of interest with an amine. An amide coupling between this amine and the linker (**59**) followed by Boc deprotection yields the diazirine-functionalised drug molecule, represented by the general structure (**63**) (Scheme 3.2). Reaction with TCO-carbonate (**64**) affords the fully functionalised target photoaffinity probe. The three steps can telescoped with chromotographic purification only required after the final step, providing an efficient method for easy access of PAL probes of a variety of different compounds of interest.

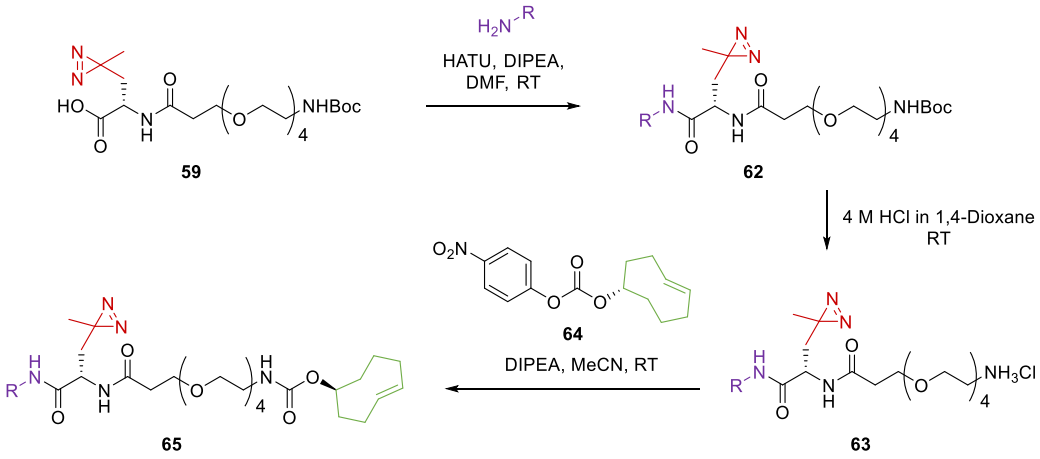

Scheme 3.2. General procedure for incorporation of photoreactive linker (59) into amine-functionalised drug compounds, with photoreactive diazirine in red, drug affinity unit in purple, and TCO functional handle in green.

With a selected linker and method for its incorporation in place, attention turned to the vector at which the linker should be positioned (and thus the position at which the

antimalarial quinazolinamine parent compound should be functionalised with an amine). It was thought that analysis of the IC_{50} data for the previously synthesised immobilised bead probes may provide direction as to the most appropriate vector for functionalisation. However, as described in **Section 2.2 – Potency Considerations for Chemical Probes (3), (34), and (51)**, it appeared that the small steric bulk of the alkyne linkers in the immobilised bead probes led to IC_{50} data that did not sufficiently distinguish between the suitability of each vector. As a result of this, all three similar vectors were considered viable positions for functionalisation using the photoreactive linker (**59**). Priority was given to functionalisation at the C-2 position due to the immobilised bead probe with linker at this position providing the highest IC_{50} value of the three immobilised bead probes. Secondly, functionalisation at the C-4 position was considered a possible alternative due to the smallest difference in IC_{50} observed on going from the parent compound (**2**) to the immobilised bead probe (**3**) functionalised at this position, potentially suggesting that changes in this region are tolerated. It was recognised that the photoreactive linker was much larger than the linker used in the design of immobilised bead probes, and thus steric factors may have a greater effect on the potency of the designed probes. Should neither of the two designed photoaffinity probes discussed provide a potent PAL probe then functionalisation at the C-6 position, or indeed further positions, was also considered. The final designs of the two target photoaffinity probes (**68**) and (**69**) based on the quinazolinamine series are indicated in Figure 3.2, with the amine-functionalised antimalarial quinazolinamine compounds (**66**) and (**67**) required for installation of the linkers also indicated.

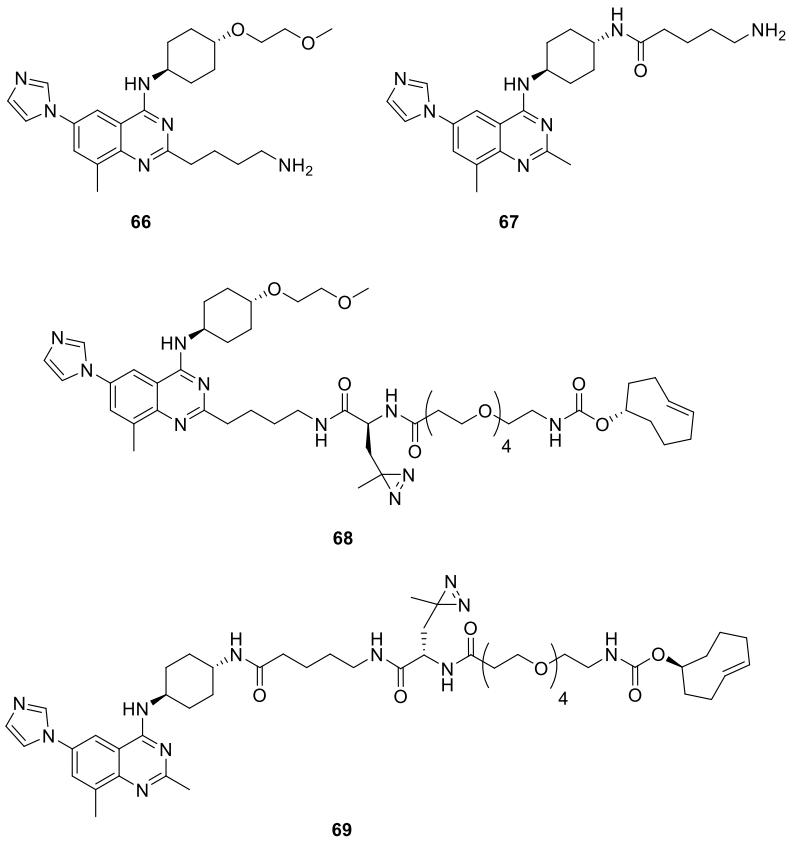

Figure 3.2. Amine-functionalised quinazolinamine compounds (66) and (67) used in the synthesis of target photoaffinity probes (68) and (69), respectively.

3.1.1 The Chemical Strategy for Synthesis of Photoaffinity Probe (68)

A challenge in the synthesis of photoaffinity probes (**68**) and (**69**) was the incorporation of the amine functionality into the requisite precursors (**66**) and (**67**), respectively. Three different methods to achieve this were originally identified in order to establish a suitable overall synthesis for chemical probe (**68**) in terms of yield and efficiency, and then to apply this to the synthesis of chemical probe (**69**) (Scheme 3.3).

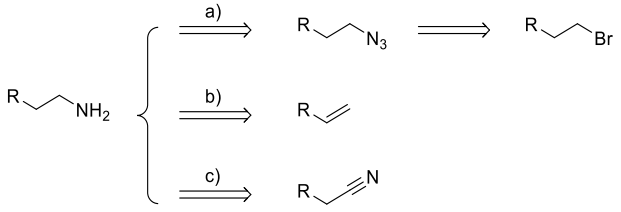

Scheme 3.3. Retrosynthetic analysis for the introduction of a free amine onto the quinazolinamine core, where R indicates the linker and core.

The three transformations investigated to introduce an amine onto the quinazolinamine core included: method (a), the reduction of an azide which itself was to be introduced *via* an S_N2 reaction between an alkyl bromide and sodium azide;[181,182] method (b), the hydroboration of an alkene followed by reaction with hydroxylamine-O-sulfonic acid;[183] and method (c) the hydrogenation of a nitrile.[182]

3.1.1.1 Investigations into the use of an azide for introduction of an amine functionality onto the quinazolinamine core

The transformation of an azide to an amine *via* a hydrogenation or Staudinger reaction[184] was considered a viable option for the introduction of the desired free amine in target quinazolinamine (**66**) due to a number of favourable properties of the azide functionality. For example, azides are easily introduced *via* simple S_N2 reactions with alkyl halides,[185] and the reduction to an amine is an environmentally-friendly transformation due to the formation of molecular nitrogen as the only side product.[186] Despite the often high reactivity of azides, they also often only act as spectators or are inert throughout organic syntheses.[187] This was considered a useful feature to ensure the azide moiety remains untouched throughout the initial steps of the synthesis of target amine (**66**). Taking into account the potential explosive nature of azides, this propensity is diminished when the number of carbon atoms is greater than the number of nitrogen atoms, and when $(N_C + N_O)/N_N \geq 3$, where N_x is the number of atoms of carbon (x = C), oxygen (x = O), and nitrogen (x = N).[185] For target compound (**66**), this value is 3.8, which is within an appopriate zone when considering the safety perspective of this synthetic route. However, high temperatures are required in early cyclisation reactions for the formation of the quinazolinamine core, and thus in order to minimise the risk of explosion the early steps of the synthetic route was designed such that a bromide functional group was initially incorporated. The azide was then introduced at a later stage *via* an S_N2 reaction.

The initial proposed synthesis for the access of target amine (**66**) *via* an azide is depicted in Scheme 3.4.

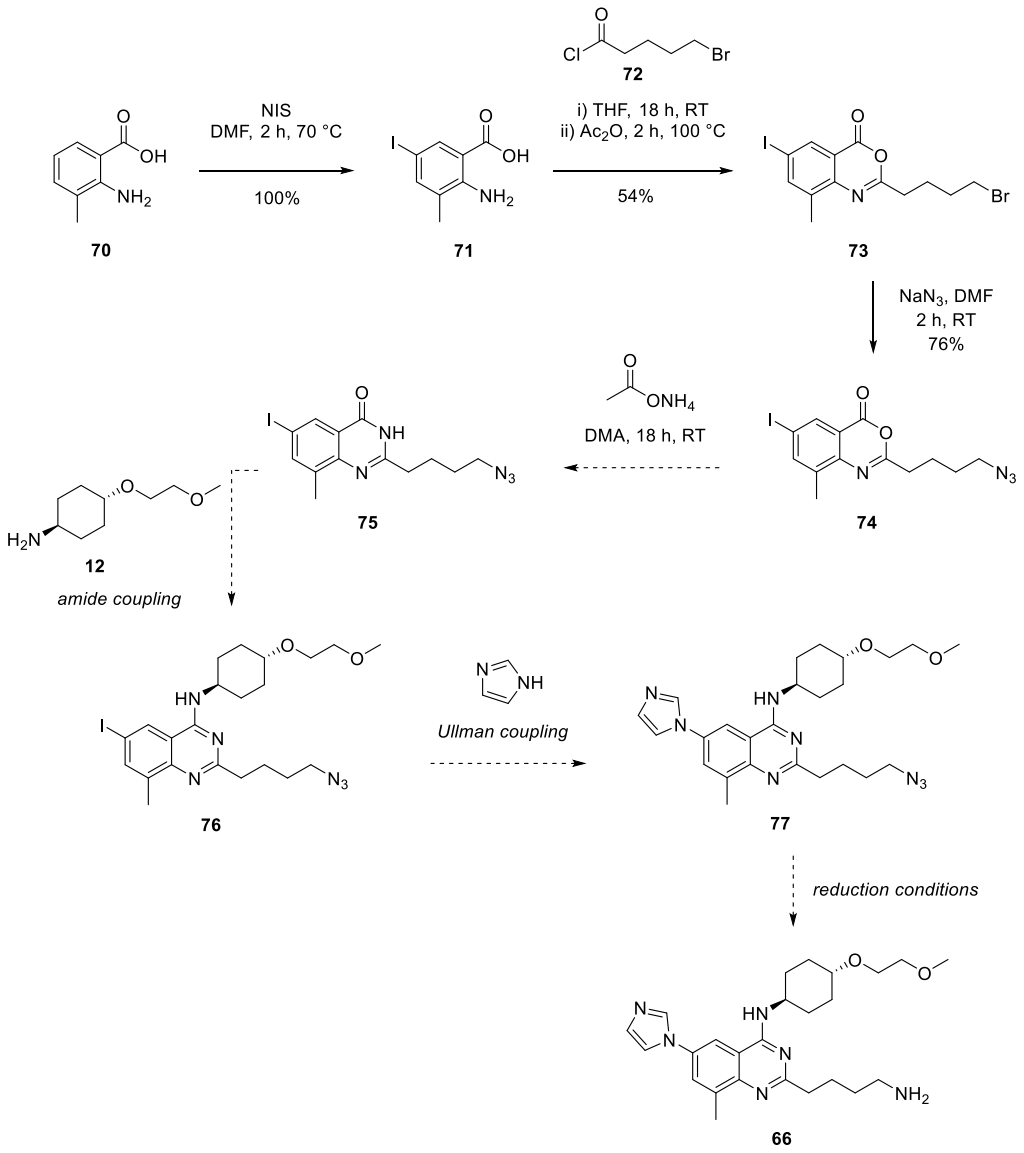

Scheme 3.4. Proposed synthesis for access of amine (66) *via* the reduction of an azide.

As mentioned in previous sections for the synthesis of immobilised bead probes, the Ullman coupling yields had been noted to be sub-optimal. As a result, the iodo-variant of the starting material aminobenzoic acid was considered a suitable substitution in order to improve reaction yields. It was predicted that due to the rate determining step of the Ullmann reaction being loss of the halide ion, the relative reactivity should thus increase with decreasing bond strength (with reactivity therefore following I > Br).[188] As a result, the first step in the synthesis towards target amine (**66**) was the iodination of aminobenzoic acid (**70**) due to a lack of commercial availability of the iodinated

precursor needed. This reaction proceeded in quantitative yield to give iodo product (**71**). Reaction with bromide-derivatised acid chloride (**72**) followed by acetic anhydride-mediated cyclisation yielded alkyl bromide (**73**). An S_N2 reaction between alkyl bromide (**73**) and sodium azide yielded the desired azide (**74**) in a 76% yield. The subsequent reaction with ammonium acetate, carried out at room temperature to minimise the risk of explosion rather than the elevated temperatures used for previous analogous reactions, to access the desired quinazolinone (**75**) proceeded with limited success. After stirring for 18 h, only 8% of product was observed by LCMS analysis, with evidence of remaining starting material and some degradation of the reaction mixture.

While these investigations were in progress, alternative approaches for the synthesis of target amine (**66**) were also attempted, as described in coming sections.

3.1.1.2 Investigations into the use of hydroboration methods for introduction of an amine functionality onto the quinazolinamine core

The well-established Brown hydroboration allows the access of alcohols from alkenes *via* the *syn*-addition of hydroboranes occuring with selective addition of the boron moiety to the least hindered carbon followed by reaction with hydrogen peroxide (Scheme 3.5, a)).[189] In later literature reports, this transformation was manipulated and extended to the synthesis of amines *via* reaction with hydroxylamine-O-sulfonic acid (HOSA) in place of hydrogen peroxide (Scheme 3.5, b)).[183,190]

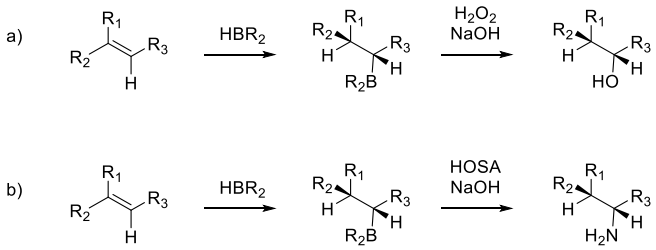

Scheme 3.5. a) Synthesis of alcohols from alkenes *via* hydroboration and reaction with hydrogen peroxide; b) synthesis of amines from alkenes *via* hydroboration and reaction with hydroxylamine-O-sulfonic acid.

This transformation was identified as a potential method for the synthesis of amine (**66**). The major benefit of this method was that the alkene functional group acting as

the starting material for this transformation was envisaged to remain intact under the experimental conditions used to construct the quinazolinamine core of (**66**). The experimental route designed is outlined in Scheme 3.6.

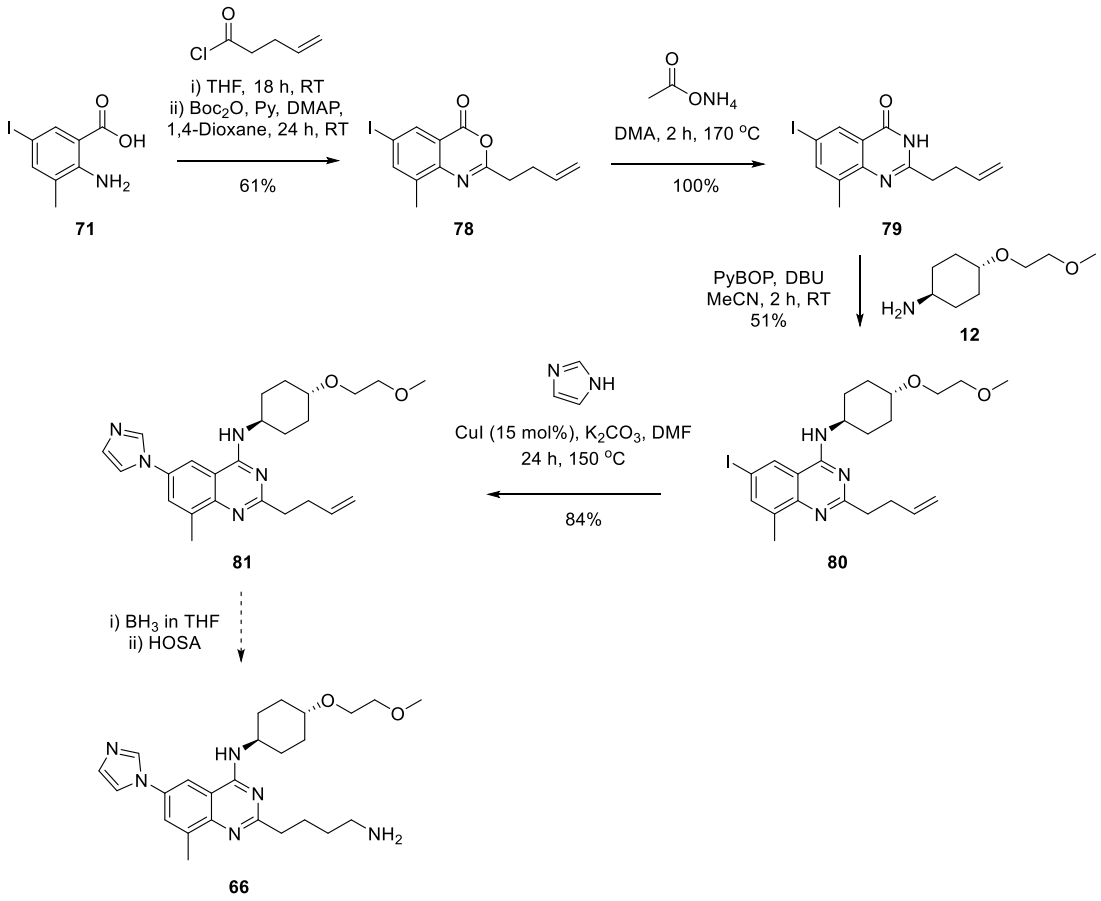

Scheme 3.6. Proposed synthetic route for the access of amine (66) *via* the hydroboration of an alkene and subsequent reaction with HOSA.

Using the iodinated starting material (**71**), reaction with 4-pentenoyl chloride followed by Boc anhydride-mediated cyclisation yielded alkene-functionalised (**78**). The Boc-anhydride and pyridine-mediated formation of the unsymmetrical anhydride of the carboxylic acid intermediate allowed facile cyclisation at room temperature, accessing substrate (**78**) in higher yields than *via* the equivalent acetic anhydride-mediated cyclisation.[191,192] Subsequent transformation using the established ammonium acetate conditions yielded the desired quinazolinone (**79**) in quantitative yield. Amide coupling with amine (**12**) afforded the alkene-functionalised quinazolinamine (**80**). Pleasingly, the Ullman coupling between (**80**) and imidazole proceeded in a high 84%

yield, indicating that the replacement of bromide with iodide on the core quiazolinamine could indeed contribute to an improvement of these coupling yields, as anticipated. The successful synthesis of alkene-functionalised quinazolinamine (**81**) indicated the stability of the alkene moiety under the reaction conditions used, as desired. However, attempts at the amination of this alkene in order to access amine (**66**) were unsuccessful. Initial efforts to form the hydroborated product using 2 equivalents of BH_3·THF yielded only unreacted starting material. When the stoichiometry of BH_3·THF was increased to 8 equivalents, the hydroborated intermediate was observed by LCMS analysis, suggesting that greater excess of borane may overcome the potential coordination of borane at heteroatoms around the molecule, thus facilitating the reaction. However, despite using anhydrous materials and thoroughly dried glassware, on addition of HOSA only the undesired alcohol product was observed by LCMS analysis and none of the desired amine. This corresponded to overall hydration of the alkene double bond (Scheme 3.7), although this product was not isolated for confirmation.

Scheme 3.7. Undesired formation of the alcohol (82) under conditions predicted to afford the amine.

Due to limited further literature precedent of the alkene to amine transformation of similar substrates using HOSA, this method to access amine (**66**) was abandoned in favour of exploring other approaches.

3.1.1.3 Investigations into nitrile hydrogenation for the introduction of an amine functionality onto the quinazolinamine core

The reduction of a nitrile to afford a primary amine is a commonly used transformation, with benefits including high atom efficiency and the ability to carry out the transformation under a variety of different conditions (for example, by metal-catalysed hydrogenations or using reducing agents such as $LiAlH_4$ or $NaBH_4$).[193,194]

The use of this transformation for the synthesis of amine (**66**) was considered a viable option due to the anticipated stability of the nitrile moiety under the reaction conditions used to construct the quinazolinamine core, and due to the wide variety of potential reduction conditions that could be tested to afford the desired amine compound (**66**). The synthetic route that was devised is illustrated in Scheme 3.8.

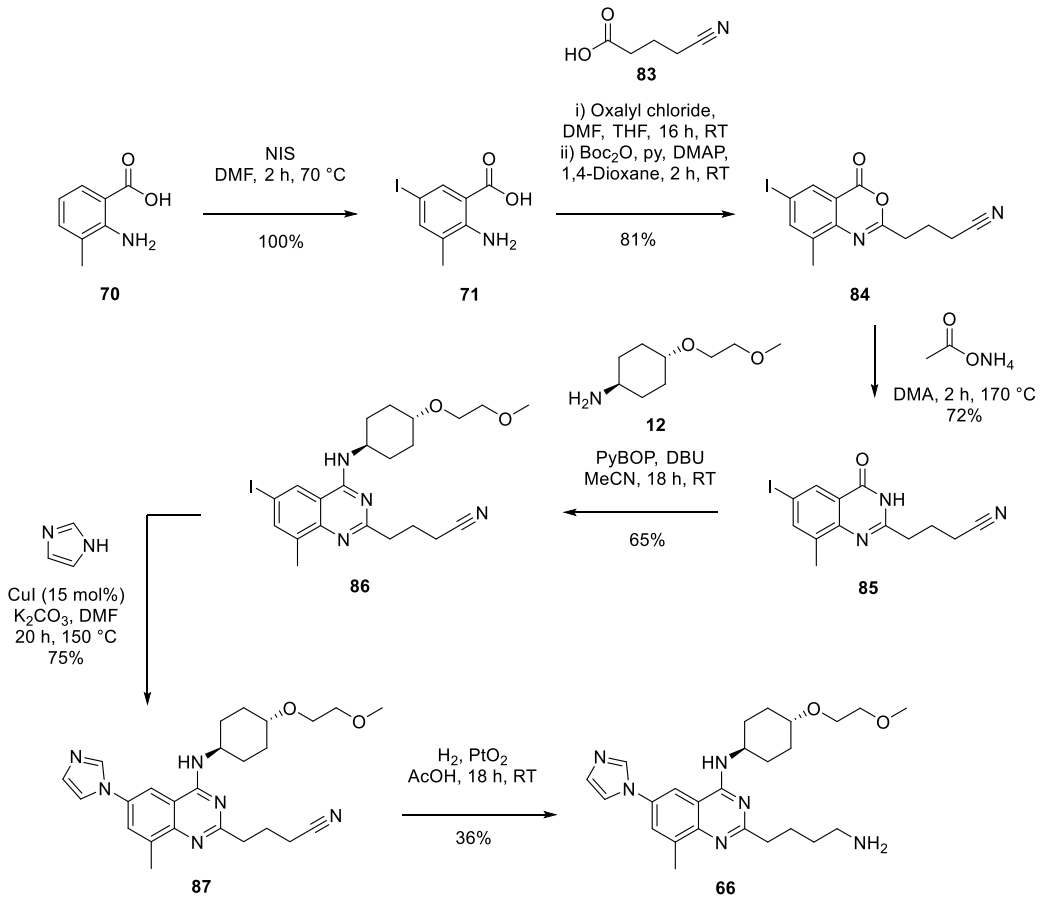

Scheme 3.8. Synthetic route for the access of amine (66) *via* the reduction of a nitrile.

Iodinated benzoic acid (**71**) was cyclised to intermediate (**84**) *via* a two step process starting with acid chloride formation of acid (**83**) for alkylation of the amino group of starting material (**71**) followed by cyclisation with Boc-anhydride, pyridine, and DMAP. The Boc-anhydride and pyridine-mediated formation of the unsymmetrical anhydride of the carboxylic acid intermediate again allowed higher yielding and facile cyclisation at room temperature.[191,192] Formation of the quinazolinamine (**86**) was achieved using the familiar conditions for condensation with ammonium acetate,

followed by amide coupling with amine (**12**). As above, Ullmann coupling of iodo-quinazolinamine (**86**) with imidazole yielded improved yields over the bromide relatives, proceeding in a highly satisfactory 75% yield and again justifying the use of the iodo starting material. The conditions chosen for the hydrogenation of nitrile (**87**) were PtO_2 in neat acetic acid under an atmosphere of hydrogen gas. These acidic conditions were chosen in order to minimise potential formation of the secondary and tertiary amines *via* reaction of the intermediate imine with starting material.[194] Reduction under these acidic conditions leads to formation of the ammonium salt which therefore prevents the further formation of these undesired amine side products.[195] In addition, due to the lower functional group tolerance of metal hydride reducing agents, these reagents were initially avoided. Although the unoptimised isolated yield of this hydrogenation reaction was low at 36%, a sufficient quantity of the desired free amine (**66**) was obtained using this method. Final access to amine (**66**) meant that installation of the photoreactive linker could be achieved *via* the chemistry outlined in **Section 3.1 – The Design and Synthesis of Appropriate Photoaffinity Chemical Probes** (Scheme 3.9). Accordingly, amine (**66**) was subjected to the telescoped reaction conditions described previously to introduce the photoactivatable diazirine group and TCO functional handle to afford target photoaffinity probe (**68**) *via* a convergent synthesis involving 14 steps overall. Due to the success of this method, attempts at the previous proposed syntheses of compound (**66**) were thus halted.

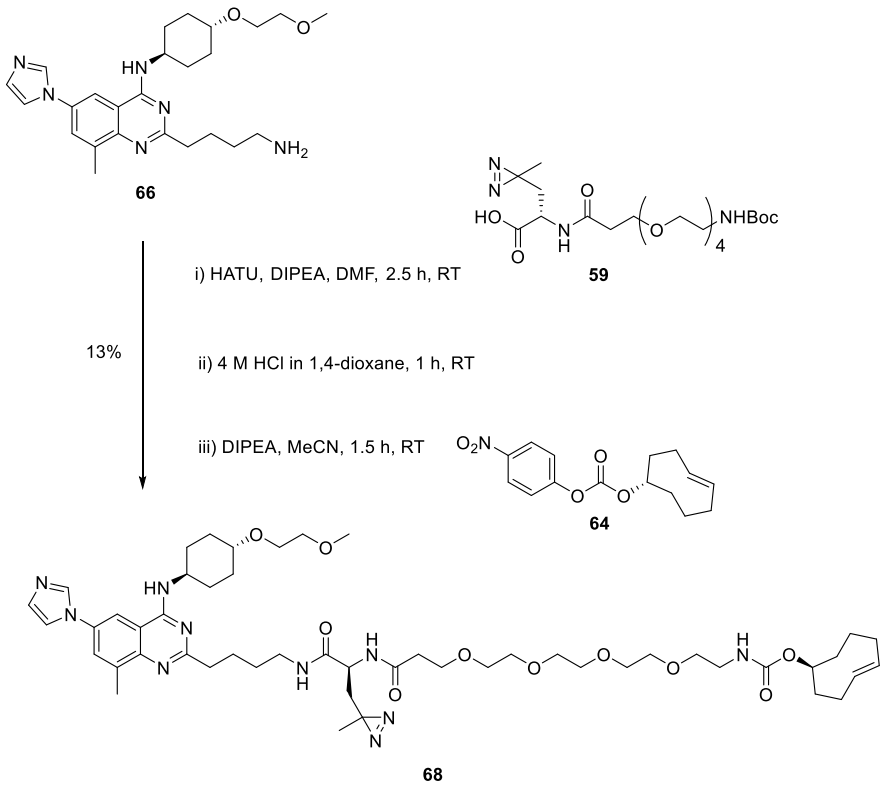

Scheme 3.9. Final installation of the photoreactive linker onto amine (66) in order to access target photoaffinity probe (68).

Of interest was the presence of the *cis*-cyclooctene isomer as a minor product (see **Chapter 5 – Experimental**). It was unclear whether this was as a result of the reaction conditions or natural isomerisation of the strained *trans* alkene on standing. The presence of this *cis* isomer was of little concern, however, due to its slow participation in the strain-promoted inverse electron demand Diels Alder reaction with the tetrazine-functionalised biotin fragment used in pull down experiments.[118] The *cis* isomer was therefore considered unreactive in comparison to its *trans* relative, and thus was expected to have a negligible impact on the ability to capture target proteins using the synthesised probe sample, except in the inevitable reduction of cross-coupling yields.

3.1.2 The Chemical Strategy for Synthesis of Photoaffinity Probe (69)

Target photoaffinity probe (**69**) was synthesised in a similar manner to immobilised bead probe (**34**), using the diaminocyclohexane fragment in order to incorporate the functionalised linker into the molecule *via* an amide coupling (Scheme 3.10). Due to

the success of the use of the iodo-varient of the starting material aminobenzoic acid for the synthesis of chemical probe (**68**), the iodinated compound (**71**) was again used as the starting material in the synthesis for chemical probe (**69**). Reduction of a nitrile was used as the method of choice for introduction of the amine functionality due to its success in the synthesis of previous photoaffinity probe (**68**).

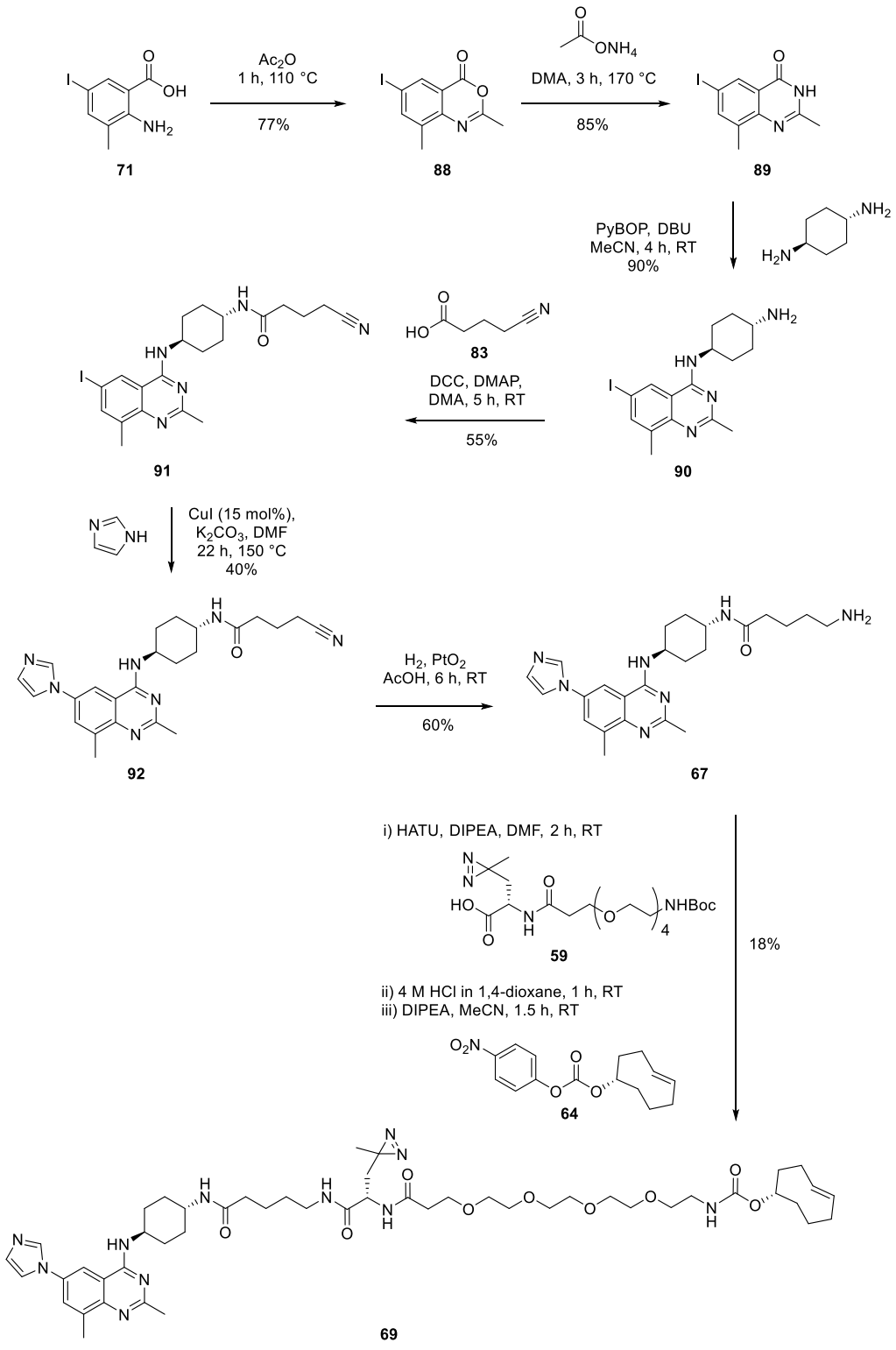

Scheme 3.10. Synthesis of target photoaffinity probe (69).

Using the established PyBOP coupling conditions, coupling between *trans*-1,4-diaminocyclohexane and quinazolinone (**89**) yielded amine (**90**) in a high 90% yield.

A subsequent amide coupling with commercially available nitrile (**83**) afforded quinazolinamine (**91**) with the desired incorporated nitrile functionality. The Ullman coupling between compound (**91**) and imidazole proceeded in a comparatively low yield of 40%, despite the previous success seen for the related Ullman coupling in the synthesis for chemical probe (**68**). This was a similar observation as seen in the synthesis of immobilised bead probe (**34**) in **Section 2.1.3 – The Chemical Strategy for Synthesis of Chemical Probe (34)**, and again it was reasoned that coordination between the amide moiety in compound (**91**) and the copper catalyst could be hindering the reaction progression. However, this hypothesis was not investigated further. Pleasingly, the nitrile reduction of compound (**92**) proceeded in a satisfactory yield of 60% to give desired amine (**67**). The free amine in (**67**) was used to incorporate the photoreactive linker using the same methodology as discussed for previous photoreactive probe (**68**). This afforded the target photoreactive chemical probe (**69**) in 18% over the three telescoped steps.

3.2 The Design and Synthesis of PI4K Photoaffinity Probe (94)

Due to the lack of any previous experience in our laboratories in the area of photoaffinity labelling in live *P. falciparum* parasites, it was considered a useful venture to synthesise a photoaffinity probe with a known protein target, in order to assess whether we could capture this target using the technique under development. This photoaffinity probe was based on an antimalarial compound developed by GSK Tres Cantos, incorporating the same photoreactive diazirine linker and TCO functional handle as the two probes based on the quinazolinamine series. Should the emerging photoaffinity assay be appropriate, it would permit successful identification of the correct target protein for this photoaffinity probe. This would provide confidence that the technique should then enable successful identification of the unknown targets of the antimalarial quinazolinamine series.

It was decided to base this probe on antimalarial compound (**93**) synthesised in our laboratories, with a structure similar to the published MMV666845,[96] previously

discussed in **Section 1.6.4.2 – Chemical Probes for Use in Affinity Capture Techniques** (Figure 3.3).

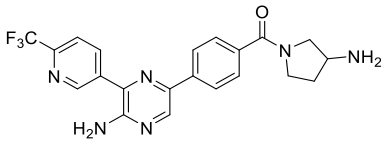

93

Figure 3.3. Antimalarial compound (93).

Antimalarial (**93**) comes from a family of PI4K inhibitors, as previously discussed. It contains a free amine which was identified as a point to which the photoreactive linker could be coupled. For antimalarial (**93**), we had confidence that this was a suitable linkage position as a result of the previously discussed study by MMV, in which a similar antimalarial molecule with the same mode of action was functionalised with a linker group at this position for use in an immobilised bead assay for chemoproteomic profiling (see **Section 1.6.4.2 – Chemical Probes for Use in Affinity Capture**).[96] Antimalarial (**93**) has an IC_{50} of 0.23 µM in the whole cell *P. falciparum* assay, corresponding to a pIC_{50} of 6.6. The probe based on antimalarial (**93**) and using the previously employed diazirine photoreactive linker and TCO functional handle was designed as the desired photoaffinity probe (**94**) (Figure 3.4). It should, however, be noted that the use of this probe in photoaffinity experiments would not act as a strong positive control as this has not been previously performed in the literature.

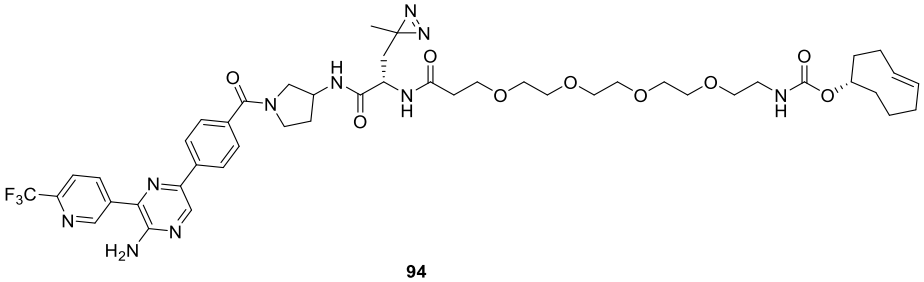

94

Figure 3.4. PI4K photoaffinity probe (94).

3.2.1 The Chemical Strategy for Synthesis of PI4K Photoaffinity Probe (94)

The synthesis devised for PI4K photoaffinity probe (**94**) is outlined in Scheme 3.11.

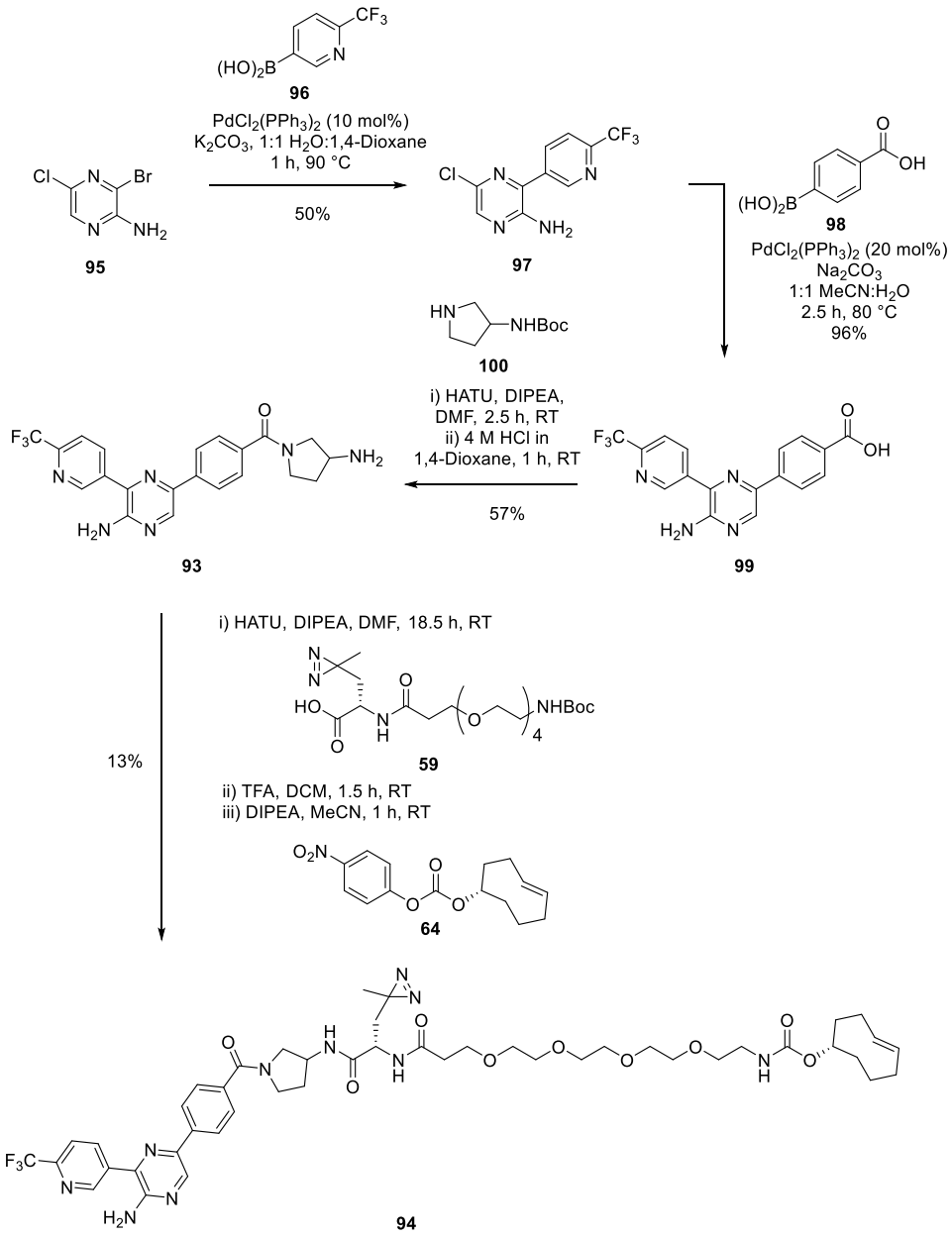

Scheme 3.11. Chemical synthesis of PI4K photoaffinity probe (94).

Bromine-selective Suzuki-Miyaura coupling between pyrazine (**95**) and boronic acid (**96**) yielded pyrazine (**97**) in a 50% yield. Subsequent Suzuki-Miyaura coupling with boronic acid (**98**) produced carboxylic acid (**99**) in a high yield of 96%, and this was then reacted with pyrrolidine (**100**) under amide coupling conditions of HATU and DIPEA. The following steps to install the diazirine photoreactive linker and TCO functional handle mimic those used for previously synthesised photoaffinity probes. However, it was observed that on purification by mass directed auto-preparative

(MDAP) HPLC after reaction with the TCO carbonate (**64**), the desired product (observed by LCMS) degraded into multiple unidentifiable products. Alternative purification methods were attempted in order to overcome the apparent instability of the product. The product was observed to be unstable to silica chromatography and it was noted that on standing in MeOH or DMSO the product also degraded rapidly. In order to avoid chromatographic purification, piperidine-4-amine was added to the reaction mixture after stirring for 1 h with the TCO carbonate (**64**) in the final step of the synthesis, in order to quench the remaining TCO carbonate (**64**). On an acidic work up, the protonated form of this side product was removed in the aqueous wash, and the remaining organic layer was concentrated *in vacuo* to yield desired product which was not purified further. These three steps afforded the desired photoaffinity probe (**94**) in a 13% yield. However, the inexplicable instability of this compound was of concern, and a deeper analysis of LCMS data was conducted in order to better understand whether this instability could have an effect on the success of PI4K protein capture in photoaffinity labelling experiments.

The synthesis of probe (**94**) was repeated and the LCMS spectrum analysed on synthesis, after dilution in DMSO, after reaction with tetrazine, and after sitting dry for 2 months followed by dilution in DMSO (to simulate the conditions that the experimental batch of PI4K probe would be subjected to due to the timescale needed for transport to GSK Tres Cantos and experimental set up) (Figure 3.5).

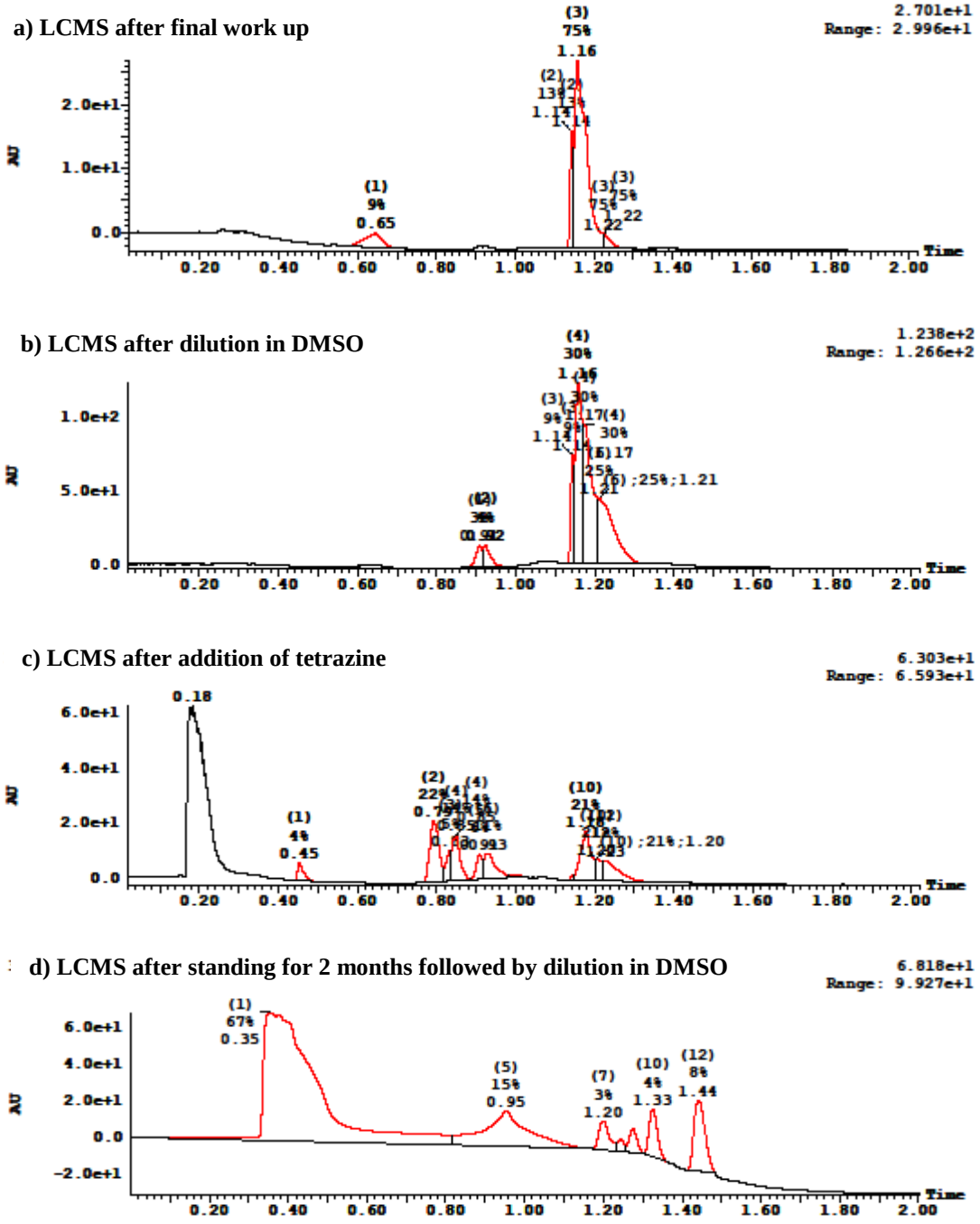

Figure 3.5. LCMS spectra of PI4K probe a) after synthesis; b) after dilution in DMSO; c) after addition of tetrazine; and d) after standing for 2 months followed by dilution in DMSO.

As can be noted from the LCMS traces, the PI4K probe is relatively clean by LCMS analysis immediately after the final work up during its synthesis (Figure 3.5, a)). There are two major peaks corresponding to product mass at retention times of 1.14 and 1.16 minutes, with the minor peak proposed to be the *cis*-isomer of the *trans*-cyclooctene. This was hypothesised due to a similar profile being observed by LCMS analysis of quinazolinamine probes (**68**) and (**69**), with the *cis* isomer seen as the minor isomer by NMR analysis (see **Chapter 5 – Experimental**). The probe was dried overnight under a nitrogen line, and the following morning dissolved in DMSO (as per the solutions used in photoaffinity labelling experiments) (Figure 3.5, b). By LCMS anaylsis, there appeared to be some degradation of the product observed by the development of a broad shoulder peak at 1.21 minutes, as well as unknown peaks appearing at 0.92 minutes. In order to test the assumption that the minor peak was the *cis*-isomer of the product, tetrazine was added to a small sample of the DMSO solution followed by shaking and instant LCMS measurement. Due to the rapid reaction kinetics of tetrazine with *trans*-cyclooctene and the comparatively negligible reaction rate with the *cis*-cyclooctene, it was predicted that a large shift in retention time for the major peak would be observed by LCMS, with the minor peak remaining relatively unchanged. As can be observed, addition of tetrazine appeared to lead to degradation of the PI4K probe (**94**) into multiple unidentifiable fragments, with it unclear whether the major or minor peaks corresponded to *trans*- or *cis*-isomers (Figure 3.5, c)). This was significant, and may suggest that the PI4K probe is unsuitable for these target identification studies. If the probe is unstable with respect to tetrazine addition, there is no guarantee that during the pull down and protein isolation steps that the desired protein targets will be effectively captured. A final LCMS of the reaction mixture after standing dry for 2 months, followed by dilution in DMSO indicated total degradation of the probe (Figure 3.5, d)). These conditions were used in order to mimick the treatment that the PI4K probe (**94**) would have been subjected to prior to use in photoaffinity labelling experiments for target identification in live *P. falciparum* parasites. This time delay in the use of the probe was as a result of the need to ship the probe from laboratories in the UK to those in Spain, and for the subsequent time taken to plan, prepare for, and conduct the photoaffinity labelling experiments. The total degradation indicates that the PI4K probe (**94**) was not suitable for photoaffinity

labelling studies, and therefore it was decided that the probe would not be used in these experiments.

3.3 Assessments of Suitability of Photoaffinity Probes (68), (69), and (94) for Use in Photoaffinity Labelling Experiments in Live *P. falciparum* Parasites

3.3.1 Potency Considerations for Photoaffinity Probes (68), (69) and (94)

Similarly to the immobilised bead probes discussed in **Chapter 2 – Results and Discussion: The Immobilised Bead Assay for Target Identification of Novel Quinazolinamine Antimalarial Compounds**, in order for the PAL probes to be suitable for use in photoaffinity labelling experiments their potencies against *P. falciparum* were desired to be of a satisfactory level (pIC_{50} >6). The *in vitro* activities of the three chemical probes (**68**), (**69**), and (**94**) were measured through use of the [^{3}H]-hypoxanthine incorporation assay used previously for potency determinations (Table 3.1).

Number	Structure	IC_{50} (μM)	pIC_{50}
68	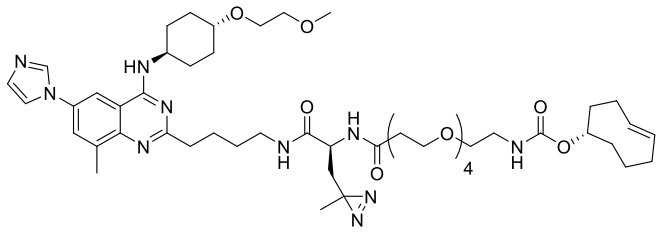	0.17	6.8
69	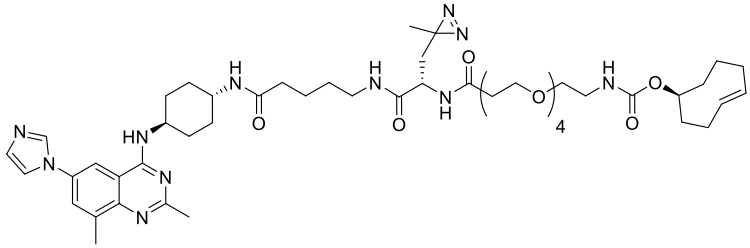	2.5	5.6
94	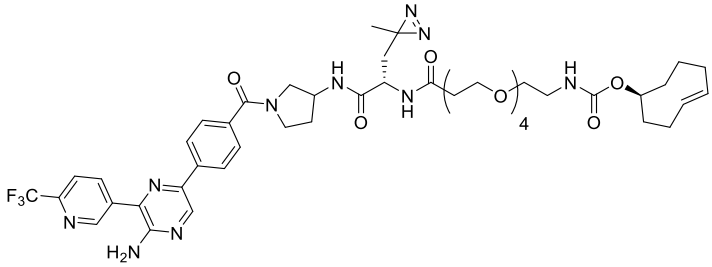	2.5	5.6

Table 3.1. Potency data for photoaffinity probes as measured in a P. falciparum [^{3}H]-hypoxanthine incorporation assay (n = 2).

As indicated by the data in Table 3.1, only photoaffinity probe (**68**) provided the desired level of potency with a pIC_{50} of 6.8. This guided the decision to use quinazolinamine photoaffinity probe (**68**) in the photoaffinity labelling experiments in live *P. falciparum* parasites as opposed to photoaffinity probe (**69**). The potency for probe (**69**) significantly dropped from that of the parent compound (pIC_{50} of 6.4) on addition of the linker and functional handle, providing a pIC_{50} of 5.6. PI4K photoaffinity probe (**94**) also showed a pIC_{50} of 5.6, reduced from 6.6 for the parent antimalarial compound (**93**). This was below the desired limit of 6 initially imposed, and provided further evidence that probe (**94**) was unsuitable for these photoaffinity labelling experiments, in addition to the stability concerns noted previously.

3.3.2 The Killing Profiles of Photoaffinity Probes (68) – (69)

The effect of antimalarial drugs is demonstrated by their ability to kill parasites and decrease the parasitaemia (a measure of the number of parasite-infected red blood cells as a percentage of total red blood cells, P%) within patients, as well as prevent recrudescence (the reappearance) of the parasites. This effect can be estimated *in vitro* by measuring the parasite killing rates, for which information about the mode of action of the antimalarial compounds can be deduced. Antimalarial compounds with the same mode of action have very similar parasite killing rate profiles. Thus, the rate profiles of compounds with unknown mode of action can be assessed based on known antimalarial rate profiles for initial indications as to their mechanisms. Possible modes of action could be excluded or envisaged based on these comparisons, although additional information would be required to confirm such indications.[196]

A routine *in vitro* parasite viability assay is carried out every 2 weeks at GSK Tres Cantos as a medium-throughput method for measuring killing rate profiles of antimalarial compounds in order to prioritise those with fast killing profiles, comparable to artemisinin. This assay was envisaged to provide a useful platform for a comparison of the killing rate profiles of the lead quinazolinamine compound (**2**) with the structurally-related photoaffinity probes (**68**) and (**69**). Should the killing rates have been substantially different between probe and parent, then this would have suggested that the addition of the photoreactive linker was leading to a change in the mechanism of action, and would have thus made the probes unsuitable for use for target identification of the parent compound.

The quinazolinamine parent compound (**2**) in the relevant *in vitro* fluorescence-activated cell sorting (FACS) assay has a moderate killing profile, defined as more than 20% parasite survival at 24 h after drug treament and less than 20% parasite survival 48 h after drug treament. This moderate killing profile was retained by the photoaffinity probes (**68**) and (**69**) as can be seen in Graph 3.1, with data gathered by Benigno Crespo and Ana Hermoso, colleagues at GSK Tres Cantos.[197]

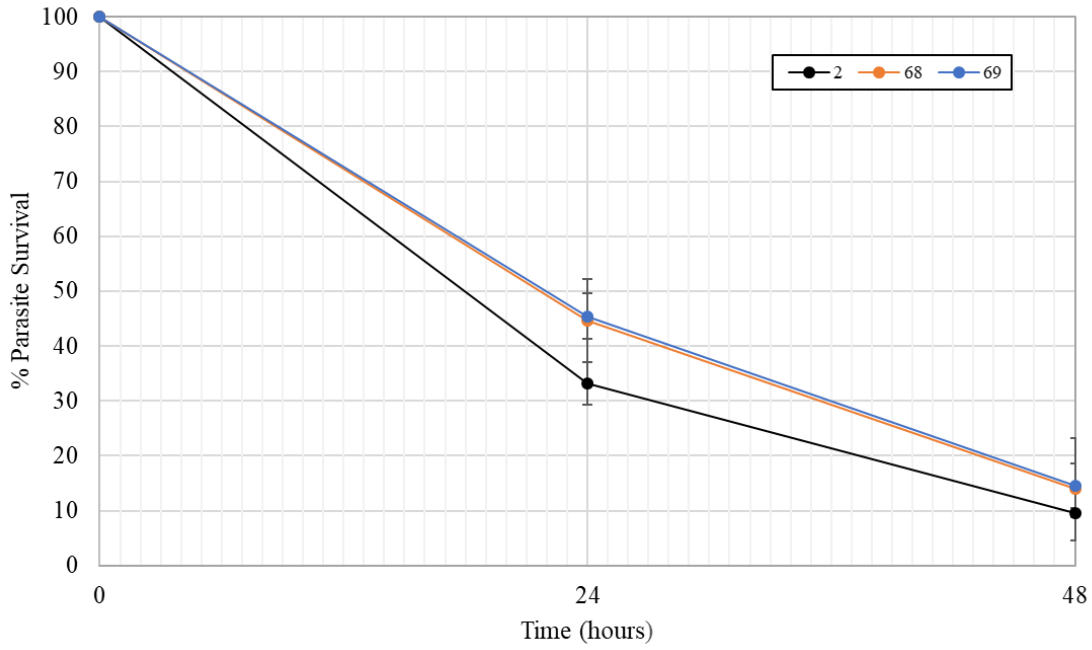

Graph 3.1 Parasite killing profiles for each of the quinazolinamine photoaffinity probes (68) and (69), lead compound (2), and four known antimalarial drugs.

The results of Graph 3.1 indicate that on addition of the photoreactive linker, there were no significant changes in parasite killing rate for either probe (**68**) or (**69**) when compared to the lead compound (**2**). This was a highly significant result, and provided experimental evidence that the photoaffinity probes designed were suitable for use in target identification studies of the antimalarial quinazolinamine series represented by parent (**2**). Although it cannot be ruled out entirely that the mode of action of the probes was not different to that of the parent, the results here provided the justification for further studies. Had the killing profiles changed significantly, this would have required the re-design and re-synthesis of alternative chemical probes for the desired target identification investigations.

3.3.3 Fluoroescence Imaging in Live *P. falciparum* Parasites

In order to visualise the accumulation of photoaffinity probe (**68**) in live parasites after irradiation with UV light, and thus have further evidence of the suitability of these probes for use in PAL experiments, an imaging experiment was required. A similar experiment had not been done before at GSK Tres Cantos, and so a new experimental

workflow was devised based on the imaging equipment available, and implemented by the author (See **Chapter 5 – Experimental**).

Samples of *P. falciparum* culture were incubated with PAL probe and then UV irradiated to trigger covalent crosslinking. Incubation with a tetrazine-derivatised fluorescent Alexa dye (AFDye™ 488)[198] facilitated the appropriate reaction with the TCO functional handle on the probe, thus allowing the visualisation of probe accumulation within the parasite cultures. The samples were subsequently incubated with a 4',6-diamidino-2-phenylindole (DAPI) dye in order to stain the DNA of the parasites. Due to the lack of DNA in human erythrocytes, this allows for the localisation of the parasites within the whole cell culture. Using a confocal microscope, images of cultures treated in this way were obtained (Figure 3.6).

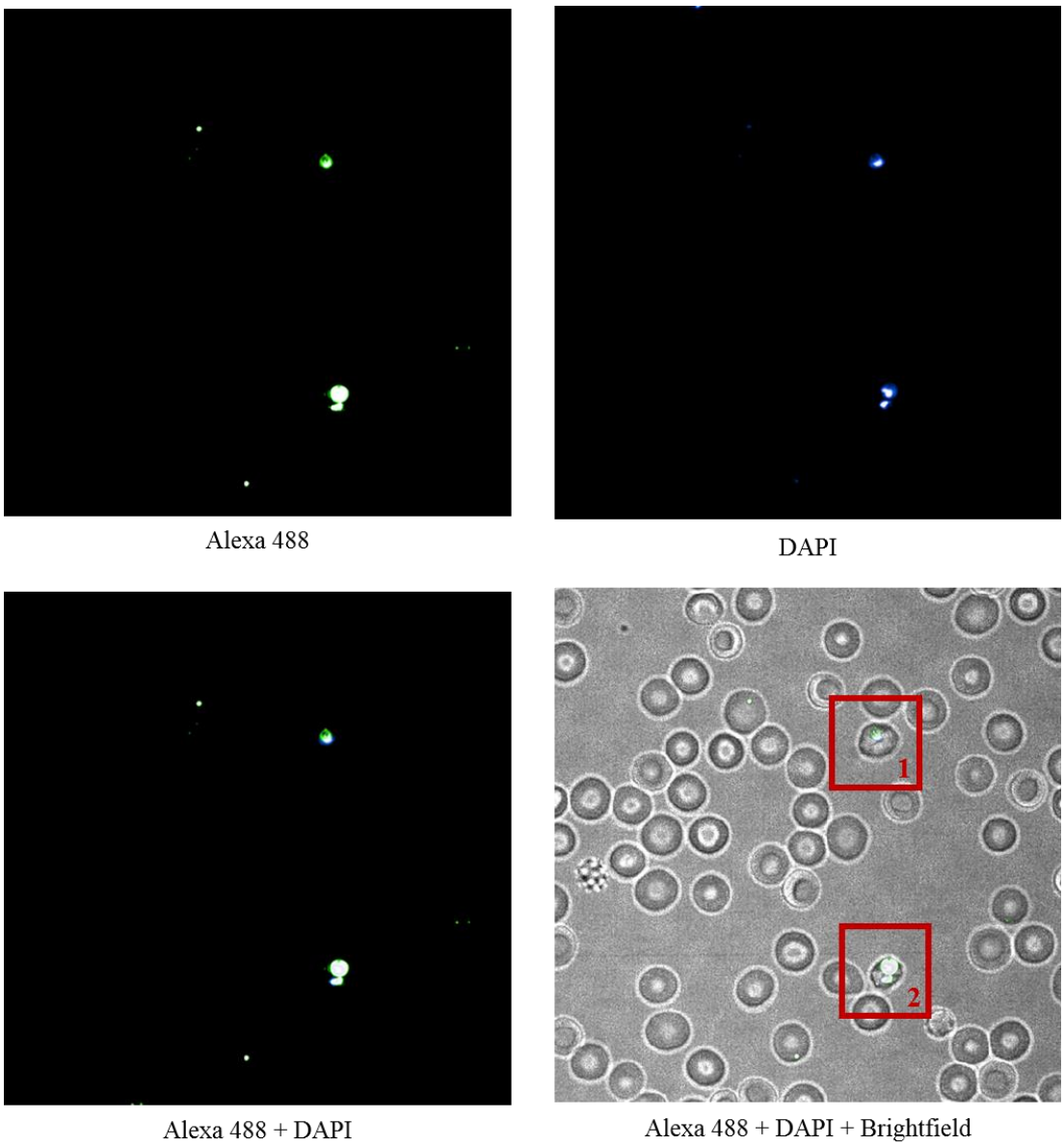

Figure 3.6. Images from imaging experiment of PAL probe in live *P. falciparum* parasites. Alexa 488 dye allows visualisation of the Alexa dye clicked onto PAL probe (green),[198] DAPI allows visualisation of parasite DNA (blue), and Brightfield allows simple visualisation of cells. Red box 1 indicates an early ring stage parasite, while red box 2 indicates a late stage trophozoite. Artefacts can also be observed in which Alexa dye is visualised as small dots corresponding to no obvious parasite or erythrocytic feature.

From Figure 3.6 it can be seen that there is an overlay of the Alexa 488 dye in green (indicating the location of PAL probe) and DAPI dye in blue (indicating the presence of parasitic DNA). Using the brightfield visualisation (used for simple visualisation of cells using white light), it is possible to observe the presence of parasites within the erythrocytes corresponding to the localisation of both probe and DAPI dyes. From

these observations, several significant conclusions can be inferred. Firstly, the PAL probe is permeable across both the erythrocytic membrane and that of the parasite, indicating its ability to reach its target within the 1 h incubation time. Secondly, the protein target of this series appears to reside within the parasite itself rather than being located in the erythrocyte cytoplasm or on its membrane. This is significant because of the presence of parasitic proteins that are exported from the parasite into the host cell, and thus suggests the protein target of the quinazolinamine series is not a member of this group of proteins (see **Section 1.3 – The Functions of Major Protein Families Across the Parasite Lifecycle**).[8,199] Finally, examples of the small, early ring stage parasites as well as the large, late stage trophozoites can be seen in the mixed-stage culture used for these experiments (see **Section 1.2 – The Malaria Lifecycle** for a description of the intraerythrocytic parasitic stages and their appearance). In addition, Figure 3.7 shows further images indicating the accumulation of PAL probe in developing final stage schizonts.

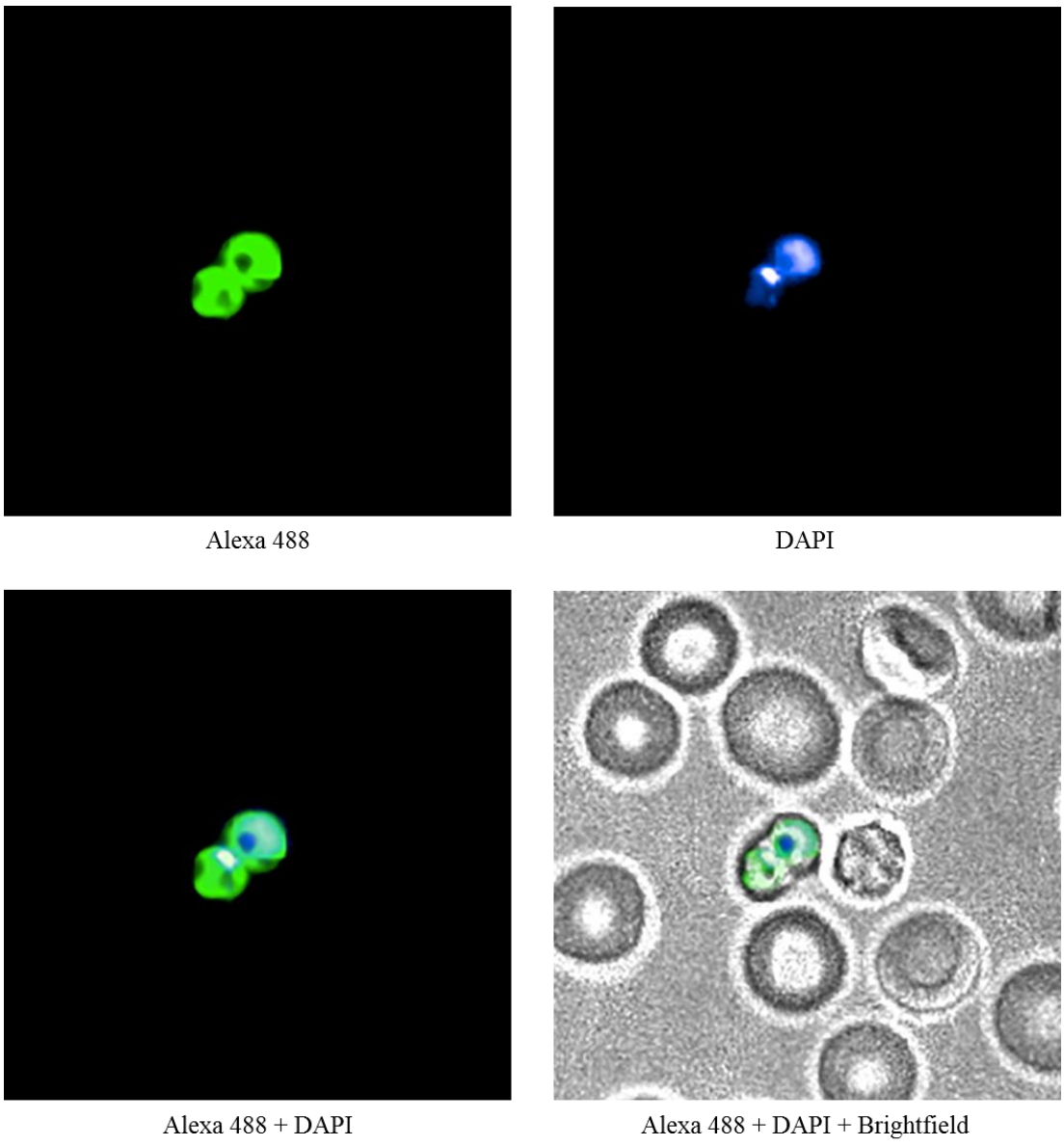

Figure 3.7. Images to show localisation of PAL probe in two trophozoite parasites within one erythrocyte (double invasion of one erythrocyte). Alexa 488 dye allows visualisation of the Alexa dye clicked onto PAL probe, DAPI allows visualisation of parasite DNA, and Brightfield allows simple visualisation of cells.

The presence of PAL probe across these different stages of the intraerythrocytic parasitic life cycle indicates that its target protein may be present in all of these stages, a favourable characteristic of a novel antimalarial series due to the increased probability of a fast killing rate profile and parasite death. Literature reports have shown that 1,832 proteins are present across all stages of the intraerythrocytic cycle, while 935 show significant changes in expression levels during these developmental

stages (See **Section 1.3 – The Functions of Major Protein Families Across the Parasite Lifecycle**).[15] The current study indicates that it is possible to capture proteins from across these different stages, thus maximising the probability of identifying the appropriate target protein.

The success of these live imaging experiments provided invaluable information that was used in the design of photoaffinity labelling experiments for target identification, described in more detail in the next section (**Section 3.4 – Considerations in the Design of an Appropriate Experimental Procedure for Photoaffinity Labelling in Live *P. falciparum* Parasites**). The imaging experiments provided support that 1 hour incubation times and 10 minute UV irradiation times were sufficient for the successful binding and crosslinking of PAL probe. Although these times were predicted to be sufficient on consultation of the literature and previous experience within our own laboratories,[128,178] it was pleasing to have evidence that these timings are appropriate for the specific PAL probes synthesised in this work. The fact that the imaging experiments also showed that the PAL probe accumulates at its target within the live parasites and not within the erythrocytic cytoplasm or membrane also provided confidence that even if the parasites were isolated from their host erythrocytes, we would not be restricting our ability to identify the target proteins of this series. This was of significance when attempting different methods for PAL for target identification within live malaria parasites (see **Section 3.4.2 – The Design of an Experimental Workflow for Photoaffinity Labelling for Target Identification in Live *P. falciparum* Parasites**).

3.4 Considerations in the Design of an Appropriate Experimental Procedure for Photoaffinity Labelling in Live *P. falciparum* Parasites

With evidence that photoreactive probe (**68**) was suitable for use in PAL experiments using *P. falciparum* cultures (see **Section 3.3 – Assessments of Suitability of Photoaffinity Probes (68), (69), and (94) for Use in Photoaffinity Labelling Experiments in Live *P. falciparum* Parasites**), attention turned to the design of a photoaffinity labelling assay for target identification. It was decided that using

standard protocols for photoaffinity labelling as previously used in our laboratories would provide suitable guidelines for buffer and lysis conditions.[167] However, photoaffinity labelling specifically in live *P. falciparum* parasites had never been performed previously in our laboratories, and so we were faced with a number of caveats as a result of culture handling and the complex parasite lifecycle. This led to a number of challenges needing to be addressed. These included considerations of the level of parasitaemia and amount of culture required for isolation of sufficient parasite protein, the proportion of parasites in different stages of the intraerythrocytic life cycle, and the actual assay workflow itself taking into account the presence of two cellular membranes (that of the erythrocytes and that of the parasites).

3.4.1 The Determination of Required Parasitaemia and Culture Volumes for Isolation of Sufficient Parasite Protein

Using the recommended buffer and lysis conditions for photoaffinity experiments meant that the amount of protein that could be extracted from the *P. falc* cultures was unknown. A crucial initial step in designing the photoaffinity labelling assay therefore involved determining the volume of culture needed in order to isolate sufficient parasite protein for pull down experiments. For pull down experiments and mass spectrometry analysis using the standard techniques in our laboratories, previous experience suggested that approximately 1 mg of parasite protein per data point would be sufficient for successful protein identification.[167]

In order to determine the amount of parasite protein that can be isolated from a *P. falc* culture treated with our desired buffers and lysis conditions, an experiment was designed using a Bradford assay for protein determination (see **Chapter 5 – Experimental**).[200] Using this experiment, it was possible to determine the amount of isolatable protein content from different volumes of *P. falciparum* culture at a parasitaemia of P10% using our photoaffinity labelling solutions and conditions (Table 3.2).

	Sample	mg/mL	Volume (µL)	Protein mass isolated (mg)
1	4 mL	0.06	250	0.02
2	8 mL	0.71	250	0.18
3	12 mL	1.26	250	0.32
4	26 mL	2.45	250	0.61

Table 3.2. Data showing the amount of protein isolated from different volumes of *P. falciparum* culture at P10%, using our photoaffinity labelling solutions and conditions.

The data indicates that even the highest volume of *P. falciparum* culture (26 mL) only afforded 0.61 mg of isolated protein content. This falls short of the target of 1 mg, and suggested that more than 26 mL of culture per data point would be necessary to obtain the required protein amount using a culture of the same composition. This was considered a difficulty, due to limitations on availability of human erythrocytes for use in these experiments, as well as the difficulties in manual handling of such large volumes of culture.

In considering how to overcome this issue, it was noted that the composition of the culture used in this Bradford assay consisted of 67% ring stage parasites, 32% trophozoites, and 1% schizonts. A photo of a representative *P. falc* culture of P3% and H2% is shown in Figure 3.8.

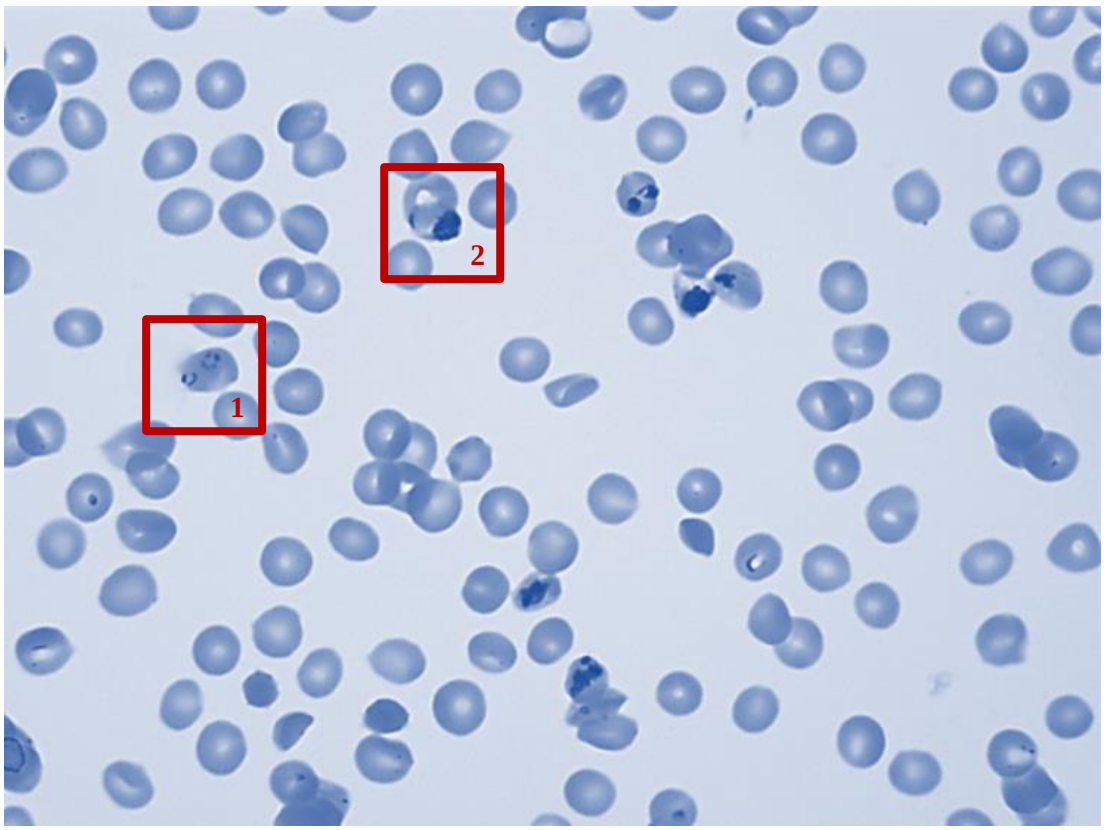

Figure 3.8. Image of a blood smear of *P. falciparum* 3D7A strain stained with Giemsa dye. Red box 1 indicates a red blood cell infected with two ring stage parasites, while red box 2 indicates a red blood cell infected with a late stage trophozoite.

This image highlights how the composition of *P. falc* cultures can be analysed, which was done when planning how to overcome the discussed issues of protein content. Firstly, the culture, obtained through standard techniques, is asynchronous (asexual stages from across the intraerythrocytic lifecycle of the parasite are present). This is generally observed for *in vitro* cultures (and was observed for the culture used in the Bradford assay) despite a high level of synchrony seen in the human host.[201,202] Secondly, the ring stage parasites are significantly smaller than the late stage trophozoites indicating a potential low return on isolated protein content in a *P. falc* culture consisting mainly of ring stage parasites. Manipulation of the *P. falc* culture composition in terms of percentage parasitaemia as well as percentage of rings and trophozoites was seen as a potential method for the preparation of cultures containing sufficient amounts of parasite protein. Considering the fact that the culture used in the Bradford assay was mainly ring stage parasites, it was thought that higher protein

amounts could be isolated from a culture of the same volume and P% but with a higher proportion of late stage parasites. However, an asynchronous culture was required in order to increase the chances of capturing all target proteins across the parasite intraerythrocytic lifecycle. Therefore, a culture with a higher percentage of trophozoites than rings, yet still with some ring stages present, was considered desirable in order to provide sufficient amounts of protein for effective pull down experiments.

Manipulation of the composition of malaria cultures can be aided through use of the sorbitol synchronisation protocol.[203] Addition of sorbitol solution and incubation triggers the lysis of erythrocytes infected with late stage parasites while leaving uninfected erythrocytes and those infected with early stage parasites undamaged, resulting in a highly synchronised culture of early stage ring parasites. This procedure is facilitated by the difference in permeability of erythrocytes hosting parasites at different stages of development, as a result of structural changes in the erythrocyte membrane induced by the parasite. Cells that are highly permeable to sorbitol (containing trophozoites or schizonts) take up sorbitol more readily than those of lower permeability (containing ring stages). The resultant swell and osmotic shock leads to cell death of the select stages of the parasite.[12] Cultures treated with this protocol maintain their synchrony for 2 – 3 lifecycles, after which asynchrony starts to develop.[204] This was identified as a suitable method for the manipulation of *P. falc* cultures in order to obtain the desired cultures with a high percentage of late stage parasites, by sorbitol synchronisation followed by further incubation of the cultures to encourage growth from the ring stages to their trophozoite stages. Allowing some asynchrony to be reintroduced would ensure the presence of some ring stage parasites, required due to reasons previously highlighted. Growth of the culture, sorbitol synchronisation, and maintenance for a further 2 – 3 lifecyles was therefore envisaged to provide the desired composition.

It was decided that the photoaffinity labelling assay would be carried out on a *P. falciparum* culture of high parasitaemia (~P10%), similar to that used for the Bradford assay, with a high percentage of late stage parasites, and that ~25 mL of culture would be used per data point. With this composition of culture and this volume, it was

reasoned that it would be possible to access sufficient quantities of isolated parasite protein for photoaffinity labelling pull down experiments, whilst taking into account the limitations on availability of human erythrocytes for these experiments, as well as difficulties in the handling of such large volumes of culture.

3.4.2 The Design of an Experimental Workflow for Photoaffinity Labelling for Target Identification in Live *P. falciparum* Parasites

Having determined the desired parameters for the *P. falciparum* cultures to be used in photoaffinity labelling experiments, the workflow for an appropriate assay was next addressed. As previously discussed, PAL probe (**68**) was identified as the most suitable probe for use in these experiments for target identification of the quinazolinamine antimalarial series. As described in the introduction (**Section 1.6 – Target Identification in Antimalarial Drug Discovery**), it is necessary to have a competitor compound in order to differentiate between background captured proteins and proteins of significance. The parent quinazolinamine compound (**2**) was used as the competitor for PAL probe (**68**) (Figure 3.9). This compound provided the control required for validation of results. Samples with no added competitor provide the baseline background information, whilst samples with added competitor are used to compare to this for analysis of significant results.

P. falciparum cultures were treated as described in the previous section, with growth carried out over 10 days (see **Chapter 5 – Experimental**), and with volumes used that allowed for 25 mL per data point. Parasitaemia had reached 6% after this time, which was lower than desired. However, due to the use of a sorbitol synchronisation after 3 days, the culture consisted of 75% mature forms and 25% ring stages, a favourable ratio. The culture was used at this composition, with the expectation that the higher proportion of mature forms would provide the added protein content needed.

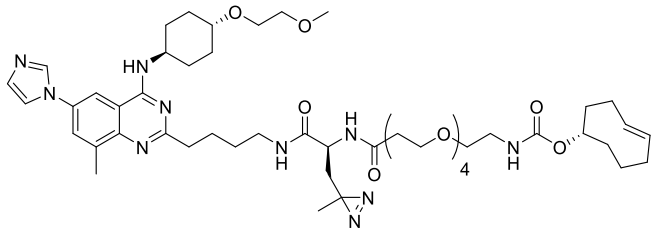

68

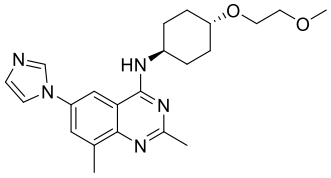

2

Figure 3.9. PAL probe (68) and related competitor compound (2) for photoaffinity labelling experiments and target identification of the antimalarial quinazolinamine series.

In the first steps of the assay protocol, incubation of the PAL probe solution with *P. falc* culture is carried out to allow for affinity binding between probe and target proteins. Three different treatment conditions of the *P. falc* cultures were used. The first of these was the treatment of culture with a solution of PAL probe only in DMSO (providing the control sample). The second was treatment of a separate sample of culture with PAL probe plus addition of a low concentration of competitor in DMSO, and the third was treatment with PAL probe plus addition of a high concentration of competitor in DMSO. A comparison of these three samples for PAL probe (**68**) would allow for identification of target proteins through the observation of a reduction in protein isolation as a result of addition of the higher concentrations of competitor compound (Figure 3.10).

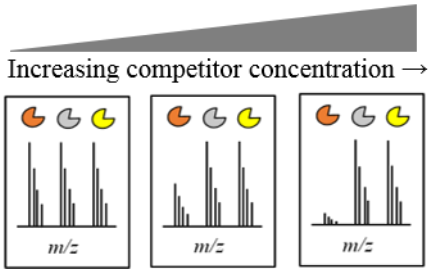

Figure 3.10. Diagram to indicate how addition of a competitor compound can be used to differentiate between background and proteins of significance. In this case, the orange protein is the target protein whilst the grey and yellow proteins are background proteins, captured as a result of non-specific binding. On addition of increasing concentrations of competitor, the amount of orange protein that is isolated is reduced, while the amount of grey and yellow protein remains constant.

When designing the subsequent steps of the assay, guidance was taken from the only report found for which photoaffinity labelling for target identification in malaria parasites was described in the literature, by Brunner *et al*.[125] (first discussed in **Section 1.6.4.3 – Chemical Probes for Use in Photoaffinity Labelling**). Two different methods were ultimately tested for a comparison of their ability to provide significant results in our hands. The first method (Method A) used the drug-treated malaria culture directly in UV irradiation steps (Figure 3.11).

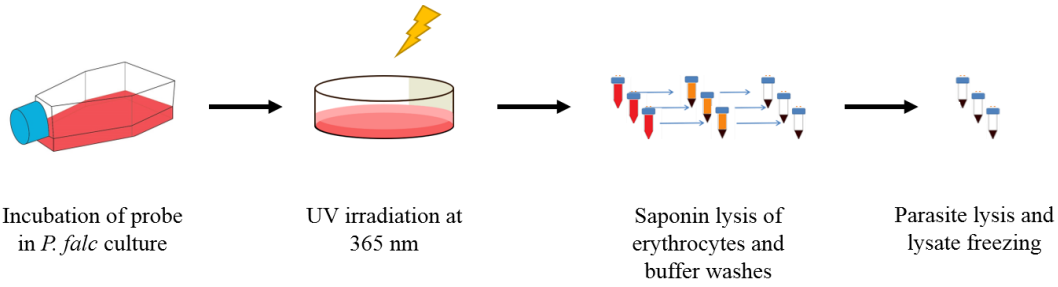

Figure 3.11. Workflow for Method A for photoaffinity labelling in live *P. falciparum* parasites.

Method A started with the growth of the appropriate *P. falciparum* culture, which was then incubated with the relevant PAL probe and competitor solution for 1 hour (which was determined to be suitable in imaging experiments described in **Section 3.3.3 – Fluorescence Imaging in Live *P. falciparum* Parasites**) using the treatment conditions described for competition experiments. The culture samples were then transferred to petri-dishes, placed in a UV microwave, and irradiated for 10 minutes at

365 nm on ice, in order to avoid an increase in temperature and potential damage to biomolecules. Each sample was collected and saponin was used to lyse the host erythrocytes, and isolate the pellets of *P. falciparum* parasites. These parasites were subsequently lysed using a parasite lysis buffer, and protein content was determined using a Bradford assay (Table 3.3).[200] The supernatants were frozen and stored at – 80 °C ready for shipment to Cellzome for pull down experiments carried out by colleagues elsewhere in our laboratories.[167]

Method A was considered to provide a suitable workflow for photoaffinity labelling in live *P. falc* parasites for target identification studies due to the ability to trigger the covalent cross-linking between probe and protein within a biologically relevant disease setting (that of the parasite living in its host erythrocyte). However, limitations of this technique included the potential for diminished cross-linking efficiency as a result of interference due to absorption by haemoglobin and thus poor radiation penetration into the parasite.[125] As a result, Method B, in which UV irradiation was carried out on isolated parasites, was also used as an attempt to overcome these potential issues (Figure 3.12). Due to the success of the imaging experiments (see **Section 3.3.3 – Fluorescence Imaging in Live *P. falciparum* Parasites**) which indicated that the probe accumulates inside the parasite, we were confident that in isolating the parasites from their host red blood cells we would not exclude the target proteins.

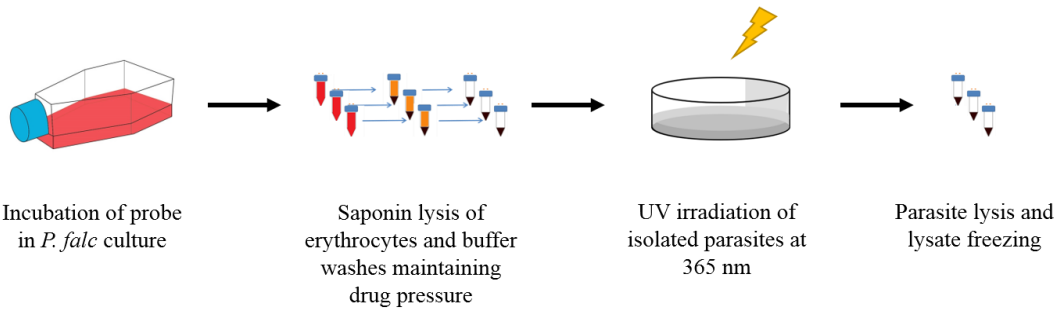

Figure 3.12. Workflow for Method B for photoaffinity labelling in live *P. falciparum* parasites.

Similarly to Method A, Method B started with the growth of the appropriate *P. falc* culture followed by incubation with the relevant PAL probe and competitor for 1 hour,

under the treatment conditions described for competition experiments. Each sample was then treated with saponin for erythrocyte lysis and the isolated parasites were UV irradiated for 10 minutes on ice. The parasites were then lysed using the parasite lysis buffer, and the protein content in the supernatant was determined using a Bradford assay (Table 3.4).[200] Supernatants were frozen and stored at – 80 °C ready for shipment to Cellzome.

Method A: PAL in *P. falc* cultures		
	Sample	**Protein mass/mg**
1A	1 µM PAL Probe (**68**) + DMSO	0.79
2A	1 µM PAL Probe (**68**) + 5 µM (**2**)	0.72
3A	1 µM PAL Probe (**68**) + 0.5 µM (**2**)	0.90

Table 3.3. Protein content isolated for each sample treated *via* Method A.

Method B: PAL in *P. falc* isolated parasites		
	Sample	**Protein mass/mg**
1B	1 µM PAL Probe (**68**) + DMSO	0.65
2B	1 µM PAL Probe (**68**) + 5 µM (**2**)	0.64
3B	1 µM PAL Probe (**68**) + 0.5 µM (**2**)	0.59

Table 3.4. Protein content isolated for each sample treated *via* Method B.

As can be noted from Tables 3.3 and 3.4, the protein content isolated for each sample fell short of the 1 mg target, although these samples were still progressed through the pull down and analysis steps. It appeared that Method B afforded less protein content per sample when compared to Method A, although the amount of undesired human host cell protein content in each of the samples compared with parasitic protein content was unknown and should be taken into account when analysing this difference. The low isolated protein content highlights one of the potential limitations of the photoaffinity labelling assay for target identification. The difficulties in growing high parasitaemia cultures (in terms of time and efficacy) make the PAL approach labour intensive, and perhaps limit the potential for a more high-throughput application.

Colleagues at Cellzome performed an affinity enrichment of the thawed lysate samples, through immobilisation of the probe-protein complex onto agarose beads *via*

an iEDDA reaction with tetrazine-derivatised biotin.[205,206] The beads were then extensively washed with appropriate buffers, before an on-bead proteolytic digest of the remaining captured proteins was performed using buffer containing trypsin. The resulting peptide components were analysed by LCMS/MS using tandem mass tag (TMT) experiments for analysis of the abundance of proteins in each treated sample (see **Section 1.6.4 – Chemoproteomic Techniques for Target Identification**).

3.5 Protein Targets Identified by the Photoaffinity Labelling Approach

Across all PAL experiments in this current study, 344 proteins were captured and identified *via* Method A, in which infected erythrocytes were UV irradiated, and 448 proteins were captured and identified *via* Method B, in which isolated parasites were UV irradiated. However, on analysis of the effect of the competitor parent compound (**2**) these numbers were significantly reduced, thus allowing differentiation between background captured proteins and captured proteins of potential significance. Results were analysed through an assessment of the fold changes in protein content isolation when compared to the control sample in which no competitor was added, which was set at a value of 1.

3.5.1 Identified Proteins Captured by Quinazolinamine Photoaffinity Probe (68)

The captured protein targets of quinazolinamine chemical probe (**68**), for which competition was observed, are indicated in Table 3.5.

Quinazolinamine Probe (68)					
Protein Name	Protein ID (new/old)	Method A (**2**) 5 µM	(**2**) 0.5 µM	Method B (**2**) 5 µM	(**2**) 0.5 µM
Apicomplexan amino acid transporter ApiAT2, putative	PF3D7_0914700/ PFI0720w	0.42	0.62	0.41	1.04
Equilibrative Nucleoside transporter 1, ENT1	PF3D7_1347200/ PF13_0252	0.45	0.81	0.41	1.09
40S ribosomal protein S8e, putative	PF3D7_1408600/ PF14_0083	0.77	0.98	0.92	1.29

Table 3.5. Table detailing the proteins captured by quinazolinamine probe (68) for which competition was observed, with numbers indicating fold changes in protein abundance on capture as a result of addition of competitor compound (2) and relative to a control in which no competitor was added (set to 1). Colours are used to highlight significant fold changes. Darker colours indicate a fold change greater than 0.5, whilst lighter colours indicate a more moderate fold change between 0.5 and 0.9.

As outlined in the table, a dose-dependent competition was observed for three proteins captured by photoaffinity probe (**68**), with two of these showing significant competition, as indicated by the colour scheme. All three proteins were captured in both Method A and Method B, although interestingly only the dose-dependent competition for 40S ribosomal protein S8e[207] was seen in Method A. Whether this shows non-reproducibility of this result and thus invalidates it, or whether it shows the superiority of Method A for target identification is currently unknown. However, the capture and dose-dependent competition seen for both the apicomplexan amino acid transporter, ApiAT2 (also known as major facilitator superfamily-related transporter, *Pf*MFR4),[208] and the equilibrative nucleoside transporter 1, ENT1,[209] in both Method A and Method B suggest a certain reproducibility, and provide evidence for these proteins being significant in the biological processes of the quinazolinamine compound (**2**). A discussion of each of the captured proteins follows.

1. Apicomplexan amino acid transporter, PfApiAT2, putative (PF3D7_0914700 and/or PFI0720w)

A selection of 10 unique peptides obtained from proteolysis were used to identify *Pf*ApiAT2 from mass spectrometry analysis as one of the captured target proteins

using Method A, whilst 12 unique peptides were found using Method B. This relatively high number of unique peptides indicates that this result is most likely reproducible.

Membrane transport proteins transfer compounds across biological membranes, playing a crucial physiological role in nutrient uptake, waste disposal (including drug disposal), metabolite transport, and the generation and maintenance of an electrochemical gradient.[210] Malaria parasites belong to the family of apicomplexan parasites: parasites that exhibit an intracellular lifecycle and that must scavenge essential nutrients including amino acids from their hosts in order to survive.[211,212] The direct uptake of these nutrients is presumed to be performed by transporters located in the membranes of the intracellular stages, although these proteins are poorly understood. However, the multi-compartment nature of the malaria parasite (due to the host cell membrane, the parasitophorous vacuole membrane, and the plasma membrane of the parasite itself) means that transporters play a key role in growth, survival, and disease propagation.[213] Indeed, membrane transport proteins are central to the blood stage proliferation of the malaria parasite through the uptake of nutrients such as pantothenic acid (a precursor of coenzyme A, crucial in metabolism)[214] or isoleucine (an amino acid not present in human haemoglobin but that is required in protein synthesis),[215] and through developing drug resistance, such as parasite resistance to chloroquine as a result of the chloroquine resistance transporter (*Pf*CRT).[210]

The *P. falciparum* apicomplexan amino acid transporter, *Pf*ApiAT2 (encoded by the PF3D7_0914700 gene, otherwise known as PFI0720w), has only recently been named as such, in February 2019.[212] Historically in the literature, this transporter has also been called the major facilitator superfamily-related transporter 4 (*Pf*MFR4), and identified as a member of the Novel Putative Transporter (NPT) family.[208,216] NPTs are predicted to contain ~12 transmembrane domains, split into 2 sets of 6 domains separated by a hydrophilic loop, and with a signature sequence between domains 2 and 3 used as a method for classifying these proteins (Figure 3.13).[211] The *Pf*ApiAT2 protein itself is predicted to contain 12 transmembrane domains, and is made up of 516 amino acids.[217]

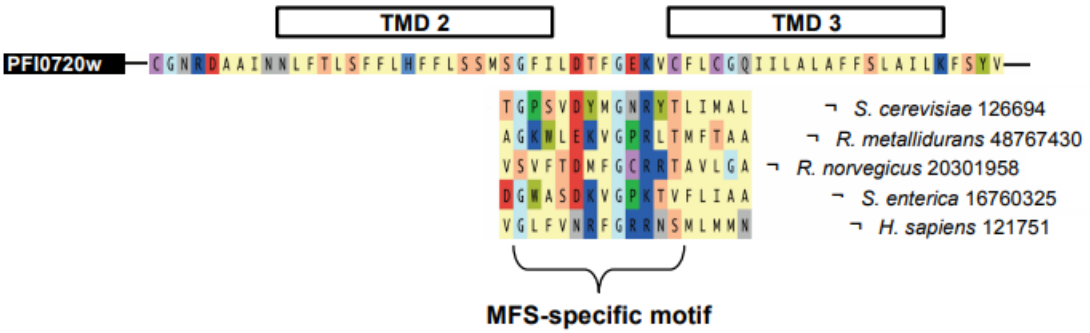

Figure 3.13. The sequence alignment of the *Pf*ApiAT2 protein between its transmembrane domains (TMDs) 2 and 3. For comparison, major facilitator superfamily-specific motifs from a range of known and putative proteins are also presented, with their NCBI accession (gi) number quoted. Residues are shaded as follows: positively charged, blue; negatively charged, red; hydroxyl, orange; amido, grey; proline, green; cysteine, purple; histidine, mid blue; glycine, light blue; tryptophan and tyrosine, olive green; remaining nonpolar, yellow. This image has been adapted from *Martin et al*.[212]

The *Pf*ApiAT2 protein is expressed across all stages of the intraerythrocytic lifecycle,[15] but is the most highly expressed 32 hours after initial parasite invasion of the host red blood cell, during the trophozoite growth stage.[217] The expression of the relevant gene from early ring stages to late schizonts suggests that the protein plays an important role in the growth and survival of the parasite.[217] The protein is localised to both the parasitophorous digestive vacuole as well as the parasite plasma membrane, and while its exact substrate remains unknown, it is believed that the protein contributes to haemoglobin catabolism either by directly exporting haemoglobin-derived proteins or indirectly maintaining the parasite homeostasis.[218] Despite the limited literature on elucidating the exact transport function of this protein, a number of reports refer to its presence and nature, or to close homologues in similar parasitic species.

The *Pf*ApiAT2 protein was identified as one of three protein targets of the potent antimalarial compound known as Torin 2 (Figure 3.14), along with phosphoribosylpyrophosphate synthetase (PF3D7_1325100) and aspartate carbamoyltransferase (PF3D7_1344800).[219]

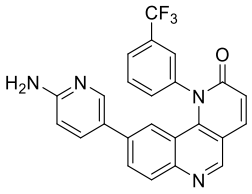

Figure 3.14. Structure of antimalarial Torin 2.[219]

Torin 2 is active not only against the asexual blood stages of the *P. falciparum* parasite, but also against the liver stage parasites[220] and the asexual gametocyte stages.[219] The compound has also been shown to completely block oocyst formation in infected mosquitos.[219] In a separate yet consistent literature report, the knockdown of the *Pf*ApiAT2 gene in mosquito-based parasites led to normal colonization of parasites within the mosquito gut but total attenuation of oocsyt development and thus sporozoite formation, suggesting this protein may be the reason for the transmission blocking effect.[210] In literature studies using *Plasmodium berghei*, Torin 2 treatment of infected hepatocytes was shown to lead to dramatic mislocalisation of proteins known to preside within the parasitophorous vacuole membrane (PVM), such as upregulated in infectious sporozoites gene 4 (UIS4) and exported protein 1 (EXP1).[220] This implies that Torin 2 may act by altering the localisation of proteins usually resident in the PVM, at least in the liver stages of the parasite.[220] These data make Torin 2 a promising compound in the development of a drug that not only treats the symptoms of malaria but that could be used in prophylactic and transmission-blocking treatments. Should these characteristics be attributed to the *Pf*ApiAT2 transporter protein, it suggests the protein can be exploited for the development of a potent curative antimalarial medicine with a novel mechanism of action. This provides exciting potential for the current series of quinazolinamine antimalarials, with *Pf*ApiAT2 being one of the captured proteins from the photoaffinity target identification studies. In addition, the potential toxicity of Torin 2 in mammalian cells was also assessed by treating HepG2 cells with high concentrations of the drug, with only partial cytotoxicity observed at the highest tested concentration (46 µM).[219] This suggests the targeting of *Pf*ApiAT2 does not trigger significant cytotoxicity issues, and is consistent with historical data obtained in our laboratories that showed low

cytotoxicity against HepG2 cells (pXC_{50} of 4.10) of our antimalarial quinazolinamine compound (**2**).

Toxoplasma gondii (the parasite causative for the infectious disease toxoplasmosis) is an experimentally tractable relative of *P. falciparum*. In a literature report, a member of the *T. gondii* NPT family from which the ApiAT2 protein comes, *Tg*NPT1 (TGME49_215490), was shown to be essential for parasite growth and survival, acting as a plasma protein membrane that transports the amino acid arginine.[212] In addition, the *Plasmodium bergei* NPT protein, *Pb*NPT1, otherwise known as the apicomplexan amino acid transporter *Pb*ApiAT8, has also been reported as an arginine transporter but with a wider substrate specificity than *Tg*NPT1, playing a major role in the crucial uptake of cationic amino acids into the intracellular malaria parasite. Similarity between *Pb*NPT1 and the *Plasmodium falciparum* orthologue, *Pf*NPT1 (PF3D7_0104800 or PFA0245W), otherwise known as *Pf*ApiAT8, provide evidence that the *Pf*NPT1 protein acts as the major arginine transporter in *Plasmodium falciparum*. Depletion of arginine in the host cell plasma as a result of the transport of this amino acid has been reported to contribute to severe clinical outcomes such as cerebral malaria, meaning the NPT1 proteins conceivably play a role in serious *Plasmodium*-induced symptoms of malaria.[212] The essential nature of these NPT proteins, in addition to the lack of human homologues of this protein family, make them attractive targets for therapeutic interventions.[211,221] These data suggest that further investigation of this protein class as a novel target for antimalarial treatment is justified and should be pursued further (Figure 3.15).

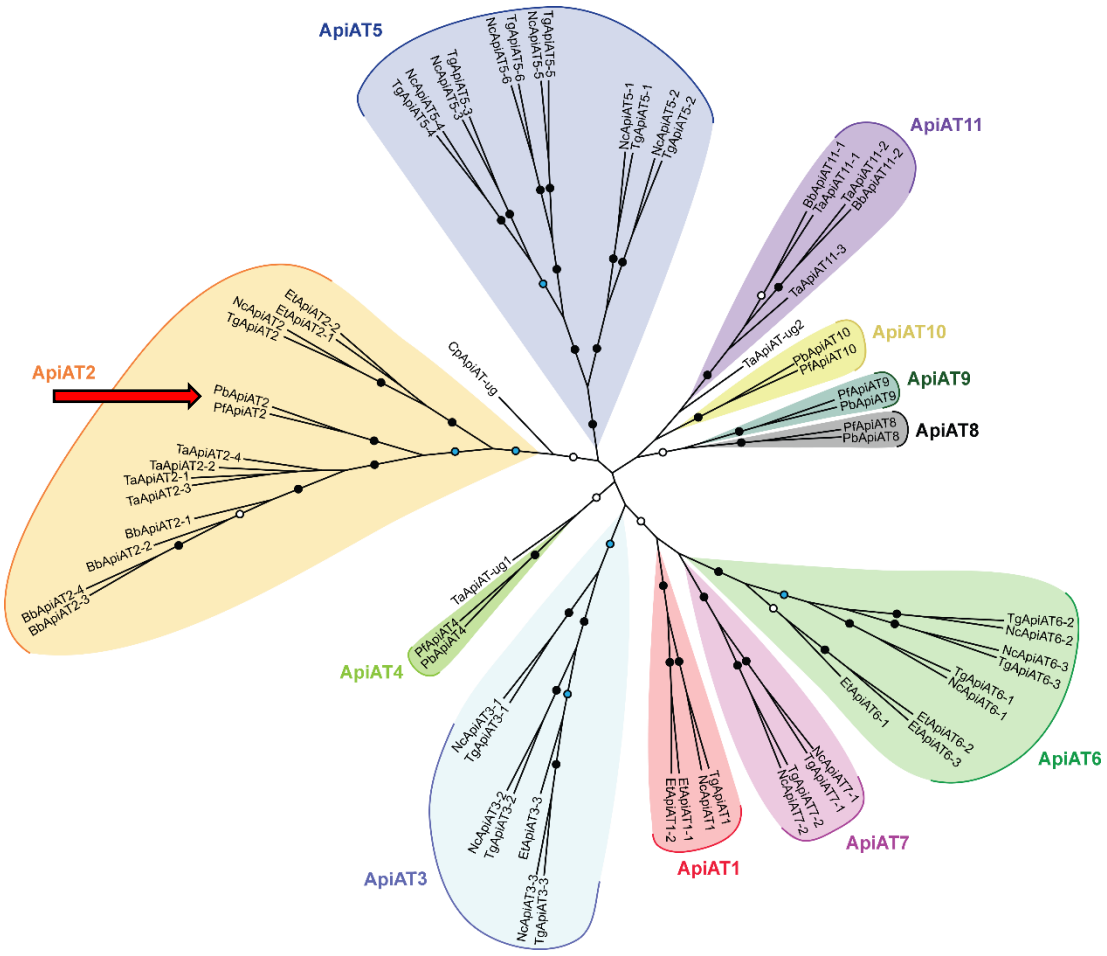

Figure 3.15. The likely phylogenetic tree of the ApiAT family of proteins, across a range of apicomplexan parasites. *Pf*ApiAT2 and *Pb*ApiAT2 are indicated by the red arrow, with clear sequence similarity. The tree was generated from analysis of sequence alignment, and is reproduced from *PLoS Pathog.* 2019, *15* (2).[212]

Whilst it is tempting to attribute the capture of *Pf*ApiAT2 to the mode of action of the antimalarial quinazolinamine (**2**), it is necessary to critically consider whether the capture of this protein could be as a result of an alternative feature of the quinazolinamine processing within the parasite, such as its transport into the parasite. For example, the human organic cation transporter 2 (OCT2/SLC22A2) contains 12 transmembrane domains like the *Pf*ApiAT2 protein, and is responsible for the absorption, distribution, and excretion of various cationic substrates in the human kidneys.[222] This function leads to the removal of these substrates into the urine, thus implicating this protein in the pharmacokinetic profiles of cationic drugs. For example, human OCT2 transports acetylsalicylate, a nonsteroidal anti-inflammatory drug; cisplatin, an anticancer drug; and metformin, an antidiabetic. In addition to these,

OCT2 transports the antimalarial drug, quinine (Figure 3.16), for which structural similarities with the antimalarial quinazolinamine (**2**) can be observed.[222] These similarities could hint at the transporter protein, *Pf*ApiAT2, acting as part of the mechanism of drug import or export for the quinazolinamine series, rather than acting as the target responsible for the mode of action of the compound. Whilst this remains to be confirmed through further studies, it should be noted that an understanding of the drug import and/or export mechanisms for antimalarials is still of importance, and can have a significant impact on understanding patient responses to drugs as a result of genetic variations of the implicated proteins amongst populations.[222]

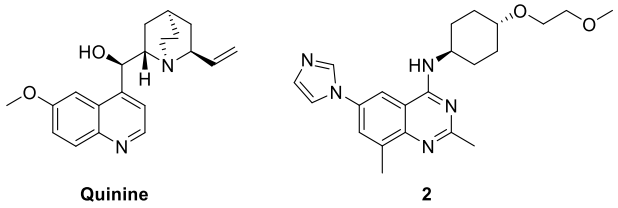

Figure 3.16. The antimalarial drug, quinine, and the antimalarial quinazolinamine (2).

2. Nucleoside transporter 1, ENT1 (PF3D7_1347200 and/or PF13_0252)

A selection of 5 unique peptides were used to identify *Pf*ENT1 from mass spectrometry analysis as one of the captured target proteins using Method A, whilst 11 unique peptides were found using Method B. These findings again indicate a good level of reproducibility in the results, and provide further evidence for the capture of the *Pf*ENT1 protein.

Similarly to *Pf*ApiAT2, captured nucleoside transporter *Pf*ENT1 is a transport protein present in the parasite plasma membrane, and expressed across all intraerythrocytic stages as well as sexual stages and sporozoites.[15,223] The function of *Pf*ENT1 has been better elucidated, however, and the protein has been identified as a low affinity, but high capacity, transporter for purine and pyrimidine nucleosides and nucleobases.[224] The *Plasmodium* parasites are autotrophic for purines, meaning they cannot synthesise them themselves but instead must salvage them from their host cells. These purines are essential for parasite survival, due to their use in RNA and DNA synthesis, as well as other cellular metabolic processes.[225] As a result, the *Pf*ENT1 protein transports

purines from the host cell cytoplasm into the parasite cytosol where they are metabolised to generate the nucleotides needed for nucleic acid synthesis, ATP generation, and intracellular signalling.[226] The majority of purines salvaged by *P. falciparum* are metabolised by a mechanism which is initiated by *Pf*ENT1-mediated transport of adenosine into the parasite cytosol, where it is metabolised by adenosine deaminase (*Pf*ADA) followed by purine nucleoside phosphorylase (*Pf*PNP) to give hypoxanthine. Hypoxanthine is then acted upon by hypoxanthine-guanine-xanthine phosphoribosyltransferase (*Pf*HGXPRT) to generate inosine 5'-monophospate (IMP), from which all other parasite purine nucleotides can be accessed (Scheme 3.12).[225,226] Unlike human cells, *Plasmodium* parasites do not contain a gene for adenosine kinase (AK) and as a result are unable to directly convert adenosine into adenosine monophosphate (AMP). The pathway outlined is thus used for generation of adenosine monophosphate (AMP), as well as adenosine diphosphate (ADP) and adenosine triphosphate (ATP), providing the energy to drive essential survival processes.[227] The essential nature of these processes has been exemplified through *Pf*ENT1-knock out studies. *Pf*ENT1-knock out strains of the *Plasmodium falciparum* parasite are not viable at physiological purine concentrations, emphasising that inhibition of this transporter protein can have profound antimalarial effects.[223,226]

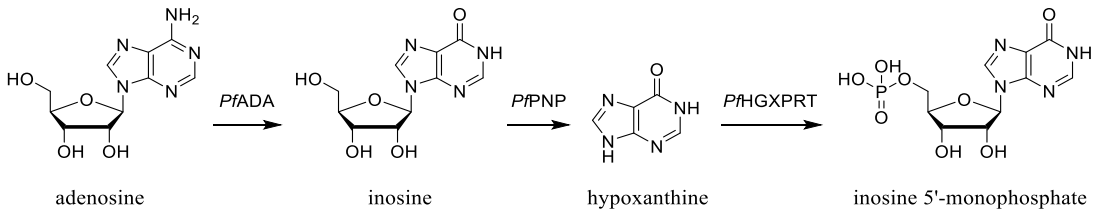

Scheme 3.12. Metabolic pathway used by *P. falc* parasites for generation of essential nucleotides.

The *Pf*ENT1 protein itself consists of 422 amino acid residues that make up 11 transmembrane domains, with the *N*-terminal region of the protein and a central hydrophilic loop being cytoplasmic (Figure 3.17).

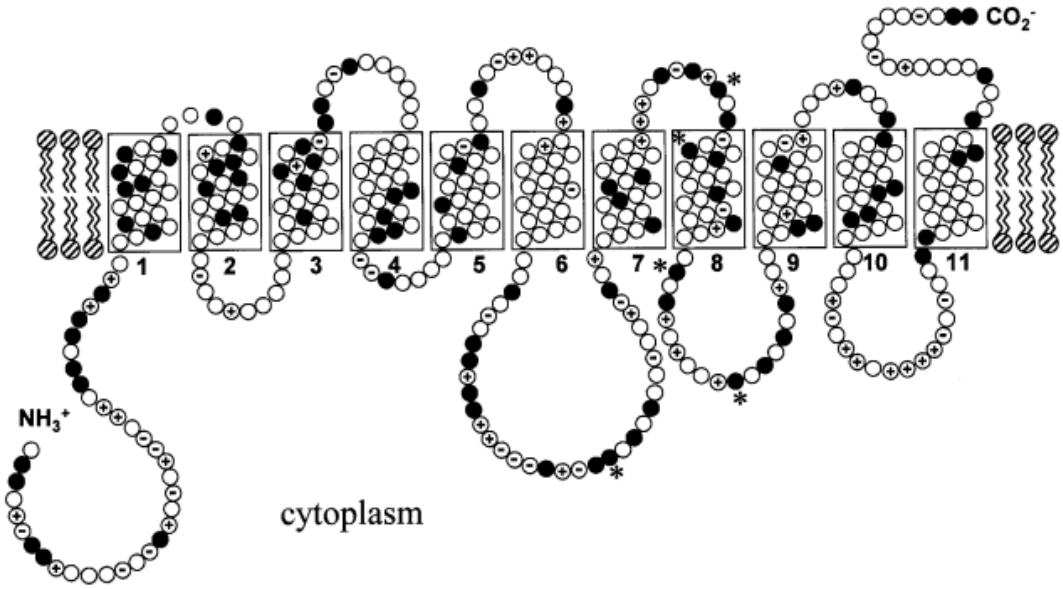

Figure 3.17. A topographical model of *Pf*ENT1, with potential membrane-specific α-helices numbered 1 – 11, basic sites (Arg, Lys, His) indicated with a +, acidic sites (Asp, Glu) indicated with a −, and uncharged residues (Ser, Thr, Gln, Asn) indicated with a black circle. This figure was originally published in *Biochem. J.* 2000, 349, 67 – 75.[224]

The presence of characteristic sequence motifs in the protein structure validates the protein as a member of the equilibrative nucleoside transporter (ENT) family, however the protein only shares 17 – 18% of its amino acid sequence with the human ENT analogue (hENT1).[223,224] This difference can be observed in the shorter extramembrane region between transmembrane domains 1 and 2 (4 amino acid residues in *Pf*ENT1 compared with 41 in hENT1), and between transmembrane domains 6 and 7 (35 amino acid residues in *Pf*ENT1 compared with 66 in hENT1).[224] These differences indicate how it is possible to develop selective inhibitors specific for the parasite transporter for use in antimalarial therapeutic treatment. Indeed, marketed drugs dipyridamole and dilazep, vasodilators used in the treatment of coronary artery disease, are inhibitors of hENT1 but not of *Pf*ENT1.[223]

In recent years, a small number of studies have attempted to identify small molecule inhibitors of the *Pf*ENT1 protein using a high throughput yeast-based growth assay.[223] The assay is based on the observation that *Saccharomyces cerevisia* yeast is sensitive to cytotoxide nucleoside analog 5-fluorouridine (5-FUrd, Figure 3.18). However, knock out yeast strains lacking the high-affinity uridine transporter FUI1 are viable.

Expression of *Pf*ENT1 in these strains restores the sensitivity to 5-fluorouridine, thus allowing selection of *Pf*ENT1 inhibitors. *Pf*ENT1-espressing FUI1-knock out yeast strains will only be viable, and therefore survive and grow, in the presence of a *Pf*ENT1 inhibitor.[223]

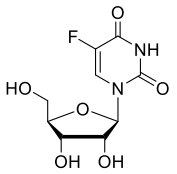

Figure 3.18. The structure of cytotoxic 5-fluorouridine (5-FUrd).

In one study reported in 2015, 64,560 compounds were screened using this assay resulting in the identification of a varied group of 171 small molecules that inhibited *Pf*ENT1. When tested against *P. falciparum* cultures, parasite growth was inhibited by these compounds.[223] Of these compounds, a number of quinazolinones (and one related pyrimidine) were identified (Figure 3.19). These compounds are perhaps of interest due to their similarity to the antimalarial quinazolinamine series investigated in this thesis. In these compounds, steric bulk is greatest at the C-2 position of the core, which provides an interesting correlation with the high potency seen for C-2 functionalised immobilised bead chemical probe (**51**) and photoaffinnity probe (**68**) (Figure 3.20).

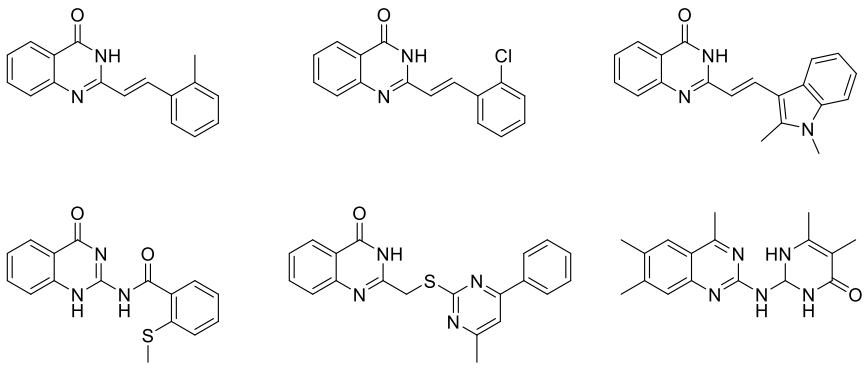

Figure 3.19. *Pf*ENT1 inhibitors identified in the literature through a yeast-based growth assay.[223]

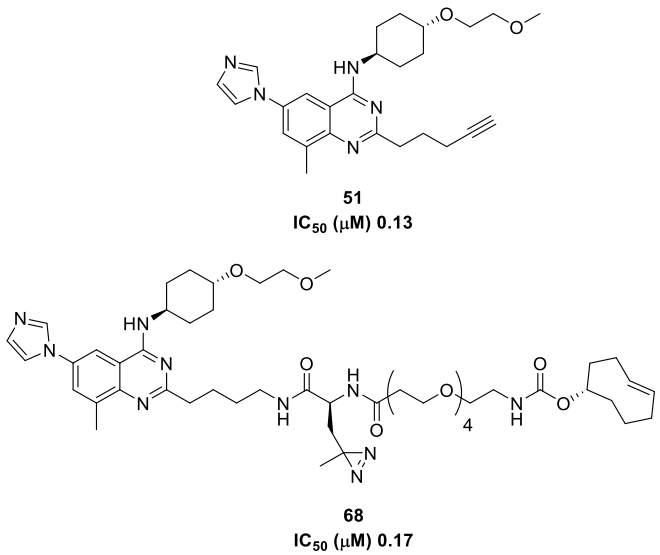

Figure 3.20. Immobilised bead probe (51) and photoaffinity probe (68), with high potency against *P. falciparum* and steric bulk at the C-2 position of the quinazolinamine core.

In a follow-up study published in 2019, GlaxoSmithKline in the United States, in collaboration with academics at the Albert Einstein College of Medicine in New York, performed a further high throughput screen of 1.8 million compounds using the yeast-based growth assay, as well as an orthogonal assay called a 'yeast kill' assay to validate their results. In the yeast kill assay, purine autotrophic yeast was grown by knock out of an essential enzyme in the purine biosynthetic pathway in yeast, ADE2. These yeast lack an endogenous adenosine transporter, and therefore cannot grow in media with adenosine as the only purine source. In contrast, ADE2-knock out yeast expressing *Pf*ENT1 can grow with only an adenosine purine source. The common factor between this assay and the yeast growth assay is inhibition of *Pf*ENT1, and thus the authors were able to identify and validate *Pf*ENT1 inhibitors from the output of these two assays.[228] Human cell toxicity and chemical properties of the hits from these assays were also assessed to identify 324 antimalarial compounds with favourable drug-like properties. The authors reported 6 of these identified *Pf*ENT1 inhibitors with improved *in vitro* potency against *P. falciparum* parasites, and improved physicochemical properties, providing promising starting points for medicinal chemistry efforts in this area (Figure 3.21).[228,229] In addition, the authors provide evidence to suggest that the vast majority of their putative *Pf*ENT1 inhibitor hits are not promiscuous, as they do

not emerge as frequent hits across other high throughput screens carried out in their laboratories.

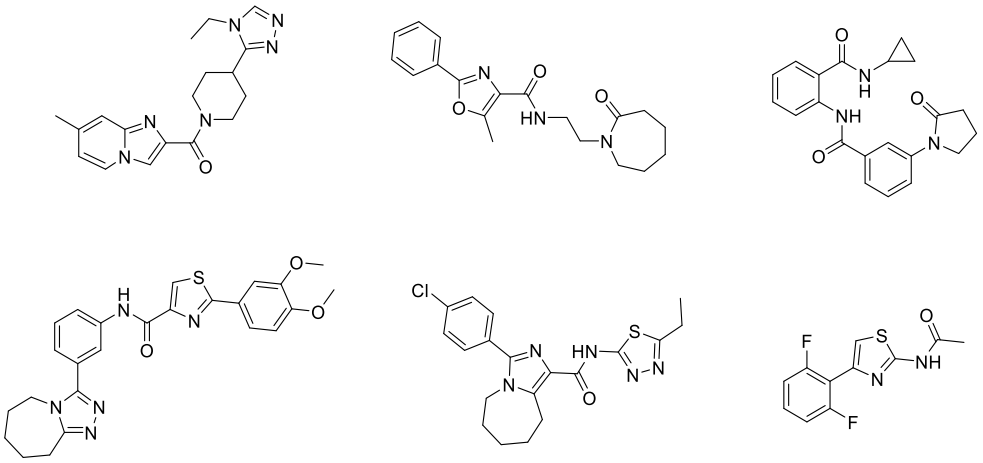

Figure 3.21. The six *Pf*ENT1 inhibitors reported by Sosa *et al.*[228]

These results provide further evidence that *Pf*ENT1 is a viable therapeutic target, with inhibitors able to provide a potentially non-toxic profile. In order to identify whether quinazolinamine compound (**2**), or indeed other similar quinazolinamines from the GSK compound library, had previously been screened in the *Pf*ENT1 yeast-based assay, a compound similarity search of our database was conducted using Helium for Excel.[230] This technique assigns a number from 0 (any compound in the search database) and 1 (exact chemical match) to describe the similarity between two compounds based on structural information such as the number and identity of atoms, bonds, rotable bonds, and the distance between chemical groups.[231,232] A similarity search of compounds in the GSK compound collection with a similarity score of greater than 0.6 when compared to the lead quinazolinamine compound (**2**) allowed us to determine that none of these compounds had been screened in the *Pf*ENT1 yeast-based assay. The direct inhibition of *Pf*ENT1 by our quinazolinamine series is thus yet to be observed, but would be a useful endeavour in the confirmation of our capture result.

The reported essential nature of the *Pf*ENT1 protein, the recent success in using this as a protein target for novel antimalarials, and a literature report indicating that the *Plasmodium vivax* analogue, *Pv*ENT1, is also a potential antimalarial target all suggest

that this is an area of antimalarial drug discovery that deserves further investigation.[233] It seems reasonable to suggest that the identification of *Pf*ENT1 as a protein target of our quinaozlinamine series should provide added impetus for further medicinal chemistry efforts around targeting this promising protein class.[234] However, as highlighted in the discussion of captured transporter *Pf*ApiAT2, whether the *Pf*ENT1 transporter is implicated in transport of the antimalarial quinazolinamine into or out of the parasite, or whether it is implicated in its mechanism of action, remains to be seen.

3. 40S ribosomal protein S8e, putative (PF3D7_1408600 and/or PF14_0083)

A selection of only 2 unique peptides were used to identify the 40S ribosomal protein S8e from mass spectrometry analysis as one of the captured target proteins using Method A, as well as using Method B. This low number of unique proteins potentially indicates less confidence in the reproducibility of this capture result. In addition to this, only limited competition was observed. This suggests a weaker interaction between this protein and our antimalarial compound than between the previously discussed captured proteins and our compound. However, an analysis of the literature precedent of this protein may still provide useful insight into an alternative possible mechanism of action of the antimalarial quinazolinamine series.

Ribosomes are macromolecular cell organelles found within archea, bacteria, and eukaryotes, consisting of one large and one small subunit per ribosome. The role of the ribosomes is to carry out translation, the process of transforming genetic information into fully synthesised proteins that demonstrate a specific phenotype.[235,236] Ribosomes perform a complex function that is essential for cellular survival, thus the targeting of ribosomal proteins provides a method for therapeutic interventions to treat disease. Indeed, drugs that target protein synthesis in the treatment of infectious diseases are ubiquitous.[237] For example, the aminoglycoside, macrolide, and lincosamide antibiotics all target the 70S prokaryotic (bacterial) ribosome, whilst the antibiotic doxycycline binds to the 30S ribosomal subunit.[238,239] Indeed, doxycycline has been clinically demonstrated to show curative effects for malaria when administered in combination with quinine, although toxicity from this combination manifests in the form of gastrointestinal issues in the largest malaria patient population, that of children and pregnant women.[239] Another promising antimalarial is

azithromycin, which has been shown to bind to the apicoplast 50S ribosomal subunit in *Plasmodium falciparum*.[239]

There is extremely limited literature around the *Plasmodium falciarum* 40S ribosomal protein S8e, with only its existence being suggested as a result of the assessment of likely orthologs between reference species (such as *S. cerevisiae*) and the query *P. falciparum* species. In one such study, sequence similarity between the *S. cerevisiae* gene YBL072C, encoding for the 40S ribosomal protein, and the PF14_0083 gene meant that this *P. falc* gene was annotated as encoding for the *P. falc* 40S ribosomal protein S8e.[237] However, the essentiality of protein synthesis and the existence of marketed drugs that target these processes suggest that an antimalarial compound acting in the same way is a viable notion. The difficulty in pursuing this line of investigation in drug discovery would most likely be obtaining sufficient selectivity between the *Plasmodium* parasitic and the human ribosomes, both being eukaryotic organisms. This difficulty is highlighted by the historical discovery of sparsomycin, initially thought to be a potential anti-tumor agent due to its binding with the eukaryotic 50S ribosomal subunit. Further investigation revealed that the compound exhibits toxicity in the form of retinopathy, due to a lack of specificity for the bacterial ribosomes over the human host ribosomes.[240]

3.6 Discussion on Results from Photoaffinity Labelling in Live Malaria Parasites

The capture of transporter proteins as potential target proteins of the antimalarial quinazolinamine series provides an interesting point for further discussion. Transporter proteins, forming part of the parasitic membrane, do not exist in their natural conformational state once parasites are lysed. This would potentially explain why the use of immobilised bead methods did not identify these membrane proteins as targets of the antimalarial quinazolinamine series, due to the use of *P. falciparum* lysates in these affinity-based experiments. Again, this could account for why the *Pf*ApiAT2 and *Pf*ENT1 proteins were not identified in the paper by Lubin *et al.* discussed in **Section 1.7 – The Identification of a Series of Antimalarial**

Quinazolinamines with a Novel Mode of Action,[128] in which lysates were also used to photoaffinity capture protein targets of the related quinazolinamine compound, BIX01294. However, in the investigations by Lubin *et al.*, the 40S ribosomal protein S8e was identified, indicating similarities in the protein capture of lysate proteins for the antimalarial quinazolinamines in their literature study and in this thesis, providing a certain validation of these results.[128] Interestingly, we did not see any capture and competition for the *P. falciparum* histone lysine methyltransferase (HKMT) proteins that have been predicted as targets of the quinazolinamine antimalarials in the literature.[148–150] This is also consistent with the paper by Lubin *et al.*, suggesting this literature hypothesis should be more vigorously scrutinised.

Transporter proteins play a key role in the growth and survival of *Plasmodium* parasites. However, only 109 transport proteins have been identified in the malaria genome, accounting for just 2.1% of the genes encoded by *P. falciparum*.[217] As a result, membrane transport proteins of the malaria parasite remain poorly understood, with their potential for use as drug targets largely unexplored. Indeed, the current view that the *Plasmodium* proteome is 'minimalistic' with regards to transporters implies that these proteins may play crucial roles, with little redundancy.[217] Compounds that inhibit a single transporter could therefore have profound effects as antimalarials, due to the lack of alternative transporters to fulfil the same role as the targeted one. The fact that membrane transport proteins rank within the top five protein targets of FDA-approved drugs (as of literature published in 2006), demonstrates the essentiality of transporters across cellular function involved in multiple different diseases, and indicates that this protein class could be worth further investigation in malaria drug discovery.[241] The capture of *Pf*ApiAT2 and *Pf*ENT1 as potential targets of the quinazolinamine series of antimalarials is thus an extremely interesting outcome, and provides added impetus for the scientific community to further examine these protein classes as a means to treat malaria. However, irrespective of whether transport proteins should be investigated as potential antimalarial targets for future antimalarials, whether the *Pf*ApiAT2 and *Pf*ENT1 proteins are indeed the target proteins responsible for the parasite killing profile of the quinazolinamine series remains to be confirmed and validated.

A number of questions as a result of certain observations remain unresolved. For example, the ability of the emerging antimalarial quinazolinamine series to inhibit the parasitic heme detoxification pathway, through blocking heme polymerisation, first discussed in **Section 1.7 – The Identification of a Series of Antimalarial Quinazolinamines with a Novel Mode of Action**, remains unexplained. The *in vitro* assay in which this ability is assessed is conducted using *P. falciparum* lysates, thus the membrane proteins *Pf*ApiAT2 and *Pf*ENT1 are disrupted and cannot be the cause of the effect observed.[146] This result reveals that the quinazolinamine series may also be targeting a protein implicated in this detoxification pathway that has not been captured during these photoaffinity labelling experiments. It is recognised, however, that the quinazolinamine series most likely demonstrates polypharmacology and that a combination of targets may be causing its potent antimalarial effects.[128] These targets may include the *Pf*ApiAT2 and *Pf*ENT1 proteins as well as one or more targets present in the parasitic lysates. This is a desirable characteristic, and although a full understanding of these processes has not yet been demonstrated, our results support the hypothesis that quinazolinamine-resistant strains will be hindered in their development as a result of polypharmacology. Alternatively, because the heme polymerisation assay is carried out *in vitro*, its results may not be directly translatable to *in vivo* investigations.

Should the *Pf*ApiAT2 and *Pf*ENT1 proteins provide the mechanism of drug transport rather than the mechanism of drug action, it suggests that the 1 hour incubation time used in the photoaffinity labelling assay protocol may not not sufficient to allow adequate diffusion of the antimalarial compound to its target site. If we analyse the killing rate profile for the quinazolinamine probe (**68**), it can be seen that after 1 hour of incubation, over 95% of parasites are still alive (Graph 3.2). This could indicate that the majority of quinazolinamine compound does not reach its target site after this time period. It is therefore proposed that the incubation time required before successful UV crosslinking between a photoreactive probe and its binding site can be achieved may be after a period of time that allows for further parasite death. This is something that would require further investigations through the analysis of captured proteins using photoaffinity probes after different time periods of incubation. These time periods would also vary depending on the antimalarial compound in question, due to their

differing parasite killing rate profiles. However, it is envisaged that this information might provide a more in depth profile of the mechanisms of drug transport, drug action, and drug export, and may help with the determination of the true role of the *Pf*ApiAT2 and *Pf*ENT1 transporter proteins in the antimalarial quinazolinamine biological pathways. It must be noted, however, that excessive parasite death as a result of long incubation times could actually hinder the capture of significant proteins, due to the death and rupture of parasites leading to a denaturing effect on the proteins in question.[242] The ideal incubation time for the capture of target proteins using our technique is therefore most likely to be dependent on a fine balance between allowing for sufficient probe-protein binding and limiting the amount of parasite death. This would be highly dependent on the unique antimalarial compound being tested, and as a result may present significant and time-consuming challenges.

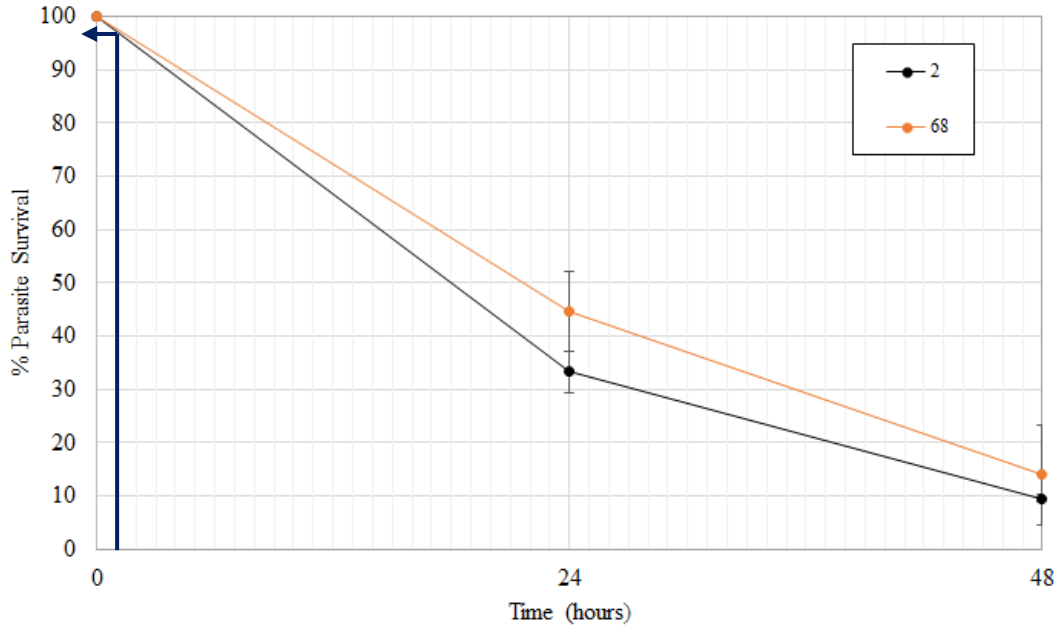

Graph 3.2. Parasite killing rate profile for antimalarial quinazolinamine probe (68) and parent compound (2). Indicated by the arrow is the percentage of parasite survival after 1 hour.

Should the *Pf*ApiAT2 and *Pf*ENT1 proteins be shown in follow-up experiments to be involved in drug transport rather than the mechanism of action of the quinazolinamine series, this knowledge could still provide a useful scientific contribution to this area of drug discovery. For example, the amino acid transporter, *Pf*AAT1 (PF3D7_0629500),

is known to transport the naturally occuring amino acid tryptophan as well as the antimalarial drug quinine. As a result, one suggested mechanism of action of quinine has been the depletion of tryptophan within the parasitic cytosol as a result of competition between the drug and the amino acid for the transporter.[243] This indicates how knowledge of drug transport can provide hypotheses for further investigations. Alternatively, transporter proteins have been heavily implicated in resistance mechanisms against antimalarial drugs. For example, the *Plasmodium falciparum* chloroquine resistance transporter (*Pf*CRT) is well known for its role in chloroquine resistance, as is the *Plasmodium falciparum* multidrug resistance protein 1 (*Pf*MDR1) which also actively translocates a number of other antimalarial drugs out of the parasite.[244] Knowledge of drug transport mechanisms is therefore crucial for improving understanding of possible mechanisms of drug resistance, and for monitoring and overcoming these.[243,245] Monitoring mutations in transporter proteins can provide explanations for resistance profiles of different *Plasmodium* parasitic strains. For example, point mutations in *Pf*MDR1 for the *P. falc* Dd2 strain have been attributed to its resistance to mefloquine in comparison to the sensitivity to mefloquine seen for the 3D7 strain. The capture of target proteins *Pf*ApiAT2 and *Pf*ENT1 is therefore of significance, regardless of whether these proteins are implicated in the mechanism of action of the quinazolinamine series or in their transport.

3.7 Chapter 3 Conclusions

The overall aim of the photoaffinity labelling investigations was to covalently capture and identify the relevant protein targets of the quinazolinamine antimalarial series represented by parent compound (**2**). This chapter reports the identification of two transporter proteins, *Pf*ApiAT2 and *Pf*ENT1, as potential protein targets of this quinazolinamine series. Specific intermediary goals were achieved in order to arrive at this conclusion. These included the design and synthesis of an appropriate photoreactive chemical probe (**68**) which showed good antimalarial potency (IC_{50} of 0.17 µM). Probe (**68**) was assessed for suitability for use in target identification studies through established techniques that included a fluorescence activated cell sorting assay to demonstrate its parasite killing rate, and to show that the moderate killing rate

profile of the parent (**2**) was conserved. Fluorescence imaging experiments provided invaluable knowledge about the localisation of probe (**68**) within the parasite, which was used in the design of two methods for photoaffinity labelling for target identification in live *P. falciparum* parasites. Method A consisted of UV irradiation and cross-linking occuring within live parasites in their host human erythrocytes, whilst Method B consisted of the isolation of live parasites from their hosts prior to UV irradiation. Both methods identified the transporter proteins, *Pf*ApiAT2 and *Pf*ENT1, as implicated in the mechanism of action of the quinazolinamine series. The capture of a larger number of proteins (448 compared to 344) using Method B suggested an improved ability to capture proteins once haemoglobin content had been reduced, a result that agrees with the result found by Brunner *et al.*[125] As a result, Method B was chosen as the preferred method for future photoaffinity labelling for antimalarial target identification experiments at GSK. The significantly reduced volumes of isolated parasites compared to the erythrocytic whole cell cultures also makes Method B preferable, as the technique is more amenable to a more high-throughput procedure.

Another aim of this thesis was to provide a comprehensive review of any captured target proteins found using the chemoproteomic techniques described. The routine affinity-based methods for target identification in *Plasmodium falciparum* lysates did not identify any significant protein targets for the quinazolinamine series. However, the identification of *Pf*ApiAT2 and *Pf*ENT1 using the more recent photoaffinity labelling technique has provided the opportunity for discussion around transporter proteins as targets for novel antimalarial medicines. Both *Pf*ApiAT2 and *Pf*ENT1 have been implicated in the literature in the transport of essential nutrients required for parasite growth. The intraerythrocytic *P. falciparum* parasites are reliant on their host human erythrocytes to supply essential nucleotides and amino acids for use in protein and DNA synthesis. Consequently, the essential nature of the *Pf*ApiAT2 and *Pf*ENT1 proteins has been demonstrated in the literature, indicating that the targeting of these protein classes could have profound antimalarial effects.[217,218,220,223,226] Should these proteins be confirmed to be the relevant protein targets of the quinazolinamine series in follow-up studies, this would quite elegantly demonstrate how their antimalarial effect is facilitated. There is, however, a possibility that the *Pf*ApiAT2 and *Pf*ENT1

proteins are implicated in the mechanism of drug transport, rather than drug action, and the potent antimalarial effect of quinazolinamine (**2**) is not actually attributable to these two proteins but to proteins in downstream biological processes. Should this be verified, the knowledge of drug transport for our quinazolinamine series still has utility in the development of a novel antimalarial. Understanding drug transport has historically been useful for the formation of further scientific hypotheses as demonstrated in the literature, as well as for contributing to the ability to understand resistance mechanims and how to overcome these.[243,245]

It is not yet possible to determine using the current data set whether the *Pf*ApiAT2 and *Pf*ENT1 proteins are the protein targets responsible for the antimalarial mechanism of action of the quinazolinamine series or whether these proteins act upstream of the protein target that is. Further investigations are required to answer this outstanding question. However, the capture of these protein targets has opened a new avenue to allow more targeted investigations into the mechanisms that surround the transport and action of our antimalarial quinazolinamine series. This study has observed that the photoaffinity labelling approach to target identification has provided results that the more established and routine affinity-based methods did not. This provides support for the future application of photoaffinity labelling for target identification in live *P. falciparum* parasites for other antimalarial series in addition to our own. These investigations have therefore contributed to the cumulative scientific knowledge around antimalarial modes of actions and how to probe these, for which there exists a pressing need for greater understanding in order to overcome the antimalarial resistance mechanisms that the *P. falciparum* parasite has developed, and is capable of developing in future.[76]

3.8 Chapter 3 Future Work

The most pertinent avenue to follow in future work for this project is the validation that the captured *Pf*ApiAT2 and *Pf*ENT1 proteins are indeed responsible for the antimalarial mechanism of action of the quinazolinamine series represented by

compound (**2**), rather than as part of the mechanisms involved in their transport. Recommendations for how this could be achieved are summarised below:

1. **Protocol adjustments:** One previously discussed hypothesis was that a longer incubation time during the initial steps of the photoaffinity labelling assay could ensure sufficient time for diffusion of probe (**68**) and parent competitor (**2**) into the parasite to reach its target binding site. Further investigations around the effects of different incubation time periods could provide valuable knowledge as to the whether the captured proteins vary across the tested time periods, thus providing insight into whether the captured *Pf*ApiAT2 and *Pf*ENT1 proteins are crucial for the antimalarial mechanism of action or whether alternative proteins also play a part.
2. **IC_{50} calculations:** In this study, three different concentrations of competitor compound were originally used (0 µM, 0.5 µM, and 5 µM in successive samples). In future iterations of this work, a greater number of samples with a wider range of competitor concentrations could be tested in order to provide the required data for IC_{50} calculations. This would be valuable for assessing the relative strength of inhibition of both *Pf*ApiAT2 and *Pf*ENT1 as well as any other proteins captured as a result of changes in the protocol as identified through the investigations discussed in point 1.
3. **Yeast-based growth and kill assays:** As discussed, GSK colleagues have published a report on the identification of *Pf*ENT1 inhibitors *via* the use of yeast-based growth and kill assays.[228] However, quinazolinamines were not screened in these investigations. In order to observe the inhibition of *Pf*ENT1 directly by quinazolinamine (**2**), future work involving the revival of the *Pf*ENT1 inhibition assays in our laboratories would be beneficial, and could provide evidence that the antimalarial effect of quinazolinamine (**2**) is due (at least in part) to *Pf*ENT1 inhibition.
4. **A replacement PI4K photoaffinity probe:** The unfortunate instability of PI4K probe (**94**) resulted in the lack of an active comparator in this study to provide evidence that the photoaffinity labelling assay itself was functional for our means. Future work could involve the synthesis of alternative PI4K photoaffinity probes to replace probe (**94**), or indeed the synthesis of alternative

photoaffinity probes with other known protein targets. This would provide additional validation of the photoaffinity labelling technique for target identification in live *P. falciparum* parasites.

Chapter 4 – An Assessment of Affinity-Based Immobilised Bead Techniques *versus* Photoaffinity Labelling Techniques in Target Identification for Malaria Drug Discovery

An interesting observation that emerges from results of the investigations in this thesis is the fact that the photoaffinity labelling technique allowed us to capture protein targets of the nascent antimalarial quinazolinamine series whereas the immobilised bead affinity-based method did not. This is an observation that is also discussed in a study by Shi *et al*, in which proteomic profiling of the kinase inhibitor dasatinib using both covalent photoaffinity probes and resin-immobilised probes found that the photoaffinity probes were much more able to access their likely intended protein targets (Figure 4.1).[242] In this study, the authors reported 84 potential Dasatinib targets identified using the Dasatinib-derived photoaffinity probe. In comparison, only 6 potential kinase targets were identified using the resin-immobilised probe.

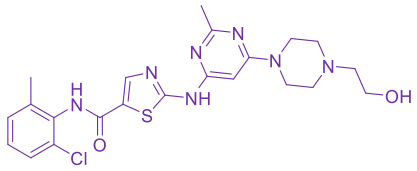

Dasatinib (BMS-354825)

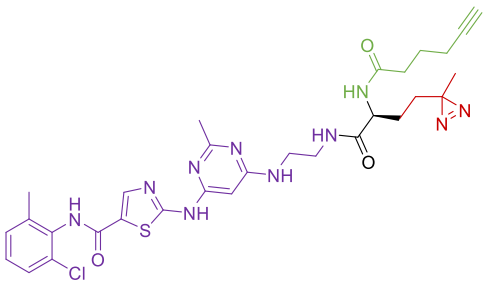

Dasatinib photoaffinity probe

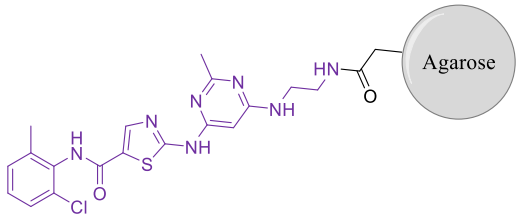

Dasatinib immobilised probe

Figure 4.1. Kinase inhibitor, Dasatinib, and the Dasatinib-based photoaffinity probe and immobilised probe used in the study by Shi *et al*,[242] with Dasatinib drug unit in purple, alkene functional handle in green, and photoreactive diazirine in red.

Despite the observations in this current study, and those of Shi *et al*,[242] direct comparisons of the photoaffinity and immobilised bead techniques are limited in the literature, and an analysis of this observation therefore aims to foster discussion of this topic.

4.1 A Direct Comparison of the Chemoproteomic Protocols Implemented in this Study

The similarities and differences of the two target identification methods as employed in this work are summarised in Table 4.1.

	Affinity-Based Technique	Photoaffinity-Based Technique
Probe potency against intraerythrocytic blood stage *P. falc* parasites	0.13 – 0.57 μM	0.17 μM
Method of capture	Affinity	Covalent
Biological sample	*P. falc* culture lysates (containing human protein content)	Live *P. falc* parasites (both in host erythrocytes and isolated)
Competitor	(**2**)	(**2**)
Immobilisation	Before protein capture	After protein capture
Protein isolation	Proteins eluted from capturing beads before proteolytic digestion	Proteins proteolytically digested on beads
Protein identification	LCMS/MS	LCMS/MS

Table 4.1. Table summarising the similarities and differences between the affinity-based and photoaffinity-based techniques for target identification used in this thesis.

In order to analyse the reasons why the photoaffinity labelling technique appeared to provide fruitful results whilst the affinity-based technque did not, we can first discount those areas where the proteomic experiments are consistent. Firstly, the potency of the chemical probes designed and used in both methods were shown to have values in the same range when tested for inhibition of the *P. falciparum* intraerythrocytic stages. Indeed, because three probes were tested in the immobilised bead assay with potencies that ranged both above and below the potency of the photoreactive chemical probe, we can assume that potency differences in the probe design were not contributing factors to the success or lack of protein target capture. In both affinity-based and photoaffinity-based methods, the quinazolinamine (**2**) was used as the competitor for competition experiments. This suggests consistency across both methods in the identification of protein targets for this particular antimalarial compound through dose-response analyses of captured proteins. Finally, LCMS/MS was used as the method of protein identification for both techniques, thus ruling this part of the protocol out of consideration when identifying reasons for differing results.

The remaining aspects as highlighted could provide insight into the observed superiority of the photoaffinity labelling technique for antimalarial target identification. A discussion of these aspects follows.

1. Method of capture

Both immobilised bead and photoaffinity labelling techniques require the initial affinity-based capture of protein targets *via* an affinity binder, in this case *via* the quinazolinamine (**2**) moiety. However, where the techniques diverge is in the subsequent steps. Photoaffinity labelling involves the covalent capture of these affinity-captured protein targets, whilst immobilised bead methods do not. Affinity interactions are facilitated by enthalpic and entropic components, which are highly dependent on the specific system in question. These components comprise factors such as binding free energy, flexibility, solvation energies, displacement of water molecules from binding sites, as well as repulsive interactions.[246] Whilst these interactions can be strong enough for effective drug action, the maximal noncovalent binding affinity between small molecules and protein binding sites has been demonstrated to plateau at around 15 kcal/mol, with the few cases of higher affinity including the biotin-avidin and biotin-streptavidin complexes.[247,248] Interactions that exceed this value have been shown to only be achieved with an element of covalent binding between drugs and protein targets, suggesting that the covalent capture in photoaffinity labelling experiments may provide a higher likelihood of success. In addition, the longer duration of capture facilitated by covalent interactions suggests that harsher purification methods can be tolerated by reducing the risk of disruption of the small molecule-protein interaction.[249] It can therefore be assumed that photoaffinity labelling provides a more effective method for protein capture in target identification studies.

2. Biological sample

The affinity-based immobilised bead assays used *P. falciparum* lysates in which to incubate the appropriate chemical probes. These lysates contained protein content from the human erythrocytes as well as the *P. falciparum* parasites (see **Chapter 5 – Experimental** for explanation of lysate collection). This is of significance, because

the parasite exports significant numbers of proteins into the erythrocytic cytoplasm which could conceivably play a role in the mechanism of action of an antimalarial drug. Whilst it was shown through fluoresence labelling experiments that the photoaffinity probe (**68**) does not target these proteins, this was unknown at the time the affinity-based experiments took place. Of concern is that this means that the actual parasitic protein content in the lysate samples is unknown. As observed in our preparation for photoaffinity labelling experiments, the parasitic protein content of *P. falciparum* cultures can be extremely low even with high volumes of culture, thus making pull down and proteomic analysis more difficult. This could be a plausible reason for the lack of target protein capture in the affinity-based methods.

In addition, the use of lysates means that membrane proteins such as the *Pf*ApiAT2 and *Pf*ENT1 proteins identified are not available for capture. The observation that the immobilised bead assays were unable to provide data for the identification of protein targets of the quinazolinamine series could therefore be explained purely on the basis of the biological sample used (lysates *versus* live parasites), should these transporter proteins be validated as the only protein targets of the quinazonlinamine (**2**). This provides another advantage for photoaffinity *versus* affinity labelling techniques: the wider range of proteins available for capture. An interesting venture would be to carry out photoaffinity labelling within the *P. falciparum* lysate samples as used in the immobilised bead assays. This could provide useful data for the discussion on whether the use of lysates or the use of affinity-based probes was the reason for the discrepancy in results between techniques.

3. Immobilisation

The affinity-based technique used in this study involved the immobilisation of the chemical probes onto solid Sepharose® beads before incubation in the relevant cell extracts. This could have a significant effect on the binding affinity of the chemical probes to their protein targets. The immobilisation of the photoaffinity-captured protein targets was only carried out after the covalent capture of the protein targets. This therefore indicates that the immobilisation step in photoaffinity labelling techniques is less likely to impede the successful capture of the appropriate protein targets compared to the affinity-based techniques. In addition, the immobilisation of

probes onto solid beads could change the mechanism of action of the chemical probe compared to the parent compound (**2**). Whilst it was possible to assess the mechanism of action of photoaffinity probe (**68**) *via* measurement of the parasite killing rate profiles, this would not be possible for the probes immobilised onto solid beads due to the need for cellular permeability. As a result, we are limited in our ability to understand whether the mode of action of immobilised probes changes compared to their parent antimalarial compound. These factors further contribute to the advantages of photoaffinity labelling over immobilised bead techniques in antimalarial target identification.

4. Protein isolation

In affinity-based immobilised bead techniques, the immobilised beads are first washed with buffer to remove any non-captured cellular proteins and to purify those captured proteins affinity-bound to the bead. An enhanced buffer is used to then disrupt the affinity interactions and isolate the captured protein targets. These are proteolytically digested to provide the peptide samples required for LCMS/MS analysis. It is feasible that the initial buffer washes could disrupt the affinity interactions between the probe and proteins should these be sufficiently weak in nature. This is possible if the immobilisation of the compound onto the beads weakens these interactions as discussed. On the other hand, should the enhanced buffer not be sufficient to disrupt these interactions, then the captured protein targets could remain bound to the bead and thus not be collected in the samples used in the LCMS/MS analysis. Both of these potential occurences would limit the ability to identify the captured protein targets. In photoaffinity labelling techniques, initial buffer washes are also used to purify the immobilised probe-protein complex during the purification steps, but due to the strong covalent bond between probe and protein the likelihood of washing away captured proteins at this point is low. The captured protein targets are then proteolytically digested whilst still immobilised onto the affinity matrix used in the purification steps. These factors overcome the potential issues that could arise using the affinity-based method, and it would be reasonable to assume that these could allow for a higher yield of isolated peptide fragments available for LCMS/MS analysis. The photoaffinity

labelling technique therefore appears to provide added advantages over the affinity-based methods.

4.2 Chapter 4 Conclusions

The side-by-side use of both affinity-based and photoaffinity-based techniques in target identification is limited in the literature, potentially as a result of the reluctance of the scientific community to report negative results. This therefore makes a direct and meaningful comparison of the overall success of each of the techniques difficult to extract. However, this study and that by Shi *et al*,[242] previously discussed in the **Chapter 4** introduction, provide evidence that there can be significant benefits of using photoaffinity labelling techniques in the place of immobilised bead techniques. Indeed, Shi *et al* advise that in future proteomic experiments, covalent probes should be used whenever possible: a conclusion which is appropriate in light of the results of this thesis. The results demonstrated in this thesis provide added evidence that photoaffinity labelling in target identification should be a more widely adopted strategy. The pertinence of our results indicates that photoaffinity labelling could have wide-reaching effects in the advancement of target identification in antimalarial drug discovery and potentially beyond.

Chapter 5 – Experimental

5.1 Synthetic Chemistry

5.1.1 General Methods

Solvents and reagents were purchased from commercial suppliers as anhydrous, and used as received unless otherwise indicated. Reactions were monitored by thin layer chromatography (TLC) or liquid chromatography-mass spectroscopy (LCMS).

5.1.2 Nuclear magnetic resonance (NMR)

NMR spectra were recorded at ambient temperature (unless otherwise stated) using standard pulse methods on a Bruker AV-400 (^{1}H = 400 MHz, ^{13}C = 101 MHz). Chemical shifts are reported in ppm and are referenced to tetramethylsilane (TMS) or the following solvent peaks: $CDCl_3$ (^{1}H = 7.27 ppm, ^{13}C = 77.00 ppm), DMSO-d_6 (^{1}H = 2.50 ppm, ^{13}C = 39.51 ppm) and MeOH-d_4 (^{1}H = 3.31 ppm, ^{13}C = 49.15 ppm). Coupling constants are quoted to the nearest 0.1 Hz, and are reported as observed using ACD NMR software. Multiplicities are given by the following abbreviations: s (singlet), d (doublet), dd (doublet of doublets), t (triplet), q (quartet), quin (quintet), sxt (sextet), m (multiplet), and br (broad). The abbreviation ‘app’ is used to indicate ‘apparent’: a signal that appears to have a certain multiplicity but that would otherwise be predicted to have a different splitting pattern, assumed to be as a result of a number of signals overlapping in the spectrum.

5.1.3 Infra-red spectroscopy (IR)

IR spectra were obtained on a Perkin Elmer Spectrum 1 machine.

5.1.4 Liquid chromatography mass spectroscopy (LCMS)

Liquid Chromatography Mass Spectroscopy (LCMS) was conducted on an Acquity UPLC CSH C18 column (50mm x 2.1mm i.d. 1.7µm packing diameter) at 40 ºC eluting with either:

Method A - 10 mM ammonium bicarbonate in water adjusted to pH 10 with ammonia solution (solvent A) and acetonitrile (solvent B); or

Method B - 0.1% v/v solution of formic acid in water (solvent A) and 0.1% v/v solution of formic acid in acetonitrile (solvent B).

The UV detection is a summed signal from wavelength of 210 nm to 350 nm. The mass spectra were recorded on a Waters ZQ spectrometer using electrospray positive and negative mode. The following elution gradients were used:

High pH modifier (Method A):

Time (min)	Flow rate (mL / min)	% A	% B
0.00	1	97	3
0.05	1	97	3
1.50	1	5	95
1.90	1	5	95
2.00	1	97	3

Formic acid modifier (Method B):

Time (min)	Flow rate (mL / min)	% A	% B
0.00	1	97	3
1.50	1	5	95
1.90	1	5	95
2.00	1	97	3

5.1.5 Mass directed auto-preparative HPLC (MDAP)

Preparative mass directed HPLC (MDAP) was conducted on an Xselect CSH C18 column (150 mm × 30 mm, 5µm packing diameter) at ambient temperature. The solvents employed were 10mM ammonium bicaronate adjusted to pH 10 with ammonia in water (solvent A) and acetonitrile (solvent B). The UV detection is a summed signal from wavelength of 210 nm to 350 nm. Mass spectra were recorded on

Waters ZQ mass spectrometer using alternate-scan positive and negative electrospray ionization. The software used was *MassLynx* 3.5 with *FractionLynx* or using equivalent alternative systems. The following elution gradient was used (High pH modifier):

Time (min)	Flow rate (mL / min)	% A	% B
0	40	70	30
1	40	70	30
20	40	15	85
20.5	40	1	99
25	40	1	99

5.1.6 High resolution mass spectroscopy (HRMS)

ESI (+) high resolution mass spectra (HRMS) were obtained on a Micromass Q-Tof 2 hybrid quadrupole time-of-flight mass spectrometer, equipped with a Z-spray interface, over a mass range of 100 – 1100 Da, with a scan time of 0.9 s and an interscan delay of 0.1 s. Reserpine was used as the external mass calibrant ($[M+H]^+$ = 609.2812 Da). The Q-Tof 2 mass spectrometer was operated in W reflectron mode to give a resolution (FWHM) of 16000-20000. Ionisation was achieved with a spray voltage of 3.2 kV, a cone voltage of 50 V, with cone and desolvation gas flows of 10-20 and 600 L/h, respectively. The source block and desolvation temperatures were maintained at 120 ºC and 250 ºC, respectively. The elemental composition was calculated using MassLynx v4.1 for the $[M+H]^+$.

An Agilent 1100 Liquid Chromatograph equipped with a model G1367A autosampler, a model G1312A binary pump, and a HP1100 model G1315B diode array detector was used. The method used was generic for all experiments. All separations were achieved using a Phenomenex Luna C18 (2) reversed phase column (100 x 2.1 mm, 3 µm particle size). Gradient elution was carried out with the mobile phases as (A) water containing 0.1% (v/v) formic acid and (B) acetonitrile containing 0.1% (v/v) formic acid. The conditions for the gradient elution were initially 5% B, increasing linearly to 100% B over 6 min, remaining at 100% B for 2.5 min then decreasing linearly to 5% B over 1 min, followed by an equilibration period of 2.5 min prior to the next

injection. The flow rate was 0.5 mL/min, temperature controlled at 35 ºC with an injection volume of between 2 to 5 µL. All samples were diluted with DMSO (99.9%) prior to LCMS analysis.

5.1.7 Purification by column chromatography

Column chromatography was conducted on a Combiflash® Rf, automated flash chromatography system, from Teledyne Isco using disposable, normal, or reverse phase, SPE Redisep or Grace cartridges (4 g to 330 g). The CombiFlash® Rf uses RFID (Radio Frequency Identification) technology to automate the setting of the parameters for purification runs and fraction collection. The system is equipped with a UV variable dual-wavelength and a Foxy® fraction collector enabling automated peak cutting, collection, and tracking.

5.1.8 Phase separators

Isolute® phase separator cartridges are fitted with a hydrophobic Teflon frit. These were used to separate organic solvent from aqueous phases under gravity.

5.1.9 Microwave

Microwave chemistry was typically performed in Biotage sealed vessels, irradiating with a Biotage Initiator™ Microwave Synthesiser.

5.1.10 Melting points

Melting points were measured on a Stuart automatic melting point apparatus, SMP40.

5.1.11 General Synthetic Procedures

General procedure for alkylation attempts of pyrazole (19)

To a microwave vial was added the detailed equivalents of 4-(4,4,5,5-tetramethyl-1,3,2-dioxaborolan-2-yl)-1*H*-pyrazole (**19**), and base (Table 2.2, reproduced from **Section 2.1.2 – The Chemical Strategy for Synthesis of Chemical Probe (3)**). The vial was capped, and evacuated and purged with N_2 before addition of a solution of the appropriate electrophilic partner in solvent. The mixture was heated to the outlined temperature for the detailed time period. Reaction outcome was assessed by LCMS analysis, and products were not isolated.

19 **20**

Entry	Reagents and Conditions	Outcome (determined by LCMS analysis)
1	Pyrazole (**19**) (1 eq.), chloroethanol (1.1 eq), Cs_2CO_3 (1 eq.), 170 °C, DMF, 18 h	No reaction
2	Pyrazole (**19**) (1 eq.), chloroethanol (1.1 eq), 1 M in THF NaHMDS (1 eq.), 100 °C, THF, 22 h[155]	12% product
3	Pyrazole (**19**) (1 eq.), chloroethanol (1.1 eq), Cs_2CO_3 (1 eq.), 100 °C, DMSO, 22 h[156]	23% product
4	Pyrazole (**19**) (1 eq.), chloroethanol (1.1 eq), NaO^{t}Bu (1 eq.), 100 °C, DMF, 22 h[157]	27% product
5	Pyrazole (**19**) (1 eq.), chloroethanol (1.1 eq), NaO^{t}Bu (1.5 eq.), 120 °C, DMF, 1 h	15% product
6	Pyrazole (**19**) (1 eq.), chloroethanol (10 eq), NaO^{t}Bu (1.5 eq.), 120 °C, DMF, 8 h	35% product
7	Pyrazole (**19**) (1 eq.), bromoethanol (10 eq), NaO^{t}Bu (1.5 eq.), 120 °C, DMF, 2 h	Degradation
8	Pyrazole (**19**) (1 eq.), bromoethanol (5 eq), NaO^{t}Bu (1.1 eq.), 100 °C, DMF, 5 h	32% product

Table 2.2. Attempts at pyrazole (19) alkylation, reproduced from Section 2.1.2 – The Chemical Strategy for Synthesis of Chemical Probe (3).

General procedure for alkylation attempts of cyclohexanol (23)

To a microwave vial was added 2-((*1r*,*4r*)-4-hydroxycyclohexyl)isoindoline-1,3-dione (**23**) and the appropriate equivalents of base (Table 2.3, reproduced from **Section 2.1.3 – The Chemical Strategy for Synthesis of Chemical Probe (34)**). The vial was capped, and evacuated and purged with N_2 before addition of a solution of the appropriate electrophilic partner in solvent. The mixture was heated to the outlined temperature for the detailed time period. Reaction outcome was assessed by LCMS analysis, and products were not isolated.

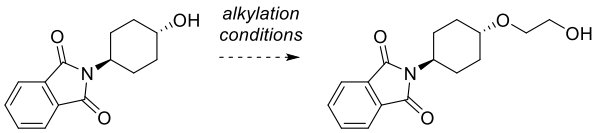

23 **24**

Entry	Reagents and Conditions	Outcome (determined by LCMS analysis)
1	2.5 M in THF oxirane, K_2CO_3, 100 °C, DMF, 24 h	No product
2	2.5 M in THF oxirane, 60% NaH in mineral oil, 100 °C, DMF, 24 h	No product
3	Bromoethanol, K_2CO_3, 100 °C, DMF, 24 h	No product
4	Bromoethanol, 60% NaH in mineral oil, 100 °C, DMF, 24 h	No product
5	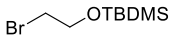 , 60% NaH in mineral oil, RT, DMF, 18 h	2% product
6	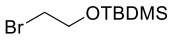 , 1 M in THF potassium bis(trimethylsilyl)amide, RT, THF, 18 h	8% product
7	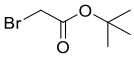 , 1 M in THF lithium bis(trimethylsilyl)amide, RT, THF, 18 h	Degradation
8	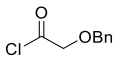 , triethylamine, DMAP, 0 °C, DCM, 6 h	No product

Table 2.3. Attempted reaction conditions for the alkylation of cyclohexanol fragment (23), reproduced from Section 2.1.3 – The Chemical Strategy for Synthesis of Chemical Probe (34).

5.1.12 Synthetic Procedures

6-(1*H*-Imidazol-1-yl)-*N*-((*1r,4r*)-4-(2-methoxyethoxy)cyclohexyl)-2,8-dimethylquinazolin-4-amine (2)

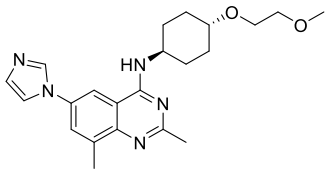

To a microwave vial was added 6-bromo-*N*-((*1r,4r*)-4-(2-methoxyethoxy)cyclohexyl)-2,8-dimethylquinazolin-4-amine (**13**) (200 mg, 0.49 mmol), 1*H*-imidazole (57 mg, 0.83 mmol), CuI (14 mg, 0.07 mmol), and K_2CO_3 (108 mg, 0.78 mmol). The vial was capped, and evacuated and purged with N_2 before addition of DMF (2 mL). The solution was heated to 150 °C and stirred at this temperature for 32 h. After this time, the solution was diluted in EtOAc (10 mL) and washed with sat. $NaHCO_3$ solution (2 × 5 mL), and brine (5 mL). The organic layer was passed through a hydrophobic frit and concentrated *in vacuo*. The crude material was purified by silica gel chromatography eluting with EtOAc in cyclohexane (0 − 100%) followed by EtOH in EtOAc (0 − 30%). The appropriate fractions were combined and concentrated *in vacuo* to yield 6-(1*H*-imidazol-1-yl)-*N*-((*1r,4r*)-4-(2-methoxyethoxy)cyclohexyl)-2,8-dimethylquinazolin-4-amine (**2**) (112 mg, 0.28 mmol, 58% yield) as a white solid; m.p. 181 – 185 °C; ν_{max}(solid): 3292, 3139, 2921, 2856, 1583, 1538, 1104, 1075, 805, 657; ^{1}H NMR (400 MHz, DMSO-d_6) δ ppm 8.30 – 8.27 (m, 2 H), 7.91 – 7.89 (m, 1 H), 7.79 (br. s., 1 H), 7.65 (d, *J* = 7.6 Hz, 1 H), 7.16 (br. s., 1 H), 4.25 – 4.13 (m, 1 H), 3.58 – 3.54 (m, 2 H), 3.46 – 3.42 (m, 2 H), 3.34 – 3.27 (m, 1 H), 3.26 (s, 3 H), 2.59 (s, 3 H), 2.49 (s, 3 H), 2.05 (app. t, *J* = 13.2 Hz, 4 H), 1.50 – 1.37 (m, 2 H), 1.35 – 1.22 (m, 2 H); ^{13}C NMR (101 MHz, DMSO-d_6) δ ppm 162.7, 158.9, 147.3, 137.1, 135.7, 132.4, 129.7, 125.2, 118.3, 112.7, 110.8, 76.9, 71.7, 66.6, 58.0, 48.7, 30.8, 29.8, 26.7, 17.5; HRMS $(M + H)^+$ calculated for $C_{22}H_{30}N_5O_2^+$ 396.2394, found 396.2401; LCMS (high pH): R_t = 0.99 mins (100%), MH^+ = 396.3.

_N_-((_1r,4r_)-4-(2-methoxyethoxy)cyclohexyl)-2,8-dimethyl-6-(1-(2-(prop-2-yn-1-yloxy)ethyl)-1_H_-pyrazol-4-yl)quinazolin-4-amine (3)

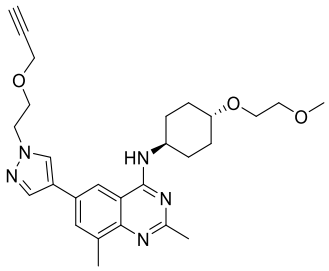

To a microwave vial was added NaH (60% dispersion in mineral oil) (32.8 mg, 0.82 mmol). The vial was capped, and evacuated and purged with N_2 before addition of 2-(4-(4-(((_1r,4r_)-4-(2-methoxyethoxy)cyclohexyl)amino)-2,8-dimethylquinazolin-6-yl)-1_H_-pyrazol-1-yl)ethan-1-ol (**21**) (120 mg, 0.27 mmol) in THF (0.8 mL). The solution was stirred at RT for 10 min before addition of 3-bromoprop-1-yne (80% in toluene) (0.30 mL, 2.73 mmol). The solution was stirred at RT for 2 h. After this time, the solution was diluted in EtOAc (10 mL). The organic layer was washed with water (2 × 5 mL), and brine (5 mL) and then passed through a hydrophobic frit and concentrated _in vacuo_. The crude material was purified by silica gel chromatography eluting with TBME in EtOAc (0 – 50%). The appropriate fractions were combined and concentrated _in vacuo_ to yield _N_-((_1r,4r_)-4-(2-methoxyethoxy)cyclohexyl)-2,8-dimethyl-6-(1-(2-(prop-2-yn-1-yloxy)ethyl)-1_H_-pyrazol-4-yl)quinazolin-4-amine (**3**) (65 mg, 0.14 mmol, 50% yield) as a yellow gum; ν_{max}(gum): 3135, 2918, 2856, 2108, 1629, 1586, 1529, 1363, 1080, 804; ^{1}H NMR (400 MHz, MeOD) δ ppm 8.12 (s, 1 H), 8.07 (s, 1 H), 7.98 (s, 1 H), 7.75 (s, 1 H), 4.37 (t, _J_ = 5.3 Hz, 2 H), 4.32 – 4.23 (m, 1 H), 4.16 (d, _J_ = 2.3 Hz, 2 H), 3.92 (t, _J_ = 5.3 Hz, 2 H), 3.67 – 3.62 (m, 2 H), 3.55 – 3.51 (m, 2 H), 3.43 – 3.35 (m, 1 H), 3.37 (s, 3 H), 2.84 (t, _J_ = 2.4 Hz, 1 H), 2.60 (s, 3 H), 2.55 (s, 3 H), 2.17 – 2.09 (m, 4 H), 1.56 – 1.35 (m, 4 H), 1 H not observed (exchangeable amine); ^{13}C NMR (101 MHz, MeOD) δ ppm 164.6, 161.1, 148.7, 138.1, 136.6, 132.0, 130.4, 129.4, 124.0, 116.5, 114.8, 80.4, 79.4, 76.4, 73.5, 69.5, 68.6, 59.3, 59.2, 53.2, 50.5, 32.3, 31.5, 26.4, 18.4; HRMS $(M + H)^+$ calculated for $C_{27}H_{36}N_5O_3^+$ 478.2813, found 478.2816; LCMS (high pH): R_t = 1.09 mins (98%), MH^+ = 478.1.

6-Bromo-2,8-dimethyl-4*H*-benzo[*d*][1,3]oxazin-4-one (10)

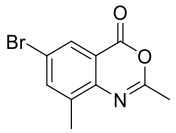

A mixture of 2-amino-5-bromo-3-methylbenzoic acid (4 g, 17.4 mmol) and acetic anhydride (16.4 ml, 174 mmol) was stirred at 110 °C under N_2 for 1.5 h, becoming an orange solution on heating. The solution was allowed to cool to RT, during which solid precipitated out of solution. The resultant mixture was filtered under vacuum and the solid washed with diethyl ether (3 × 2 mL). The solid was dried under N_2 to yield 6-bromo-2,8-dimethyl-4*H*-benzo[d][1,3]oxazin-4-one (**10**) (3.75 g, 14.8 mmol, 85% yield) as a white solid; m.p. 169 – 176 °C; ν_{max}(solid): 2928, 1738, 1641, 1521, 1429, 1238, 1182, 1023, 789, 618; ^{1}H NMR (400 MHz, DMSO-d_6) δ ppm 8.00 – 7.96 (m, 2 H), 2.45 (s, 3 H), 2.41 (s, 3 H); ^{13}C NMR (101 MHz, DMSO-d_6) δ ppm 159.7, 158.4, 143.6, 139.5, 137.6, 127.2, 119.6, 118.1, 21.2, 16.3; HRMS $(M + H)^+$ calculated for $C_{10}H_9BrNO_2^+$ 253.9811, found 253.9820; LCMS (high pH): R_t = 1.18 mins (100%), MH^+ = 254.2, 256.0.

6-Bromo-2,8-dimethylquinazolin-4(3*H*)-one (11)

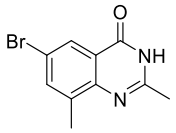

A mixture of 6-bromo-2,8-dimethyl-4*H*-benzo[*d*][1,3]oxazin-4-one (**10**) (3.75 g, 14.8 mmol) and ammonium acetate (2.28 g, 29.5 mmol) in DMA (30 mL) was stirred at 170 °C under N_2 for 4 h. The solution was allowed to cool to RT, during which a solid precipitated out of solution. The mixture was filtered under vacuum and the solid washed with MeCN (2 × 5 mL). The solid was dried under N_2 to afford 6-bromo-2,8-dimethylquinazolin-4(3*H*)-one (**11**) (3.16 g, 12.5 mmol, 85% yield) as a white solid; m.p. 303 – 310 °C; ν_{max}(solid): 3024, 2871, 1681, 1625, 1455, 873, 797, 632, 602, 528; ^{1}H NMR (400 MHz, DMSO-d_6) δ ppm 12.32 (br. s., 1 H), 7.97 (d, J = 2.0 Hz, 1 H), 7.80 (d, J = 2.3 Hz, 1 H), 2.48 (s, 3 H), 2.36 (s, 3 H); ^{13}C NMR (101 MHz, DMSO-d_6) δ ppm 160.8, 153.9, 146.5, 137.8, 136.9, 125.3, 122.0, 117.6, 21.8, 16.8; HRMS $(M + H)^+$ calculated for $C_{10}H_{10}BrN_2O^+$ 252.9971, found 252.9973; LCMS (high pH): R_t = 0.92 mins (100%), MH^+ = 253.2, 255.3.

(*1r,4r*)-4-(2-Methoxyethoxy)cyclohexanamine (12)

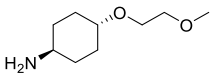

To a hydrogenation flask was added Pd/C (10% wt, 0.26 g, 2.46 mmol) . The flask was evacuated and purged with N_2. (*1r,4r*)-*N,N*-dibenzyl-4-(2-methoxyethoxy)cyclohexan-1-amine (**16**) (5.80 g, 16.4 mmol) in EtOH (40 mL) was added under vacuum, and washed through with further EtOH (10 mL). The flask was evacuated and purged with N_2 again before being flushed with hydrogen and then connected to a hydrogen burette. The solution was left to stir under hydrogen for 24 h. After this time, the reaction solution was filtered through celite. The bed and flask was washed with further EtOH (10 mL) and also filtered through celite. The combined EtOH washes were concentrated *in vacuo* to yield (*1r,4r*)-4-(2-methoxyethoxy)cyclohexan-1-amine (**12**) (2.34 g, 13.5 mmol, 82% yield) as a grey oil; ν_{max}(oil): 3408, 2933, 2850, 1555, 1454, 1379, 1106, 490; ^{1}H NMR (400 MHz, DMSO-d_6) δ ppm 3.52 – 3.48 (m, 2 H), 3.43 – 3.39 (m, 2 H), 3.24 (s, 3 H), 3.21 – 3.12 (m, 1 H), 2.56 – 2.48 (m, 1 H), 1.94 – 1.87 (m, 2 H), 1.77 – 1.69 (m, 2 H), 1.44 (br. s, 2 H), 1.19 – 0.96 (m, 4 H); ^{13}C NMR (101 MHz, $CDCl_3$) δ ppm 78.0, 72.3, 67.4, 59.0, 49.9, 34.5, 30.7; HRMS $(M + H)^+$ calculated for $C_9H_{20}NO_2^+$ 174.1489, found 174.1494; no chromophore for LCMS. Spectroscopic data is consistent with literature reports.[250]

6-Bromo-*N*-((*1r,4r*)-4-(2-methoxyethoxy)cyclohexyl)-2,8-dimethylquinazolin-4-amine (13)

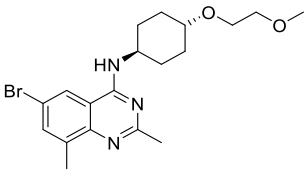

To a round bottomed flask was added 6-bromo-2,8-dimethylquinazolin-4(3*H*)-one (**11**) (1.00 g, 3.95 mmol), and PyBOP (3.08 g, 5.93 mmol). The vial was capped, and evacuated and purged with N_2 before addition of MeCN (20 mL), (*1r,4r*)-4-(2-methoxyethoxy)cyclohexan-1-amine (**12**) (1.37 g, 7.90 mmol), and DBU (1.19 mL, 7.90 mmol). The mixture was stirred at RT for 24 h. After this time, the solution was diluted in EtOAc (20 mL), and washed with water (2 × 10 mL), and brine (10 mL).

The organic layer was passed through a hydrophobic frit, and concentrated *in vacuo*. The crude material was purified by silica gel chromatography eluting with EtOAc in cyclohexane + 1% NEt_3 (0 – 40%). The appropriate fractions were combined and concentrated *in vacuo* to yield 6-bromo-*N*-((*1r*,*4r*)-4-(2-methoxyethoxy)cyclohexyl)-2,8-dimethylquinazolin-4-amine (**13**) (1.34 g, 3.28 mmol, 83% yield) as a white solid; m.p. 130 – 132 °C; ν_{max}(solid): 3363, 2934, 2860, 1577, 1531, 1364, 1344, 1133, 1106, 869, 804, 595, 543; ^{1}H NMR (400 MHz, DMSO-d_6) δ ppm 8.36 (d, *J* = 1.8 Hz, 1 H), 7.73 (d, *J* = 7.5 Hz, 1 H), 7.71 − 7.69 (m, 1 H), 4.20 – 4.09 (m, 1 H), 3.56 – 3.33 (m, 2 H), 3.45 – 3.41 (m, 2 H), 3.31 – 3.26 (m, 1 H), 3.25 (s, 3 H), 2.50 (s, 3 H), 2.45 (s, 3 H), 2.08 – 1.93 (m, 4 H), 1.48 – 1.36 (m, 2 H), 1.32 – 1.20 (m, 2 H); ^{13}C NMR (101 MHz, $CDCl_3$) δ ppm 163.9, 158.0, 148.2, 138.9, 135.3, 120.4, 117.3, 113.8, 77.7, 72.4, 67.6, 59.1, 49.0, 30.7, 30.6, 27.0, 17.5; HRMS $(M + H)^+$ calculated for $C_{19}H_{27}BrN_3O_2^+$ 408.1281, found 408.1295; LCMS (high pH): R_t = 1.28 mins (100%), MH^+ = 408.3, 410.2.

(*1r*,*4r*)-4-(Dibenzylamino)cyclohexanol (15)

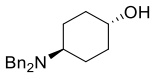

To a solution of (*1r*,*4r*)-4-aminocyclohexan-1-ol (**14**) (10.0 g, 87 mmol) in MeCN (200 mL) was added (bromomethyl)benzene (22.7 mL, 191 mmol) and K_2CO_3 (36.0 g, 260 mmol). The mixture was stirred at 70 °C for 20 h. After this time, the mixture was diluted in EtOAc (200 mL) and washed with water (2 × 100 mL), and brine (100 mL). The organic layer was passed through a hydrophobic frit and concentrated *in vacuo*. The crude material was purified by silica gel chromatography eluting with TBME in cyclohexane (0 – 75%). The appropriate fractions were combined and concentrated *in vacuo* to yield (*1r*,*4r*)-4-(dibenzylamino)cyclohexan-1-ol (**15**) (22.6 g, 76 mmol, 88% yield) as a white solid; m.p. 108 – 110 °C; ν_{max}(solid): 3263, 2929, 2858, 1493, 1452, 1063, 746, 695; ^{1}H NMR (400 MHz, $CDCl_3$) δ ppm 7.38 – 7.34 (m, 4 H), 7.32 – 7.26 (m, 4 H), 7.24 – 7.19 (m, 2 H), 3.62 (s, 4 H), 3.60 – 3.49 (m, 1 H), 2.54 (tt, *J* = 11.8, 3.5 Hz, 1 H), 2.05 – 1.97 (m, 2 H), 1.95 – 1.87 (m, 2 H), 1.50 – 1.38 (m, 2 H), 1.26 – 1.14 (m, 2 H), 1 H not observed (exchangeable alcohol); HRMS $(M + H)^+$ calculated for $C_{20}H_{26}NO^+$ 296.2009, found 296.2011; LCMS (high pH): R_t = 1.33 mins (98%), MH^+ = 296.3. Spectroscopic data is consistent with literature reports.[250]

(*1r,4r*)-*N,N*-Dibenzyl-4-(2-methoxyethoxy)cyclohexanamine (16)

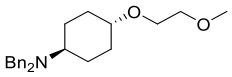

To a solution of (*1r,4r*)-4-(dibenzylamino)cyclohexan-1-ol (**15**) (22.1 g, 74.7 mmol) and 1-bromo-2-methoxyethane (29.5 mL, 314 mmol) in THF (150 mL) was added NaH (60% dispersion in mineral oil) (14.9 g, 374 mmol). The mixture was stirred at 50 °C for 64 h over the weekend. After this time, the reaction was cooled to 0 °C and the remaining NaH was quenched with IPA (75 mL). The solution was separated with NH_4Cl (100 mL), and EtOAc (100 mL). The aqueous layer was washed with EtOAc (2 × 50 mL) and the combined organic layers were passed through a hydrophobic frit and concentrated *in vacuo*. The crude material was purified by silica gel chromatography eluting with EtOAc in cyclohexane (0 – 30%). The appropriate fractions were combined and concentrated *in vacuo* to yield (*1r,4r*)-*N,N*-dibenzyl-4-(2-methoxyethoxy)cyclohexan-1-amine (**16**) (21.4 g, 60.5 mmol, 81% yield) as a yellow oil; ν_{max}(oil): 3029, 2931, 2858, 2799, 1493, 1453, 1359, 1250, 1107, 737, 698; ^{1}H NMR (400 MHz, $CDCl_3$) δ ppm 7.41 – 7.36 (m, 4 H), 7.33 – 7.28 (m, 4 H), 7.25 – 7.20 (m, 2 H), 3.64 (s, 4 H), 3.63 – 3.59 (m, 2 H), 3.55 – 3.51 (m, 2 H), 3.39 (s, 3 H), 3.27 – 3.18 (m, 1 H), 2.56 (tt, *J* = 11.8, 3.5 Hz, 1 H), 2.15 – 2.08 (m, 2 H), 1.98 – 1.91 (m, 2 H), 1.46 – 1.36 (m, 2 H), 1.26 – 1.14 (m, 2 H); ^{13}C NMR (101 MHz, $CDCl_3$) δ ppm 140.8, 128.4, 128.1, 126.6, 78.5, 72.3, 67.3, 59.0, 57.2, 54.1, 31.4, 26.0; HRMS $(M + H)^+$ calculated for $C_{23}H_{32}NO_2^+$ 354.2428, found 354.2434; LCMS (high pH): R_t = 1.54 mins (99%), MH^+ = 354.4.

***N*-((*1r,4r*)-4-(2-methoxyethoxy)cyclohexyl)-2,8-dimethyl-6-(1*H*-pyrazol-4-yl)quinazolin-4-amine (17)**

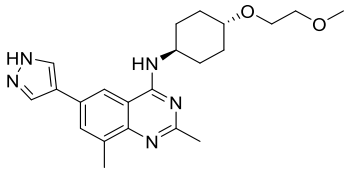

To a microwave vial was added 4-(4,4,5,5-tetramethyl-1,3,2-dioxaborolan-2-yl)-1*H*-pyrazole (261 mg, 1.38 mmol), 6-bromo-*N*-((*1r,4r*)-4-(2-methoxyethoxy)cyclohexyl)-2,8-dimethylquinazolin-4-amine (**13**) (250 mg, 0.61 mmol), K_2CO_3 (423 mg, 3.06

mmol), and $PdCl_2$(dppf) (135 mg, 0.18 mmol). The vial was capped, and evacuated and purged with N_2 before addition of DME (5 mL) and water (1.00 mL). The solution was stirred at 100 °C for 24 h. The solution was allowed to cool to RT before being diluted in EtOAc (20 mL), and washed with water (2 × 5 mL), and brine (5 mL). The organic layer was passed through a hydrophobic frit and concentrated *in vacuo*. The crude material was purified by silica gel chromatography eluting with EtOAc in TBME (0 – 50%). The appropriate fractions were combined and concentrated *in vacuo* to yield *N*-((*1r*,*4r*)-4-(2-methoxyethoxy)cyclohexyl)-2,8-dimethyl-6-(1*H*-pyrazol-4-yl)quinazolin-4-amine (**17**) (83 mg, 0.21 mmol, 34% yield) as an off-white solid; m.p. 185 – 190 °C; ν_{max}(solid): 2936, 2860, 1577, 1523, 1509, 1358, 1102, 804; ^{1}H NMR (400 MHz, MeOD) δ ppm 8.18 (s, 1 H), 8.10 (s, 2 H), 7.81 (s, 1 H), 4.34 – 4.26 (m, 1 H), 3.69 – 3.64 (m, 2 H), 3.58 – 3.53 (m, 2 H), 3.43 – 3.35 (m, 1 H), 3.39 (s, 3 H), 2.63 (s, 3 H), 2.58 (s, 3 H), 2.20 – 2.11 (m, 4 H), 1.58 – 1.37 (m, 4 H), 2 H not observed (exchangeable); ^{13}C NMR (101 MHz, MeOD) δ ppm 163.0, 159.5, 147.1, 135.0, 130.7, 129.0, 121.8, 115.1, 113.2, 77.8, 71.9, 67.1, 57.7, 49.0, 30.8, 29.9, 24.8, 16.9, 2 C not observed; HRMS $(M + H)^+$ calculated for $C_{22}H_{30}N_5O_2^+$ 396.2394, found 396.2388; LCMS (high pH): R_t = 0.94 mins (99%), MH^+ = 396.5.

2-(4-(4-(((*1r*,*4r*)-4-(2-Methoxyethoxy)cyclohexyl)amino)-2,8-dimethylquinazolin-6-yl)-1*H*-pyrazol-1-yl)ethanol (21)

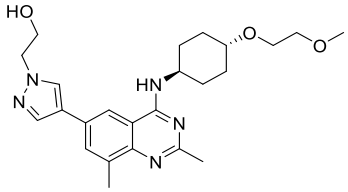

To a microwave vial was added *N*-((*1r*,*4r*)-4-(2-methoxyethoxy)cyclohexyl)-2,8-dimethyl-6-(1*H*-pyrazol-4-yl)quinazolin-4-amine (**17**) (278 mg, 0.70 mmol), and K_2CO_3 (117 mg, 0.84 mmol). The vial was capped, and evacuated and purged with N_2 before addition of DMF (3 mL). The solution was stirred at RT for 10 min before addition of oxirane (2.5 M in THF) (0.31 mL, 0.77 mmol). The solution was heated to 100 °C and stirred for a further 3 h. After this time, the solution was diluted in EtOAc (10 mL), and washed with water (2 × 5 mL), and brine (5 mL). The organic layer was passed through a hydrophobic frit and concentrated *in vacuo*. The crude material was

purified by silica gel chromatography eluting with EtOAc in TBME (0 – 80%). The appropriate fractions were combined and concentrated *in vacuo* to yield 2-(4-(4-(((*1r,4r*)-4-(2-methoxyethoxy)cyclohexyl)amino)-2,8-dimethylquinazolin-6-yl)-1*H*-pyrazol-1-yl)ethan-1-ol (**21**) (150 mg, 0.34 mmol, 49% yield), as a yellow oil; ν_{max}(oil): 3344, 2934, 2860, 1578, 1528, 1364, 1089, 803, 735; ^{1}H NMR (400 MHz, MeOD) δ ppm 8.14 – 8.12 (m, 1 H), 8.10 (s, 1 H), 7.99 (s, 1 H), 7.78 – 7.75 (m, 1 H), 4.32 – 4.24 (m, 3 H), 3.96 – 3.91 (m, 2 H), 3.67 – 3.63 (m, 2 H), 3.56 – 3.51 (m, 2 H), 3.38 (s, 3 H), 3.41 – 3.34 (m, 1 H), 2.61 (s, 3 H), 2.56 (s, 3 H), 2.19 – 2.07 (m, 4 H), 1.58 – 1.36 (m, 4 H), 2 H not observed (exchangeable); ^{13}C NMR (101 MHz, DMSO-d_6) δ ppm 162.1, 159.3, 147.7, 136.7, 135.5, 130.3, 128.7, 128.1, 121.9, 115.5, 113.4, 77.5, 72.2, 67.2, 60.5, 58.6, 54.9, 49.0, 31.4, 30.4, 27.3, 18.0; HRMS $(M + H)^+$ calculated for $C_{25}H_{35}N_4O_3^+$ 440.2656, found 440.2658; LCMS (high pH): R_t = 0.90 mins (100%), MH^+ = 440.4.

2-((*1r,4r*)-4-Hydroxycyclohexyl)isoindoline-1,3-dione (23)

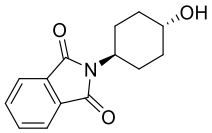

To a round bottomed flask was added (*1r,4r*)-4-aminocyclohexan-1-ol (0.86 g, 7.43 mmol) and phthalic anhydride (1.00 g, 6.75 mmol). The flask was equipped with a reflux condenser and the mixture was heated to gentle boiling at 200 °C under N_2 for 30 min. After this time, the solution was cooled under N_2 to RT. The resultant solid was filtered under vacuum and washed with water (2 × 10 mL). The white solid was collected to yield 2-((*1r,4r*)-4-hydroxycyclohexyl)isoindoline-1,3-dione (**23**) (1.14 g, 4.65 mmol, 69% yield); ν_{max}(solid): 3384, 2930, 2855, 1766, 1699, 1374, 1056, 719; ^{1}H NMR (400 MHz, DMSO-d_6) δ ppm 7.86 – 7.80 (m, 4 H) 4.62 (d, *J* = 4.5 Hz, 1 H), 3.96 (tt, *J* = 12.3, 3.9 Hz, 1 H), 3.51 – 3.40 (m, 1 H), 2.20 – 2.07 (m, 2 H), 1.96 – 1.89 (m, 2 H), 1.72 – 1.64 (m, 2 H), 1.33 – 1.21 (m, 2 H); HRMS $(M + H)^+$ calculated for $C_{14}H_{16}NO_3^+$ 246.1125, found 246.1130; LCMS (high pH): R_t = 0.81 mins (95%), MH^+ = 246.2. Spectroscopic data is consistent with literature reports.[251,252]

(*1r,4r*)-4-((6-Bromo-2,8-dimethylquinazolin-4-yl)amino)cyclohexanol (26)

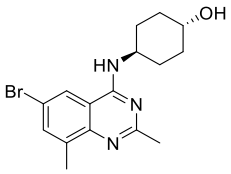

To a microwave vial was added (*1r,4r*)-4-aminocyclohexan-1-ol (455 mg, 3.95 mmol), 6-bromo-2,8-dimethylquinazolin-4(3*H*)-one (**11**) (500 mg, 1.98 mmol), and PyBOP (1.54 g, 2.96 mmol). The vial was capped, and evacuated and purged with N_2 before addition of MeCN (5 mL), and DBU (0.60 mL, 3.95 mmol). The mixture was stirred at RT for 18 h. After this time, the mixture was separated with EtOAc (10 mL), and water (10 mL). The organic layer was washed with water (5 mL), and brine (5 mL), and then passed through a hydrophobic frit, and concentrated *in vacuo*. The crude material was purified by silica gel chromatography eluting with EtOAc in cyclohexane + 1% NEt_3 (0 – 50%). The appropriate fractions were combined and concentrated *in vacuo* to yield (*1r,4r*)-4-((6-bromo-2,8-dimethylquinazolin-4-yl)amino)cyclohexan-1-ol (**26**) (590 mg, 1.68 mmol, 85% yield) as a white solid; m.p. 93 – 97 °C; ν_{max}(solid): 3325, 2933, 2858, 1579, 1531, 1419, 1355, 1084, 1022, 865, 809, 801; ^{1}H NMR (400 MHz, DMSO-d_6) δ ppm 8.36 (d, *J* = 1.8 Hz, 1 H), 7.72 (d, *J* = 7.8 Hz, 1 H), 7.69 – 7.65 (m, 1 H), 4.54 (d, *J* = 4.5 Hz, 1 H), 4.18 – 4.08 (m, 1 H), 3.49 – 3.38 (m, 1 H), 3.17 (d, *J* = 5.3 Hz, 3 H), 2.44 (s, 3 H), 1.96 – 1.85 (m, 4 H), 1.48 – 1.36 (m, 2 H), 1.34 – 1.22 (m, 2 H); ^{13}C NMR (101 MHz, DMSO-d_6) δ ppm 163.5, 158.6, 148.2, 138.2, 135.2, 123.0, 116.7, 114.5, 69.0, 49.2, 34.8, 30.4, 27.3, 17.6; HRMS $(M + H)^+$ calculated for $C_{16}H_{21}BrN_3O^+$ 350.0863, found 350.0870; LCMS (formic): R_t = 0.51 mins (99%), MH^+ = 350.4, 352.3.

_N_-((_1r,4r_)-4-((6-(1_H_-Imidazol-1-yl)-2,8-dimethylquinazolin-4-yl)amino)cyclohexyl)hexanamide (30)

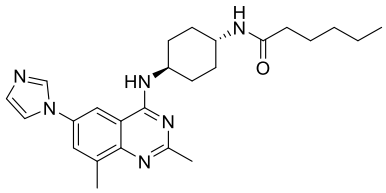

To a microwave vial was added _N_-((_1r,4r_)-4-((6-bromo-2,8-dimethylquinazolin-4-yl)amino)cyclohexyl)hexanamide (**33**) (28 mg, 0.06 mmol), CuI (1.79 mg, 9.39 µmol), K_2CO_3 (13.8 mg, 0.10 mmol), and imidazole (7.2 mg, 0.11 mmol). The vial was capped, and evacuated and purged with N_2 before addition of DMF (1 mL). The solution was heated to 150 °C and stirred for 48 h. After this time, the solution was cooled to RT and diluted in EtOAc (5 mL). The solution was washed with water (2 × 3 mL), and brine (3 mL). The organic layer was passed through a hydrophobic frit and concentrated *in vacuo*. The crude material was purified by mass directed auto-preparative HPLC (MDAP, HpH). The appropriate fractions were combined and concentrated *in vacuo* to yield _N_-((_1r,4r_)-4-((6-(1_H_-imidazol-1-yl)-2,8-dimethylquinazolin-4-yl)amino)cyclohexyl)hexanamide (**30**) (9 mg, 0.02 mmol, 33% yield) as a white solid; m.p. 249 – 254 °C; ν_{max}(solid): 3349, 3291, 2930, 2854, 1627, 1528, 1452, 1105, 1069, 799, 589; ^{1}H NMR (400 MHz, DMSO-d_6) δ ppm 8.30 – 8.27 (m, 2 H), 7.92 – 7.89 (m, 1 H), 7.80 – 7.78 (m, 1 H), 7.70 (d, J = 7.9 Hz, 1 H), 7.66 (d, J = 7.6 Hz, 1 H), 7.15 (s, 1 H), 4.24 – 4.13 (m, 1 H), 3.63 – 3.51 (m, 1 H), 2.59 (s, 3 H), 2.49 (s, 3 H), 2.06 – 1.98 (m, 4 H), 1.90 – 1.83 (m, 2 H), 1.54 – 1.40 (m, 4 H), 1.37 – 1.18 (m, 6 H), 0.86 (t, J = 7.0 Hz, 3 H); ^{13}C NMR (151 MHz, DMSO-d_6) δ ppm 171.7, 163.2, 159.4, 147.9, 137.6, 136.2, 132.9, 130.3, 125.7, 118.8, 113.3, 111.3, 49.1, 47.6, 36.0, 31.8, 31.34, 31.31, 27.3, 25.5, 22.3, 18.0, 14.4; HRMS $(M + H)^+$ calculated for $C_{25}H_{35}N_6O^+$ 435.2867, found 435.2869; LCMS (high pH): R_t = 1.10 mins (99%), MH^+ = 435.1.

(*1r,4r*)-*N*^{1}-(6-Bromo-2,8-dimethylquinazolin-4-yl)cyclohexane-1,4-diamine (32)

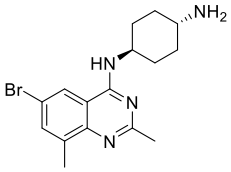

To a microwave vial was added 6-bromo-2,8-dimethylquinazolin-4(3*H*)-one (**11**) (500 mg, 1.98 mmol), (*1r,4r*)-cyclohexane-1,4-diamine (451 mg, 3.95 mmol) and PyBOP (1.54 g, 2.96 mmol). The vial was capped, and evacuated and purged with N_2 before addition of DBU (0.60 mL, 3.95 mmol) and MeCN (12 mL). The solution was stirred at RT for 2.5 h. After this time, the mixture was diluted in EtOAc (30 mL) and washed with water (2 × 10 mL), and brine (10 mL). The organic layer was passed through a hydrophobic frit and concentrated *in vacuo*. The crude material was purified by silica gel chromatography eluting with EtOAc in cyclohexane + 1% NEt_3 (0 – 100%). The appropriate fractions were combined and concentrated *in vacuo* to yield (*1r,4r*)-N^1-(6-bromo-2,8-dimethylquinazolin-4-yl)cyclohexane-1,4-diamine (**32**) (676 mg, 1.94 mmol, 98% yield), as an orange gum; ν_{max}(solid): 3285, 2929, 2864, 1650, 1576, 1535, 1088, 830, 566; ^{1}H NMR (400 MHz, DMSO-d_6) δ ppm 8.36 (s, 1 H), 7.75 (d, *J* = 7.6 Hz, 1 H), 7.69 (s, 1 H), 4.19 – 4.07 (m, 1 H), 3.30 (br. s, 2 H), 2.68 – 2.63 (m, 1 H), 2.51 (s, 3 H), 2.44 (s, 3 H), 1.90 (app. d, *J* = 12.3 Hz, 2 H), 1.83 (app. d, *J* = 12.1 Hz, 2 H), 1.47 – 1.36 (m, 2 H), 1.23 – 1.12 (m, 2 H); ^{13}C NMR (101 MHz, DMSO-d_6) δ ppm 163.5, 158.6, 148.2, 138.2, 135.2, 123.0, 116.7, 114.5, 50.3, 49.3, 35.3, 31.1, 27.3, 17.6; HRMS $(M + H)^+$ calculated for $C_{16}H_{22}BrN_4^+$ 349.1022, found 349.1025; LCMS (high pH): R_t = 1.22 mins (99%), MH^+ = 349.2, 351.2.

***N*-((*1r,4r*)-4-((6-bromo-2,8-dimethylquinazolin-4-yl)amino)cyclohexyl)hexanamide (33)**

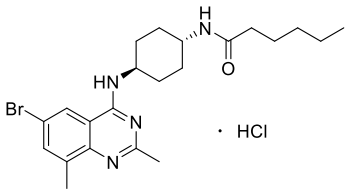

To a microwave vial was added (*1r,4r*)-*N*^{1}-(6-bromo-2,8-dimethylquinazolin-4-yl)cyclohexane-1,4-diamine (**32**) (150 mg, 0.43 mmol). The vial was capped, and

evacuated and purged with N_2 before addition of THF (5 mL), and then hexanoyl chloride (0.06 mL, 0.45 mmol) dropwise. The solution was stirred at RT for 3 h. After this time, the solution was diluted in EtOAc (20 mL) and washed with water (2 × 10 mL), and brine (10 mL). The organic layer was passed through a hydrophobic frit and concentrated *in vacuo* to yield *N*-((*1r*,*4r*)-4-((6-bromo-2,8-dimethylquinazolin-4-yl)amino)cyclohexyl)hexanamide (**33**) (164 mg, 0.34 mmol, 79% yield), as the chloride salt, and as a white solid; m.p. 265 – 272 °C (dec.); ν_{max}(solid): 3415, 3275, 2927, 2855, 1638, 1557, 1520, 1422, 1341, 798, 545; ^{1}H NMR (400 MHz, DMSO-d_6) δ ppm 8.37 (d, *J* = 2.0 Hz, 1 H), 7.79 (d, *J* = 7.6 Hz, 1 H), 7.72 – 7.69 (m, 1 H), 7.65 (d, *J* = 7.9 Hz, 1 H), 4.20 – 4.09 (m, 1 H), 3.60 – 3.49 (m, 1 H), 2.51 (br. s., 3 H), 2.45 (s, 3 H), 2.04 (t, *J* = 7.4 Hz, 2 H), 1.96 (d, *J* = 10.3 Hz, 2 H), 1.84 (d, *J* = 10.6 Hz, 2 H), 1.54 – 1.40 (m, 4 H), 1.37 – 1.18 (m, 6 H), 0.86 (t, *J* = 7.1 Hz, 3 H); ^{13}C NMR (151 MHz, DMSO-d_6) δ ppm 171.7, 163.5, 158.6, 148.2, 138.2, 135.2, 123.0, 116.8, 114.5, 49.1, 47.6, 36.0, 31.8, 31.3, 31.1, 27.3, 25.5, 22.3, 17.6, 14.4; HRMS $(M + H)^+$ calculated for $C_{22}H_{32}BrN_4O^+$ 447.1754, found 447.1755; LCMS (high pH): R_t = 1.32 mins (100%), MH^+ = 447.4, 449.4.

_N_-((*1r*,*4r*)-4-((6-(1*H*-imidazol-1-yl)-2,8-dimethylquinazolin-4-yl)amino)cyclohexyl)hex-5-ynamide (34)

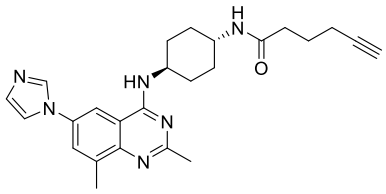

To a microwave vial was added *N*-((*1r*,*4r*)-4-((6-bromo-2,8-dimethylquinazolin-4-yl)amino)cyclohexyl)hex-5-ynamide (**36**) (183 mg, 0.41 mmol), imidazole (48 mg, 0.70 mmol), CuI (12 mg, 0.06 mmol), and K_2CO_3 (91 mg, 0.66 mmol). The vial was capped, and evacuated and purged with N_2 before addition of DMF (2 mL). The solution was stirred at 150 °C for 24 h. After this time, the solution was allowed to cool to RT and then diluted in EtOAc (20 mL), and washed with sat. $NaHCO_3$ solution (2 × 10 mL), and brine (10 mL). The organic layer was passed through a hydrophobic frit and concentrated *in vacuo*. The crude material was purified by silica gel chromatography eluting with EtOAc in TBME (0 – 75%). The appropriate fractions

were combined and concentrated *in vacuo* to yield *N*-((*1r*,*4r*)-4-((6-(1*H*-imidazol-1-yl)-2,8-dimethylquinazolin-4-yl)amino)cyclohexyl)hex-5-ynamide (**34**) (65 mg, 0.15 mmol, 37% yield) as a white solid; m.p. 241 – 246 °C; ν_{max}(solid): 3354, 3300, 3260, 2935, 2855, 2140, 1645, 1532, 1341, 1065, 804, 636, 624; ^{1}H NMR (400 MHz, DMSO-d_6) δ ppm 8.28 (s, 2 H), 7.90 (d, *J* = 1.2 Hz, 1 H), 7.78 (d, *J* = 1.2 Hz, 1 H), 7.73 (d, *J* = 7.9 Hz, 1 H), 7.69 (d, *J* = 7.6 Hz, 1 H), 7.15 (s, 1 H), 4.24 – 4.14 (m, 1 H), 3.63 – 3.51 (m, 1 H), 2.77 (t, *J* = 2.7 Hz, 1 H), 2.59 (s, 3 H), 2.48 (s, 3 H), 2.19 – 2.11 (m, 4 H), 2.06 – 1.97 (m, 2 H), 1.91 – 1.83 (m, 2 H), 1.71 (quin., *J* = 7.4 Hz, 2 H), 1.52 – 1.40 (m, 2 H), 1.38 – 1.26 (m, 2 H); ^{13}C NMR (101 MHz, DMSO-d_6) δ ppm 171.0, 163.2, 159.4, 147.8, 137.6, 136.2, 132.9, 130.3, 125.7, 118.8, 113.3, 111.3, 84.6, 71.9, 49.1, 47.7, 34.8, 31.8, 31.3, 27.3, 24.8, 18.0, 17.9; HRMS $(M + H)^+$ calculated for $C_{25}H_{31}N_6O^+$ 431.2554, found 431.2554; LCMS (high pH): R_t = 0.96 mins (98%), MH^+ = 431.4.

_N_-((*1r*,*4r*)-4-((6-Bromo-2,8-dimethylquinazolin-4-yl)amino)cyclohexyl)hex-5-ynamide (36)

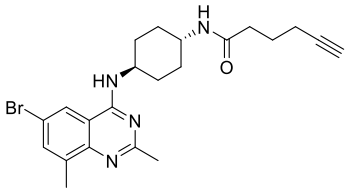

To a microwave vial was added (*1r*,*4r*)-*N*^{1}-(6-bromo-2,8-dimethylquinazolin-4-yl)cyclohexane-1,4-diamine (**32**) (367 mg, 1.05 mmol), DCC (217 mg, 1.05 mmol), and DMAP (12 mg, 0.11 mmol). The vial was capped, and evacuated and purged before addition of DMF (4 mL), and hex-5-ynoic acid (0.12 mL, 1.05 mmol). The solution was stirred at RT for 16 h. After this time, the solution was diluted in EtOAc (20 mL), and washed with water (2 × 10 mL), and brine (10 mL). The organic layer was passed through a hydrophobic frit and concentrated *in vacuo*. The crude material was purified by silica gel chromatography eluting with EtOAc in cyclohexane + 1% NEt_3 (0 – 60%). The appropriate fractions were combined and concentrated *in vacuo* to yield *N*-((*1r*,*4r*)-4-((6-bromo-2,8-dimethylquinazolin-4-yl)amino)cyclohexyl)hex-5-ynamide (**36**) (211 mg, 0.48 mmol, 45% yield) as a colourless gum; ν_{max}(gum): 3358, 3318, 3254, 2929, 2849, 2147, 1653, 1524, 1347, 1112, 879, 791, 633, 613; ^{1}H

NMR (400 MHz, DMSO-d_6) δ ppm 8.37 (d, *J* = 1.7 Hz, 1 H), 7.78 (d, *J* = 7.6 Hz, 1 H), 7.72 (d, *J* = 7.9 Hz, 1 H), 7.71 – 7.69 (m, 1 H), 4.19 – 4.09 (m, 1 H), 3.60 – 3.50 (m, 1 H), 2.77 (t, *J* = 2.6 Hz, 1 H), 2.51 (br. s., 3 H), 2.45 (s, 3 H), 2.19 – 2.12 (m, 4 H), 1.96 (app. d, *J* = 10.6 Hz, 2 H), 1.85 (app. d, *J* = 10.6 Hz, 2 H), 1.67 (quin, *J* = 7.3 Hz, 2 H), 1.51 – 1.40 (m, 2 H), 1.36 – 1.24 (m, 2 H); ^{13}C NMR (DMSO-d_6) δ ppm 171.0, 163.5, 158.6, 148.2, 138.2, 135.2, 123.0, 116.7, 114.5, 84.6, 71.9, 49.1, 47.6, 34.8, 31.8, 31.1, 27.3, 24.8, 17.9, 17.6; HRMS $(M + H)^+$ calculated for $C_{22}H_{28}BrN_4O^+$ 443.1441, found 443.1441; LCMS (high pH): R_t = 1.19 mins (100%), MH^+ = 443.3, 445.3.

6-Bromo-2-(2-bromoethyl)-8-methyl-4*H*-benzo[*d*][*1,3*]oxazin-4-one (39)

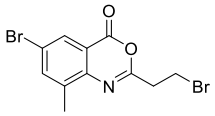

To a round bottomed flask was added 2-amino-5-bromo-3-methylbenzoic acid (420 mg, 1.83 mmol). The vial was evacuated and purged with N_2 before addition of THF (4 mL). To the mixture was added 3-bromopropanoyl chloride (0.22 mL, 2.19 mmol) dropwise. The solution was stirred for 2 h. After this time, the solution was concentrated *in vacuo*. DMAP (0.94 mg, 7.67 µmol) was added, and the flask was evacuated and purged with N_2. A solution of of Boc_2O (0.02 mL, 0.08 mmol) in 1,4-dioxane (10 mL), and pyridine (0.12 mL, 1.51 mmol) was added. The mixture was stirred at RT for 3 h. After this time, the solution was diluted in EtOAc (20 mL), and washed with water (3 × 10 mL) and then brine (2 × 10 mL). The organic layer was passed through a hydrophobic frit and concentrated *in vacuo*. The crude material was purified by silica gel chromatography eluting with Et_2O in cyclohexane (0 – 40%). The appropriate fractions were combined and concentrated *in vacuo* to yield 6-bromo-2-(2-bromoethyl)-8-methyl-4*H*-benzo[*d*][*1,3*]oxazin-4-one (**39**) (247 mg, 0.71 mmol, 47% yield) as a white solid; ^{1}H NMR (400 MHz, DMSO-d_6) δ ppm 8.05 – 8.02 (m, 2 H), 3.86 (t, *J* = 6.5 Hz, 2 H), 3.31 (t, *J* = 6.5 Hz, 2 H), 3.30 (s, 3 H); LCMS (high pH): R_t = 1.34 mins (71%), MH^+ = 345.9, 348.0, 350.0. Facile bromide elimination occurred on standing to form the undesired alkene (**42**), as observed by LCMS analysis, and precluded further characterisation.

6-(1*H*-Imidazol-1-yl)-*N*-((*1r,4r*)-4-(2-methoxyethoxy)cyclohexyl)-8-methylquinazolin-4-amine (44)

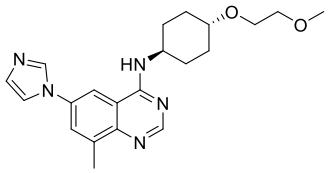

To a microwave vial was added 6-bromo-*N*-((*1r,4r*)-4-(2-methoxyethoxy)cyclohexyl)-8-methylquinazolin-4-amine (**46**) (405 mg, 1.03 mmol), imidazole (119 mg, 1.75 mmol), CuI (29.3 mg, 0.15 mmol), and K_2CO_3 (227 mg, 1.643 mmol). The vial was capped, and evacuated and purged with N_2 before addition of DMF (5 mL). The solution was stirred at 150 °C for 26 h. After this time, the solution was diluted in EtOAc (30 mL) and washed with sat. $NaHCO_3$ solution (2 × 20 mL), and brine (20 mL). The aqueous layer was extracted with EtOAc (2 × 20 mL). The combined organic layers were passed through a hydrophobic frit and concentrated *in vacuo*. The crude material was purified by silica gel chromatography eluting with EtOAc in TBME (0 – 100%) and then EtOH in EtOAc (0 – 20%). The appropriate fractions were combined and concentrated *in vacuo* to yield 6-(1*H*-imidazol-1-yl)-*N*-((*1r,4r*)-4-(2-methoxyethoxy)cyclohexyl)-8-methylquinazolin-4-amine (**44**) (233 mg, 0.61 mmol, 60% yield) as a white solid; m.p. 187 – 191 °C; ν_{max}(solid): 3254, 3121, 2939, 1586, 1533, 1504, 1096, 1058, 845, 807, 781, 659; ^{1}H NMR (400 MHz, $CDCl_3$) δ ppm 8.76 (s, 1 H), 7.85 (br. s., 1 H), 7.66 – 7.63 (m, 1H), 7.63 – 7.61 (m, 1 H), 7.34 (br. s., 1 H), 7.26 (br. s., 1 H), 6.19 (d, *J* = 7.5 Hz, 1 H), 4.38 – 4.27 (m, 1 H), 3.69 – 3.65 (m, 2 H), 3.60 – 3.56 (m, 2 H), 3.42 (s, 3 H), 3.41 – 3.33 (m, 1 H), 2.77 (s, 3 H), 2.33 – 2.36 (m, 2 H), 2.21 – 2.14 (m, 2 H), 1.62 – 1.38 (m, 4 H); ^{13}C NMR (101 MHz, DMSO-d_6) δ ppm 158.9, 154.4, 146.7, 137.8, 133.2, 129.9, 125.2, 118.2, 114.7, 110.8, 109.5, 76.9, 71.6, 66.7, 58.0, 49.1, 30.7, 29.8, 17.4; HRMS $(M + H)^+$ calculated for $C_{21}H_{28}N_5O_2^+$ 382.2238, found 382.2234; LCMS (high pH): R_t = 0.84 (97%), MH^+ = 382.4.

6-Bromo-8-methylquinazolin-4(3*H*)-one (45)

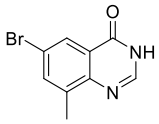

To a round bottomed flask was added 2-amino-5-bromo-3-methylbenzoic acid (1.00 g, 4.35 mmol). The flask was evacuated and purged with N_2 before addition of formamide (3.47 mL, 87.0 mmol). The mixture was stirred at 140 °C under N_2 for 22 h. After 20 min of heating, the mixture formed a clear orange solution, turning to a tan brown slurry overnight. After this time, the mixture was added to ice and water (10 mL) and stirred for 15 min. The mixture was then filtered under vacuum and the filter cake washed with water (5 mL). The filter cake was collected to yield 6-bromo-8-methylquinazolin-4(3*H*)-one (**45**) (964 mg, 4.03 mmol, 93% yield) as an off-white solid; m.p. 299 – 305 °C; ν_{max}(solid): 3074, 2877, 1687, 1607, 1449, 1404, 1328, 1269, 879, 798, 527, 512; ^{1}H NMR (400 MHz, DMSO-d_6) δ ppm 12.41 (br. s., 1 H), 8.16 (s, 1 H), 8.04 (d, J = 2.2 Hz, 1 H), 7.87 – 7.85 (m, 1 H), 2.52 (s, 3 H); ^{13}C NMR (101 MHz, DMSO-d_6) d ppm 159.8, 146.3, 145.0, 138.6, 137.0, 125.4, 124.0, 118.7, 16.8; HRMS $(M + H)^+$ calculated for $C_9H_8BrN_2O^+$ 238.9815, found 238.9813; LCMS (high pH): R_t = 0.77 mins (99%), MH^+ = 238.8, 240.8. Spectroscopic data is consistent with literature reports.[250]

6-Bromo-*N*-((*1r,4r*)-4-(2-methoxyethoxy)cyclohexyl)-8-methylquinazolin-4-amine (46)

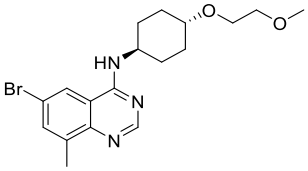

To a microwave vial was added (*1r,4r*)-4-(2-methoxyethoxy)cyclohexan-1-amine (**12**) (675 mg, 3.90 mmol), 6-bromo-8-methylquinazolin-4(3*H*)-one (**45**) (466 mg, 1.95 mmol), and PyBOP (1.52 g, 2.92 mmol). The vial was capped, and evacuated and purged with N_2 before addition of MeCN (5 mL), and DBU (0.59 mL, 3.90 mmol). The mixture was stirred at RT for 2.5 h. After this time, the mixture was separated with EtOAc (10 mL), and water (10 mL). The organic layer was washed with water (5 mL), and brine (5 mL) and then passed through a hydrophobic frit and concentrated *in*

vacuo. The crude material was purified by silica gel chromatography eluting with EtOAc in cyclohexane (0 – 50%). The appropriate fractions were combined and concentrated *in vacuo* to yield 6-bromo-*N*-((*1r*,*4r*)-4-(2-methoxyethoxy)cyclohexyl)-8-methylquinazolin-4-amine (**46**) (443 mg, 1.12 mmol, 58% yield) as an orange oil; ν_{max}(oil): 3352, 2934, 2862, 1602, 1580, 1533, 1485, 1097, 841, 806; ^{1}H NMR (400 MHz, DMSO-d_6) δ ppm 8.51 (s, 1 H), 8.43 (d, *J* = 1.8 Hz, 1 H), 7.91 (d, *J* = 7.5 Hz, 1 H), 7.76 (d, *J* = 1.0 Hz, 1 H), 4.20 – 4.08 (m, 1 H), 3.57 – 3.53 (m, 2 H), 3.45 – 3.41 (m, 2 H), 3.32 – 3.27 (m, 1 H), 3.25 (s, 3 H), 2.54 (s, 3 H), 2.08 – 1.94 (m, 4 H), 1.49 – 1.37 (m, 2 H), 1.32 – 1.21 (m, 2 H); ^{13}C NMR (101 MHz, $CDCl_3$-*d*) δ ppm 158.1, 154.7, 147.5, 139.5, 135.6, 120.59, 118.6, 115.8, 77.7, 72.4, 67.6, 59.1, 49.4, 30.8, 30.6, 17.6; HRMS $(M + H)^+$ calculated for $C_{18}H_{25}BrN_3O_2^+$ 394.1125, found 394.1128; LCMS (high pH): R_t = 1.12 mins (100%), MH^+ = 394.3, 396.2.

3-(Benzyloxy)propanoic acid (49)

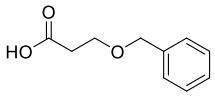

β-Lactone (0.44 mL, 6.94 mmol) and phenylmethanol (1.87 mL, 18.0 mmol) were stirred in a round bottomed flask at 75 °C for 28 h. After this time, the solution was allowed to cool to RT before careful addition of 2 M NaOH (150 mL, 300 mmol). The solution was stirred at RT for a further 1 h and then extracted with DCM (3 × 100 mL). The aqueous layer was then acidified by addition of 2 M HCl (200 mL) and extracted with Et_2O (3 × 150 mL). The Et_2O washes were combined and concentrated *in vacuo* to yield 3-(benzyloxy)propanoic acid (**49**) (637 mg, 3.53 mmol, 51% yield) as a yellow oil; ν_{max}(oil): 3031, 2871, 1711, 1453, 1187, 1100, 1067, 736, 697; ^{1}H NMR (400 MHz, $CDCl_3$-*d*) δ ppm 7.40 – 7.27 (m, 5 H), 4.57 (s, 2 H), 3.77 (t, *J* = 6.3 Hz, 2 H), 2.68 (t, *J* = 6.3 Hz, 2 H); ^{13}C NMR (101 MHz, $CDCl_3$-*d*) δ ppm 177.2, 137.8, 128.4, 127.69, 127.66, 73.1, 65.2, 34.9; HRMS $(M + Na)^+$ calculated for $C_{10}H_{12}NaO_3^+$ 203.0679, found 203.0676; LCMS (high pH): R_t = 0.45 mins (85%), MH^- = 179.2. Spectroscopic data is consistent with literature reports.[253]

6-(1*H*-Imidazol-1-yl)-*N*-((*1r,4r*)-4-(2-methoxyethoxy)cyclohexyl)-8-methyl-2-(pent-4-yn-1-yl)quinazolin-4-amine (51)

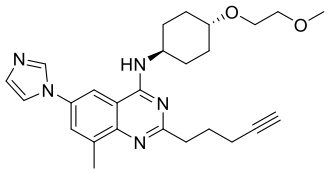

To a microwave vial was added imidazole (53 mg, 0.77 mmol), CuI (13 mg, 0.07 mmol), and K_2CO_3 (100 mg, 0.73 mmol). The vial was capped, and evacuated and purged with N_2 before addition of a solution of 6-bromo-*N*-((*1r,4r*)-4-(2-methoxyethoxy)cyclohexyl)-8-methyl-2-(pent-4-yn-1-yl)quinazolin-4-amine (**55**) (209 mg, 0.45 mmol) in DMF (2 mL). The solution was stirred at 150 °C for 16 h. After this time, the solution was allowed to cool to RT and then diluted in EtOAc (20 mL), and washed with sat. $NaHCO_3$ solution (2 × 10 mL), and brine (10 mL). The organic layer was passed through a hydrophobic frit and concentrated *in vacuo*. The crude material was purified by silica gel chromatography eluting with EtOAc in cyclohexane (0 – 75%). The appropriate fractions were combined and concentrated *in vacuo* to yield 6-(1*H*-imidazol-1-yl)-*N*-((*1r,4r*)-4-(2-methoxyethoxy)cyclohexyl)-8-methyl-2-(pent-4-yn-1-yl)quinazolin-4-amine (**51**) (98 mg, 0.22 mmol, 48% yield) as a colourless gum; ν_{max}(gum): 3243, 3115, 2928, 2860, 1581, 1537, 1451, 1096, 1073, 915, 872, 664; ^{1}H NMR (400 MHz, $CDCl_3$) δ ppm 7.84 – 7.82 (m, 1 H), 7.56 – 7.54 (m, 1 H), 7.54 – 7.52 (m, 1 H), 7.33 – 7.32 (m, 1 H), 7.24 – 7.22 (m, 1 H), 5.80 (d, *J* = 7.3 Hz, 1 H), 4.35 – 4.24 (m, 1 H), 3.68 – 3.65 (m, 2 H), 3.59 – 3.55 (m, 2 H), 3.41 (s, 3 H), 3.41 – 3.32 (m, 1 H), 3.01 (t, *J* = 7.3 Hz, 2 H), 2.73 (s, 3 H), 2.39 (td, *J* = 7.2, 2.4 Hz, 2 H), 2.32 – 2.24 (m, 2 H), 2.20 – 2.11 (m, 4 H), 1.99 (t, *J* = 2.7 Hz, 1 H), 1.60 – 1.48 (m, 2 H), 1.45 – 1.33 (m, 2 H); ^{13}C NMR (151 MHz, $CDCl_3$) δ ppm 166.0, 158.9, 148.4, 139.1, 135.8, 132.8, 130.2, 126.4, 118.7, 112.9, 111.0, 84.5, 77.5, 72.1, 68.1, 67.3, 58.9, 49.2, 38.4, 30.52, 30.46, 26.6, 18.0, 17.7; HRMS $(M + H)^+$ calculated for $C_{26}H_{34}N_5O_2^+$ 448.2707, found 448.2712; LCMS (high pH): R_t = 1.19 mins (97%), MH^+ = 448.3.

6-Bromo-8-methyl-2-(pent-4-yn-1-yl)-4*H*-benzo[*d*][1,3]oxazin-4-one (53)

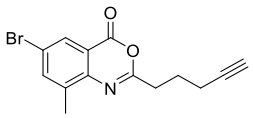

To a microwave vial was added 2-amino-5-bromo-3-methylbenzoic acid (378 mg, 1.64 mmol). The vial was capped, and evacuated and purged with N_2 before addition of THF (2 mL). The solution was stirred for 5 min at RT before slow addition of a solution of hex-5-ynoyl chloride (257 mg, 1.97 mmol) in THF (2 mL). The mixture was stirred at RT for 18 h overnight. The pink solution was then concentrated *in vacuo* before being replaced into a microwave vial, which was then capped, and evacuated and purged with N_2. Acetic anhydride (1.38 mL, 14.6 mmol) was added and the mixture was stirred at 110 °C for 1 h. After this time, the solution was diluted in EtOAc (20 mL), and washed with water (2 × 10 mL), and brine (2 × 10 mL). The organic layer was passed through a hydrophobic frit and concentrated *in vacuo*. The crude material was purified by silica gel chromatography eluting with TBME in cyclohexane (0 – 15%). The appropriate fractions were combined and concentrated *in vacuo* to yield 6-bromo-8-methyl-2-(pent-4-yn-1-yl)-4*H*-benzo[*d*][1,3]oxazin-4-one (**53**) (379 mg, 1.24 mmol, 85% yield) as a white solid; m.p. 86 – 90 °C; ν_{max}(solid): 3298, 3076, 2965, 2920, 2137, 1763, 1645, 1247, 784, 649, 626; ^{1}H NMR (400 MHz, DMSO-d_6) δ ppm 8.03 – 7.99 (m, 2 H), 2.81 (t, *J* = 2.6 Hz, 1 H), 2.77 (t, *J* = 7.3 Hz, 2 H), 2.48 (s, 3 H), 2.36 (td, *J* = 7.1, 2.7 Hz, 2 H), 1.94 (quin, *J* = 7.2 Hz, 2 H); ^{13}C NMR (101 MHz, DMSO-d_6) δ ppm 161.6, 158.4, 143.4, 139.4, 137.7, 127.2, 119.6, 118.4, 83.7, 71.7, 32.8, 24.1, 17.0, 16.2; HRMS $(M + H)^+$ calculated for $C_{14}H_{13}BrNO_2^+$ 306.0124, found 306.0127; LCMS (high pH): R_t = 1.35 mins (88%), MH^+ = 306.1, 308.1.

6-Bromo-8-methyl-2-(pent-4-yn-1-yl)quinazolin-4(3*H*)-one (54)

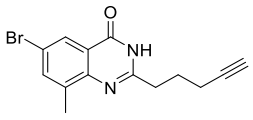

To a microwave vial was added 6-bromo-8-methyl-2-(pent-4-yn-1-yl)-4*H*-benzo[*d*][1,3]oxazin-4-one (**53**) (350 mg, 1.14 mmol) and ammonium acetate (176 mg, 2.29 mmol). The vial was capped, and evacuated and purged with N_2 before addition of DMA (2.5 mL). The solution was stirred at 170 °C for 1.5 h. After this time, the

solution was allowed to cool to RT and then diluted in EtOAc (20 mL) and washed with water (2 × 10 mL), and brine (10 mL). The organic layer was then passed through a hydrophobic frit and concentrated *in vacuo* to yield 6-bromo-8-methyl-2-(pent-4-yn-1-yl)quinazolin-4(3*H*)-one (**54**) (317 mg, 1.04 mmol, 91 % yield), as a colourless gum; ν_{max}(solid): 3303, 3021, 2879, 2150, 1667, 1615, 1458, 807, 796, 656, 628; ^{1}H NMR (400 MHz, DMSO-d_6) δ ppm 12.33 (br. s., 1 H), 7.99 (d, *J* = 1.8 Hz, 1 H), 7.82 (br. s., 1 H), 2.79 (t, *J* = 2.4 Hz, 1 H), 2.71 (t, *J* = 7.4 Hz, 2 H), 2.50 (s, 3 H), 2.30 (td, *J* = 7.0, 2.5 Hz, 2 H), 2.00 – 1.88 (m, 2 H); ^{13}C NMR (101 MHz, DMSO-d_6) δ ppm 160.8, 156.2, 146.3, 138.0, 136.8, 125.3, 122.3, 117.8, 83.9, 71.6, 33.2, 25.0, 17.2, 16.7; HRMS $(M + H)^+$ calculated for $C_{14}H_{14}BrN_2O^+$ 305.0284, found 305.0290; LCMS (high pH): R_t = 1.17 mins (96%), MH^+ = 305.1, 307.1.

6-Bromo-*N*-((*1r*,*4r*)-4-(2-methoxyethoxy)cyclohexyl)-8-methyl-2-(pent-4-yn-1-yl)quinazolin-4-amine (55)

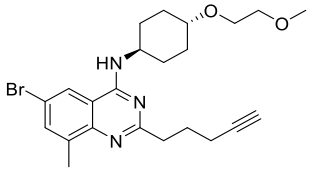

To a microwave vial was added 6-bromo-8-methyl-2-(pent-4-yn-1-yl)quinazolin-4(3*H*)-one (**54**) (284 mg, 0.93 mmol) and PyBOP (726 mg, 1.40 mmol). The vial was capped, and evacuated and purged with N_2 before addition of DBU (0.28 mL, 1.86 mmol) and a solution of (*1r*,*4r*)-4-(2-methoxyethoxy)cyclohexan-1-amine (**12**) (322 mg, 1.86 mmol) in MeCN (7 mL). The solution was stirred at RT for 1.5 h. After this time, the solution was diluted in EtOAc (30 mL), and washed with water (2 × 10 mL), and brine (10 mL). The organic layer was passed through a hydrophobic frit and concentrated *in vacuo*. The crude material was purified by silica gel chromatography eluting with TBME in cyclohexane (0 – 50%). The appropriate fractions were combined and concentrated *in vacuo* to yield 6-bromo-*N*-((*1r*,*4r*)-4-(2-methoxyethoxy)cyclohexyl)-8-methyl-2-(pent-4-yn-1-yl)quinazolin-4-amine (**55**) (274 mg, 0.60 mmol, 64% yield) as a yellow gum; ν_{max}(gum): 3358, 3295, 2933, 2869, 2153, 1574, 1527, 1448, 1412, 1364, 1131, 1093, 872, 805, 632; ^{1}H NMR (400 MHz, $CDCl_3$) δ ppm 7.61 – 7.59 (m, 2 H), 5.27 (d, *J* = 7.3 Hz, 1 H), 4.27 – 4.16 (m, 1 H), 3.68 – 3.64 (m, 2 H), 3.59 – 3.54 (m, 2 H), 3.41 (s, 3 H), 3.39 – 3.31 (m, 1 H), 2.96 (t,

J = 7.3 Hz, 2 H), 2.63 (s, 3 H), 2.36 (td, *J* = 7.2, 2.7 Hz, 2 H), 2.29 – 2.21 (m, 2 H), 2.17 – 2.07 (m, 4 H), 1.97 (t, *J* = 2.6 Hz, 1 H), 1.58 – 1.46 (m, 2 H), 1.36 – 1.25 (m, 2 H); ^{13}C NMR (400 MHz, $CDCl_3$) δ ppm 165.8, 158.0, 148.1, 139.2, 135.2, 120.4, 117.4, 114.1, 84.7, 77.6, 72.3, 68.3, 67.5, 59.1, 49.3, 38.6, 30.64, 30.61, 26.8, 18.2, 17.5; HRMS $(M + H)^+$ calculated for $C_{23}H_{31}BrN_3O_2^+$ 460.1594, found 460.1601; LCMS (high pH): R_t = 1.48mins (94%), MH^+ = 460.3, 462.3.

(*S*)-2,2-Dimethyl-22-((3-methyl-3*H*-diazirin-3-yl)methyl)-4,20-dioxo-3,8,11,14,17-pentaoxa-5,21-diazatricosan-23-oic acid (59)

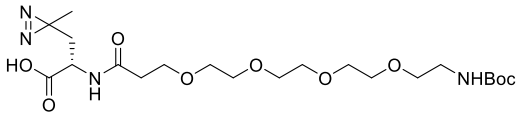

To a microwave vial was added 2,2-dimethyl-4-oxo-3,8,11,14,17-pentaoxa-5-azaicosan-20-oic acid (272 mg, 0.74 mmol), *N*-hydroxysuccinimide(103 mg, 0.89 mmol), and EDC.HCl (157 mg, 0.82 mmol). The vial was capped, and evacuated and purged with N_2 before addition of DCM (1.5 mL). The solution was stirred at RT for 20 h. After this time, the solution was concentrated *in vacuo*. The crude material was diluted in EtOAc (10 mL), and washed with water (3 mL), and brine (3 mL). The organic layer was passed through a hydrophobic frit and concentrated *in vacuo* to give the activated ester intermediate. To a separate solution of $NaHCO_3$ (99 mg, 1.18 mmol) in water (2 mL) was added (*S*)-2-amino-3-(3-methyl-3*H*-diazirin-3-yl)propanoic acid (84 mg, 0.59 mmol). This solution was stirred at RT for 10 minutes before addition of the activated ester intermediate dissolved in 1,4-dioxane (2 mL). The combined solution was stirred at RT for a further 18 h and then concentrated *in vacuo*. The residue was dissolved in water (8 mL) and EtOAc (8 mL). 1 M aqueous HCl (2.95 mL, 2.95 mmol) was added and the emulsion was stirred vigorously for 10 min. The organic layer was separated, and the aqueous layer was washed with EtOAc (2 × 5 mL). The combined organic layers were passed through a hydrophobic frit before being concentrated *in vacuo*. The crude material was purified by silica gel chromatography eluting with EtOAc in cyclohexane (0 – 100%) and then with EtOH in EtOAc (0 – 100%). The appropriate fractions were combined and concentrated *in vacuo* to yield (*S*)-2,2-dimethyl-22-((3-methyl-3*H*-diazirin-3-yl)methyl)-4,20-dioxo-3,8,11,14,17-pentaoxa-5,21-diazatricosan-23-oic acid (**59**) (148 mg, 0.30 mmol, 51% yield) as a

colourless oil; ν_{max}(oil): 3321, 2975, 2926, 2872, 1704, 1653, 1532, 1249, 1102; ^{1}H NMR (400 MHz, MeOD) δ ppm 4.39 (dd, *J* = 9.6, 4.7 Hz, 1 H), 3.82 – 3.75 (m, 2 H), 3.67 – 3.58 (m, 12 H), 3.51 (t, *J* = 5.5 Hz, 2 H), 3.24 – 3.20 (m, 2 H), 2.62 – 2.49 (m, 2 H), 2.03 (dd, *J* = 15.0, 4.7 Hz, 1 H), 1.58 (dd, *J* = 15.0, 9.6 Hz, 1 H), 1.44 (s, 9 H), 1.05 (s, 3 H), 3 H not observed (exchangeable); ^{13}C NMR (151 MHz, DMSO-d_6) δ ppm 172.6, 169.7, 155.5, 77.5, 69.72, 69.67, 69.6, 69.5, 69.4, 69.1, 66.7, 48.4, 39.6, 36.4, 36.0, 28.2, 24.5, 19.5, 1 C not observed; HRMS $(M + H)^+$ calculated for $C_{21}H_{39}N_4O_9^+$ 491.2712, found 491.2716; LCMS (high pH): R_t = 0.61 mins (100%), MH^+ = 491.4.

2-(4-Aminobutyl)-6-(1*H*-imidazol-1-yl)-*N*-((*1r,4r*)-4-(2-methoxyethoxy)cyclohexyl)-8-methylquinazolin-4-amine (66)

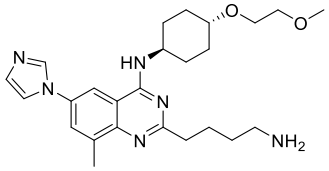

To a hydrogenation flask containing platinum(IV) oxide (243 mg, 1.07 mmol) was added a solution of 4-(6-(1*H*-imidazol-1-yl)-4-(((*1r,4r*)-4-(2-methoxyethoxy)cyclohexyl)amino)-8-methylquinazolin-2-yl)butanenitrile (**87**) (370 mg, 0.83 mmol) in acetic acid (4.0 mL, 70 mmol). The solution was stirred under H_2 for 18 h. After this time, the reaction mixture was diluted in water (20 mL) and then made basic through addition of 2 M NaOH. The mixture was extracted with EtOAc (3 × 10 mL) and the combined organic layers were passed through a hydrophobic frit and concentrated *in vacuo*. The crude material was purified by gold silica gel chromatography eluting with EtOAc + 1% NEt_3 in cyclohexane + 1% NEt_3 (0 – 100%), and then EtOH in EtOAc + 1% NEt_3 (0 – 100%). The appropriate fractions were combined and concentrated *in vacuo* to yield 2-(4-aminobutyl)-6-(1*H*-imidazol-1-yl)-*N*-((*1r,4r*)-4-(2-methoxyethoxy)cyclohexyl)-8-methylquinazolin-4-amine (**66**) (136 mg, 0.30 mmol, 36% yield) as an orange gum; ν_{max}(gum): 3260, 3083, 2933, 2858, 1569, 1535, 1436, 1398, 1371, 1100, 1071, 649; ^{1}H NMR (600 MHz, $CDCl_3$) δ ppm 7.83 (s, 1 H), 7.54 (s, 1 H), 7.51 – 7.49 (m, 1 H), 7.31 (s, 1 H), 7.23 (s, 1 H), 5.74 (d, *J* = 7.7 Hz, 1 H), 4.32 – 4.25 (m, 1 H), 3.68 – 3.65 (m, 2 H), 3.58 – 3.55 (m, 2 H), 3.41 (s, 3 H), 3.39 – 3.33 (m, 1 H), 2.91 (t, *J* = 7.5 Hz, 2 H), 2.78 (t, *J* = 7.0 Hz, 2 H), 2.73

(s, 3 H), 2.30 – 2.25 (m, 2 H), 2.19 – 2.13 (m, 2 H), 1.94 (quin, *J* = 7.6 Hz, 2 H), 1.63 - 1.49 (m, 4 H), 1.42 - 1.34 (m, 2 H), 2 H not observed (exchangeable); ^{13}C NMR (101 MHz, DMSO-d_6) δ ppm 166.8, 158.8, 148.8, 138.1, 134.3, 132.3, 130.2, 126.4, 118.7, 112.8, 111.0, 77.5, 72.1, 67.3, 58.9, 49.2, 42.0, 39.4, 33.4, 30.51, 30.45, 25.1, 17.7; HRMS $(M + H)^+$ calculated for $C_{25}H_{39}N_6O_2^+$ 453.2973, found 453.2975; LCMS (high pH): R_t = 1.07 mins (95%), MH^+ = 453.4.

_N_-((*1r,4r*)-4-((6-(1*H*-imidazol-1-yl)-2,8-dimethylquinazolin-4-yl)amino)cyclohexyl)-5-aminopentanamide (67)

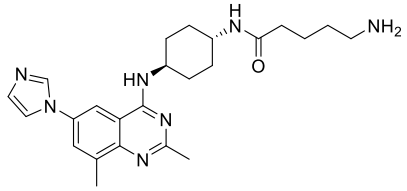

To a hydrogenation flask containing platinum(IV) oxide (142 mg, 0.62 mmol) was added a solution of *N*-((*1r,4r*)-4-((6-(1*H*-imidazol-1-yl)-2,8-dimethylquinazolin-4-yl)amino)cyclohexyl)-4-cyanobutanamide (**92**) (207 mg, 0.48 mmol) in acetic acid (2.2 mL, 38 mmol). The solution was stirred under H_2 for 6 h. After this time, the reaction mixture was diluted in water and then made basic through addition of 2 M NaOH. The mixture was extracted with EtOAc (3 × 20 mL) and the combined organic layers were passed through a hydrophobic frit and concentrated *in vacuo*. The crude material was purified by silica gel chromatography eluting with EtOAc + 1% NEt_3 in cyclohexane + 1% NEt_3 (0 – 100%), and then EtOH in EtOAc + 1% NEt_3 (0 – 100%). The appropriate fractions were combined and concentrated *in vacuo* to yield *N*-((*1r,4r*)-4-((6-(1*H*-imidazol-1-yl)-2,8-dimethylquinazolin-4-yl)amino)cyclohexyl)-5-aminopentanamide (**67**) (125 mg, 0.29 mmol, 60% yield) as a white solid; m.p. 185 – 193 °C (dec.); ν_{max}(solid): 3268, 3043, 2930, 1634, 1537, 1398, 1065, 802, 656; ^{1}H NMR (400 MHz, DMSO-d_6) δ ppm 8.30 – 8.29 (m, 2 H), 7.92 – 7.89 (m, 1 H), 7.80 – 7.79 (m, 1 H), 7.72 – 7.68 (m, 2 H), 7.17 – 7.16 (m, 1 H), 4.24 – 4.13 (m, 1 H), 3.63 – 3.52 (m, 1 H), 3.29 (app. s, 2 H), 2.59 (s, 3 H), 2.56 – 2.48 (m, 2 H), 2.49 (s, 3 H), 2.08 – 1.98 (m, 4 H), 1.91 – 1.85 (m, 2 H), 1.55 – 1.40 (m, 4 H), 1.38 – 1.26 (m, 4 H); ^{13}C NMR (151 MHz, DMSO-d_6) δ ppm 162.7, 158.9, 147.3, 137.1, 135.7, 132.4, 129.8, 125.2, 118.3, 112.8, 110.8, 109.5, 48.6, 47.1, 41.3, 35.4, 32.7, 31.3, 30.8, 26.7, 22.8,

17.5; HRMS $(M + H)^+$ calculated for $C_{24}H_{34}N_7O^+$ 436.2819, found 436.2823; LCMS (high pH): R_t = 0.92 mins (100%), MH^- = 434.4.

(*R*,*E*)-cyclooct-4-en-1-yl ((*S*)-23-(6-(1*H*-imidazol-1-yl)-4-(((*1r*,*4S*)-4-(2-methoxyethoxy)cyclohexyl)amino)-8-methylquinazolin-2-yl)-17-((3-methyl-3*H*-diazirin-3-yl)methyl)-15,18-dioxo-3,6,9,12-tetraoxa-16,19-diazatricosyl)carbamate (68)

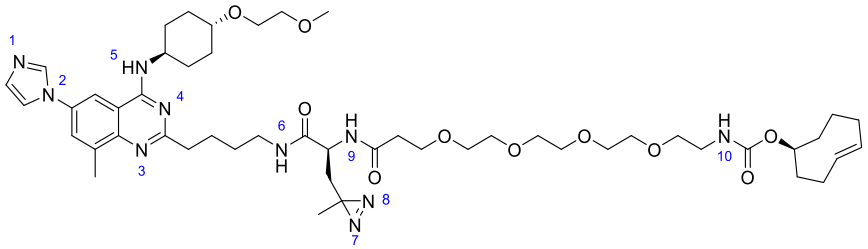

A microwave vial containing HATU (20 mg, 0.05 mmol) was capped, and evacuated and purged with N_2 before addition of a solution of (*S*)-2,2-dimethyl-22-((3-methyl-3*H*-diazirin-3-yl)methyl)-4,20-dioxo-3,8,11,14,17-pentaoxa-5,21-diazatricosan-23-oic acid (**59**) (26 mg, 0.05 mmol) in DMF (0.10 mL) and DIPEA (0.03 mL, 0.15 mmol). The solution was stirred at RT for 30 min before addition of a solution of 2-(4-aminobutyl)-6-(1*H*-imidazol-1-yl)-*N*-((*1r*,*4r*)-4-(2-methoxyethoxy)cyclohexyl)-8-methylquinazolin-4-amine (**66**) (22 mg, 0.05 mmol) in DMF (0.15 mL). The solution was stirred at RT for a further 2 h. After this time, the solution was diluted in EtOAc (3 mL), and washed with water (1 mL), and brine (1 mL). The organic layer was passed through a hydrophobic frit and concentrated *in vacuo*. The crude material was diluted in MeOH (0.5 mL) and passed through an SCX column. This was washed with 2 M NH_3 in MeOH (5 mL), and the basic filtrate was concentrated *in vacuo*. The crude material was diluted in 4 M HCl in 1,4-dioxane (1 mL, 4.00 mmol) and the solution stirred at RT for 1 h. After this time, the solution was concentrated in vacuo to yield the chloride salt intermediate. The intermediate was diluted in MeCN (0.20 mL), DIPEA (0.04 mL, 0.24 mmol) and (*S*,*E*)-cyclooct-4-en-1-yl (4-nitrophenyl) carbonate (16 mg, 0.05 mmol) was added. The solution was stirred at RT for 1.5 h. After this time, the solution was diluted in EtOAc (1 mL) and washed with water (1 mL), and brine (1 mL). The organic layer was passed through a hydrophobic frit and concentrated *in vacuo*. The crude material was purified by auto-preparative HPLC

(HpH). The appropriate fractions were combined and concentrated *in vacuo* to yield (*S*,*E*)-cyclooct-4-en-1-yl ((*S*)-23-(6-(1*H*-imidazol-1-yl)-4-(((*1r*,*4S*)-4-(2-methoxyethoxy)cyclohexyl)amino)-8-methylquinazolin-2-yl)-17-((3-methyl-3*H*-diazirin-3-yl)methyl)-15,18-dioxo-3,6,9,12-tetraoxa-16,19-diazatricosyl)carbamate (**68**) (6 mg, 6 µmol, 13% yield) as a colourless gum. A *cis* impurity was observed by NMR; ν_{max}(gum): 3301, 3050, 2930, 2865, 1691, 1649, 1572, 1535, 1455, 1260, 1102, 1020, 732; ^{1}H NMR (600 MHz, MeOD) δ ppm 8.24 (s, 1 H), 8.18 (d, *J* = 1.8 Hz, 1 H), 7.83 (s, 1 H), 7.69 (s, 1 H), 7.19 (s, 1 H), 5.96 – 5.62 (m, 1 H, *trans* alkene H), 5.61 – 5.56 (m, 1 H, *cis* alkene H), 5.55 – 5.49 (m, 1 H, *trans* alkene H), 4.33 – 4.25 (m, 2 H), 3.75 (t, *J* = 6.1 Hz, 2 H), 3.68 – 3.65 (m, 2 H), 3.63 – 3.57 (m, 14 H), 3.56 – 3.48 (m, 4 H), 3.43 – 3.36 (m, 2 H), 3.38 (s, 1 H), 3.29 – 3.21 (m, 3 H), 2.86 (t, *J* = 7.5 Hz, 2 H), 2.69 (s, 3 H), 2.52 (t, *J* = 6.2 Hz, 2 H), 2.39 – 2.30 (m, 1 H), 2.27 – 2.20 (m, 3 H), 2.19 – 2.14 (m, 5 H), 2.07 – 2.02 (m, 1 H), 1.99 (dd, *J* = 14.9, 5.0 Hz, 1 H), 1.93 – 1.87 (m, 2 H), 1.86 – 1.78 (m, 1 H), 1.77 – 1.71 (m, 1 H), 1.68 – 1.61 (m, 3 H), 1.57 (dd, *J* = 13.0, 4.6 Hz, 1 H), 1.54 – 1.40 (m, 6 H), 1.34 – 1.21 (m, 2 H), 1.03 (s, 3 H), a 1:4 mixture of *cis* and *trans* isomers therefore additional alkene peaks are observed, 3 H not observed (exchangeable); ^{13}C NMR (151 MHz, $CDCl_3$) δ ppm 171.9, 170.4, 166.5, 159.0, 156.4, 136.0, 135.41, 135.38, 131.7, 130.5, 126.6, 118.8, 113.1, 111.09, 110.0, 77.6, 72.3, 70.5, 70.33, 70.25, 70.22, 70.15, 67.5, 67.1, 59.1, 49.6, 49.5, 41.1, 40.8, 39.65, 39.62, 39.1, 36.8, 36.4, 34.3, 32.7, 30.7, 30.6, 29.9, 29.7, 29.0, 28.0, 25.3, 23.94, 23.91, 19.76, 19.73, 18.0, 17.9, 1.0, a 1:4 mixture of *cis* and *trans* isomers therefore additional alkene peaks are observed; ^{15}N NMR (600 MHz, MeOD-d_4) δ ppm 77 (N-10), 115 (N-6), 184 (N-2), 233 (N-3 or N-4), 260 (N-1), 491 (N-7 and N-8), three nitrogen peaks not observed due to broadening effects (N-3 or N-4, N-5, N-9), characteristic diazirine peak seen at 491 ppm; HRMS $(M + H)^+$ calculated for $C_{50}H_{77}N_{10}O_{10}^+$ 977.5819, found 977.5825; LCMS (high pH): R_t = 1.20 mins (88%), MH^+ = 977.6.

(*S*,*E*)-Cyclooct-4-en-1-yl ((*S*)-24-(((*1r*,*4S*)-4-((6-(1*H*-imidazol-1-yl)-2,8-dimethylquinazolin-4-yl)amino)cyclohexyl)amino)-17-((3-methyl-3*H*-diazirin-3-yl)methyl)-15,18,24-trioxo-3,6,9,12-tetraoxa-16,19-diazatetracosyl)carbamate (69)

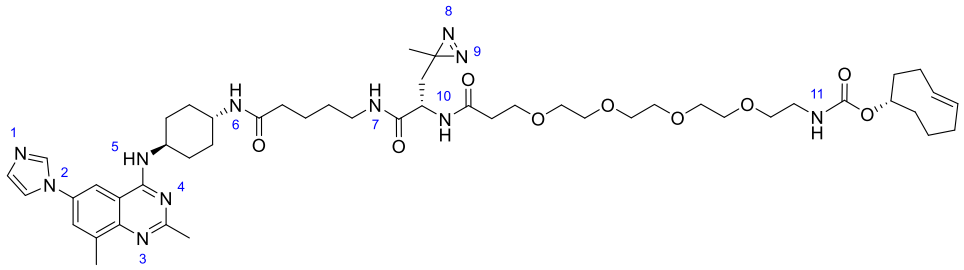

A microwave vial containing HATU (27 mg, 0.07 mmol) was capped, and evacuated and purged with N_2 before addition of a solution of (*S*)-2,2-dimethyl-22-((3-methyl-3*H*-diazirin-3-yl)methyl)-4,20-dioxo-3,8,11,14,17-pentaoxa-5,21-diazatricosan-23-oic acid (**59**) (35 mg, 0.07 mmol) in DMF (0.10 mL) and DIPEA (0.034 mL, 0.19 mmol). The solution was stirred at RT for 30 min before addition of a solution of *N*-((*1r*,*4r*)-4-((6-(1*H*-imidazol-1-yl)-2,8-dimethylquinazolin-4-yl)amino)cyclohexyl)-5-aminopentanamide (**67**) (28 mg, 0.06 mmol) in DMF (0.15 mL). The solution was stirred at RT for a further 1.5 h. After this time, the solution was diluted in EtOAc (3 mL), and washed with water (1 mL), and brine (1 mL). The organic layer was passed through a hydrophobic frit and concentrated *in vacuo*. The crude material was diluted in 4 M HCl in 1,4-dioxane (1 mL, 4.00 mmol) and the solution stirred at RT for 1 h, before being concentrated *in vacuo* to yield the chloride salt intermediate. The intermediate was diluted in MeCN (0.15 mL), DIPEA (0.056 mL, 0.32 mmol) and (*S*,*E*)-cyclooct-4-en-1-yl (4-nitrophenyl) carbonate (21 mg, 0.07 mmol) was added. The solution was stirred at RT for 1.5 h. After this time, the solution was diluted in EtOAc (1 mL) and washed with water (0.5 mL), and brine (0.5 mL). The organic layer was passed through a hydrophobic frit and concentrated *in vacuo*. The crude material was purified by auto-preparative HPLC (HpH). The appropriate fractions were combined and concentrated *in vacuo* to yield (*S*,*E*)-cyclooct-4-en-1-yl ((*S*)-24-(((*1r*,*4S*)-4-((6-(1*H*-imidazol-1-yl)-2,8-dimethylquinazolin-4-yl)amino)cyclohexyl)amino)-17-((3-methyl-3*H*-diazirin-3-yl)methyl)-15,18,24-trioxo-3,6,9,12-tetraoxa-16,19-diazatetracosyl)carbamate (**69**) (11 mg, 0.01 mmol, 18% yield) as a colourless gum. A *cis* impurity was observed by NMR; ν_{max}(gum):

3286, 3053, 2929, 2860, 1697, 1637, 1535, 1436, 1264, 1100, 989, 733; ^{1}H NMR (600 MHz, MeOD) δ ppm 8.23 (s, 1 H), 8.19 (d, *J* = 1.8 Hz, 1 H), 7.83 – 7.81 (m, 1 H), 7.69 (s, 1 H), 7.19 (s, 1 H), 5.71 – 5.64 (m, 1 H, *trans* alkene H), 5.63 – 5.57 (m, 1 H, *cis* alkene H), 5.57 – 5.50 (m, 1 H, *trans* alkene H), 4.34 – 4.27 (m, 3 H), 3.79 (t, *J* = 6.1 Hz, 2 H), 3.67 – 3.57 (m, 18 H), 3.56 – 3.49 (m, 2 H), 3.27 – 3.18 (m, 5 H), 2.68 (s, 3 H), 2.59 (s, 3 H), 2.55 (t, *J* = 6.1 Hz, 2 H), 2.40 – 2.31 (m, 1 H), 2.28 – 2.17 (m, 5 H), 2.14 (d, *J* = 11.7 Hz, 2 H), 2.00 (dd, *J* = 14.9, 5.0 Hz, 3 H), 1.71 – 1.51 (m, 11 H), 1.50 – 1.41 (m, 2 H), 1.35 – 1.22 (m, 2 H), 1.05 (s, 3 H), a 1:4 mixture of *cis* and *trans* isomers therefore additional alkene peaks are observed, ; ^{13}C NMR (151 MHz, MeOD) δ ppm 175.4, 174.1, 173.3, 170.6, 165.9, 161.3, 149.4, 139.3, 137.4, 136.7, 134.7, 132.9, 130.6, 127.5, 120.11 (*trans* alkene), 120.05 (*cis* alkene), 114.9, 112.85 (*trans* alkene), 112.82 (*cis* alkene), 111.7, 71.88, 71.86, 71.84, 71.76, 71.70, 71.6, 71.3, 68.5, 51.3, 50.6, 49.9, 42.3, 42.0, 40.4, 38.2, 37.9, 36.9, 35.6, 34.0, 32.9, 32.4, 31.1, 30.0, 29.3, 26.7, 25.2, 24.6, 20.2, 18.5, a 1:4 mixture of *cis* and *trans* isomers therefore additional alkene peaks are observed; ^{15}N NMR (600 MHz, MeOD-d_4) δ ppm 498 (N-8, N-9), 255 (N-1), 238 (N-3), 232 (N-4), 189 (N-2), 126 (N-10), five nitrogen peaks not observed due to broadening effects (N-2, N-5, N-6, N-7, N-11), characteristic diazirine peak seen at 498 ppm; HRMS $[(M + 2\ H)^{2+}]/2$ calculated for $C_{49}H_{75}N_{11}O_9^{2+}$ 480.7869, found 480.7876; LCMS (high pH): R_t = 1.12 mins (93%), MH^- = 958.7.

2-Amino-5-iodo-3-methylbenzoic acid (71)

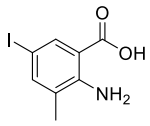

NIS (7.04 g, 31.3 mmol) was added to a solution of 2-amino-3-methylbenzoic acid (4.73 g, 31.3 mmol) in DMF (50 mL). The mixture was stirred at 70 °C under N_2 for 2 h. After this time, the solution was allowed to cool to RT and was concentrated *in vacuo*. The resulting residue was dispersed in water (100 mL) and the suspension was filtered *in vacuo*. The solid was washed with water (50 mL) and then dried to give 2-amino-5-iodo-3-methylbenzoic acid (**71**) (8.69 g, 31.4 mmol, 100% yield) as a brown solid; m.p. 212 – 217 °C (dec.); ν_{max}(solid): 3504, 3381, 2966, 1665, 1562, 1310, 1224, 877, 855, 791, 682, 587; ^{1}H NMR (400 MHz, DMSO-d_6) δ ppm 7.86 (d, *J* = 2.0 Hz, 1

H), 7.44 (d, *J* = 2.2, 1 H), 3.31 (br. s, 2 H), 2.08 (s, 3 H), carboxylic acid 1 H not seen; ^{13}C NMR (101 MHz, DMSO-d_6) δ ppm 168.7, 149.3, 141.6, 136.7, 126.4, 111.6, 74.4, 17.0; HRMS $(M + H)^+$ calculated $C_8H_9INO_2^+$ 277.9672, found 277.9689; LCMS (high pH): R_t = 0.56 mins (97%), MH^+ = 278.1.

2-(4-Bromobutyl)-6-iodo-8-methyl-4*H*-benzo[*d*][*1,3*]oxazin-4-one (73)

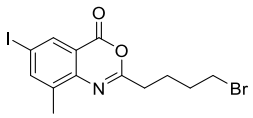

To a round bottomed flask containing 2-amino-5-iodo-3-methylbenzoic acid (**71**) (1.80 g, 6.50 mmol) was added THF (15 mL) under N_2, followed by dropwise addition of 5-bromopentanoyl chloride (1.04 mL, 7.80 mmol). The solution was stirred at RT for 18 h. After this time, the mixture was concentrated *in vacuo*. The residue was then diluted in acetic anhydride (3.52 ml, 37.3 mmol) and the mixture was stirred at 110 °C under N_2 for 2 h. The solution was allowed to cool to RT and was filtered under vacuum. The solid was washed with MeOH (2 × 2 mL) and collected and then diluted in water (10 mL). The mixture was filtered under vacuum and washed with further water (2 × 3 mL). Starting material was washed through into the filtrate where it precipitated out. The solid on the filter was collected to yield 2-(4-bromobutyl)-6-iodo-8-methyl-4*H*-benzo[*d*][*1,3*]oxazin-4-one (**73**) (0.85 g, 2.01 mmol, 54% yield) as a white solid; m.p. 109 – 112 °C; ν_{max}(solid): 2948, 2925, 1756, 1458, 1236, 1251, 790, 772, 558; ^{1}H NMR (400 MHz, DMSO-d_6) δ ppm 8.18 – 8.16 (m, 1 H), 8.13 – 8.12 (m, 1 H), 3.60 (t, *J* = 6.6 Hz, 2 H), 2.71 (t, *J* = 7.1 Hz, 2 H), 2.44 (s, 3 H), 2.01 – 1.82 (m, 4 H); ^{13}C NMR (101 MHz, $CDCl_3$-*d*) δ ppm 161.5, 158.7, 145.7, 144.2, 138.0, 134.6, 118.3, 91.9, 33.7, 32.9, 31.8, 24.3, 16.6; HRMS $(M + H)^+$ calculated for $C_{13}H_{14}BrINO2^+$ 421.9247, found 421.9246; LCMS (high pH): R_t = 1.49 mins (95%), MH^+ = 422.0, 424.1.

2-(4-Azidobutyl)-6-iodo-8-methyl-4*H*-benzo[*d*][*1,3*]oxazin-4-one (74)

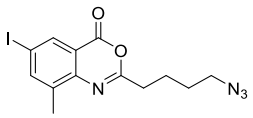

To a microwave vial was added 2-(4-bromobutyl)-6-iodo-8-methyl-4*H*-benzo[*d*][1,3]oxazin-4-one (**73**) (276 mg, 0.65 mmol) and sodium azide (42.5 mg, 0.65 mmol). The vial was capped and evacuated and purged with N_2 before addition of DMF (3 mL). The mixture was stirred at RT for 2 h. After this time, the solution was diluted in EtOAc (10 mL) and washed with saturated aq. $NaHCO_3$ solution (10 mL) and brine (10 mL). The organic layer was passed through a hydrophobic frit and concentrated *in vacuo* to yield 2-(4-azidobutyl)-6-iodo-8-methyl-4*H*-benzo[*d*][1,3]oxazin-4-one (**74**) (190 mg, 0.50 mmol, 76% yield) as an off-white solid; m.p. not measured due to potential explosive nature of azide; ν_{max}(solid): 2984, 2867, 2093, 1736, 1649, 1457, 1256, 1137, 791, 768; ^{1}H NMR (400 MHz, DMSO-d_6) δ ppm 8.17 (d, *J* = 1.5 Hz, 1 H), 8.13 (d, *J* = 1.5 Hz, 1 H), 3.40 (t, *J* = 6.6 Hz, 2 H), 2.71 (t, *J* = 7.1 Hz, 2 H) 2.45 (s, 3 H), 1.84 - 1.76 (m, 2 H) 1.73 - 1.67 (m, 2 H); ^{13}C NMR (101 MHz, DMSO-d_6) δ ppm 162.4, 158.7, 145.6, 144.2, 137.9, 133.8, 118.9, 93.1, 50.9, 33.8, 28.0, 22.8, 16.5; HRMS $(M + H)^+$ calculated for $C_{13}H_{14}IN_4O_2^+$ 385.0156, found 385.0160; LCMS (high pH): R_t = 1.44 mins (84%), MH^+ = 385.0.

2-(But-3-en-1-yl)-6-iodo-8-methyl-4*H*-benzo[*d*][*1,3*]oxazin-4-one (78)

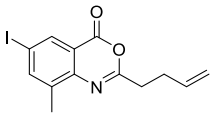

A microwave vial containing 2-amino-5-iodo-3-methylbenzoic acid (**71**) (1.00 g, 3.61 mmol) was capped and evacuated and purged with N_2. THF (8 mL) was added followed by dropwise addition of pent-4-enoyl chloride (0.48 mL, 4.33 mmol). The solution was stirred at RT for 18 h. After this time, the solution was concentrated *in vacuo*. To the flask was added Boc_2O (0.84 mL, 3.62 mmol), DMAP (0.04 g, 0.36 mmol), and 1,4-dioxane (20 mL). Pyridine (0.29 mL, 3.62 mmol) was added slowly and the solution was stirred at RT under N_2 for 24 h. After this time, the mixture was diluted in EtOAc (30 mL), and washed with water (2 × 10 mL), and brine (2 × 10 mL). The organic layer was passed through a hydrophobic frit and concentrated *in vacuo*.

The crude material was purified by silica gel chromatography eluting with TBME in cyclohexane (0 – 5%). The appropriate fractions were combined and concentrated *in vacuo* to yield 2-(but-3-en-1-yl)-6-iodo-8-methyl-4*H*-benzo[*d*][1,3]oxazin-4-one (**78**) (756 mg, 2.22 mmol, 61% yield) as yellow crystals; m.p. 60 – 64 °C; ν_{max}(solid): 3071, 2916, 1754, 1741, 1637, 1460, 1427, 1308, 1143, 963, 906, 879, 790, 540, 469; ^{1}H NMR (400 MHz, DMSO-d_6) δ ppm 8.14 (d, *J* = 1.5 Hz, 1 H), 8.11 - 8.09 (m, 1 H), 5.97 - 5.87 (m, 1 H), 5.17 – 5.10 (m, 1 H), 5.05 – 5.00 (m, 1 H), 2.76 (t, *J* = 7.5 Hz, 2 H), 2.53 - 2.46 (m, 2 H), 2.42 (s, 3 H); ^{13}C NMR (101 MHz, DMSO-d_6) δ ppm 161.5, 158.0, 145.1, 143.6, 137.4, 136.7, 133.2, 118.2, 115.8, 92.6, 33.2, 29.0, 15.9; HRMS $(M + H)^+$ calculated for $C_{13}H_{13}INO_2^+$ 341.9985, found 341.9989; LCMS (high pH): R_t = 1.45 mins (99%), MH^+ = 342.2.

2-(But-3-en-1-yl)-6-iodo-8-methylquinazolin-4(3*H*)-one (79)

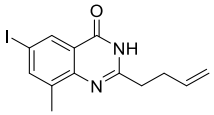

To a microwave vial was added 2-(but-3-en-1-yl)-6-iodo-8-methyl-4*H*-benzo[*d*][1,3]oxazin-4-one (**78**) (648 mg, 1.90 mmol) and ammonium acetate (293 mg, 3.80 mmol). The vial was capped, and evacuated and purged with N_2 before addition of DMA (8 mL). The solution was stirred at 170 °C for 2 h. After this time, the solution was diluted in EtOAc (10 mL), and washed with water (2 × 3 mL), and brine (3 mL). The organic layer was passed through a hydrophobic frit and concentrated *in vacuo.* The crude material was diluted in DCM (10 mL) and then filtered under vacuum. The solid was washed with DCM (3 × 2 mL) and then collected to yield 2-(but-3-en-1-yl)-6-iodo-8-methylquinazolin-4(3*H*)-one (**79**) (646 mg, 1.90 mmol, 100% yield), as a white solid; m.p. 242 – 248 °C; ν_{max}(solid): 3163, 3023, 2920, 2869, 1673, 1615, 1455, 922, 877, 802, 656, 528; ^{1}H NMR (400 MHz, DMSO-d_6) δ ppm 12.31 (br. s, 1 H), 8.19 (d, *J* = 1.7 Hz, 1 H), 7.98 – 7.95 (m, 1 H), 5.95 – 5.84 (m, 1 H), 5.12 – 5.05 (m, 1 H), 5.01 – 4.97 (m, 1 H), 2.74 – 2.69 (m, 2 H), 2.54 – 2.52 (m, 2 H), 2.48 (s, 3 H); ^{13}C NMR (101 MHz, DMSO-d_6) δ ppm 160.6, 156.3, 146.7, 142.4, 137.7, 137.1, 131.6, 122.4, 115.5, 90.3, 33.7, 30.3, 16.5; HRMS $(M + H)^+$ calculated for $C_{13}H_{14}IN_2O^+$ 341.0145, found 341.0152; LCMS (high pH): R_t = 1.25 mins (99%), MH^+ = 341.2.

2-(But-3-en-1-yl)-6-iodo-*N*-((*1r*,*4r*)-4-(2-methoxyethoxy)cyclohexyl)-8-methylquinazolin-4-amine (80)

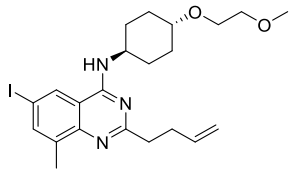

To a round bottomed flask was added 2-(but-3-en-1-yl)-6-iodo-8-methylquinazolin-4(3*H*)-one (**79**) (0.62 g, 1.82 mmol), (*1r*,*4r*)-4-(2-methoxyethoxy)cyclohexan-1-amine (**12**) (0.63 mg, 3.65 mmol), and PyBOP (1.42 g, 2.73 mmol). The vial was capped, and evacuated and purged with N_2 before addition of MeCN (10mL) and DBU (0.55 mL, 3.65 mmol). The mixture was stirred at RT for 2 h. After this time, the mixture was diluted in EtOAc (20 mL), and washed with water (2 × 10 mL), and brine (10 mL). The organic layer was passed through a hydrophobic frit and concentrated *in vacuo*. The crude material was purified by silica gel chromatography eluting with TBME in cyclohexane (0 – 20%). The appropriate fractions were combined and concentrated *in vacuo* to yield 2-(but-3-en-1-yl)-6-iodo-*N*-((*1r*,*4r*)-4-(2-methoxyethoxy)cyclohexyl)-8-methylquinazolin-4-amine (**80**) (458 mg, 0.92 mmol, 51% yield) as a white solid; m.p. 99 – 101 °C; ν_{max}(solid): 3362, 3089, 2930, 2863, 1571, 1528, 1354, 1097, 807, 470; ^{1}H NMR (400 MHz, DMSO-d_6) δ ppm 8.51 (d, *J* = 1.5 Hz, 1 H), 7.86 – 7.83 (m, 1 H), 7.77 (d, *J* = 7.4 Hz, 1 H), 5.98 – 5.87 (m, 1 H), 5.07 (app. dq, *J* = 17.2, 2.0 Hz, 1 H), 4.96 – 4.91 (m, 1 H), 4.18 – 4.08 (m, 1 H), 3.57 – 3.54 (m, 2 H), 3.45 – 3.42 (m, 2 H), 3.34 – 3.27 (m, 1 H), 3.26 (s, 3 H), 2.82 – 2.76 (m, 2 H), 2.57 – 2.50 (m, 2 H), 2.49 (s, 3 H), 2.10 – 1.95 (m, 4 H), 1.48 – 1.36 (m, 2 H), 1.33 – 1.21 (m, 2 H); ^{13}C NMR (101 MHz, DMSO-d_6) δ ppm 165.1, 157.8, 147.9, 140.0, 138.5, 137.5, 128.7, 114.7, 114.6, 88.7, 76.8, 71.6, 66.6, 58.0, 48.9, 38.5, 31.4, 30.7, 29.5, 16.7; HRMS $(M + H)^+$ calculated for $C_{22}H_{31}IN_3O_2^+$ 496.1455, found 496.1462; LCMS (high pH): R_t = 1.58 mins (94%), MH^+ = 496.3.

2-(But-3-en-1-yl)-6-(1*H*-imidazol-1-yl)-*N*-((*1r,4r*)-4-(2-methoxyethoxy)cyclohexyl)-8-methyl-3,4-dihydroquinazolin-4-amine (81)

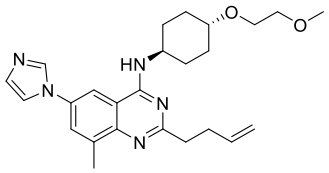

To a microwave vial was added 2-(but-3-en-1-yl)-6-iodo-*N*-((*1r,4r*)-4-(2-methoxyethoxy)cyclohexyl)-8-methyl-3,4-dihydroquinazolin-4-amine (**80**) (365 mg, 0.74 mmol), CuI (21 mg, 0.11 mmol), K_2CO_3 (163 mg, 1.18 mmol), and imidazole (85 mg, 1.25 mmol). The vial was capped, and evacuated and purged with N_2 before addition of DMF (3 mL). The solution was stirred at 150 °C for 24 h. After this time, the solution was diluted in EtOAc (10 mL) and washed with sat. $NaHCO_3$ solution (2 × 5 mL), and brine (2 × 5 mL). The organic layer was passed through a hydrophobic frit and concentrated *in vacuo.* The crude material was purified by silica gel chromatography eluting with TBME in EtOAc (0 – 100%). The appropriate fractions were combined and concentrated *in vacuo* to yield 2-(But-3-en-1-yl)-6-(1*H*-imidazol-1-yl)-*N*-((*1r,4r*)-4-(2-methoxyethoxy)cyclohexyl)-8-methyl-3,4-dihydroquinazolin-4-amine (**81**) (268 mg, 0.62 mmol, 84% yield) as an off-white solid; m.p. 122 – 125 °C; ν_{max}(solid): 3300, 3094, 2932, 2860, 1742, 1626, 1582, 1536, 1101, 1062, 908, 807, 657; ^{1}H NMR (400 MHz, DMSO-d_6) δ ppm 8.32 – 8.26 (m, 2 H), 7.93 – 7.90 (m, 1 H), 7.79 (br. s., 1 H), 7.67 (d, *J* = 7.4 Hz, 1 H), 7.16 (br. s., 1 H), 6.00 – 5.89 (m, 1 H), 5.12 – 5.06 (m, 1 H), 4.97 – 4.92 (m, 1 H), 4.22 – 4.12 (m, 1 H), 3.58 – 5.54 (m, 2 H), 3.46 – 3.42 (m, 2 H), 3.36 – 3.27 (m, 1 H), 3.26 (s, 3 H), 2.86 – 2.81 (m, 2 H), 2.60 (s, 3 H), 2.61 – 2.53 (m, 2 H), 2.12 – 2.02 (m, 4 H), 1.50 – 1.37 (m, 2 H), 1.36 – 1.23 (m, 2 H); ^{13}C NMR (101 MHz, DMSO-d_6) d ppm 164.8, 159.0, 147.2, 138.5, 137.2, 135.6, 132.5, 129.8, 125.1, 118.2, 114.6, 113.0, 110.8, 76.9, 71.6, 66.6, 58.0, 49.0, 38.4, 31.5, 30.7, 29.7, 17.4; HRMS $(M + H)^+$ calculated for $C_{25}H_{34}N_5O_2^+$ 436.2707, found 436.2714; LCMS (high pH): R_t = 1.25 mins (98%), MH^+ = 436.4.

4-(6-Iodo-8-methyl-4-oxo-4*H*-benzo[*d*][1,3]oxazin-2-yl)butanenitrile (84)

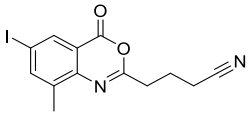

To a round bottomed flask which had been dried with a heat gun, and evacuated and purged with N_2 was added 4-cyanobutanoic acid (4.3 mL, 43 mmol), THF (100 mL), and DMF (0.034 mL, 0.43 mmol). Oxalyl chloride (4.0 mL, 46 mmol) was added dropwise and the solution stirred at RT until effervescence subsided suggesting the acid chloride had formed. A separate round bottomed flask containing 2-amino-5-iodo-3-methylbenzoic acid (**71**) (12.6 g, 46 mmol) was evacuated and purged with N_2 before addition of THF (100 mL). To this was slowly added the solution containing the acid chloride. The solution was stirred at RT for 16 h. After this time, the mixture was concentrated *in vacuo*. The crude material was added to a round bottomed flask along with Boc_2O (10.1 mL, 43 mmol), and DMAP (0.53 g, 4.33 mmol). The flask was evacuated and purged with N_2 before addition of 1,4-dioxane (100 mL) and pyridine (3.5 mL, 43.3 mmol). The solution was stirred at RT for 2 h. After this time, the solution was diluted in EtOAc (200 mL), and washed with water (3 × 10 mL) and then brine (2 × 10 mL). The organic layer was passed through a hydrophobic frit and concentrated in vacuo. The crude material was purified by silica gel chromatography eluting with TBME in cyclohexane (0 – 80%). The appropriate fractions were combined and concentrated *in vacuo* to yield 4-(6-iodo-8-methyl-4-oxo-4*H*-benzo[*d*][1,3]oxazin-2-yl)butanenitrile (**84**) (12.4 g, 35 mmol, 81% yield) as an off-white solid; m.p. 125 – 129 °C; ν_{max}(solid): 3060, 2243, 1741, 1651, 1462, 1310, 1239, 1147, 1090, 971, 790; ^{1}H NMR (400 MHz, DMSO-d_6) δ ppm 8.18 (d, J = 1.5 Hz, 1 H), 8.14 – 8.13 (m, 1 H), 2.77 (t, J = 7.1 Hz, 2 H), 2.68 (t, J = 7.3 Hz, 2 H), 2.44 (s, 3 H), 2.04 (quin, J = 7.2 Hz, 2 H); ^{13}C NMR (101 MHz, DMSO-d_6) δ ppm 160.8, 158.0, 145.1, 143.6, 137.4, 133.2, 120.2, 118.5, 92.7, 32.6, 21.1, 15.9, 15.4; HRMS $(M + H)^+$ calculated for $C_{13}H_{12}IN_2O_2^+$ 354.9938, found 354.9949; LCMS (high pH): R_t = 1.23 mins (100%), MH^+ = 355.0.

4-(6-Iodo-8-methyl-4-oxo-3,4-dihydroquinazolin-2-yl)butanenitrile (85)

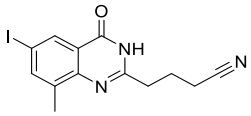

To a microwave vial was added 4-(6-iodo-8-methyl-4-oxo-4*H*-benzo[d][1,3]oxazin-2-yl)butanenitrile (**84**) (606 mg, 1.71 mmol) and ammonium acetate (264 mg, 3.42 mmol). The vial was capped, and evacuated and purged with N_2 before addition of DMA (5 mL). The solution was stirred at 170 °C for 2 h. The solution was allowed to cool to RT before being diluted in EtOAc (15 mL). The organic layer was washed with water (5 mL), and brine (5 mL). Product precipitated and the organic layer was filtered under vacuum. The solid was collected to yield 4-(6-iodo-8-methyl-4-oxo-3,4-dihydroquinazolin-2-yl)butanenitrile (**85**) (305 mg, 0.86 mmol, 51% yield), as a white solid. The filtrate was passed through a hydrophobic frit and concentrated *in vacuo*. This crude material was purified by silica gel chromatography eluting with EtOAc in cyclohexane (0 – 50%). The appropriate fractions were combined and concentrated *in vacuo* to yield 4-(6-iodo-8-methyl-4-oxo-3,4-dihydroquinazolin-2-yl)butanenitrile (**85**) (128 mg, 0.36 mmol, 21% yield), as a white solid, giving 433 mg (1.22 mmol) of product overall (72%); m.p. 229 – 231 °C; ν_{max}(solid): 3162, 3080, 2948, 2246, 1681, 1622, 1462, 1418, 1200, 883, 798, 782, 603, 525; ^{1}H NMR (400 MHz, DMSO-d_6) δ ppm 12.32 (br. s., 1 H), 8.21 − 8.19 (m, 1 H), 7.99 − 7.97 (m, 1 H), 2.73 (t, J = 7.3 Hz, 2 H), 2.64 (t, J = 7.1 Hz, 2 H), 2.48 (s, 3 H), 2.06 (quin, J = 7.2 Hz, 2 H); ^{13}C NMR (101 MHz, DMSO-d_6) δ ppm 160.6, 155.4, 146.5, 142.4, 137.7, 131.6, 122.6, 120.3, 90.5, 32.8, 21.7, 16.5, 15.6; HRMS $(M + H)^+$ calculated for $C_{13}H_{13}IN_3O^+$ 354.0098, found 354.0110; LCMS (high pH): R_t = 1.04 mins (99%), MH^+ = 354.1.

4-(6-Iodo-4-(((*1r*,*4r*)-4-(2-methoxyethoxy)cyclohexyl)amino)-8-methylquinazolin-2-yl)butanenitrile (86)

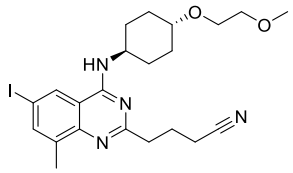

To a microwave vial was added 4-(6-iodo-8-methyl-4-oxo-3,4-dihydroquinazolin-2-yl)butanenitrile (**85**) (384 mg, 1.09 mmol), and PyBOP (849 mg, 1.63 mmol). The vial was evacuated and purged with N_2 before addition of a solution of (*1r*,*4r*)-4-(2-methoxyethoxy)cyclohexan-1-amine (**12**) (377 mg, 2.175 mmol) in MeCN (5 mL), followed by DBU (0.33 mL, 2.18 mmol). The mixture was left to stir at RT for 18 h. After this time, the solution was diluted in EtOAc (20 mL), and washed with water (2 × 10 mL), and brine (10 mL). The organic layer was passed through a hydrophobic frit, and concentrated *in vacuo*. The crude material was purified by silica gel chromatography eluting with EtOAc in cyclohexane (0 – 50%). The appropriate fractions were combined and concentrated *in vacuo* to yield 4-(6-iodo-4-(((*1r*,*4r*)-4-(2-methoxyethoxy)cyclohexyl)amino)-8-methylquinazolin-2-yl)butanenitrile (**86**) (357 mg, 0.702 mmol, 65% yield) as a white solid; m.p. 160 – 163 °C; ν_{max}(solid): 3368, 2929, 2860, 2250, 1573, 1521, 1366, 1080, 872, 803, 552, 461; ^{1}H NMR (400 MHz, DMSO-d_6) δ ppm 8.52 (s, 1 H), 7.86 (s, 1 H), 7.83 (d, *J* = 7.4 Hz, 1 H), 4.17 – 4.07 (m, 1 H), 3.57 – 3.53 (m, 2 H), 3.45 – 3.41 (m, 2 H), 3.35 – 3.27 (m, 1 H), 3.26 (s, 3 H), 2.81 (t, *J* = 7.3 Hz, 2 H), 2.64 (t, *J* = 7.1 Hz, 2 H), 2.49 (s, 3 H), 2.11 – 1.95 (m, 6 H), 1.49 – 1.36 (m, 2 H), 1.33 – 1.21 (m, 2 H); ^{13}C NMR (101 MHz, DMSO-d_6) δ ppm 164.2, 157.8, 147.8, 140.2, 137.6, 128.7, 120.6, 114.8, 89.0, 76.8, 71.6, 66.6, 58.0, 49.0, 37.5, 30.7, 29.5, 23.1, 16.7, 15.8; HRMS $(M + H)^+$ calculated for $C_{22}H_{30}IN_4O_2^+$ 509.1408, found 509.1416; LCMS (high pH): R_t = 1.37 mins (99%), MH^+ = 509.4.

4-(6-(1*H*-Imidazol-1-yl)-4-(((*1r*,*4r*)-4-(2-methoxyethoxy)cyclohexyl)amino)-8-methylquinazolin-2-yl)butanenitrile (87)

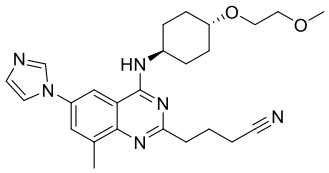

To a microwave vial was added 4-(6-iodo-4-(((*1r*,*4r*)-4-(2-methoxyethoxy)cyclohexyl)amino)-8-methylquinazolin-2-yl)butanenitrile (**86**) (304 mg, 0.60 mmol), CuI (17 mg, 0.09 mmol), K_2CO_3 (132 mg, 0.96 mmol), and imidazole (69 mg, 1.02 mmol). The vial was capped, and evacuated and purged with N_2 before addition of DMF (2 mL). The solution was stirred at 150 °C for 20 h. After this time, the solution was diluted in EtOAc (10 mL) and washed with sat. $NaHCO_3$ solution (2 × 5 mL), and brine (5 mL). The organic layer was passed through a hydrophobic frit and concentrated *in vacuo*. The crude material was purified by silica gel chromatography eluting with EtOAc + 1% NEt_3 in TBME (0 – 100%). The appropriate fractions were combined and concentrated *in vacuo* to yield 4-(6-(1*H*-Imidazol-1-yl)-4-(((*1r*,*4r*)-4-(2-methoxyethoxy)cyclohexyl)amino)-8-methylquinazolin-2-yl)butanenitrile (**87**) (202 mg, 0.45 mmol, 75% yield) as a colourless gum; ν_{max}(gum): 3276, 3118, 2934, 2860, 2245, 1573, 1535, 1499, 1454, 1100, 1063, 804, 658; ^{1}H NMR (400 MHz, DMSO-d_6) δ ppm 8.31 – 8.27 (m, 2 H), 7.95 – 7.93 (m, 1 H), 7.80 – 7.79 (m, 1 H), 7.73 (d, *J* = 7.4 Hz, 1 H), 7.17 – 7.16 (m, 1 H), 4.22 – 4.11 (m, 1 H), 3.58 – 3.54 (m, 2 H), 3.46 – 3.42 (m, 2 H), 3.39 – 3.28 (m, 1 H), 3.26 (s, 3 H), 2.89 – 2.83 (m, 2 H), 2.66 (t, *J* = 7.1 Hz, 2 H), 2.61 (s, 3 H), 2.14 – 2.01 (m, 6 H), 1.50 – 1.37 (m, 2 H), 1.36 – 1.24 (m, 2 H); ^{13}C NMR (101 MHz, DMSO-d_6) δ ppm 163.9, 159.0, 147.2, 137.3, 135.7, 132.6, 129.8, 125.2, 120.7, 118.2, 113.1, 110.8, 76.9, 71.7, 66.6, 58.0, 49.1, 37.5, 30.8, 29.7, 23.2, 17.4, 15.9; HRMS $(M + H)^+$ calculated for $C_{25}H_{33}N_6O_2^+$ 449.2660, found 449.2664; LCMS (high pH): R_t = 1.04 mins (100%), MH^+ = 449.5.

6-Iodo-2,8-dimethyl-4*H*-benzo[*d*][1,3]oxazin-4-one (88)

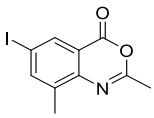

To a round bottomed flask was added 2-amino-5-iodo-3-methylbenzoic acid (**71**) (2.00 g, 7.22 mmol) and acetic anhydride (6.81 ml, 72.2 mmol). The mixture was heated to 110 °C under N_2 for 1 h. After this time, the solution was cooled to RT and a precipitate formed. The mixture was filtered under vacuum and the solid washed with Et_2O (2 × 10 mL). The solid was collected to yield 6-iodo-2,8-dimethyl-4*H*-benzo[d][1,3]oxazin-4-one (**88**) (1.68 g, 5.58 mmol, 77% yield), as brown crystals; m.p. 175 – 178 °C; ν_{max}(solid): 2923, 1736, 1648, 1460, 1312, 1239, 1182, 966, 887, 789, 768, 614, 469; ^{1}H NMR (400 MHz, $CDCl_3$-*d*) δ ppm 8.34 (d, *J* = 1.5 Hz, 1 H), 7.94 – 7.92 (m, 1 H), 2.49 (s, 3 H), 2.46 (s, 3 H); ^{13}C NMR (101 MHz, $CDCl_3$-*d*) δ ppm 159.4, 158.7, 145.7, 144.4, 137.7, 134.5, 118.1, 91.7, 21.5, 16.6; HRMS (M + H)$^+$ calculated for $C_{10}H_9INO_2^+$ 301.9672, found 301.9677; LCMS (high pH): R_t = 1.22 mins (97%), MH^+ = 302.1.

6-Iodo-2,8-dimethylquinazolin-4(3*H*)-one (89)

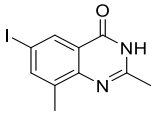

To a round bottomed flask was added 6-iodo-2,8-dimethyl-4*H*-benzo[d][1,3]oxazin-4-one (**88**) (2.00 g, 6.64 mmol) and ammonium acetate (1.02 g, 13.3 mmol). The flask was evacuated and purged with N_2 before addition of DMA (15 mL). The mixture was stirred at 170 °C for 3 h. After this time, the mixture was allowed to cool to RT and was filtered under vacuum. The solid was washed with MeCN (2 × 10 mL) and then collected to yield 6-iodo-2,8-dimethylquinazolin-4(3*H*)-one (**89**) (1.70 g, 5.66 mmol, 85% yield) as a white solid; m.p. 308 – 312 °C; ν_{max}(solid): 3156, 3023, 2874, 1679, 1622, 1455, 1297, 1184, 877, 800, 782, 627, 526; ^{1}H NMR (400 MHz, DMSO-d_6) δ ppm 12.30 (br. s., 1 H), 8.18 (d, *J* = 1.5 Hz, 1 H), 7.95 – 7.94 (m, 1 H), 2.45 (s, 3 H), 2.35 (s, 3 H); ^{13}C NMR (101 MHz, DMSO-d_6) δ ppm 161.1, 154.5, 147.3, 142.9, 138.1, 132.1, 122.8, 90.7, 22.3, 17.2; HRMS (M + H)$^+$ calculated for $C_{10}H_{10}IN_2O^+$ 300.9832, found 300.9838; LCMS (high pH): R_t = 0.95 mins (100%), MH^+ = 301.1.

(*1r,4r*)-N^1-(6-Iodo-2,8-dimethylquinazolin-4-yl)cyclohexane-1,4-diamine (90)

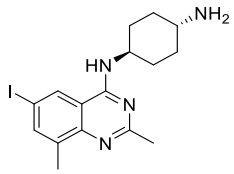

To a microwave vial was added 6-iodo-2,8-dimethylquinazolin-4(3*H*)-one (**89**) (1.57 g, 5.23 mmol), (*1r,4r*)-cyclohexane-1,4-diamine (1.20 g, 10.5 mmol) and PyBOP (4.08 g, 7.85 mmol). The vial was capped, and evacuated and purged with N_2 before addition of DBU (1.58 mL, 10.5 mmol) and MeCN (12 mL). The solution was stirred at RT for 4 h. After this time, the mixture was diluted in EtOAc (30 mL) and washed with water (2 × 10 mL), and brine (10 mL). The organic layer was passed through a hydrophobic frit and concentrated *in vacuo.* The crude material was diluted in DCM (5 mL) and after precipitation, was filtered under vacuum. The filtrate was loaded onto a silica gel column and purified by silica gel chromatography eluting with EtOAc in cyclohexane + 1% NEt_3 (0 – 100%) and then EtOH in EtOAc (0 – 60%). The appropriate fractions were combined and concentrated *in vacuo* to yield (*1r,4r*)-N^1-(6-iodo-2,8-dimethylquinazolin-4-yl)cyclohexane-1,4-diamine (**90**) (1.87 g, 4.72 mmol, 90% yield), as an off-white solid; m.p. 173 – 177 °C; ν_{max}(solid): 3450, 3284, 2929, 2860, 1574, 1533, 831, 556; ^{1}H NMR (400 MHz, DMSO-d_6) δ ppm 8.50 (s, 1 H), 7.83 (s, 1 H), 7.74 (d, *J* = 7.6 Hz, 1 H), 4.18 – 4.07 (m, 1 H), 3.30 (br .s, 2 H), 2.59 – 2.53 (m, 1 H), 2.47 (s, 3 H), 2.44 (s, 3 H), 1.89 (d, *J* = 11.1 Hz, 2 H), 1.82 (d, *J* = 12.8 Hz, 2 H), 1.48 – 1.36 (m, 2 H), 1.21 – 1.09 (m, 2 H); ^{13}C NMR (101 MHz, DMSO-d_6) δ ppm 163.5, 158.2, 148.5, 140.5, 137.9, 129.2, 115.0, 89.1, 50.4, 49.3, 35.7, 31.2, 27.3, 17.3; HRMS $(M + H)^+$ calculated for $C_{16}H_{22}IN_4^+$ 397.0884, found 397.0886; LCMS (high pH): R_t = 1.05 mins (100%), MH^+ = 397.0.

4-Cyano-*N*-((*1r,4r*)-4-((6-iodo-2,8-dimethylquinazolin-4-yl)amino)cyclohexyl)butanamide (91)

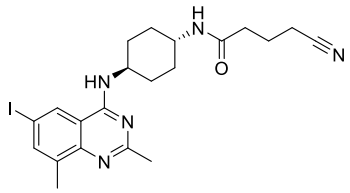

To a microwave vial was (*1r,4r*)-N^1-(6-iodo-2,8-dimethylquinazolin-4-yl)cyclohexane-1,4-diamine (**90**) (1.22 g, 3.08 mmol), 4-cyanobutanoic acid (0.35 g, 3.08 mmol), DCC (0.64 g, 3.08 mmol), and DMAP (0.04 g, 0.31 mmol). The vial was capped, and evacuated and purged with N_2 before addition of DMA (10 mL). The solution was stirred at RT for 5 h. After this time, the mixture was diluted in EtOAc (20 mL) and washed with water (2 × 10 mL), and then brine (10 mL). The organic layer was filtered under vacuum. The filtrate was then passed through a hydrophobic frit and concentrated *in vacuo*. The crude material was diluted in DCM (3 mL) and then filtered under vacuum. The solid was collected to yield 4-cyano-*N*-((*1r,4r*)-4-((6-iodo-2,8-dimethyl-3,4-dihydroquinazolin-4-yl)amino)cyclohexyl)butanamide (**91**) (617 mg, 1.26 mmol, 41% yield), as a white solid. The filtrate was concentrated *in vacuo* and purified by silica gel chromatography eluting with EtOAc in TBME (0 – 50%). The appropriate fractions were combined and concentrated *in vacuo* to yield 4-cyano-*N*-((*1r,4r*)-4-((6-iodo-2,8-dimethyl-3,4-dihydroquinazolin-4-yl)amino)cyclohexyl)butanamide (**91**) (211 mg, 0.43 mmol, 14% yield), as a white solid, giving 828 mg (1.69 mmol) of product overall (55%); m.p. 184 – 189 °C; ν_{max}(solid): 3397, 3294, 2937, 2260, 1636, 1531, 1344, 547; ^{1}H NMR (400 MHz, DMSO-d_6) δ ppm 8.51 – 8.49 (m, 1 H), 7.85 – 7.77 (m, 3 H), 4.20 – 4.10 (m, 1 H), 3.62 – 3.51 (m, 1 H), 2.52 – 2.49 (m, 2H), 2.47 (m, 3 H), 2.45 (s, 3 H), 2.19 (t, *J* = 7.4 Hz, 2 H), 2.00 − 1.93 (m, 2 H), 1.91 − 1.84 (m, 2 H), 1.78 (quin, *J* = 7.3 Hz, 2 H), 1.52 – 1.40 (m, 2 H), 1.36 – 1.24 (m, 2 H); ^{13}C NMR (101 MHz, DMSO-d_6) δ ppm 169.8, 162.9, 157.7, 148.0, 140.1, 137.4, 128.7, 120.3, 114.5, 88.7, 48.5, 47.2, 33.8, 31.2, 30.6, 26.8, 21.2, 16.8, 15.8; HRMS $(M + H)^+$ calculated for $C_{21}H_{27}IN_5O^+$ 492.1255, found 492.1264; LCMS (high pH): R_t = 1.14 mins (100%), MH^+ = 492.3.

_N_-((_1r,4r_)-4-((6-(1_H_-imidazol-1-yl)-2,8-dimethylquinazolin-4-yl)amino)cyclohexyl)-4-cyanobutanamide (92)

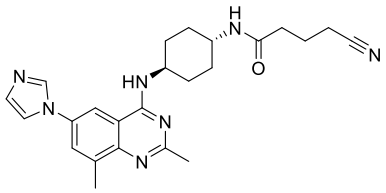

To a microwave vial was added 4-cyano-_N_-((_1r,4r_)-4-((6-iodo-2,8-dimethyl-3,4-dihydroquinazolin-4-yl)amino)cyclohexyl)butanamide (**91**) (600 mg, 1.22 mmol), CuI (35 mg, 0.18 mmol), K_2CO_3 (270 mg, 1.95 mmol), and imidazole (141 mg, 2.08 mmol). The vial was capped, and evacuated and purged with N_2 before addition of DMF (5 mL). The solution was stirred at 150 °C for 22 h. After this time, the solution was diluted in EtOAc (10 mL) and washed with sat. $NaHCO_3$ solution (2 × 5 mL), and brine (5 mL). The organic layer was passed through a hydrophobic frit and concentrated *in vacuo*. The crude material was purified by silica gel chromatography eluting with EtOAc in TBME (0 – 100%) followed by EtOH in EtOAc (0 – 40%). The appropriate fractions were combined and concentrated *in vacuo* to yield _N_-((_1r,4r_)-4-((6-(1_H_-imidazol-1-yl)-2,8-dimethyl-3,4-dihydroquinazolin-4-yl)amino)cyclohexyl)-4-cyanobutanamide (**92**) (209 mg, 0.48 mmol, 40% yield), as a white solid; m.p. 276 – 277 °C; ν_{max}(solid): 3393, 3289, 2936, 2855, 2248, 1638, 1532, 1310, 801, 731; ^{1}H NMR (400 MHz, DMSO-d_6) δ ppm 8.28 (s, 2 H), 7.92 – 7.90 (m, 1 H), 7.84 (d, J = 7.6 Hz, 1 H), 7.80 – 7.79 (m, 1 H), 7.70 (d, J = 7.9 Hz, 1 H), 7.15 (s, 1 H), 4.25 – 4.13 (m, 1 H), 3.66 – 3.53 (m, 1 H), 2.59 (s, 3 H), 2.53 – 2.50 (m, 2 H), 2.49 (s, 3 H), 2.19 (t, J = 7.4 Hz, 2 H), 2.02 (app. d, J = 10.3 Hz, 2 H), 1.89 (app. d, J = 10.3 Hz, 2 H), 1.78 (quin, J = 7.3 Hz, 2 H), 1.52 – 1.40 (m, 2 H), 1.39 – 1.27 (m, 2 H); ^{13}C NMR (101 MHz, DMSO-d_6) δ ppm 169.8, 162.7, 158.9, 147.3, 137.1, 135.7, 132.4, 129.8, 125.2, 120.3, 118.3, 112.7, 110.8, 48.6, 47.2, 33.8, 31.2, 30.7, 26.7, 21.2, 17.5, 15.8; HRMS $(M + H)^+$ calculated for $C_{24}H_{30}N_7O^+$ 432.2508, found 432.2506; LCMS (high pH): R_t = 0.87 mins (100%), MH^+ = 432.4.

(4-(5-Amino-6-(6-(trifluoromethyl)pyridin-3-yl)pyrazin-2-yl)phenyl)(3-aminopyrrolidin-1-yl)methanone (93)

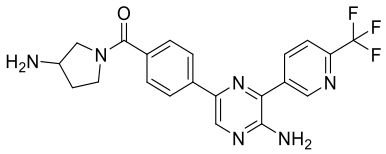

To a microwave vial was added 4-(5-amino-6-(6-(trifluoromethyl)pyridin-3-yl)pyrazin-2-yl)benzoic acid (**99**) (74 mg, 0.21 mmol), and HATU (78 mg, 0.21 mmol). The vial was capped, and evacuated and purged with N_2 before addition of DMF (0.40 mL), and DIPEA (0.09 mL, 0.52 mmol). The solution was stirred at RT for 30 min before addition of a solution of *tert*-butyl pyrrolidin-3-ylcarbamate (32 mg, 0.17 mmol) in DMF (0.20 mL). The solution was stirred at RT for a further 2 h. After this time, the solution was diluted in EtOAc (10 mL), and washed with water (3 mL), aqueous LiCl solution (3 mL), and brine (3 mL). The organic layer was passed through a hydrophibic frit and concentrated *in vacuo*. The crude residue was diluted in 4 M HCl in 1,4-dioxane (1.72 mL, 6.87 mmol) and stirred at RT for 1 h. The mixture was then separated with EtOAc (10 mL) and water (10 mL). The aqueous layer was made basic by addition of 2 M NaOH (5 mL), and was then extracted with EtOAc (3 × 5 mL). The combined organic layers were passed through a hydrophobic frit and concentrated in vacuo to yield (4-(5-amino-6-(6-(trifluoromethyl)pyridin-3-yl)pyrazin-2-yl)phenyl)(3-aminopyrrolidin-1-yl)methanone (**93**) (42 mg, 0.10 mmol, 57% yield) as a yellow gum; ν_{max}(gum): 3317, 3195, 2950, 1603, 1434, 1414, 1322, 1131, 1091, 850; ^{1}H NMR (400 MHz, MeOD-d_6) δ ppm 9.18 - 9.15 (m, 1 H), 8.60 (s, 1 H), 8.50 (dd, *J* = 8.1, 1.7 Hz, 1 H), 8.10 (s, 1 H), 8.07 (s, 1 H), 7.96 (d, *J* = 8.1 Hz, 1 H), 7.63 (app. t, *J* = 8.5 Hz, 2 H), 5.48 (s, 2 H), 3.83 - 3.48 (m, 5 H), 2.65 (s, 2 H), 2.25 - 2.07 (m, 1 H), 1.88 - 1.74 (m, 1 H); ^{13}C NMR (151 MHz, MeOD-d_6) δ ppm 163.0, 157.7, 152.8, 149.6, 148.0, 140.0, 139.8, 139.2, 137.8, 137.4, 128.7, 127.6, 124.6, 114.5, 88.6, 48.7, 30.5, 26.8, 16.8; HRMS $(M + H)^+$ calculated for $C_{21}H_{20}F_3N_6O^+$ 429.1645, found 429.1647; LCMS (high pH): R_t = 0.83 mins (100%), MH^+ = 429.3.

(*S*,*E*)-cyclooct-4-en-1-yl ((*17S*)-18-((1-(4-(5-amino-6-(4-(trifluoromethyl)phenyl)pyrazin-2-yl)benzoyl)pyrrolidin-3-yl)amino)-17-((3-methyl-3*H*-diazirin-3-yl)methyl)-15,18-dioxo-3,6,9,12-tetraoxa-16-azaoctadecyl)carbamate (94)

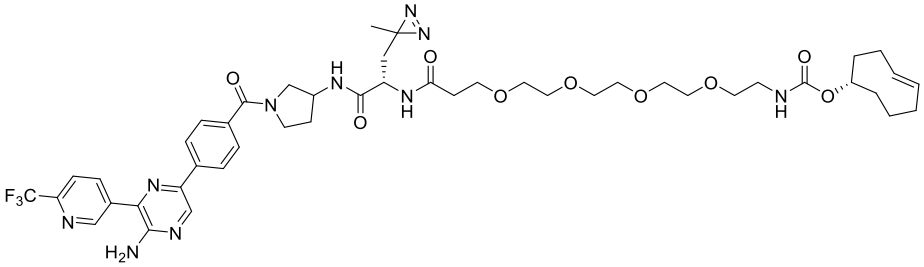

To a microwave vial containing HATU (64 mg, 0.17 mmol), which had been evacuated and purged with N_2, was added a solution of (*S*)-2,2-dimethyl-22-((3-methyl-3*H*-diazirin-3-yl)methyl)-4,20-dioxo-3,8,11,14,17-pentaoxa-5,21-diazatricosan-23-oic acid (**59**) (82 mg, 0.17 mmol) in DMF (0.2 mL) followed by DIPEA (0.08 mL, 0.45 mmol). The solution was stirred at RT for 30 mins and then a solution of (4-(5-amino-6-(6-(trifluoromethyl)pyridin-3-yl)pyrazin-2-yl)phenyl)(3-aminopyrrolidin-1-yl)methanone (**93**) (48 mg, 0.11 mmol) in DMF (0.20 mL) was added. The solution was stirred at RT for a further 18 h. After this time, the solution was diluted in EtOAc (5 mL), and washed with water (2 mL), and brine (2 mL). The organic layer was passed through a hydrophobic frit and concentrated *in vacuo*. The crude material was purified by solid-phase extraction using a 5 g silica cartridge and eluting with EtOAc in cyclohexane (0 – 100%), followed by EtOH in EtOAc (0 – 0%). The appropriate fractions were combined and concentrated *in vacuo* to yield crude intermediate. This was diluted in DCM (1 mL), and TFA (0.22 mL, 2.80 mmol) was added. The solution was stirred at RT for 1.5 h. The solution was then diluted again in DCM (5 mL), and washed with water (2 mL), and brine (2 mL). Protonated product entered the aqueous layer. The aqueous layer was made basic through addition of 2 M NaOH, and was then extracted with EtOAc (2 × 5 mL). These organic washes were combined, passed through a hydrophobic frit, and concentrated *in vacuo*. The crude material was diluted in MeCN (1 mL) and DIPEA (0.06 mL, 0.34 mmol). (*S*,*E*)-cyclooct-4-en-1-yl (4-nitrophenyl) carbonate (16 mg, 0.06 mmol) was added. The solution was stirred at RT for 1 h. To the reaction mixture was added piperidin-4-amine (3.56 µL, 0.03 mmol). The solution was stirred at RT for 30 min before being concentrated *in vacuo*. The

crude residue was diluted in DCM (1 mL), and washed with 2 M HCl (3 × 1 mL) followed by saturated aq. $NaHCO_3$ solution (5 × 1 mL) and then brine (1 mL). The organic layer was passed through a hydrophobic frit and concentrated under N_2 to yield (*S*,*E*)-cyclooct-4-en-1-yl ((*17S*)-18-((1-(4-(5-amino-6-(4-(trifluoromethyl)phenyl)pyrazin-2-yl)benzoyl)pyrrolidin-3-yl)amino)-17-((3-methyl-3*H*-diazirin-3-yl)methyl)-15,18-dioxo-3,6,9,12-tetraoxa-16-azaoctadecyl)carbamate (**94**) (14 mg, 0.01 mmol, 13% yield) as a yellow gum; ^{1}H NMR (400 MHz, DMSO-d_6) δ ppm 9.16 (s, 1 H), 8.73 (s, 1 H), 8.45 (dd, *J* = 8.1, 1.7 Hz, 1 H), 8.41 – 8.3 (m, 1 H), 8.16 – 7.96 (m, 5 H), 7.67 – 7.54 (m, 3 H), 5.69 – 5.59 (m, 1 H), 5.56 – 5.44 (m, 1 H), 5.25 – 5.22 (m, 0.5 H), 5.20 – 5.16 (m, 0.5 H), 4.75 – 4.69 (m, 1 H), 4.37 – 4.11 (m, 2 H), 3.75 – 3.36 (m, 16 H), 3.25 – 3.07 (m, 4 H), 2.44 – 2.31 (m, 2 H), 2.19 – 2.06 (m, 2 H), 2.04 – 1.91 (m, 3 H), 1.83 – 1.74 (m, 2 H), 1.71 – 1.53 (m, 6 H), 1.53 – 1.42 (m, 2 H), 1.33 – 1.11 (m, 6 H), 1.02 (d, *J* = 13.5 Hz, 2 H), 0.95 (s, 1 H), 0.89 – 0.79 (m, 2 H), additional peaks observed due to rotamers and assumed cis/trans isomerisation of alkene double bond; LCMS (high pH): R_t = 1.17 mins (60%), MH^- = 951.4. Product instability precluded further characterisation (see **Section 3.2.1 – The Chemical Strategy for Synthesis of PI4K Photoaffinity Probe (94)**).

5-Chloro-3-(6-(trifluoromethyl)pyridin-3-yl)pyrazin-2-amine (97)

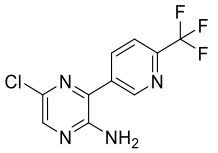

To a microwave vial was added 3-bromo-5-chloropyrazin-2-amine (5 g, 24.0 mmol), $PdCl_2(PPh_3)_2$ (1.68 g, 2.40 mmol), and K_2CO_3 (3.98 g, 28.8 mmol). The vial was capped, and evacuated and purged with N_2 before addition of 1,4-dioxane (50 mL), and water (50 mL). The mixture was heated to 90 °C and a solution of (6-(trifluoromethyl)pyridin-3-yl)boronic acid (5.04 g, 26.4 mmol) in 1,4-dioxane (20 mL) and water (20 mL) was added slowly over 10 min. The mixture was stirred at 90 °C for 1 h. The solution was cooled to RT and then added to water (70 mL). The aqueous layer was extracted with DCM (3 × 50 mL) and the combined organic layers were passed through a hydrophobic frit and concentrated *in vacuo*. The crude material was purified by silica gel chromatography eluting with TBME in cyclohexane (0 – 40%).

The appropriate fractions were combined and concentrated *in vacuo* to yield 5-chloro-3-(6-(trifluoromethyl)pyridin-3-yl)pyrazin-2-amine (**97**) (3.27 g, 11.9 mmol, 50% yield), as an off-white solid; m.p. 168 – 171 °C; ν_{max}(gum): 3469, 3311, 3193, 1615, 1442, 1338, 1129, 1090, 1020, 861, 743, 641; ^{1}H NMR (400 MHz, DMSO-d_6) δ ppm 9.02 (d, *J* = 2.0 Hz, 1 H), 8.35 (dd, *J* = 8.1, 1.5 Hz, 1 H), 8.15 (s, 1 H), 8.01 (d, *J* = 7.9 Hz, 1 H), 6.74 (s, 2 H); ^{13}C NMR (101 MHz, DMSO-d_6) δ ppm 152.7, 149.4, 146.1, 141.4, 137.9, 135.3, 134.1, 133.8, 122.9, 120.7; HRMS $(M + H)^+$ calculated for $C_{10}H_7ClF_3N_4^+$ 275.0306, found 275.0307; LCMS (high pH): R_t = 1.02 mins (100%), MH^- = 273.2.

4-(5-Amino-6-(6-(trifluoromethyl)pyridin-3-yl)pyrazin-2-yl)benzoic acid (99)

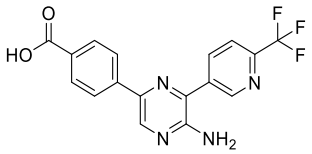

To a round bottomed flask was added 5-chloro-3-(6-(trifluoromethyl)pyridin-3-yl)pyrazin-2-amine (**97**) (3.17 g, 11.5 mmol), 4-boronobenzoic acid (2.11 g, 12.7 mmol), Na_2CO_3 (2.45 g, 23.1 mmol), $PdCl_2(PPh_3)_2$ (1.62 g, 2.31 mmol), water (25 mL), and MeCN (25 mL). The flask was placed under N_2 and the mixture stirred at 80 °C for 2.5 h. After this time, the mixture was cooled to RT and filtered under vacuum. The filtrate was diluted in EtOAc (25 mL) and washed with water (15 mL), 2 M HCl (15 mL), and brine (15 mL). The organic layer was discarded and the aqueous layer was left to stand for 1 h at RT before being filtered under vacuum and the solid collected to yield 4-(5-amino-6-(6-(trifluoromethyl)pyridin-3-yl)pyrazin-2-yl)benzoic acid (**99**) (3.98 g, 11.1 mmol, 96% yield) as a yellow solid; m.p. 390 – 399 °C (dec.); ν_{max}(solid): 3420, 3309, 3138, 1692, 1338, 1174, 1129, 1023, 858, 773, 696, 497; ^{1}H NMR (400 MHz, DMSO-d_6) δ ppm 9.15 (d, *J* = 2.0 Hz, 1 H), 8.76 (s, 1 H), 8.46 (dd, *J* = 8.0, 1.6 Hz, 1 H), 8.16 – 8.10 (m, 2 H), 8.05 – 7.96 (m, 3 H), 6.81 (s, 2 H), 1 H not observed (exchangeable carboxylic acid); ^{13}C NMR (101 MHz, DMSO-d_6) δ ppm 167.1, 153.0, 149.7, 145.9, 145.6, 140.4, 140.2, 138.7, 137.9, 136.6, 134.0, 129.7, 124.8, 120.6, 120.3; HRMS $(M + H)^+$ calculated for $C_{17}H_{12}F_3N_4O_2^+$ 361.0907, found 361.0909; LCMS (high pH): R_t = 0.63 mins (99%), MH^+ = 361.1.

5.2 Biology

5.2.1 Reagents and materials

Standard antimalarial drugs were provided by GlaxoSmithKline and Medicines for Malaria Venture. Reagents were purchased from commercial suppliers and used as received unless otherwise indicated.

5.2.2 Preparation of solutions and buffers

Albumax solution:

The following were combined using distilled water:

- Albumax II (100 g/L)
- D-sucrose (40 g/L)
- L-glutamine (6 g/L)

Hypoxanthine solution:

Prepared using distilled water:

- Hypoxathine (2 g/L)

100 mM Na_3VO_4 solution

Prepared as follows:

- Na_3VO_4 (9.2 g) was dissolved in 400 mL distilled water
- The pH was adjusted to 10.0 using 18% HCl.
- The solution was boiled until it turned colourless, and then cooled to RT.
- The volume was adjusted to 450 mL distilled water, and then the pH was asjusted to 10.0 using 1 M NaOH.
- The solution was made up to 500 mL with distilled water and store at – 20 °C.

PBS buffer:

The following were combined using distilled water:

- NaCl (8 g/L)
- KCl (0.2 g/L)

- Na_2HPO_4 (1.44 g/L)
- KH_2PO_4 (0.24 g/L)
- The pH was adjusted to 7.4 using HCl.

HBSS buffer (no calcium, no magnesium, no phenol red):

The following were combined using distilled water:

- NaCl (8 g/L)
- KCl (0.4 g/L)
- Na_2HPO_4 (48 mg/L)
- KH_2PO_4 (60 mg/L)
- $NaHCO_3$ (0.35 g/L)
- D-Glucose (1 g/L)

5 x DP buffer

The following were combined using distilled water for stock solutions:

- 1 M Tris-HCl pH 7.4 (250 mL)
- 87% glycerol (288 mL)
- 1 M $MgCl_2$ (7.5 mL)
- 5 M NaCl (150 mL)
- 100 mM Na_3VO_4 solution (50 mL)
- The volume was adjusted to 1 L with sterile deionised water.

1 x DP buffer

The following were combined using distilled water for stock solutions:

- 5 x DP buffer (200 mL)
- 25 mM NaF (50 mL from 500 mM stock)
- 1 mM DTT (1 mL from 1 M stock, added just prior to use)
- The volume was adjusted to 1 L with sterile deionised water.
- The buffer was stored at 4 °C and used within a week. If DTT was added, the buffer was used within a day.
- For a 1 x DP buffer with 0.4% IGEPAL CA-630 or 0.2% IGEPAL CA-630, the appropriate volume of 20% IGEPAL CA-630 was added.

Enhanced 2 x sample buffer

The following were combined using distilled water for stock solutions:

- 200 mM Tris HCl (200 mL of 1 M stock)
- 250 mM Tris Base (30.29 g)
- 20% glycerol (235.3 mL of 85% glycerol stock)
- 4% SDS (200 mL of 20% SDS stock)
- 0.01% bromophenol blue (10 mL of 1 % stock)
- The volume was adjusted to 1 L using distilled water.

Parasite lysis buffer for immobilised bead experiments

The following were combined using distilled water for stock solutions (*Note: for the 0.02% IGEPAL CA-630 varient, add 0.01 mL IGEPAL CA-630 instead of 0.4 mL):*

- 5 x DP buffer (20 mL)
- Deionised water (6 mL)
- IGEPAL CA-630 (0.4 mL)
- 0.5 M NaF (0.5 mL)
- 1 Roche EDTA-free protease inhibitor tablet
- Calyculin was added to a final concentration of 50 nM.

Parasite lysis buffer for PAL experiments

The following were combined using distilled water for stock solutions:

- 1 x DP buffer without DTT (25 mL)
- 20% IGEPAL CA-630 (1 mL)
- 20% SDS (625 µL)
- 1 Roche EDTA-free protease inhibitor tablet
- 1 µL per 1 mL of benzonase (added just prior to use)

0.25 x LDS sample buffer/50 mM DTT

The following were combined using distilled water for stock solutions:

- 4 x NuPAGE LDS sample buffer (62.5 µL)
- Deionised water (887.5 µL)
- 1 mM DTT (50 µL)

Wash buffer 1

The following were combined using distilled water for stock solutions:

- 1 M HEPES pH 8.5 (5 mL)
- 5 M NaCl (8 mL)
- 20% SDS (2.5 mL)
- The volume was adjusted to 100 mL with sterile deionised water.

Wash buffer 2

The following were combined using distilled water for stock solutions:

- 1 M HEPES pH 8.5 (15 mL)
- 5 M NaCl (24 mL)
- The volume was adjusted to 300 mL with sterile deionised water.

Wash buffer 3

The following were combined using distilled water for stock solutions:

- 1 M HEPES pH 8.5 (15 mL)
- Urea (36 g)
- The volume was adjusted to 300 mL with sterile deionised water.
- The buffer was prepared fresh and used within a day.

Wash buffer 4

The following were combined using distilled water for stock solutions:

- 1 M HEPES pH 8.5 (7 mL)
- Sterile deionised water (133 mL)

Digestion buffer

The following were combined using distilled water for stock solutions unless otherwise stated (per 20 samples):

- 100 mM TCEP (65 µL)
- 100 mM CAA (195 µL)
- 50 mM HEPES pH 8.5 (1027 µL for PAL experiments, 1014 µL otherwise)

- 0.4 µg LysC/µL in 1 M HEPES pH 8.5 stock (6.5 µL for PAL experiments, 13 µL otherwise)
- 0.4 µg Trypsin/µL in 1 M HEPES pH 8.5 stock (6.5 µL for PAL experiments, 13 µL otherwise)

Stop solution (2.5% NH_2OH in 0.1 M HEPES)

The following were combined using distilled water for stock solutions:

- 50% NH_2OH (50 µL)
- 0.1 M HEPES pH 8.5 (950 µL)

5.2.3 *P. falciparum* culture information

The culture growth and maintenance of *P. falciparum* intraerythrocytic stage parasites is carried out routinely at GSK Tres Cantos through traditional techniques, and these were used for the growth of parasites for use in these investigations.[12,254] *P. falc* pellets of the 3D7A strain, cloned from the NF54 strain which itself was originally derived from a patient living in the Netherlands,[255,256] are stored at − 80°C until required. These are thawed and then cultivated in suitable media supplemented with appropriate serum and human erythrocytes, under a gaseous atmosphere of 2 – 5% CO_2 and 5 – 10% O_2, with intermittent change of medium and provision of fresh erythrocytes as the number of parasites increases.[202,204] Malaria cultures are usually described by a percentage parasitaemia (P%), the percentage of infected erythrocytes taking into account the whole erythrocytic population, along with a percentage hematocrit (H%), which is the percentage of erythrocytes by volume in the entire culture, taking into account all media, serum, and supplements.

RPMI 1640, originally developed to culture human leukocytes, is the medium of choice for *P. falciparum* culture maintenance and consists of essential amino acids and vitamins, and a sodium bicarbonate buffer system that, under a 5 – 10% CO_2 atmosphere, maintains a physiological pH which is critical for growth of the parasite.[204] Controling the pH of *P. falc* cultures can be difficult due to the large quantities of lactic acid produced by the parasite during glycolysis.[257] As a result, maintaining a low percentage parasitaemia of 2 – 5% through removal and replacement

of erythrocytes and media can lead to longer culture maintenance times. RPMI 1640 does not contain proteins, lipids, or growth factors, and so in *P. falc* cultures this media is supplemented with serum. Although 10% human serum provides optimal growth conditions, limitations in terms of cost and supply mean that other types of mamallian serum are often used.[202] Bovine serum albumin, a serum derived from cows, is often used as a replacement and is used in our laboratories.[202,204,258] Further supplementation of the medium and serum mixture with hypoxanthine, a naturally occuring purine derivative, is required due to the parasite's inability to synthesise its own purines for use in DNA and protein synthesis, and thus survival.[47,48] Finally, addition of human erythrocytes to the cultures provides the host cells for the *P. falciparum* parasites and facilitates the asexual reproduction required for survival through providing a source of haemoglobin.[202]

In the current study, *P. falciparum* strain 3D7A was obtained from the Malaria Research and Reference Reagent Resource Centre (MR4), and human erythrocytes were obtained from the Spanish Red Cross Blood Bank. The human biological samples were sourced ethically and their research use was in accord with the terms of the informed consents under an IRB/EC approved protocol. The parasite strain was cultured using modified versions of the method described by Trager et al.[254] Briefly, parasites were cultured using RPMI-1640, which was completed by supplementation with 0.5% Albumax solution and 150 µM hypoxanthine solution, at 2% haematocrit under an atmosphere of 90% N_2, 5% CO_2, 5% O_2 at 37 °C. The complete medium was prepared fresh before use and prewarmed to 37 °C. Erythrocytes were washed with incomplete RPMI-1640 by centrifugation at RT at 800 g for 10 min, and used within 2 weeks.

5.2.4 Determination of parasitaemia in blood smears of *P. falciparum* cultures

A 0.25 mL aliquot of the appropriate malaria culture was centrifuged and the supernatant was aspirated. The erythrocyte pellet was smeared onto a glass slide, dried, fixed in methanol, and then dried again. The slide was then incubated in a Giemsa stain (Giemsa azur eosin methylene blue for microscopy) for 5 min at RT. The slide was washed with distilled water, and then dried, and visualised under a microscope.

Parasitaemia was determined through visual counting of infected erythrocytes as a percentage of total erythrocyte population within a specific field of view, and averaging the results.

5.2.5 [^{3}H]-Hypoxanthine incorporation assay for determination of *P. falc* IC_{50} [168]

The [^{3}H]-hypoxanthine incorporation assay coupled with a scintillation proximity asaay is a method used to determine the whole-cell *in vitro* potencies of antimalarial compounds, and was carried out by colleagues at GSK Tres Cantos for this study.[259] This is determined by measurement of the reduction in parasitaemia after treatment with the compound, observed through incorporation of radioactive [^{3}H]-hypoxanthine into the parasite.[168]

A culture of 3D7A strain parasitized erythrocytes (0.5% parasitaemia and 2% haematocrit) in complete RPMI-1640 was exposed to 3-fold serial dilutions of the compound in DMSO in 96-well plates (100 µL). Plates were incubated for 24h at 37ºC, 5% CO_2, 5% O_2, 90% N_2. After 24h incubation, 0.2 µCi (8 µL for each well in the 96-well plate) of a stock solution of ^{3}H-hypoxanthine (0.025 µCi/µL) in RMPI-1640 was added and plates were incubated for a further 24h.

The plates were frozen after this time until required. The plates were thawed and parasites were harvested on Filtermat A glass fiber filters (PerkinElmer) using a Cell Harvester 96 (Tomtec, CT, USA). The filters were dried and melted on MeltiLex scintillator sheets (PerkinElmer) in order to determine the incorporation of ^{3}H-hypoxanthine by measuring radioactivity using a MicroBeta plate counter (PelkinElmer). Raw data are normalized to the level of incorporation of the positive control (parasitized erythrocytes with DMSO i.e. 0% inhibition) and the negative control (parasitized erythrocytes exposed to 25 µM artesunate, i.e. 100% inhibition) as follows:

$$100 - \left[\frac{100 \times (unknown - negative\ control)}{(positive\ control - negative\ control)}\right]$$

IC_{50} values are determined using XL-FIT Excel software based on the inhibition of growth data obtained with the formula above in Excel, and fitted with CL-Fit software with a 2-parameter equation. This equation has a lower data limit of 0 (the background

is corrected), and an upper data limit of 100 (the data range is corrected), and is as follows:

$$y = \frac{100\%}{1 + (\frac{x}{IC_{50}})^s}$$

Where *s* is the slope factor. This assumes that *y* decreases with increasing *x*.

5.2.6 The immobilised bead assay for target identification of antimalarial quinazolinamines

The immobilised bead assay is used for the proteomic profiling of complex protein samples using the affinity-based capture of relevant protein targets of a synthesised chemical probe. For antimalarial target identification, this requires the prior isolation of appropriate parasite lysate, and the immobilisation of the synthesised chemical probe onto commercially available agarose-derivatised beads. Blocked beads, to which no chemical probe is conjugated, act as a control. Parasite lysate is then incubated with blocked or capturing beads, or the free antimalarial compound for 1 h. A second incubation step involves addition of fresh capturing beads to each of these samples to trigger competitive binding to protein targets. Bead samples are then washed to elute non-captured proteins, and then the captured proteins are eluted and proteolytically digested. Salts and remaining detergents are removed from peptide samples before digested peptide fragments are sequenced and analysed by LCMS/MS to identify their parent proteins using the quantitative TMT labelling method. Synthetic chemistry was conducted by the author of this study, whilst *P. falciparum* lysate preparation was carried out by Olalla Sanz at GSK Tres Cantos,[260] and the subsequent pull down experiments were conducted by colleagues at Cellzome.[167]

P. falciparum lysate preparation. A 3D7 *P. falciparum* strain is grown at 2% haematocrit in human erythrocytes (obtained from the local blood bank) to yield a parasitaemia level of up to 15% as per the standard conditions.[254] *P. falciparum* cultures are synchronised by sorbitol treatment. This is carried out first by centrifugation of the parasite culture at 37 °C at 1900 rpm for 5 min, and then discarding the supernatant. The pellet is incubated with 10 volumes of prewarmed sorbitol (5%) at 37 °C for 5 min. The pellet is then washed twice with complete RPMI

using the parameters of 37 °C at 1900 rpm for 5 min. The pellets are resuspended in complete RPMI medium with red blood cells (H2%, P0.5%) and grown to the appropriate parasitaemia level. Once this level is reached, infected red blood cells are isolated using VarioMACS magnetic columns. The culture is then centrifuged (4 °C, 1900 rpm, 5 min) and washed twice with PBS buffer. Pellets are then resuspended in lysis buffer and cell disruption is carried out by sonication (Vibra Cell Sonics, ultrasonic Processor 750 Watt 20 KHz). The samples are incubated on ice for 30 min, and then centrifuged at 4 °C for 20,000 g for 10 min. The supernatant is transferred to precooled ultracentrifuge tubes and centrifuged again at 4 °C at 140,000 g for 1 h. The supernatant is transferred into a fresh precooled eppendorf and the protein concentration determined by a Bradford assay.[200] Aliquots are prepared with 5 mg per eppendorf, and then frozen and stored at – 80 °C until use.

Preparation of capturing beads. A 75% slurry (1 mL) of NHS-Sepharose 4 Fast Flow beads (provided in isopropanol from GE Healthcare, #17-0906-01) was centrifuged. The supernatant was discarded, and the beads washed three times with DMSO (10 mL). A 1:1 slurry of beads and DMSO was prepared, and 3-azido-1-propanamine (10 µL of 100 mM stock solution) and triethylamine (7.5 µL) were added. The beads were incubated on a shaker at RT overnight. Ethanolamine (50 µL) was added to the bead slurry, and the beads were incubated on a shaker at RT for a further 6 hours. Beads were then washed twice with DMSO (10 mL) and three times with isopropanol (10 mL). A 1:1 slurry of beads and isopropanol was prepared and the slurry was stored at – 20 °C. When needed, 2 mL of bead slurry (1 mL of settled beads) were centrifuged and the supernatant was discarded. The beads were washed three times with aqueous *t*BuOH (50% *t*BuOH in water). The appropiate chemical probe solution (10 µL of 100 mM stock solution) was added to the bead slurry. A premixed solution of $CuSO_4$ (5 µL of 100 mM solution in water) and *tris*(3-hydroxypropyltriazolylmethyl)amine (THPTA) (20 µL of 50 mM solution in water) was next added to the bead slurry. Freshly prepared sodium-L-ascorbate solution (12.5 µL of 200 mM stock solution in water) was added, and the bead slurry was incubated on a shaker at RT for at least 2 hours. The bead slurry was centrifuged and the supernatant was discarded. The beads were washed with 0.2 M ethylenediaminetetraacetic acid disodium salt (EDTA-Na_2) solution until the blue colour disappeared. The beads were then washed with 2 × 10

mL each of water, DMSO, and isopropanol, and then stored as a 1:1 slurry of beads and isopropanol at – 20 °C.

Preparation of blocked beads. Blocked beads are used as a control. The NHS active group on the NHS-Sepharose 4 Fast Flow beads is 'blocked' by treating the beads the same way as for the capturing beads, except without any 3-azido-1-propanamine. A 75% slurry (1 mL) of NHS-Sepharose 4 Fast Flow beads was transferred into a centrifuge tube and centrifuged. The supernatant was discarded, and the beads washed three times with DMSO (10 mL). A 1:1 slurry of beads and DMSO was prepared, and triethylamine (7.5 µL) was added. The beads were incubated on a shaker at RT overnight. Ethanolamine (50 µL) was added to the bead slurry, and the beads were incubated on a shaker at RT for a further 6 hours. Beads were then washed twice with DMSO (10 mL) and three times with isopropanol (10 mL). A 1:1 slurry of beads and isopropanol was prepared and the slurry was stored at – 20 °C. Before use, the slurry was thawed, centrifuged, and the supernatant was discarded to leave 1 mL of blocked beads.

Competition experiments overview. Each competition experiment comprised 10 samples processed in two steps (see Table 5.1).

Sample	1st Step	2nd Step
1	lysate + blocked beads + DMSO	lysate from 1st step (supernatant) + capturing beads
2	lysate + blocked beads + DMSO	lysate from 1st step (supernatant) + capturing beads
3	lysate + capturing beads + DMSO	lysate from 1st step (non-binding fraction) + fresh capturing beads
4	lysate + capturing beads + DMSO	lysate from 1st step (non-binding fraction) + fresh capturing beads
5	1st conc. of competitor compound + lysate	lysate from 1st step + capturing beads
6	2nd conc. of competitor compound + lysate	lysate from 1st step + capturing beads
7	3rd conc. of competitor compound + lysate	lysate from 1st step + capturing beads
8	4th conc. of competitor compound + lysate	lysate from 1st step + capturing beads
9	5th conc. of competitor compound + lysate	lysate from 1st step + capturing beads
10	6th conc. of competitor compound + lysate	lysate from 1st step + capturing beads

Table 5.1. Table to indicate the two steps in the processing of each sample in each competition experiment.

For samples 1 – 4, the same amount of DMSO is added as used for the compound competition samples. These samples are used as controls. Samples 5 – 10 are used for

the competition experiments, from high to low concentration of competitor. The volumes of each reagent used are outlined in Table 5.2.

Reagent	1st Step	2nd Step
Lysate	0.6 mL	0.5 mL
Dry beads	21 µL	17.5 µL
Competitor (**2**) (200x stock solution in DMSO)	3 µL	-

Table 5.2. Overview of reagent volumes used in both incubation steps.

The first incubation step was performed with a 20% increased input of material to ensure that the second incubation step could be carried out with exactly 500 µL of pre-incubated lysate.

Preparation of diluted lysate. A 3 mg lysate pellet per data point was thawed in a water bath at RT and then diluted in 1 x DP buffer to reduce the detergent concentration from 0.8% to 0.4%. The lysate was then diluted with further 1 x DP buffer to reach a final protein concentration of 5 mg/mL (determined using the protein content values found in the Bradford assay). The diluted lysate was then centrifuged (4 °C, 33,500 rpm, 20 min) and the cleared lysate transferred into fresh falcon tubes and kept on ice.

Preparation of compound dilutions (samples 5 – 10). A 200x stock solution (at 2 mM) of competitor compound (**2**) was prepared in anhydrous DMSO. A dilution series was then prepared using a 1:6 dilution factor. Using the 200x stock solution as the highest concentration of competitor, aliquots of 3 µL per dilution solution were used for samples 5 – 10 in the first incubation step (ensuring a final solvent concentration of 0.5% DMSO in competition experiments).

Washing and equilibration of affinity matrix. In order to have 21 µL of required beads for all the samples in Table 5.1, 250 µL capturing beads and 50 µL blocking beads were transferred to two separate 15 mL tubes each containing 10 mL 1 x DP buffer without IGEPAL CA-630, whilst working on ice. The tubes were centrifuged, and the supernatant was discarded. This was repeated once more, and then the beads were similarly washed with 1 x DP buffer containing 0.4% IGEPAL CA-630. The beads were then resuspended in 1 x DP buffer containing 0.4% IGEPAL CA-630 to get a 5% bead slurry.

Competition experiments – first incubation step. To wells in a 96 well filter plate, corresponding to samples 1 – 4, 420 µL of appropriate 5% bead slurry (i.e. 21 µL of

dry capturing or blocked beads) were transferred for each sample as per step 1 in Table 5.1. In this first incubation step, to each well corresponding to samples 1 – 10 was added 0.6 mL precleared lysate. Next, 3 µL of the appropriate competitor (**2**) stock solution was added to the respective wells corresponding to samples 5 – 10, and 3 µL of DMSO was added to the remaining wells. The samples were incubated for 1 h at 4 °C with overhead rotation with cooling in a cold room.

Competition experiments – second incubation step. A second 96 well filter plate was prepared containing 350 µL of 5% capturing bead slurry per sample well (i.e. 17.5 µL dry beads). The pre-incubated samples from the first incubated step were transferred to the second 96 well plate containing capturing beads. This second plate was then incubated for a further 1 h at 4 °C with overhead rotation and cooling in the cold room.

Plate washing. After incubation, the filter plate was spun down at 1200 rpm for 1 min at 4 °C. Beads were washed first with 1 x DP buffer with 0.4% IGEPAL CA-630 (10 mL) and secondly with 1 x DP buffer containing 0.2% IGEPAL CA-630 (5 mL) using a MultiScreen HTS Vacuum Manifold. After these washes, the plate was placed on top of a waste collection plate and the assembly was centrifuged for 2 mins at 1200 rpm at 4 °C. The flow-through was discarded.

Protein elution. To each well was added 50 µL of 2 x enhanced sample buffer. The plate was closed using a fresh bottom mat, and incubated at 50 °C in an incubator being shaken for 30 mins at 140 rpm. The filter plate was then placed onto a fresh 96 well collection plate and the assembly was centrifuged for 2 min at 1200 rpm at RT. The 96 well plate containing the eluate was sealed with aluminium foil and stored at – 20 °C.

Protein digestion. To each well was added 40 µL of digestion buffer. The plate was placed on top of a collection plate and shaked overnight at RT and 500 rpm on a Titramax orbital shaker. The peptides were then eluted by centrifugation for 1 min at 1000 g and collected in the collection plate. Peptide samples were then labelled with TMT reagent as per the general procedure (**Section 5.2.11 – Chemical peptide labelling using TMT reagents**).

KCl-based clean up. After the TMT labelling and pooling, all peptide samples contain HEPES, potential bead remnants, and detergent remnants. In order to purify samples, they were subjected to KCl-based SDS removal and desalting. Dried samples were

dissolved in pre-warmed saturated KCl solution (~5M at 38 °C) and centrifuged, in order to separate insoluble potassium dodecyl sulfate (and bead remnants) from the peptide-containing supernatant. An SPE plate (Oasis HLB 96-well μElution Plate, Waters, #186001828BA) was activated by washing through 0.1 mL of 80% MeCN and 0.5% TFA solution. The plate was equilibrated by loading 0.2% TFA, and the filtrate was discarded. The supernatants from the KCl precipitated samples were loaded into the SPE plate and the plate was centrifuged slowly for 5 min at 900 rpm. Samples were washed with 0.1 mL 4% TFA followed by centrifugation. The SPE plate was placed on a collection plate. To each well was added 0.2 mL 80% MeCN, 0,5% TFA followed by 1 min centrifugation. The purified peptide-containing eluate was collected and lypholised. Samples were then subjected to LCMS/MS acquisition and analysis as per the general procedure (**Section 5.2.12 – LCMS/MS acquisition and analysis for protein identification**).

5.2.7 Fluorescence-activated cell sorting (FACS) for parasite killing rate studies[261]

The FACS assay provides the means to measure the parasite killing kinetics of antimalarial compounds. *P. falciparum* blood stage cultures are incubated in the presence of the antimalarial compound for 24 h or 48 h. The antimalarial compound is then removed through appropriate washes, and the culture samples are added to erythrocytes pre-labelled with intracellular dye to allow their subsequent identification. The ability of viable parasites from the treated cultures to re-establish infection in the labelled erythrocytes can then be analysed by two-colour flow cytometry after the labelling of parasite DNA. Stained erythrocytes containing stained parasites are as a result of a new infection by parasites surviving after the antimalarial incubation step. The capacity for the antimalarial compound to eliminate parasite viability within 24 h or 48 h is thus determined.[261] A sample of *P. falciparum* culture not treated with any antimalarial compound and progressed to the invasion of pre-labelled erythrocytes step is used as a control to indicate maximum parasite viability. This FACS assay was conducted by Benigno Crespo and Ana Hermoso, colleagues at GSK Tres Cantos.[197]

Erythrocyte labelling. Erythrocytes were labelled with CFDA-SE by incubation of the required volume at 1% haematocrit in RPMI 1640, with a CFDA-SE concentration of 10 µM at 37 °C for 2 h. The suspension was then washed with complete medium and the labelled erythrocytes were resuspended in complete medium to give 1% haematocrit, and then incubated for 30 min at 37 °C. Erythrocytes were then washed twice with RPMI-1640, diluted to 1% haematocrit, and stored at 4 °C for up to 24 h.

Drug treatment and infection of labelled erythrocytes. Conditions were chosen to mimic those used for the standard [^{3}H]-hypoxanthine incorporation assay for IC_{50} determination (2% haematocrit, 0.5% parasitaemia, with greater than 80% ring stages). Asynchronous cultures were incubated under shaking conditions to avoid multiple infections per erythrocyte. A culture volume of 50 µL per well with parasites at 4% haematocrit and 0.5% parasitaemia was dispensed into 96 well plates containing 50 µL of complete media with previously diluted drugs prepared at 2 × their final concentration to give a final volume of 100 µL per well and a final drug concentration of 10 × IC_{50}, unless the IC_{50} is above 1 µM in which case a set dose of 10 µM was used to avoid potential toxic responses at higher doses. Each drug was tested in triplicate. The plates were then incubated for 24 or 48 h using standard incubation techniques. The drug was renewed every 24 h throughout the treatment period by retiring old media from the cultured wells and adding the same volume with fresh drug. Drug was removed following either 24 or 48 h of exposure. This was achieved by removing 80 µL of media containing drug, leaving 20 µL in the well to which 200 µL of fresh media was added (1/10 dilution). Plates were centrifuged for 4 min at 600 g at RT, and 180 µL of media was then removed. The remaining 20 µL, containing the infected erythrocytes, was resuspended in 100 µL of complete media (1/5 dilution). Following this drug removal, 70 µL of washed infected erythrocytes was transferred to a new microtitre plate containing 130 µL of CFDA-SE-labelled, non-infected erythrocytes (1/3 dilution) at 2% haematocrit in complete media. Plates were incubated for 48 h in the dark to allow new infections to develop in labelled erythrocytes as a measure of viable parasites. Control wells contained no drug and were exposed for 0 h before progression to the parasite invasion step.

Parasite labelling. Following incubation, parasite cultures were washed with PBS. Plates containing cultured parasites were centrifuged, the supernatants were aspirated,

and the erythrocytes were suspended in Hoechst 33342 solution (1.2 µg/mL in RPMI-1640), and then incubated for 20 min in the dark. Cells were then fixed by addition of 20 µL of 0.25% gluteraldehyde and stored at 4 °C protected from the light.

Fluorescence-activated cell sorting (FACS). Following parasite staining, each sample was transferred to cytometry tubes and acquired in a Attune NXT flow cytometer equipped with a 405 nm violet laser and a 488 nm blue laser. Hoechst 33342 was excited by the violet laser, and CFDA-SE was excited by the blue laser. Samples were analysed using Microsoft Excel.

Data analysis and validation. Parasitised CFDA-SE-stained erythrocytes represent new infections that have been established from parasites surviving drug treatment. Quantification of CFDA-SE-stained erythrocytes was used to evaluate parasite viability following drug treatment. Assuming no bias in reinvasion of dyed or non-dyed erythrocytes, the total number of new infections was estimated as 3/2 of the number of infected, labelled erythrocytes (due to the three fold dilution of the treated erythrocytes in labelled erythrocytes). Parasite viability was calculated as the percentage of infected CFDA-SE-stained erythrocytes in drug-treated samples at 24 or 48 h versus infected CFDA-SE-stained erythrocytes in control samples at time 0, i.e. controls allow normalisation to a parasite viability of 100% before drug treatment. The results were presented as the mean of this normalised percentage ± the standard error of the mean. All statistical analyses were performed using Microsoft Excel.

5.2.8 Confocal imaging for visualising probe localisation in *P. falciparum* parasites

The accumulation of photoaffinity probe compound (**68**) in live parasites can be visualised through incubation of the probe in *P. falciparum* cultures, followed by UV irradiation to trigger covalent crosslinking. The TCO functional handle on the probe is then reacted with a tetrazine-derivatised dye to allow for visualisation, with a culture sample in which no probe is added used as a control. These experiments were conducted by the author of this study, with guidance from Olalla Sanz and Pedro Alfonso Torres-Gomez at GSK Tres Cantos.[262]

Reagents. AFDye™ 488 Tetrazine was sourced from Click Chemistry Tools as a fluorescent group that absorbs at 493 nm and reacts with *trans*-cyclooctene groups

with fast kinetics (up to 30,000 $M^{-1}s^{-1}$). In addition, 4',6-diamidino-2-phenylindole (DAPI) was used as a blue-fluorescent DNA stain to locate parasitic content within the *P. falciparum* cultures. DAPI is excited by the violet (405 nm) laser line and thus these spectral properties make it suitable for use with AFDye™ 488.

Culture information. An 8 mL sample of *P. falciparum* culture (H2%, P3.5%) was centrifuged and resuspended in complete RMPI-1640 media without phenol red, to avoid potential interference during the UV cross-linking step.

Probe treatment. The two conditions tested for imaging include:

1. Malaria culture treated with PAL probe and UV cross-linked.
2. Malaria culture not treated with PAL probe (negative control).

A 6 mL sample of malaria culture (H2%, P3.5%), in media without phenol red, was incubated with 5 µM of PAL probe for 1 h. In parallel, an untreated 2 mL sample of the malaria culture (H3%, P3.5%) was also incubated for 1 h. Cultures were then washed with cold PBS. The probe-treated pellet was resuspended in 4 mL of cold PBS, and then UV irradiated for 10 min in the UV photo cross-linker. The untreated malaria culture was kept at RT during this time. Both samples were then centrifuged, and the supernatant was aspirated. Each sample was resuspended in 700 µL of culture media (without phenol red) and fixed by addition of 70 µL of 0.025% gluteraldehyde (to give a final concentration of 0.0025%). The samples were incubated for 10 min at RT, and then centrifuged. The supernatant was aspirated, and the erythrocyte pellet was resuspended in 1% BSA in HBSS. The samples were incubated for 1 h at RT, centrifuged, and the supernatant was aspirated. The samples were washed once with 0.05% Tween in HBSS and then incubated in 10 µg/mL of AFDye 488 Tetrazine solution, for 1 h at RT. Each sample was then washed twice with 0.05% Tween in HBSS solution, and resuspended in 5µg/mL DAPI in HBSS and incubated for 30 min at RT. These stained samples were washed once with HBSS, centrifuged and then the supernatant was aspirated. The pellets were resuspended in 150 µL of HBSS and transferred to a 96 Perkin Elmer Cell Carrier Ultra plate, treated with collagen for better adherence of cells. 1/3 dilutions were carried out to give 6 different concentrations. The plate was centrifuged and then transferred to a a Perkin Elmer Opera Phenix™ high-content imaging system,, avoiding movements and agitations. This system provides high-resolution images of cell-culture models using advanced

spinning-disk technology called Synchrony™ Optics. The technology reduces spectral cross talk by placing excitation lasers into two groups such that spectrally neighbouring laser lines are in different light paths, allowing for up to four channels of simultaneous imaging. Automated confocal imaging was performed, with images acquired using a 40x water objective, and using two lasers (Alexa 488; 488 nm excitation line, 520 nm emission filter; 405 nm for DAPI-stained parasites) and brightfield visualisation. Image analysis was performed in Harmony Software (Perkin Elmer). Images were visually assessed for suitability in terms of cell crowding, and then edited with the second sample providing the background control. This background fluorescence was subtracted from that seen for the first sample to provide normalised images.

5.2.9 Determination of parasitic protein content in different volumes of *P. falciparum* culture

The determination of parasitic protein content in different volumes of the same *P. falciparum* culture (i.e. at the same % hematocrit and % parasitaemia) can be determined through isolation of the parasites from their host erythrocytes, followed by a Bradford assay as per standard protocols.[200] A 50 mL *P. falc* culture (P9.7%, H10%) was distributed amongst 4 different falcon tubes in volumes of 4 mL, 8 mL, 12 mL, and 26 mL. Saponin was then added to each falcon tube to cause selective erythrocyte lysis. Saponin, a surfactant that interacts with cellular membranes, makes the lipid bilayer membrane of red blood cells permeable to macromolecules, which can be observed by the total loss of red hameoglobin from the culture, removed by centrifugation and buffer washes.[263] The parasite membrane remains intact during this process, allowing isolation of the live parasite pellets from their host human red blood cells.[264] Next, parasite lysis followed by centrifugation and aspiration of the supernatant provided the parasite lysate. This was used in a Bradford assay, in which a Coomassie Brilliant Blue G-250 dye is used to bind to protein. The binding of the dye to protein causes a shift in its absorption maximum from 465 to 595 nm. The increase in absorption at 595 nm is monitored to give a value for protein content, using known protein amounts of a standard of λ-globulin for comparison.[200] *P. falciparum*

cultures were prepared by Jose Luis Llergo-Largo, and the rest of the experiment was carried out by the author of this study with guidance from Olalla Sanz.[260,265]

Culture information. *Day 1:* A 30 mL *P. falciparum* culture (H2%, P0.5%) was incubated as per standard conditions.

Day 4: The culture were centrifuged, and the supernatant was aspirated and discarded. The pellet was resuspended in complete RPMI and fresh erythrocytes to give 1 flask of 100 mL at 5% haematocrit.

Day 11: A Giemsa-stained blood smear indicated that parasitaemia had reached 3.8%.

Day 12: A Giemsa-stained blood smear indicated that parasitaemia had reached 5.2%. The culture was centrifuged, and the supernatant was aspirated and discarded. Fresh RPMI media was added to give 1 flask of 100 mL at 5% haematocrit.

Day 13: A Giemsa-stained blood smear indicated that parasitaemia had reached 6%. The culture was centrifued, and the supernatant was aspirated and discarded. Fresh RPMI media was added to give 1 flask of 100 mL at 5% haematocrit.

Day 14: A Giemsa-stained blood smear indicated that parasitaemia had reached 9.7%, with 67% ring stages and 33% mature forms. This culture (H5%, P9.7%) was used in the following experiment.

Culture treatment. A 100 mL *P. falciparum* culture (H5%, P9.7%) was centrifuged, and the supernatant was aspirated. The pellet was resuspended in 50 mL of RPMI media to give a culture of haematocrit 10%. This culture was distributed into 4 different falcon tubes in volumes of 4 mL, 8 mL, 12 mL, and 26 mL. To each falcon tube was added 10 µL of saponin per mL of culture. The cultures were incubated for 5 min at RT. Each sample was then washed with PBS until the supernatant became transparent. The samples were centrifuged, and the supernatant aspirated between washes. To each of the 4 parasite pellets was added 250 µL of parasite lysis buffer (without benzonase). The sample was pipetted up and down 10 times, and then 20 µL of each sample was transferred to separate 1.5 mL eppendorfs. The samples were centrifuged for 20 min at 20,000 g at RT, and the supernatant was used in a Bradford assay for determination of protein content.[200]

Bradford assay for determination of protein content. To each well of a 250 µL microplate was added 200 µL of MilliQ water, as well as either the standard (λ-globuline), or sample solution, with each sample assayed by triplicates. 50 uL of

Coomassie G-250 dye was then added to each well, and the plate was shaken for 5 min. The protein content in each sample was determined in an M5 Spectramax Microplate Reader (λ = 595 nm). A standard curve was produced (Graph 5.1).

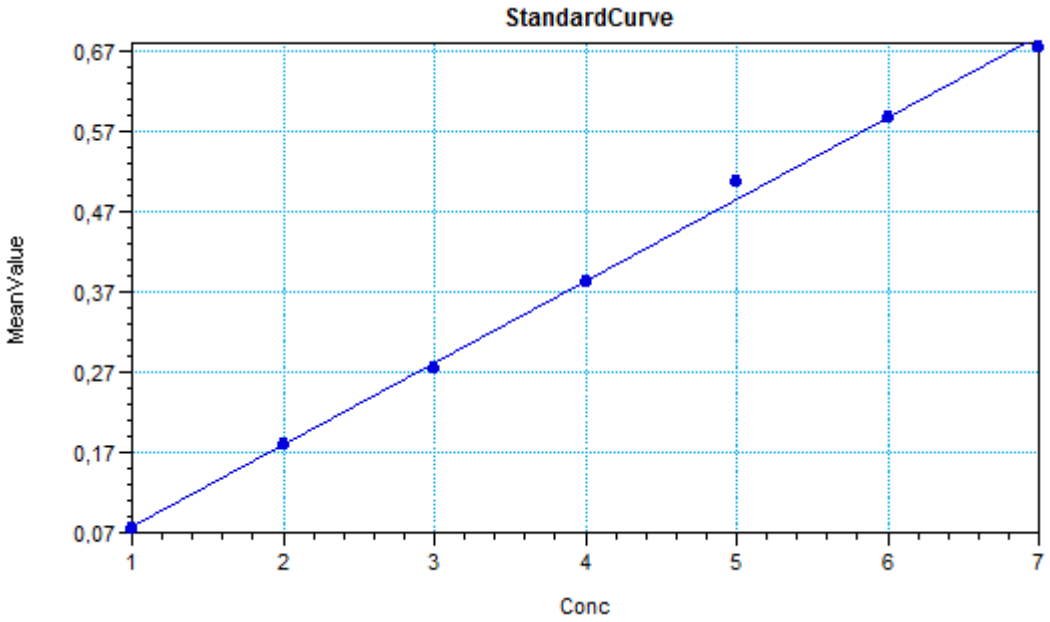

Graph 5.1. Standard curve for Bradford assay.

The average protein content for each sample was determined as per Table 5.3 below. Standard samples 1 and 2 gave results below the range indicated by the control, and thus were determined by extrapolation.

	Sample	mg/mL	Volume (µL)	Protein mass isolated (mg)
1	4 mL	0.06	250	0.02
2	8 mL	0.71	250	0.18
3	12 mL	1.26	250	0.32
4	26 mL	2.45	250	0.61

Table 5.3. Parasitic protein content in P. falciparum culture (H10%, P9.7%) samples of differing volumes.

5.2.10 Photoaffinity labelling for target identification of antimalarial quinazolinamines

Photoaffinity labelling can be used to covalently capture protein targets of a photoreactive chemical probe within complex protein mixtures thus enabling the

isolation and identification of these proteins using LCMS/MS. In antimalarial drug discovery for *P. falciparum*, this requires the growth of an appropriate *P. falciparum* culture at a high parasitaemia, followed by incubation of this culture with the appropriate concentrations of photoaffinity probe and free drug competitor to allow for affinity binding to protein targets. UV irradiation facilitates the covalent crosslinking. In these experiments, either UV irradiation of the whole blood stage cultures or of the isolated parasites is conducted depending on which method is under investigation. Subsequent parasite lysis allows access of the parasite lysate, for which a Bradford assay is used to determine protein content. These lysates are diluted to the same protein concentration, and then dosed with neutravidin agarose beads, which are previously functionalised with a tetrazine derivatised biotin reagent *via* exploitation of the strong interaction between neutravidin and biotin. The tetrazine functional handle reacts rapidly with the TCO functional handle incorporated into the photoaffinity probe. Non-covalently bound proteins are washed away, and the purified captured proteins are proteolytically digested. The peptide fragments are further purified to remove salts, detergents, and bead remnants. They are then labelled with appropriate TMT reagents before being sequenced using LCMS/MS for protein identification. The chemical syntheses and the subsequent steps up until the preparation of capturing beads were carried out by the author of this study, with guidance from Olalla Sanz.[260] The pull down experiments were carried out by colleagues at Cellzome.[167]

Equipment. A CL-1000 UV Crosslinker bought from Analytik Jena US LLC was used for UV irradiation of samples.

Culture information. *Day 1:* One flask containing 100 mL of *P. falc* culture (H2%, P0.3%) was scaled up over 10 days. The flask was incubated as per standard conditions.

Day 3: The *P. falciparum* culture was determined to be at 5% parasitaemia through a Giemsa-stained blood smear. A sorbitol synchronisation was carried out. The culture was centrifuged at 1900 rpm for 5 min at 37 °C. The supernatant was aspirated and discarded, and the pellets were resuspended in 10 volumes of pre-warmed sorbitol (5%), and incubated for 5 min at 37 °C. The pellets were then twice washed with complete RPMI, centrifuged and the supernatant was aspirated. The pellets were again

resuspended in complete RPMI medium and fresh erythrocytes to give 6 flasks of 100 mL/flask at 2.5% haematocrit.

Day 7: A Giemsa-stained blood smear indicated that parasitaemia was at 4%. The cultures were centrifuged, and the supernatant was aspirated and discarded. The pellets were resuspended in complete RPMI and fresh erythrocytes to give 6 flasks of 100 mL/flask at 5% haematocrit.

Day 9: A Giemsa-stained blood smear indicated parasitaemia had reached 6%. The cultures were centrifuged, and the supernatant was aspirated and discarded. The pellets were resuspended in complete RPMI and fresh erythrocytes to maintain 6 flasks of 100 mL/flask at 5% haematocrit.

Day 10: A Giemsa-stained blood smear indicated that parasitaemia remained at 6%, with 25% at ring stages and 75% of parasites as mature forms. The cultures (H5%, P6%) were centrifuged, and the supernatant was aspirated and discarded. The pellets were resuspended in 300 mL of complete RPMI media without phenol red to give a culture of 10% haematocrit and 6% parasitaemia.

Treatment of P. falciparum cultures. 150 mL of malaria culture (H10%, P6%) was split into 3 flasks of 50 mL each. These were treated as follows, with the volume of DMSO added kept constant between samples and never exceeding 2%, and the final concentrations of each compound as indicated:

1. 1 µM PAL probe (**68**) in DMSO
2. 1 µM PAL probe (**68**) + 5 µM parent compound (**2**) in DMSO
3. 1 µM PAL probe (**68**) + 0.5 µM parent compound (**2**) in DMSO

The 3 flasks were incubated for 1 h at 37 °C, in an atmosphere of 90% N_2, 5% CO_2, and 5% O_2. Each sample was then split into two to give 6 flasks of 25 mL each.

Method A: Photoaffinity labelling in P. falciparum cultures. One 25 mL flask of each sample (1A – 3A) was UV irradiated at 365 nm for 10 min on ice. Each sample was then collected in separate falcon tubes and 250 µL of saponin was added to each. The samples were shaken and incubated for 5 min at RT, and then centrifuged. The supernatant was aspirated and the remaining pellet was washed with PBS buffer three times, with centrifugation and aspiration between each wash. To each isolated parasite pellet was then added 250 µL of parasite lysis buffer (with benzonase added just prior to use). The samples were pipetted up and down 10 times and then incubated for 35

min at RT to complete the lysis and allow the benzonase to digest nucleic acids. The homogenates were cleared by centrifugation for 40 min at 20,000 g at RT. The supernatants were transferred into fresh eppendorfs and 20 µL of each sample was taken for protein determination using a Bradford assay in an M5 Spectramax (λ = 595 nm). The lysates were frozen on dry ice and stored at – 80 °C until use in pull-down experiments.

Method B: Photoaffinity labelling in isolated P. falciparum parasites. The remaining 25 mL flasks for each sample (1B – 3B) were transferred to separate falcon tubes and 250 µL of saponin was added to each. The cultures were shaken and incubated at RT for 5 min, and then centrifuged and the supernatant was aspirated. Each pellet was washed with treated PBS solution that maintained the drug pressure of each compound in the respective sample. The isolated parasite pellets were then diluted in 2 mL each of complete RPMI media without phenol red and then UV irradiated at 365 nm for 10 min on ice. Each sample was then transferred to separate falcon tubes, and 250 µL of parasite lysis buffer (with benzonase added just prior to use) was added to each sample. The samples were pipetted up and down 10 times, and then incubated for 35 min at RT. The homogenates were cleared by centrifugation for 40 min at 20,000 g at RT, and the supernatants were transferred into fresh eppendorfs. 20 µL of each sample was taken for protein concentration determination using a Bradford assay in an M5 Spectramax (λ = 595 nm). The lysates were frozen on dry ice and stored at – 80 °C until used for pull-down experiments.

Bradford assay for determination of protein content in parasite lysates. To each well of a 250 µL microplate was added 200 µL of MilliQ water, as well as either the standard (λ-globuline) with SDS, or sample solution, with each sample assayed by triplicates. 50 uL of Coomassie G-250 dye was then added to each well, and the plate was shaken for 5 min. The protein content in each sample was determined in an M5 Spectramax Microplate Reader (λ = 595 nm). A standard curve was produced (Graph 5.2).

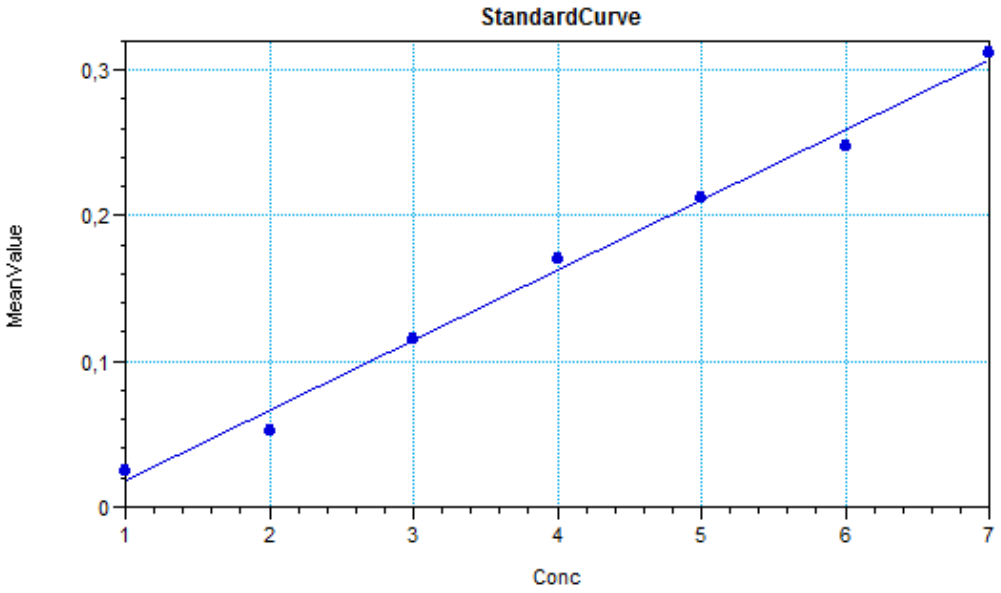

Graph 5.2. Standard curve for Bradford assay.

The average protein content for each sample was determined as per the tables below:

METHOD A: PAL in *P. falc* cultures			
	Sample	**mg/mL**	**Volume**
1A	1 µM PAL Probe (**68**) + DMSO	3.15	250 µL
2A	1 µM PAL Probe (**68**) + 5 µM (**2**)	2.86	250 µL
3A	1 µM PAL Probe (**68**) + 0.5 µM (**2**)	3.60	250 µL

Table 5.4. Parasite protein content in each sample treated as per Method A.

METHOD B: PAL in *P. falc* parasites			
	Sample	**mg/mL**	**Volume**
1B	1 µM PAL Probe (**68**) + DMSO	2.60	250 µL
2B	1 µM PAL Probe (**68**) + 5 µM (**2**)	2.57	250 µL
3B	1 µM PAL Probe (**68**) + 0.5 µM (**2**)	2.35	250 µL

Table 5.5. Parasite protein content in each sample treated as per Method B.

Preparation of capturing beads. The preparation of beads involves the immobilisation of biotin-tetrazine onto agarose beads, the blocking of beads with biotin, and then the equilibration of the coupled beads with DP buffer with 0.4% IGEPAL CA-630. 300 µL of dry high capacity Neutravidin Agarose beads (Thermo Scientific, #29204) were

washed three times with PBS buffer by dilution, mixing, centrifugation and aspiration of the wash buffer supernatant. A 1:1 slurry of beads and PBS buffer was prepared after the last wash step, and 1.20 µL of a 50 mM tetrazine-PEG_4-biotin (sourced from Jena Bioscience, #CLK-027-25) stock solution in DMSO was added. The tube was closed and inverted several times to ensure bead resuspension. The beads were incubated overnight at 4 °C under overhead rotation. The beads were then blocked with biotin to block any remaining neutravidin sites. A 3 µL aliquot of a 100 mM biotin stock solution in DMSO was added to the tube containing 300 µL of beads. The tube was closed and inverted several times, and then incubated for 30 mins at 4 °C under overhead rotation. The beads were then transferred to a 15 mL tube and washed three times with 1 x DP buffer containing 0.4% IGEPAL CA-630. After the last wash step, a 5% bead slurry in DP buffer containing 0.4% IGEPAL CA-630 was prepared (i.e. a volume of 6 mL for 300 µL beads). The bead slurry was stored on ice.

Preparation of diluted cell lysates. Treated *P. falciparum* lysate samples were thawed and then diluted on ice to 0.4% IGEPAL CA-630 with 1 x DP buffer containing 0.5% SDS and Roche Protease Inhibitors (1 protease inhibitor per 25 mL buffer). The lysates were then diluted to an equal protein concentration between samples (maintaining the maximum possible concentration) with further 1 x DP buffer containing 0.5% SDS and Roche Protease Inhibitors (1 protease inhibitor per 25 mL buffer) with 0.4% IGEPAL CA-630. Lysates were then centrifuged for 20 min at 4 °C at 33,500 rpm. The supernatants were transferred to fresh tubes and kept on ice.

Incubation of lysates with capturing beads. From each diluted sample was transferred 500 µL to separate wells in a 96 well filter plate containing 17.5 µL each of prepared capturing beads. The filter plate was incubated for 1 h at 4 °C with overhead rotation. The filter plate was then spun down at 1200 rpm for 1 min at 4 °C and samples were washed firstly with 1 x DP buffer containing 0.4% IGEPAL CA-630 and 0.5% SDS (5 × 2 mL), and then with 1 x DP buffer containing 0.2% IGEPAL CA-630 and 0.5% SDS (5 × 1 mL). The filter plate was placed on top of a waste collection plate and the assembly was centrifuged at 1200 rpm for 1 min at 4 °C.

Elution of non-covalently bound proteins. 50 µL of 0.25 x NuPAGE LDS sample buffer (Invitrogen, #NP0007) containing 50 mM DTT was added to each well, and the plate was incubated at 50 °C for 30 min with shaking at 140 rpm. The filter plate was

placed on top of a waste collection plate and the assembly was centrifuged at 1200 rpm for 2 min at RT. The eluates were discarded and the filter plate containing the beads retained. The beads were washed with wash buffer 1 (5 mL) and then centrifuged at 1200 rpm for 1 min at RT. The beads were then washed with wash buffer 2 (15 mL), wash buffer 3 (15 mL), and wash buffer 4 (5 mL) and centrifuged at 1200 rpm for 1 min at RT between washes, with the eluates discarded.

On bead digestion. To each well of the filter plate containing the washed beads was added 60 µL of freshly prepared digestion buffer. The plate was incubated overnight at 700 rpm in a thermomixer at RT. The filter plate was then placed on a fresh 96-well plate and the assembly was centrifuged at 1200 rpm for 2 mins at RT. To each well containing the beads was then added 60 µL of 50 mM HEPES buffer, and the plate was incubated at 700 rppm in a thermomixer for 4 mins at RT. The filter plate was then placed onto a fresh 96-well plate and the assembly was centrifuged at 1200 rpm for 2 mins at RT. This wash fraction was combined with the eluate from the previous wash and the samples were frozen at −80 °C and then lyophilised. The peptide samples were then labelled with TMT reagent as per the general procedure (**Section 5.2.11 – Chemical peptide labelling using TMT reagents**).

C18SCX clean-up. After TMT labelling and pooling, all peptide samples contain HEPES, potential bead remnants, and detergent remnants. In order to purify samples, they were subjected to stage tip-based C18SCX purification which combines salt/detergent/bead removal in a single approach. This approach allows the purification of low mass samples (<10 µg). Dried peptide samples were dissolved in 100 µL of 6% TFA (in distilled water) and the pH was checked to ensure it was less than 4. These solutions were loaded onto a layer of C18 material (octadecyl C18 47mm Extraction Disks, Empore/3M, #2215), which had been pre-wetted with MeOH, and filtered. The peptide samples were washed with 100 µL of 0.5% TFA, 2% MeCN, and then eluted to an SCX filter (cation 47 mm Extraction Disks, Empore/3M, #2251) through addition of 100 µL of 0.5% TFA in 60% MeCN. Samples were washed once more through the SCX column with 200 µL 0.5% TFA in 60% MeCN to remove remaining detergents. Peptides were then eluted from the SCX column by addition of 50 µL of 5% NH_3 in 80% MeCN. This was repeated twice. The purified peptide-containing eluate was collected and lypholised. Samples were then subjected to LCMS/MS acquisition and

analysis as per the general procedure (**Section 5.2.12 – LCMS/MS acquisition and analysis for protein identification**).

5.2.11 Chemical peptide labelling using TMT reagents

Digested peptide samples were suspended in 10 µL of distilled water in separate wells of the appropriately sized plate. To each sample was added 10 µL of appropriate TMT reagent (TMT10plex™ Isobaric Mass Tagging Kit, #90113 sourced from GE, Thermo Scientific). The plate was sealed, and incubated for 1 h at RT with shaking at 500 rpm on a Titramax shaker. The stop solution was prepared shortly before the end of the incubation time. Non-reacted TMT reagent was quenched by addition of 5 µL per sample of stop solution to each well. The plate was incubated for 15 min at RT, shaking at 500 rpm on a Titramax shaker. All of the samples were then combined in one 1.5 mL tube. Each well was washed with 10 µL wash solution and pooled into the same 1.5 mL tube. This solution was lypholised.

5.2.12 LCMS/MS acquisition and analysis for protein identification

The Q ExactivePlus mass spectrometer has a high performance quadrupole precursor ion selector and an Orbitrap mass analyser. The quadrupole is used for the selection of precursor ions to generate MS/MS data for identification of the selected peptide. The Orbitrap is used for the determination of the exact mass of the parent ions in MS1 scans and of peptide fragments and TMT reporter ion signals generated by high-energy collisional dissociation (HCD) in the HCD cell for MS2 scans. Peptides were separated using a Ultimate 3000 HPLC system (Thermo Fisher Scientific) with Chromeleon software on a 50 cm × 100 µM Nano C18 column (Reprosil®) at 55 °C. Elution was performed using a gradient of 2 – 40% MeCN in 0.1% formic acid over 200 min. Samples were injected into a Q ExactivePlus mass spectrometer (Thermo Fisher Scientific), performing 10 scan events. MS spectra were acquired using a 70,000 resolution with an ion target of 3×10^6. High energy collisional dissociation scans (for MS2) were performed with a normalised collision energy of 33%, and at 30,000 resolution with an ion target of 2×10^5. The instrument was operated with Tune 2.8 and Xcalibur 4.0.27.19. Mascot 2.5 (Matrix Science) and an in-house version of

isobarQuant were used for protein identification and quantification as per literature procedures.[266] A 10-ppm mass tolerance for peptide precursors and 20 mDa (HCD) mass tolerance for fragment ions was selected. Carbamidomethylation of cysteine residues and TMT modification of lysine residues were set as fixed modifications. *N*-terminal acetylation of proteins and TMT modification of peptide *N*-termini were set as variable modifications. Spectra were matched to peptides and filtered according to the following criteria: false-discovery rate <1%; mascot ion score >15; signal-to-background ratio of the precursor ion >4; and signal-to-interference >0.5. Fold changes were calculated by dividing the MS2 signal achieved for proteins in samples containing competitor compound by the sample without competition. Fold-changes were corrected for isotope purity and adjusted for interference caused by co-eluting nearly isobaric peaks.[267] Protein quantification was derived from individual spectra matching to distinct peptides by using sum-based bootstrap algorithm.[268,269]

References

(1) Cowman, A. F.; Healer, J.; Marapana, D.; Marsh, K. Malaria: Biology and Disease. *Cell* **2016**, *167* (3), 610–624.

(2) Phillips, M. A.; Burrows, J. N.; Manyando, C.; van Huijsduijnen, R. H.; Van Voorhis, W. C.; Wells, T. N. C. Malaria. *Nat. Rev. Dis. Prim.* **2017**, *3*, 17050.

(3) Bartoloni, A.; Zammarchi, L. Clinical Aspects of Uncomplicated and Severe Malaria. *Mediterr. J. Hematol. Infect. Dis.* **2012**, *4* (1), e2012026.

(4) *WHO | Malaria Fact Sheet*; World Health Organization, 2018.

(5) Vaughan, A. M.; Aly, A. S. I.; Kappe, S. H. I. Malaria Parasite Pre-Erythrocytic Stage Infection: Gliding and Hiding. *Cell Host Microbe* **2008**, *4* (3), 209–218.

(6) Silvie, O.; Mota, M. M.; Matuschewski, K.; Prudencio, M. Interactions of the Malaria Parasite and Its Mammalian Host. *Curr. Opin. Microbiol.* **2008**, *11* (4), 352–359.

(7) Bosch, J.; Buscaglia, C. A.; Krumm, B.; Ingason, B. P.; Lucas, R.; Roach, C.; Cardozo, T.; Nussenzweig, V.; Hol, W. G. J. Aldolase Provides an Unusual Binding Site for Thrombospondin-Related Anonymous Protein in the Invasion Machinery of the Malaria Parasite. *Proc. Natl. Acad. Sci.* **2007**, *104* (17), 7015–7020.

(8) Marti, M.; Baum, J.; Rug, M.; Tilley, L.; Cowman, A. F. Signal-Mediated Export of Proteins from the Malaria Parasite to the Host Erythrocyte. *Journal of Cell Biology* **2005**, 587–592.

(9) Flammersfeld, A.; Lang, C.; Flieger, A.; Pradel, G. Phospholipases during Membrane Dynamics in Malaria Parasites. *International Journal of Medical Microbiology* **2018**, *308* (1), 129–141.

(10) Mundwiler-Pachlatko, E.; Beck, H. P. Maurer's Clefts, the Enigma of *Plasmodium Falciparum*. *Proceedings of the National Academy of Sciences of the United States of America* **2013**, *110* (50), 19987–19994.

(11) Sam-Yellowe, T. Y. The Role of the Maurer's Clefts in Protein Transport in *Plasmodium Falciparum*. *Trends in Parasitology* **2009**, *25* (6), 277–284.

(12) Radfar, A.; Méndez, D.; Moneriz, C.; Linares, M.; Marín-García, P.; Puyet, A.; Diez, A.; Bautista, J. M. Synchronous Culture of *Plasmodium Falciparum* at High Parasitemia Levels. *Nat. Protoc.* **2009**, *4* (12), 1899–1915.

(13) Bennink, S.; Kiesow, M. J.; Pradel, G. The Development of Malaria Parasites in the Mosquito Midgut. *Cellular Microbiology* **2016**, *18* (7), 905–918.

(14) Florens, L.; Washburn, M. P.; Raine, J. D.; Anthony, R. M.; Grainger, M.; Haynes, J. D.; Moch, J. K.; Muster, N.; Sacci, J. B.; Tabb, D. L.; et al. A Proteomic View of the

Plasmodium Falciparum Life Cycle. *Nature* **2002**, *419* (6906), 520–526.

(15) Pease, B. N.; Huttlin, E. L.; Jedrychowski, M. P.; Talevich, E.; Harmon, J.; Dillman, T.; Kannan, N.; Doerig, C.; Chakrabarti, R.; Gygi, S. P.; et al. Global Analysis of Protein Expression and Phosphorylation of Three Stages of *Plasmodium Falciparum* Intraerythrocytic Development. *J. Proteome Res.* **2013**, *12* (9), 4028–4045.

(16) Frischknecht, F.; Matuschewski, K. *Plasmodium* Sporozoite Biology. *Cold Spring Harb. Perspect. Med.* **2017**, *7*, a025478.

(17) van den Berg, R. A.; Coccia, M.; Ballou, W. R.; Kester, K. E.; Ockenhouse, C.; Vekemans, J.; Jongert, E.; Didierlaurent, A.; van der Most, R. G. Predicting RTS,S Vaccine-Mediated Protection from Transcriptomes in a Malaria-Challenge Clinical Trial. *Front. Immunol.* **2017**, *8* (557), 1–13.

(18) Kumar, H.; Tolia, N. H. Getting in: The Structural Biology of Malaria Invasion. *PLoS Pathog.* **2019**, *15* (9), e1007943.

(19) Garcia, J. E.; Puentes, A.; Patarroyo, M. E. Developmental Biology of Sporozoite-Host Interactions in *Plasmodium Falciparum* Malaria: Implications for Vaccine Design. *Clinical Microbiology Reviews*. **2006**, 686–707.

(20) Triglia, T.; Tham, W.-H.; Hodder, A.; Cowman, A. F. Reticulocyte Binding Protein Homologues Are Key Adhesins during Erythrocyte Invasion by *Plasmodium Falciparum*. *Cell Microbiol.* **2009**, *11* (11), 1671–1687.

(21) Crosnier, C.; Bustamante, L. Y.; Bartholdson, S. J.; Bei, A. K.; Theron, M.; Uchikawa, M.; Mboup, S.; Ndir, O.; Kwiatkowski, D. P.; Duraisingh, M. T.; et al. Basigin Is a Receptor Essential for Erythrocyte Invasion by *Plasmodium Falciparum*. *Nature* **2011**, *480*, 534–537.

(22) Gafan, C.; Wilson, J.; Berger, L. C.; Berger, B. J. Characterization of the Ornithine Aminotransferase from *Plasmodium Falciparum*. *Mol. Biochem. Parasitol.* **2001**, *118* (1), 1–10.

(23) Krause, R. G. E.; Goldring, J. P. D. Phosphoethanolamine-N-Methyltransferase Is a Potential Biomarker for the Diagnosis of P. Knowlesi and *P. Falciparum* Malaria. *PLoS One* **2018**, *13* (3), e0193833.

(24) Senczuk, A. M.; Reeder, J. C.; Kosmala, M. M.; Ho, M. *Plasmodium Falciparum* Erythrocyte Membrane Protein 1 Functions as a Ligand for P-Selectin. *Blood* **2001**, *98* (10), 3132–3135.

(25) Robert-Paganin, J.; Robblee, J. P.; Auguin, D.; Blake, T. C. A.; Bookwalter, C. S.; Krementsova, E. B.; Moussaoui, D.; Previs, M. J.; Jousset, G.; Baum, J.; et al. Plasmodium Myosin A Drives Parasite Invasion by an Atypical Force Generating

Mechanism. *Nat. Commun.* **2019**, *10* (1), 3286.

(26) Mayer, D. C. G.; Kaneko, O.; Hudson-Taylor, D. E.; Reid, M. E.; Miller, L. H. Characterization of a *Plasmodium Falciparum* Erythrocyte-Binding Protein Paralogous to EBA-175. *Proc. Natl. Acad. Sci. U. S. A.* **2001**, *98* (9), 5222–5227.

(27) Dvorin, J. D.; Martyn, D. C.; Patel, S. D.; Grimley, J. S.; Collins, C. R.; Hopp, C. S.; Bright, A. T.; Westenberger, S.; Winzeler, E.; Blackman, M. J.; et al. A Plant-like Kinase in *Plasmodium Falciparum* Regulates Parasite Egress from Erythrocytes. *Science* **2010**, *328* (5980), 910–912.

(28) Collins, C. R.; Hackett, F.; Strath, M.; Penzo, M.; Withers-Martinez, C.; Baker, D. A.; Blackman, M. J. Malaria Parasite CGMP-Dependent Protein Kinase Regulates Blood Stage Merozoite Secretory Organelle Discharge and Egress. *PLoS Pathog.* **2013**, *9* (5), e1003344.

(29) Ward, P.; Equinet, L.; Packer, J.; Doerig, C. Protein Kinases of the Human Malaria Parasite *Plasmodium Falciparum*: The Kinome of a Divergent Eukaryote. *BMC Genomics* **2004**, *5*, 79.

(30) Carlton, J. M.; Angiuoli, S. V; Suh, B. B.; Kooij, T. W.; Pertea, M.; Silva, J. C.; Ermolaeva, M. D.; Allen, J. E.; Selengut, J. D.; Koo, H. L.; et al. Genome Sequence and Comparative Analysis of the Model Rodent Malaria Parasite Plasmodium Yoelii Yoelii. *Nature* **2002**, *419* (6906), 512–519.

(31) Tadesse, F. G.; Meerstein-Kessel, L.; Gonçalves, B. P.; Drakeley, C.; Ranford-Cartwright, L.; Bousema, T. Gametocyte Sex Ratio: The Key to Understanding *Plasmodium Falciparum* Transmission? *Trends in Parasitology* **2019**, *35* (3), 226–238.

(32) Suresh, N.; Haldar, K. Mechanisms of Artemisinin Resistance in *Plasmodium Falciparum* Malaria. *Current Opinion in Pharmacology* **2018**, *42*, 46–54.

(33) World Health Organization. *Guidelines for the Treatment of Malaria*, 3rd ed.; **2015**.

(34) Institute of Medicine (US) Committee on the Economics of Antimalarial Drugs. *Saving Lives, Buying Time: Economics of Malaria Drugs in an Age of Resistance*; National Academies Press (US), **2004**.

(35) Klein, E. Y. Antimalarial Drug Resistance: A Review of the Biology and Strategies to Delay Emergence and Spread. *Int. J. Antimicrob. Agents* **2013**, *41* (4), 311–317.

(36) Achan, J.; Mwesigwa, J.; Edwin, C. P.; D'alessandro, U. Malaria Medicines to Address Drug Resistance and Support Malaria Elimination Efforts. *Expert Rev. Clin. Pharmacol.* **2018**, *11* (1), 61–70.

(37) Slater, A. F. G. Chloroquine: Mechanism of Drug Action and Resistance in *Plasmodium Falciparum*. *Pharmacol. Ther.* **1993**, *57* (2–3), 203–235.

(38) Cottrell, G.; Musset, L.; Hubert, V.; Bras, J. Le; Clain, J. Emergence of Resistance to Atovaquone-Proguanil in Malaria Parasites: Insights from Computational Modeling and Clinical Case Reports. *Antimicrob. Agents Chemother.* **2014**, *58* (8), 4504–4514.

(39) Price, R. N.; Uhlemann, A.-C.; Brockman, A.; McGready, R.; Ashley, E.; Phaipun, L.; Patel, R.; Laing, K.; Looareesuwan, S.; White, N. J.; et al. Mefloquine Resistance in *Plasmodium Falciparum* and Increased Pfmdr1 Gene Copy Number. *Lancet (London, England)* **2004**, *364* (9432), 438–447.

(40) Su, X.-Z.; Miller, L. H. The Discovery of Artemisinin and the Nobel Prize in Physiology or Medicine. *Sci. China. Life Sci.* **2015**, *58* (11), 1175–1179.

(41) Miller, L. H.; Su, X. Artemisinin: Discovery from the Chinese Herbal Garden. *Cell* **2011**, *146* (6), 855–858.

(42) Blasco, B.; Leroy, D.; Fidock, D. A. Antimalarial Drug Resistance: Linking *Plasmodium Falciparum* Parasite Biology to the Clinic. *Nat. Med.* **2017**, *23* (8), 917–928.

(43) Cui, L.; Mharakurwa, S.; Ndiaye, D.; Rathod, P. K.; Rosenthal, P. J. Antimalarial Drug Resistance: Literature Review and Activities and Findings of the ICEMR Network. *Am. J. Trop. Med. Hyg.* **2015**, *93* (3), 57–68.

(44) Nosten, F.; White, N. J. Artemisinin-Based Combination Treatment of *Falciparum* Malaria. *Am. J. Trop. Med. Hyg.* **2007**, *77* (6), 181–192.

(45) Edwards, R. L.; Odom John, A. R. Muddled Mechanisms: Recent Progress towards Antimalarial Target Identification. *F1000Research* **2016**, *5*, 2514.

(46) Dziekan, J. M.; Yu, H.; Chen, D.; Dai, L.; Wirjanata, G.; Larsson, A.; Prabhu, N.; Sobota, R. M.; Bozdech, Z.; Nordlund, P. Identifying Purine Nucleoside Phosphorylase as the Target of Quinine Using Cellular Thermal Shift Assay. *Sci. Transl. Med.* **2019**, *11* (473), eaau3174.

(47) Cassera, M. B.; Zhang, Y.; Hazleton, K. Z.; Schramm, V. L. Purine and Pyrimidine Pathways as Targets in *Plasmodium Falciparum*. *Curr. Top. Med. Chem.* **2011**, *11* (16), 2103–2115.

(48) Ting, L.-M.; Shi, W.; Lewandowicz, A.; Singh, V.; Mwakingwe, A.; Birck, M. R.; Ringia, E. A. T.; Bench, G.; Madrid, D. C.; Tyler, P. C.; et al. Targeting a Novel *Plasmodium Falciparum* Purine Recycling Pathway with Specific Immucillins. *J. Biol. Chem.* **2005**, *280* (10), 9547–9554.

(49) Le Bras, J.; Durand, R. The Mechanisms of Resistance to Antimalarial Drugs in *Plasmodium Falciparum*. *Fundam. Clin. Pharmacol.* **2003**, *17* (2), 147–153.

(50) Chinappi, M.; Via, A.; Marcatili, P.; Tramontano, A. On the Mechanism of

Chloroquine Resistance in *Plasmodium Falciparum*. *PLoS One* **2010**, *5* (11), e14064.

(51) Calderón, F.; Wilson, D. M.; Gamo, F.-J. Antimalarial Drug Discovery: Recent Progress and Future Directions. *Prog. Med. Chem.* **2013**, *52*, 97–151.

(52) Schroeder, R. L.; Gerber, J. P. Chloroquine and Hydroxychloroquine Binding to Melanin: Some Possible Consequences for Pathologies. *Toxicol. Reports* **2014**, *1*, 963–968.

(53) Nzila, A. M.; Mberu, E. K.; Sulo, J.; Dayo, H.; Winstanley, P. A.; Sibley, C. H.; Watkins, W. M. Towards an Understanding of the Mechanism of Pyrimethamine-Sulfadoxine Resistance in *Plasmodium Falciparum*: Genotyping of Dihydrofolate Reductase and Dihydropteroate Synthase of Kenyan Parasites. *Antimicrob. Agents Chemother.* **2000**, *44* (4), 991–996.

(54) Vinayak, S.; Alam, M. T.; Mixson-Hayden, T.; McCollum, A. M.; Sem, R.; Shah, N. K.; Lim, P.; Muth, S.; Rogers, W. O.; Fandeur, T.; et al. Origin and Evolution of Sulfadoxine Resistant *Plasmodium Falciparum*. *PLoS Pathog.* **2010**, *6* (3), e1000830.

(55) Srivastava, I. K.; Rottenberg, H.; Vaidya, A. B. Atovaquone, a Broad Spectrum Antiparasitic Drug, Collapses Mitochondrial Membrane Potential in a Malarial Parasite. *J. Biol. Chem.* **1997**, *272* (7), 3961–3966.

(56) Staines, H. M.; Burrow, R.; Teo, B. H.-Y.; Chis Ster, I.; Kremsner, P. G.; Krishna, S. Clinical Implications of Plasmodium Resistance to Atovaquone/Proguanil: A Systematic Review and Meta-Analysis. *J. Antimicrob. Chemother.* **2018**, *73* (3), 581–595.

(57) Srivastava, I. K.; Vaidya, A. B. A Mechanism for the Synergistic Antimalarial Action of Atovaquone and Proguanil. *Antimicrob. Agents Chemother.* **1999**, *43* (6), 1334–1339.

(58) Korsinczky, M.; Chen, N.; Kotecka, B.; Saul, A.; Rieckmann, K.; Cheng, Q. Mutations in *Plasmodium Falciparum* Cytochrome b That Are Associated with Atovaquone Resistance Are Located at a Putative Drug-Binding Site. *Antimicrob. Agents Chemother.* **2000**, *44* (8), 2100–2108.

(59) Wong, W.; Bai, X.-C.; Sleebs, B. E.; Triglia, T.; Brown, A.; Thompson, J. K.; Jackson, K. E.; Hanssen, E.; Marapana, D. S.; Fernandez, I. S.; et al. Mefloquine Targets the *Plasmodium Falciparum* 80S Ribosome to Inhibit Protein Synthesis. *Nat. Microbiol.* **2017**, *2*, 17031.

(60) Basco, L. K.; Gillotin, C.; Gimenez, F.; Farinotti, R.; Le Bras, J. In Vitro Activity of the Enantiomers of Mefloquine, Halofantrine and Enpiroline against *Plasmodium Falciparum*. *Br. J. Clin. Pharmacol.* **1992**, *33* (5), 517–520.

(61) Karle, J. M.; Olmeda, R.; Gerena, L.; Milhous, W. K. *Plasmodium Falciparum*: Role of Absolute Stereochemistry in the Antimalarial Activity of Synthetic Amino Alcohol Antimalarial Agents. *Exp. Parasitol.* **1993**, *76* (4), 345–351.

(62) Reed, M. B.; Saliba, K. J.; Caruana, S. R.; Kirk, K.; Cowman, A. F. Pgh1 Modulates Sensitivity and Resistance to Multiple Antimalarials in *Plasmodium Falciparum*. *Nature* **2000**, *403* (6772), 906–909.

(63) Sanchez, C. P.; Anurag, D.; Stein, W. D.; Lanzer, M. Transporters as Mediators of Drug Resistance in *Plasmodium Falciparum*. *Int. J. Parasitol.* **2012**, *40* (10), 1109–1118.

(64) Klonis, N.; Creek, D. J.; Tilley, L. Iron and Heme Metabolism in *Plasmodium Falciparum* and the Mechanism of Action of Artemisinins. *Current Opinion in Microbiology* **2013**, 722–727.

(65) Tilley, L.; Straimer, J.; Gnädig, N. F.; Ralph, S. A.; Fidock, D. A. Artemisinin Action and Resistance in *Plasmodium Falciparum*. *Trends Parasitol.* **2016**, *32* (9), 682–696.

(66) Morris, C. A.; Duparc, S.; Borghini-Fuhrer, I.; Jung, D.; Shin, C. S.; Fleckenstein, L. Review of the Clinical Pharmacokinetics of Artesunate and Its Active Metabolite Dihydroartemisinin Following Intravenous, Intramuscular, Oral or Rectal Administration. *Malaria Journal* **2011**, *10*, 263.

(67) Hughes, J. P.; Rees, S. S.; Kalindjian, S. B.; Philpott, K. L. Principles of Early Drug Discovery. *British Journal of Pharmacology* **2011**, 1239–1249.

(68) Mohs, R. C.; Greig, N. H. Drug Discovery and Development: Role of Basic Biological Research. *Alzheimer's and Dementia: Translational Research and Clinical Interventions* **2017**, 651–657.

(69) GSK. *The GlaxoSmithKline Pocket Guide to Drug Metabolism and Pharmacokinetics (DMPK)*; **2018**.

(70) Schenone, M.; Dančík, V.; Wagner, B. K.; Clemons, P. A. Target Identification and Mechanism of Action in Chemical Biology and Drug Discovery. *Nat. Chem. Biol.* **2013**, *9* (4), 232–240.

(71) Moffat, J. G.; Vincent, F.; Lee, J. A.; Eder, J.; Prunotto, M. Opportunities and Challenges in Phenotypic Drug Discovery: An Industry Perspective. *Nat. Rev. Drug Discov.* **2017**, *16* (8), 531–543.

(72) Hovlid, M. L.; Winzeler, E. A. Phenotypic Screens in Antimalarial Drug Discovery. *Trends Parasitol.* **2016**, *32* (9), 697–707.

(73) Swinney, D. C. Phenotypic vs. Target-Based Drug Discovery for First-in-Class Medicines. *Clin. Pharmacol. Ther.* **2013**, *93* (4), 299–301.

(74) Ziegler, S.; Pries, V.; Hedberg, C.; Waldmann, H. Target Identification for Small Bioactive Molecules: Finding the Needle in the Haystack. *Angew. Chemie Int. Ed.* **2013**, *52* (10), 2744–2792.

(75) Gardner, M. J.; Hall, N.; Fung, E.; White, O.; Berriman, M.; Hyman, R. W.; Carlton, J. M.; Pain, A.; Nelson, K. E.; Bowman, S.; et al. Genome Sequence of the Human Malaria Parasite *Plasmodium Falciparum*. *Nature* **2002**, *419* (6906), 498–511.

(76) Lin, J. T.; Juliano, J. J.; Wongsrichanalai, C. Drug-Resistant Malaria: The Era of ACT. *Curr. Infect. Dis. Rep.* **2010**, *12* (3), 165–173.

(77) Olliaro, P. Mode of Action and Mechanisms of Resistance for Antimalarial Drugs. *Pharmacol. Ther.* **2001**, *89* (2), 207–219.

(78) Zheng, X. S.; Chan, T.-F.; Zhou, H. H. Genetic and Genomic Approaches to Identify and Study the Targets of Bioactive Small Molecules. *Chem. Biol.* **2004**, *11* (5), 609–618.

(79) Katsila, T.; Spyroulias, G. A.; Patrinos, G. P.; Matsoukas, M.-T. Computational Approaches in Target Identification and Drug Discovery. *Comput. Struct. Biotechnol. J.* **2016**, *14*, 177–184.

(80) Cuatrecasas, P.; Wilchek, M.; Anfinsen, C. B. Selective Enzyme Purification by Affinity Chromatography. *Proc. Natl. Acad. Sci. U. S. A.* **1968**, *61* (2), 636–643.

(81) Ong, S.-E.; Schenone, M.; Margolin, A. A.; Li, X.; Do, K.; Doud, M. K.; Mani, D. R.; Kuai, L.; Wang, X.; Wood, J. L.; et al. Identifying the Proteins to Which Small-Molecule Probes and Drugs Bind in Cells. *Proc. Natl. Acad. Sci. U. S. A.* **2009**, *106* (12), 4617–4622.

(82) Drewes, G.; Knapp, S. Chemoproteomics and Chemical Probes for Target Discovery. *Trends Biotechnol.* **2018**, *36* (12), 1275–1286.

(83) Zhang, Y.; Fonslow, B. R.; Shan, B.; Baek, M. C.; Yates, J. R. Protein Analysis by Shotgun/Bottom-up Proteomics. *Chemical Reviews*. **2013**, 2343–2394.

(84) Swearingen, K. E.; Lindner, S. E. Plasmodium Parasites Viewed through Proteomics. *Trends Parasitol.* **2018**, *34* (11), 945–960.

(85) Yates, J. R. *Mass Spectrometry and the Age of the Proteome*; John Wiley & Sons, Ltd, **1998**; Vol. 33.

(86) Steen, H.; Mann, M. The ABC's (and XYZ's) of Peptide Sequencing. *Nature Reviews Molecular Cell Biology* **2004**, *5* (9), 699–711.

(87) Fenn, J. B.; Mann, M.; Meng, C. K.; Wong, S. F.; Whitehouse, C. M. Electrospray Ionization for Mass Spectrometry of Large Biomolecules. *Science*. **1989**, *246* (4926), 64–71.

(88) Angel, T. E.; Aryal, U. K.; Hengel, S. M.; Baker, E. S.; Kelly, R. T.; Robinson, E. W.; Smith, R. D. Mass Spectrometry-Based Proteomics: Existing Capabilities and Future Directions. *Chemical Society Reviews* **2012**, *41* (10), 3912–3928.

(89) Xie, F.; Liu, T.; Qian, W. J.; Petyuk, V. A.; Smith, R. D. Liquid Chromatography-Mass Spectrometry-Based Quantitative Proteomics. *Journal of Biological Chemistry*. **2011**, *286* (29), 25443–25449.

(90) Zhang, L.; Elias, J. E. Relative Protein Quantification Using Tandem Mass Tag Mass Spectrometry. *Methods in Molecular Biology*; Humana Press Inc. **2017**, *1550*, 185–198.

(91) Thompson, A.; Schäfer, J.; Kuhn, K.; Kienle, S.; Schwarz, J.; Schmidt, G.; Neumann, T.; Hamon, C. Tandem Mass Tags: A Novel Quantification Strategy for Comparative Analysis of Complex Protein Mixtures by MS/MS. *Anal. Chem.* **2003**, *75* (8), 1895–1904.

(92) Arrowsmith, C. H.; Audia, J. E.; Austin, C.; Baell, J.; Bennett, J.; Blagg, J.; Bountra, C.; Brennan, P. E.; Brown, P. J.; Bunnage, M. E.; et al. The Promise and Peril of Chemical Probes. *Nat. Chem. Biol.* **2015**, *11* (8), 536–541.

(93) Moustakim, M.; Felce, S. L.; Zaarour, N.; Farnie, G.; McCann, F. E.; Brennan, P. E. Target Identification Using Chemical Probes. *Methods Enzymol.* **2018**, *610*, 27–58.

(94) Jeffery, D. A.; Bogyo, M. Chemical Proteomics and Its Application to Drug Discovery. *Curr. Opin. Biotechnol.* **2003**, *14* (1), 87–95.

(95) Bantscheff, M.; Drewes, G. Chemoproteomic Approaches to Drug Target Identification and Drug Profiling. *Bioorg. Med. Chem.* **2012**, *20* (6), 1973–1978.

(96) Paquet, T.; Le Manach, C.; Cabrera, D. G.; Younis, Y.; Henrich, P. P.; Abraham, T. S.; Lee, M. C. S.; Basak, R.; Ghidelli-Disse, S.; Lafuente-Monasterio, M. J.; et al. Antimalarial Efficacy of MMV390048, an Inhibitor of Plasmodiumphosphatidylinositol-4-Kinase. *Sci. Transl. Med.* **2017**, *9* (387), eaad9735.

(97) Médard, G.; Pachl, F.; Ruprecht, B.; Klaeger, S.; Heinzlmeir, S.; Helm, D.; Qiao, H.; Ku, X.; Wilhelm, M.; Kuehne, T.; et al. Optimized Chemical Proteomics Assay for Kinase Inhibitor Profiling. *J. Proteome Res.* **2015**, *14* (3), 1574–1586.

(98) Bantscheff, M.; Eberhard, D.; Abraham, Y.; Bastuck, S.; Boesche, M.; Hobson, S.; Mathieson, T.; Perrin, J.; Raida, M.; Rau, C.; et al. Quantitative Chemical Proteomics Reveals Mechanisms of Action of Clinical ABL Kinase Inhibitors. *Nat. Biotechnol.* **2007**, *25* (9), 1035–1044.

(99) Smith, E.; Collins, I. Photoaffinity Labeling in Target- and Binding-Site Identification. *Future Med. Chem.* **2015**, *7* (2), 159–183.

(100) Diamandis, E. P.; Christopoulos, T. K. The Biotin-(Strept)Avidin System: Principles and Applications in Biotechnology. *Clin. Chem.* **1991**, *37* (5), 625–636.

(101) Jain, A.; Cheng, K. The Principles and Applications of Avidin-Based Nanoparticles in Drug Delivery and Diagnosis. *Journal of Controlled Release* **2017**, *245*, 27–40.

(102) Chivers, C. E.; Koner, A. L.; Lowe, E. D.; Howarth, M. How the Biotin-Streptavidin Interaction Was Made Even Stronger: Investigation via Crystallography and a Chimaeric Tetramer. *Biochem. J.* **2011**, *435* (1), 55–63.

(103) Ge, S.-S.; Chen, B.; Wu, Y.-Y.; Long, Q.-S.; Zhao, Y.-L.; Wang, P.-Y.; Yang, S. Current Advances of Carbene-Mediated Photoaffinity Labeling in Medicinal Chemistry. *RSC Adv.* **2018**, *8* (51), 29428–29454.

(104) Murale, D. P.; Hong, S. C.; Haque, M. M.; Lee, J. S. Photo-Affinity Labeling (PAL) in Chemical Proteomics: A Handy Tool to Investigate Protein-Protein Interactions (PPIs). *Proteome Science* **2017**, *15*, 14.

(105) Hermanson, G. T. Photo-Chemical Reactions. *Bioconjugate Techniques* **2008,** 204–208.

(106) Dormán, G.; Nakamura, H.; Pulsipher, A.; Prestwich, G. D. The Life of Pi Star: Exploring the Exciting and Forbidden Worlds of the Benzophenone Photophore. *Chem. Rev.* **2016**, *116* (24), 15284–15398.

(107) Guo, H.; Li, Z. Developments of Bioorthogonal Handle-Containing Photo-Crosslinkers for Photoaffinity Labeling. *Medchemcomm* **2017**, *8* (8), 1585–1591.

(108) Kempf, K.; Raja, A.; Sasse, F.; Schobert, R. Synthesis of Penicillenol C1 and of a Bis-Azide Analogue for Photoaffinity Labeling. *J. Org. Chem.* **2013**, *78* (6), 2455–2461.

(109) Inui, H.; Sawada, K.; Oishi, S.; Ushida, K.; McMahon, R. J. Aryl Nitrene Rearrangements: Spectroscopic Observation of a Benzazirine and Its Ring Expansion to a Ketenimine by Heavy-Atom Tunneling. *J. Am. Chem. Soc.* **2013**, *135* (28), 10246–10249.

(110) Preston, G. W.; Wilson, A. J. Photo-Induced Covalent Cross-Linking for the Analysis of Biomolecular Interactions. *Chem. Soc. Rev.* **2013**, *42* (8), 3289.

(111) Das, J. Aliphatic Diazirines as Photoaffinity Probes for Proteins: Recent Developments. *Chem. Rev.* **2011**, *111* (8), 4405–4417.

(112) Brunner, J.; Senn, H.; Richards, F. M. 3-Trifluoromethyl-3-Phenyldiazirine. A New Carbene Generating Group for Photolabeling Reagents. *J. Biol. Chem.* **1980**, *255* (8), 3313–3318.

(113) Brunner, J. New Photolabelling and Crosslinking Methods. *Annu. Rev. Biochem.* **1993**, *62*, 483–514.

(114) Hill, J. R.; Robertson, A. A. B. Fishing for Drug Targets: A Focus on Diazirine Photoaffinity Probe Synthesis. *J. Med. Chem.* **2018**, *61* (16), 6945–6963.

(115) McKay, C. S.; Finn, M. G. Click Chemistry in Complex Mixtures: Bioorthogonal Bioconjugation. *Chem. Biol.* **2014**, *21* (9), 1075–1101.

(116) Knall, A.-C.; Slugovc, C. Inverse Electron Demand Diels–Alder (IEDDA)-Initiated Conjugation: A (High) Potential Click Chemistry Scheme. *Chem. Soc. Rev.* **2013**, *42* (12), 5131–5142.

(117) Davies, S.; Qiao, L.; Oliveira, B.; Navo, C.; Jiménez-Osés, G.; Bernardes, G. J. L. Tetrazine-triggered Release of Carboxylic-acid Containing Molecules for Activation of an Anti-inflammatory Drug. *ChemBioChem* **2019**, *20* (12), 1541–1546.

(118) Blackman, M. L.; Royzen, M.; Fox, J. M. Tetrazine Ligation: Fast Bioconjugation Based on Inverse-Electron-Demand Diels-Alder Reactivity. *J. Am. Chem. Soc.* **2008**, *130* (41), 13518–13519.

(119) Thalhammer, F.; Wallfahrer, U.; Sauer, J. Reaktivität Einfacher Offenkettiger Und Cyclischer Dienophile Bei Diels-Alder-Reaktionen Mit Inversem Elektronenbedarf. *Tetrahedron Lett.* **1990**, *31* (47), 6851–6854.

(120) Devaraj, N. K.; Weissleder, R. Biomedical Applications of Tetrazine Cycloadditions. *Acc. Chem. Res* **2011**, *44* (9), 816–827.

(121) Selvaraj, R.; Fox, J. M. *trans*-Cyclooctene - a Stable, Voracious Dienophile for Bioorthogonal Labeling. *Curr. Opin. Chem. Biol.* **2013**, *17* (5), 753–760.

(122) Colca, J. R.; McDonald, W. G.; Waldon, D. J.; Leone, J. W.; Lull, J. M.; Bannow, C. A.; Lund, E. T.; Mathews, W. R. Identification of a Novel Mitochondrial Protein ("MitoNEET") Cross-Linked Specifically by a Thiazolidinedione Photoprobe. *Am. J. Physiol. Metab.* **2004**, *286* (2), 252–260.

(123) Lee, K.; Ban, H. S.; Naik, R.; Hong, Y. S.; Son, S.; Kim, B.-K.; Xia, Y.; Song, K. Bin; Lee, H.-S.; Won, M. Identification of Malate Dehydrogenase 2 as a Target Protein of the HIF-1 Inhibitor LW6 Using Chemical Probes. *Angew. Chemie Int. Ed.* **2013**, *52* (39), 10286–10289.

(124) Kotake, Y.; Sagane, K.; Owa, T.; Mimori-Kiyosue, Y.; Shimizu, H.; Uesugi, M.; Ishihama, Y.; Iwata, M.; Mizui, Y. Splicing Factor SF3b as a Target of the Antitumor Natural Product Pladienolide. *Nat. Chem. Biol.* **2007**, *3* (9), 570–575.

(125) Brunner, R.; Ng, C. L.; Aissaoui, H.; Akabas, M. H.; Boss, C.; Brun, R.; Callaghan, P. S.; Corminboeuf, O.; Fidock, D. A.; Frame, I. J.; et al. UV-Triggered Affinity Capture Identifies Interactions between the *Plasmodium Falciparum* Multidrug Resistance Protein 1 (PfMDR1) and Antimalarial Agents in Live Parasitized Cells. *J. Biol. Chem.*

2013, *288* (31), 22576–22583.

(126) Berman, A.; Shearing, L. N.; Ng, K. F.; Jinsart, W.; Foley, M.; Tilley, L. Photoaffinity Labelling of *Plasmodium Falciparum* Proteins Involved in Phospholipid Transport. *Mol. Biochem. Parasitol.* **1994**, *67* (2), 235–243.

(127) Penarete-Vargas, D. M.; Boisson, A.; Urbach, S.; Chantelauze, H.; Peyrottes, S.; Fraisse, L.; Vial, H. J. A Chemical Proteomics Approach for the Search of Pharmacological Targets of the Antimalarial Clinical Candidate Albitiazolium in *Plasmodium Falciparum* Using Photocrosslinking and Click Chemistry. *PLoS One* **2014**, *9* (12), e113918.

(128) Lubin, A. S.; Rueda-Zubiaurre, A.; Matthews, H.; Baumann, H.; Fisher, F. R.; Morales-Sanfrutos, J.; Hadavizadeh, K. S.; Nardella, F.; Tate, E. W.; Baum, J.; et al. Development of a Photo-Cross-Linkable Diaminoquinazoline Inhibitor for Target Identification in *Plasmodium Falciparum*. *ACS Infect. Dis.* **2018**, *4* (4), 523–530.

(129) Desneves, J.; Thorn, G.; Berman, A.; Galatis, D.; La Greca, N.; Sinding, J.; Foley, M.; Deady, L. W.; Cowman, A. F.; Tilley, L. Photoaffinity Labeling of Mefloquine-Binding Proteins in Human Serum, Uninfected Erythrocytes and *Plasmodium Falciparum*-Infected Erythrocytes. *Mol. Biochem. Parasitol.* **1996**, *82* (2), 181–194.

(130) Gowda, A. S. P.; Madhunapantula, S. V.; Achur, R. N.; Valiyaveettil, M.; Bhavanandan, V. P.; Gowda, D. C. Structural Basis for the Adherence of Plasmodium Falciparum-Infected Erythrocytes to Chondroitin 4-Sulfate and Design of Novel Photoactivable Reagents for the Identification of Parasite Adhesive Proteins. *J. Biol. Chem.* **2006**, *282*, 916–928.

(131) Foley, M.; Deady, L. W.; Ng, K.; Cowman, A. F.; Tilley, L. Photoaffinity Labeling of Chloroquine-Binding Proteins in *Plasmodium Falciparum*. *J. Biol. Chem.* **1994**, *269* (9), 6955–6961.

(132) McNamara, C.; Winzeler, E. A. Target Identification and Validation of Novel Antimalarials. *Future Microbiol.* **2011**, *6* (6), 693–704.

(133) Gamo, F.-J.; Sanz, L. M.; Vidal, J.; de Cozar, C.; Alvarez, E.; Lavandera, J.-L.; Vanderwall, D. E.; Green, D. V. S.; Kumar, V.; Hasan, S.; et al. Thousands of Chemical Starting Points for Antimalarial Lead Identification. *Nature* **2010**, *465* (7296), 305–310.

(134) Young, R. J. Physical Properties in Drug Design. In *Tactics in Contemporary Drug Design: Topics in Medicinal Chemistry Vol 9*; Springer Berlin Heidelberg, **2014**; 1–68.

(135) Priest, B. T.; Bell, I. M.; Garcia, M. L. Role of HERG Potassium Channel Assays in Drug Development. *Channels (Austin)* **2008**, *2* (2), 87–93.

(136) Danker, T.; Möller, C. Early Identification of HERG Liability in Drug Discovery Programs by Automated Patch Clamp. *Front. Pharmacol.* **2014**, *5*, 203.

(137) Leeson, P. D.; Springthorpe, B. The Influence of Drug-like Concepts on Decision-Making in Medicinal Chemistry. *Nat. Rev. Drug Discov.* **2007**, *6* (11), 881–890.

(138) Leeson, P. D.; Young, R. J. Molecular Property Design: Does Everyone Get It? *ACS Med. Chem. Lett.* **2015**, *6* (7), 722–725.

(139) Roberts, J.; Baker, B.; Ignacio Martin Hernando, J.; del Rio, R.; Cabanillas, A.; Chaparro-Martin, M.; Hirst, D.; Patel, V.; Poole, D.; Tape, D.; et al. Unpublished Work. **2019**.

(140) Spillman, N. J.; Kirk, K. The Malaria Parasite Cation ATPase PfATP4 and Its Role in the Mechanism of Action of a New Arsenal of Antimalarial Drugs. *Int. J. Parasitol. Drugs Drug Resist.* **2015**, *5* (3), 149–162.

(141) Singh, A.; Maqbool, M.; Mobashir, M.; Hoda, N. Dihydroorotate Dehydrogenase: A Drug Target for the Development of Antimalarials. *Eur. J. Med. Chem.* **2017**, *125*, 640–651.

(142) Roncales-Poza, M.; Mata, L.; Neria Serrano, F. GSK Unpublished Work. **2016**.

(143) Roncales-Poza, M.; Neria Serrano, F. GSK Unpublished Work. **2016**.

(144) Gomez-Lorenzo, M. D. G.; Lafuente-Monasterio, M. J.; Prats, S. GSK Unpublished Work. **2017**.

(145) Neria Serrano, F. GSK Unpublished Work. **2016**.

(146) Tripathi, A. K.; Khan, S. I.; Walker, L. A.; Tekwani, B. L. Spectrophotometric Determination of de Novo Hemozoin/β-Hematin Formation in an in Vitro Assay. *Anal. Biochem.* **2004**, *325* (1), 85–91.

(147) Cozar-Gallardo, C. De; Crespo-Fernandez, B.; Llergo-Largo, J. L. GSK Unpublished Work. **2015**.

(148) Sundriyal, S.; Chen, P. B.; Lubin, A. S.; Lueg, G. A.; Li, F.; White, A. J. P.; Malmquist, N. A.; Vedadi, M.; Scherf, A.; Fuchter, M. J. Histone Lysine Methyltransferase Structure Activity Relationships That Allow for Segregation of G9a Inhibition and Anti-*Plasmodium* Activity. *Medchemcomm* **2017**, *8* (5), 1069–1092.

(149) Sundriyal, S.; Malmquist, N. A.; Caron, J.; Blundell, S.; Liu, F.; Chen, X.; Srimongkolpithak, N.; Jin, J.; Charman, S. A.; Scherf, A.; et al. Development of Diaminoquinazoline Histone Lysine Methyltransferase Inhibitors as Potent Blood-Stage Antimalarial Compounds. *ChemMedChem* **2014**, *9* (10), 2360–2373.

(150) Malmquist, N. A.; Moss, T. A.; Mecheri, S.; Scherf, A.; Fuchter, M. J. Small-Molecule Histone Methyltransferase Inhibitors Display Rapid Antimalarial Activity against All

Blood Stage Forms in *Plasmodium Falciparum*. *Proc. Natl. Acad. Sci. U. S. A.* **2012**, *109* (41), 16708–16713.

(151) Traquete, R.; Henderson, E.; Picaud, S.; Cal, P. M. S. D.; Sieglitz, F.; Rodrigues, T.; Oliveira, R.; Filippakopoulos, P.; Bernardes, G. J. L. Evaluation of Linker Length Effects on a BET Bromodomain Probe. *Chem. Commun.* **2019**, *55* (68), 10128–10131.

(152) Wright, M. H.; Sieber, S. A. Chemical Proteomics Approaches for Identifying the Cellular Targets of Natural Products. *Natural Product Reports* **2016**, *33* (5), 681–708.

(153) Lee, J. H.; Lee, H. B.; Andrade, J. D. Blood Compatibility of Polyethylene Oxide Surfaces. *Prog. Polym. Sci.* **1995**, *20* (6), 1043–1079.

(154) Wan, Z.-K.; Wacharasindhu, S.; Levins, C. G.; Lin, M.; Tabei, K.; Mansour, T. S. The Scope and Mechanism of Phosphonium-Mediated S_NAr Reactions in Heterocyclic Amides and Ureas. **2007**, *72* (26), 10194–10210.

(155) Perry, B.; Beevers, R.; Bennett, G.; Buckley, G.; Crabbe, T.; Gowers, L.; James, L.; Jenkins, K.; Lock, C.; Sabin, V.; et al. Optimization of a Series of Multi-Isoform PI3 Kinase Inhibitors. *Bioorg. Med. Chem. Lett.* **2008**, *18* (19), 5299–5302.

(156) Andrea Dawn Basso. WO 2009/017701 A2, **2009**.

(157) Bondy, S. S.; Cannizzaro, C. E.; Chou, C.-H.; Halcomb, R. L.; HU, Y. E.; Link, J. O.; Liu, Q.; Schroeder, S. D.; Tse, W. C.; Zhang, J. R. WO 2013/006738 A1, **2013**.

(158) Abdel-Hafez, A. A.-M. Synthesis and Anticonvulsant Evaluation of N-Substituted-Isoindolinedione Derivatives. *Arch. Pharm. Res.* **2004**, *27* (5), 495–501.

(159) Yokoyama, M.; Okano, T.; Sakurai, Y.; Kikuchi, A.; Ohsako, N.; Nagasaki, Y.; Kataoka, K. Synthesis of Poly(Ethylene Oxide) with Heterobifunctional Reactive Groups at Its Terminals by an Anionic Initiator. *Bioconjug. Chem.* **1992**, *3* (4), 275–276.

(160) Chaparro-Martin, M.; Ignacio Martin Hernando, J. GSK Unpublished Work. **2019**.

(161) Böttcher, T.; Sieber, S. A. Showdomycin as a Versatile Chemical Tool for the Detection of Pathogenesis-Associated Enzymes in Bacteria. *J. Am. Chem. Soc.* **2010**, *132* (20), 6964–6972.

(162) Zeiler, E.; Braun, N.; Böttcher, T.; Kastenmüller, A.; Weinkauf, S.; Sieber, S. A. Vibralactone as a Tool to Study the Activity and Structure of the ClpP1P2 Complex from Listeria Monocytogenes. *Angew. Chemie - Int. Ed.* **2011**, *50* (46), 11001–11004.

(163) Staub, I.; Sieber, S. A. β-Lactams as Selective Chemical Probes for the in Vivo Labeling of Bacterial Enzymes Involved in Cell Wall Biosynthesis, Antibiotic Resistance, and Virulence. *J. Am. Chem. Soc.* **2008**, *130* (40), 13400–13409.

(164) Minisci, F.; Bernardi, R.; Bertini, F.; Galli, R.; Perchinummo, M. Nucleophilic

Character of Alkyl Radicals—VI : A New Convenient Selective Alkylation of Heteroaromatic Bases. *Tetrahedron* **1971**, *27* (15), 3575–3579.

(165) Sherwood, T. C.; Li, N.; Yazdani, A. N.; Dhar, T. G. M. Organocatalyzed, Visible-Light Photoredox-Mediated, One-Pot Minisci Reaction Using Carboxylic Acids via *N*-(Acyloxy)Phthalimides. *J. Org. Chem.* **2018**, *83* (5), 3000–3012.

(166) Li, A.-H.; Moro, S.; Forsyth, N.; Melman, N.; Ji, X.; Jacobson, K. A. Synthesis, CoMFA Analysis, and Receptor Docking of 3,5-Diacyl-2,4-Dialkylpyridine Derivatives as Selective A_3 Adenosine Receptor Antagonists. *J. Med. Chem.* **1999**, *42* (4), 706–721.

(167) Lehmann, S.; Eberl, C. H.; Ghidelli-Disse, S.; Klos-Hudak, M. GSK Unpublished Work. **2018**.

(168) de Cózar, C.; Caballero, I.; Colmenarejo, G.; Sanz, L. M.; Álvarez-Ruiz, E.; Gamo, F.-J.; Cid, C. Development of a Novel High-Density [^{3}H]-Hypoxanthine Scintillation Proximity Assay To Assess *Plasmodium Falciparum* Growth. *Antimicrob. Agents Chemother.* **2016**, *60* (10), 5949–5956.

(169) Freeman-Cook, K. D.; Hoffman, R. L.; Johnson, T. W. Lipophilic Efficiency: The Most Important Efficiency Metric in Medicinal Chemistry. *Future Medicinal Chemistry*. **2013**, *5* (2), 113–115.

(170) Presolski, S. I.; Hong, V. P.; Finn, M. G. Copper-Catalyzed Azide-Alkyne Click Chemistry for Bioconjugation. *Current Protocols in Chemical Biology* **2011**.

(171) Berg, R.; Straub, B. F. Advancements in the Mechanistic Understanding of the Copper-Catalyzed Azide-Alkyne Cycloaddition. *Beilstein Journal of Organic Chemistry*, **2013**, 2715–2750.

(172) Anand, A.; Kulkarni, M. V. Click Chemistry Approach for the Regioselective Synthesis of Iso-Indoline-1,3-Dione-Linked 1,4 and 1,5 Coumarinyl 1,2,3-Triazoles and Their Photophysical Properties. *Synth. Commun.* **2017**, *47* (7), 722–733.

(173) Kaul, G.; Amiji, M. Long-Circulating Poly(Ethylene Glycol)-Modified Gelatin Nanoparticles for Intracellular Delivery. *Pharm. Res.* **2002**, *19* (7), 1061–1067.

(174) Knop, K.; Hoogenboom, R.; Fischer, D.; Schubert, U. S. Poly(Ethylene Glycol) in Drug Delivery: Pros and Cons as Well as Potential Alternatives. *Angew. Chemie Int. Ed.* **2010**, *49* (36), 6288–6308.

(175) Caliceti, P.; Veronese, F. M. Pharmacokinetic and Biodistribution Properties of Poly(Ethylene Glycol)–protein Conjugates. *Adv. Drug Deliv. Rev.* **2003**, *55* (10), 1261–1277.

(176) McNamee, C. E.; Yamamoto, S.; Higashitani, K. Effect of the Physicochemical

Properties of Poly(Ethylene Glycol) Brushes on Their Binding to Cells. *Biophys. J.* **2007**, *93* (1), 324–334.

(177) Duffy, S.; Avery, V. M. *Plasmodium Falciparum in vitro* Continuous Culture Conditions: A Comparison of Parasite Susceptibility and Tolerance to Anti-Malarial Drugs throughout the Asexual Intra-Erythrocytic Life Cycle. *Int. J. Parasitol. Drugs drug Resist.* **2017**, *7* (3), 295–302.

(178) Eberl, C. H.; Vappiani, J.; Wagner, A. J.; Lehmann, S.; Muelbaier, M.; Bantscheff, M. Unpublished Work. **2018**.

(179) Suchanek, M.; Radzikowska, A.; Thiele, C. Photo-Leucine and Photo-Methionine Allow Identification of Protein-Protein Interactions in Living Cells. *Nat. Methods* **2005**, *2* (4), 261–267.

(180) Tanaka, Y.; Bond, M. R.; Kohler, J. J. Photocrosslinkers Illuminate Interactions in Living Cells. *Molecular BioSystems*. **2008**, *4* (6), 473–480.

(181) Scriven, E. F. V.; Turnbull, K. Azides: Their Preparation and Synthetic Uses. *Chem. Rev.* **1988**, *88* (2), 297–368.

(182) Larock, R. C. *Comprehensive Organic Transformations: A Guide to Functional Group Preparations*; John Wiley & Sons, Inc., **1999**.

(183) Brown, H. C.; Kim, K.-W.; Srebnik, M.; Bakthan, S. Organoboranes for Synthesis. 7. An Improved General Synthesis of Primary Amines from Alkenes via Hydroboration-Organoborane Chemistry. *Tetrahedron* **1987**, *43* (18), 4071–4078.

(184) Staudinger, H.; Meyer, J. Über Neue Organische Phosphorverbindungen III. Phosphinmethylenderivate Und Phosphinimine. *Helv. Chim. Acta* **1919**, *2* (1), 635–646.

(185) Bräse, S.; Gil, C.; Knepper, K.; Zimmermann, V. Organic Azides: An Exploding Diversity of a Unique Class of Compounds. *Angew. Chemie Int. Ed.* **2005**, *44* (33), 5188–5240.

(186) Intrieri, D.; Zardi, P.; Caselli, A.; Gallo, E. Organic Azides: " *Energetic Reagents* " for the *Inter* Molecular Amination of C–H Bonds. *Chem. Commun.* **2014**, *50* (78), 11440–11453.

(187) Brase, S.; Banert, K. *Organic Azides: Syntheses and Applications*; John Wiley & Sons, Hoboken, **2009**.

(188) H. B. Goodbrand; Hu, N.-X. Ligand-Accelerated Catalysis of the Ullmann Condensation: Application to Hole Conducting Triarylamines. **1999**, *64* (2), 670–674.

(189) Brown, H. C.; Zweifel, G. A Stereospecific *cis* Hydration of the Double Bond in Cyclic Derivatives. *J. Am. Chem. Soc.* **1959**, *81* (1), 247–247.

(190) Wallace, R. G. Hydroxylamine-*O*-Sulfonic Acid - a Versatile Synthetic Reagent. *Aldrichimica Acta* **1980**, *13* (1), 3–11.

(191) Mohapatra, D.; Datta, A. Di-*Tert*-Butyl Pyrocarbonate Mediated Cyclodehydration of *N*-Acyl Amino Acids into Functionalized Oxazoles and Acylanthranils. *Syn. Lett.* **2000**, *1996* (11), 1129–1130.

(192) Pozdnev, V. F. Activation of Carboxylic Acids by Pyrocarbonates. Application of Di-*Tert*-Butyl Pyrocarbonate as Condensing Reagent in the Synthesis of Amides of Protected Amino Acids and Peptides. *Tetrahedron Lett.* **1995**, *36* (39), 7115–7118.

(193) Levay, K.; Hegedus, L. Selective Heterogenous Catalytic Hydrogenation of Nitriles to Primary Amines. *Period. Polytech. Chem. Eng.* **2018**, *62* (4), 476–488.

(194) Bagal, D. B.; Bhanage, B. M. Recent Advances in Transition Metal-Catalyzed Hydrogenation of Nitriles. *Adv. Synth. Catal.* **2015**, *357* (5), 883–900.

(195) Gomez, S.; Peters, J. A.; Maschmeyer, T. The Reductive Amination of Aldehydes and Ketones and the Hydrogenation of Nitriles: Mechanistic Aspects and Selectivity Control. *Adv. Synth. Catal.* **2002**, *344* (10), 1037–1057.

(196) Sanz, L. M.; Crespo, B.; De-Cózar, C.; Ding, X. C.; Llergo, J. L.; Burrows, J. N.; García-Bustos, J. F.; Gamo, F.-J. *P. Falciparum* In Vitro Killing Rates Allow to Discriminate between Different Antimalarial Mode-of-Action. *PLoS One* **2012**, *7* (2), e30949.

(197) Crespo, B.; Hermoso, A. GSK Unpublished Work. **2019**.

(198) LLC, C. C. T. AFDye 488 Tetrazine Product No. 1361. **2019**.

(199) Marti, M.; Spielmann, T. Protein Export in Malaria Parasites: Many Membranes to Cross. *Current Opinion in Microbiology*. **2013**, *16* (4), 445–451.

(200) Bradford, M. M. A Rapid and Sensitive Method for the Quantitation of Microgram Quantities of Protein Utilizing the Principle of Protein-Dye Binding. *Anal. Biochem.* **1976**, *72* (1–2), 248–254.

(201) Ranford-Cartwright, L. C.; Sinha, A.; Humphreys, G. S.; Mwangi, J. M. New Synchronization Method for *Plasmodium Falciparum*. *Malar. J.* **2010**, *9*, 170.

(202) Schuster, F. L. Cultivation of Plasmodium Spp. *Clin. Microbiol. Rev.* **2002**, *15* (3), 355–364.

(203) Lambros, C.; Vanderberg, J. P. Synchronization of Plasmodium Falciparum Erythrocytic Stages in Culture. *J. Parasitol.* **1979**, *65* (3), 418.

(204) Trigg, P. I. Recent Advances in Malaria Parasite Cultivation and Their Application to Studies on Host-Parasite Relationships: A Review. *Bull. World Heal. Organ.* **1985**, *63* (2), 387–398.

(205) Thermo Scientific. NeutrAvidin Agarose Resins #29204 https://assets.thermofisher.com/TFS-Assets/LSG/manuals/MAN0011319_NeutrAvidin_Agarose_Resins_UG.pdf (accessed Nov 14, 2019).

(206) Jena Bioscience. Tetrazine-PEG4-Biotin #CLK-027-25 https://www.jenabioscience.com/images/PDF/CLK-027.pdf (accessed Nov 14, 2019).

(207) PlasmoDB Plasmodium Genomics Resource. PF3D7_1408600 40S ribosomal protein S8e, putative https://plasmodb.org/plasmo/app/record/gene/PF3D7_1408600 (accessed Nov 14, 2019).

(208) PlasmoDB Plasmodium Genomics Resource. PF3D7_0914700 major facilitator superfamily-related transporter, putative https://plasmodb.org/plasmo/app/record/gene/PF3D7_0914700 (accessed Nov 14, 2019).

(209) PlasmoDB Plasmodium Genomics Resource. PF3D7_1347200 nucleoside transporter 1 https://plasmodb.org/plasmo/app/record/gene/PF3D7_1347200 (accessed Nov 14, 2019).

(210) Kenthirapalan, S.; Waters, A. P.; Matuschewski, K.; Taco, &; Kooij, W. A. Functional Profiles of Orphan Membrane Transporters in the Life Cycle of the Malaria Parasite. *Nat. Commun.* **2016**, *7* (10519).

(211) Rajendran, E.; Hapuarachchi, S. V; Miller, C. M.; Fairweather, S. J.; Cai, Y.; Smith, N. C.; Cockburn, I. A.; Bröer, S.; Kirk, K.; van Dooren, G. G. Cationic Amino Acid Transporters Play Key Roles in the Survival and Transmission of Apicomplexan Parasites. *Nat. Commun.* **2017**, *8*, 14455.

(212) Parker, K. E. R.; Fairweather, S. J.; Rajendran, E.; Blume, M.; McConville, M. J.; Bröer, S.; Kirk, K.; van Dooren, G. G. The Tyrosine Transporter of Toxoplasma Gondii Is a Member of the Newly Defined Apicomplexan Amino Acid Transporter (ApiAT) Family. *PLoS Pathog.* **2019**, *15* (2), e1007577.

(213) Martin, R. E.; Ginsburg, H.; Kirk, K. Membrane Transport Proteins of the Malaria Parasite. *Molecular Microbiology*. **2009**, *74* (3), 519–528.

(214) Saliba, K. J.; Horner, H. A.; Kirk, K. Transport and Metabolism of the Essential Vitamin Pantothenic Acid in Human Erythrocytes Infected with the Malaria Parasite *Plasmodium Falciparum*. *J. Biol. Chem.* **1998**, *273* (17), 10190–10195.

(215) Martin, R. E.; Kirk, K. Transport of the Essential Nutrient Isoleucine in Human Erythrocytes Infected with the Malaria Parasite *Plasmodium Falciparum*. *Blood* **2007**, *109* (5), 2217–2224.

(216) Parker, K. E. R.; Fairweather, S. J.; Rajendran, E.; Blume, M.; McConville, M. J.; Bröer, S.; Kirk, K.; Dooren, G. G. van. Characterization of the Apicomplexan Amino Acid Transporter (ApiAT) Family in *Toxoplasma Gondii*. *bioRxiv* **2018**, 306993.

(217) Martin, R. E.; Henry, R. I.; Abbey, J. L.; Clements, J. D.; Kirk, K. The "permeome" of the Malaria Parasite: An Overview of the Membrane Transport Proteins of *Plasmodium Falciparum*. *Genome Biol.* **2005**, *6* (3), R26.

(218) Cobbold, S. A.; Chua, H. H.; Nijagal, B.; Creek, D. J.; Ralph, S. A.; McConville, M. J. Metabolic Dysregulation Induced in *Plasmodium Falciparum* by Dihydroartemisinin and Other Front-Line Antimalarial Drugs. *J. Infect. Dis.* **2016**, *213* (2), 276–286.

(219) Sun, W.; Tanaka, T. Q.; Magle, C. T.; Huang, W.; Southall, N.; Huang, R.; Dehdashti, S. J.; McKew, J. C.; Williamson, K. C.; Zheng, W. Chemical Signatures and New Drug Targets for Gametocytocidal Drug Development. *Sci. Rep.* **2015**, *4*, 3743.

(220) Hanson, K. K.; Ressurreicao, A. S.; Buchholz, K.; Prudencio, M.; Herman-Ornelas, J. D.; Rebelo, M.; Beatty, W. L.; Wirth, D. F.; Hanscheid, T.; Moreira, R.; et al. Torins Are Potent Antimalarials That Block Replenishment of *Plasmodium* Liver Stage Parasitophorous Vacuole Membrane Proteins. *Proc. Natl. Acad. Sci. U. S. A.* **2013**, *110* (30), 2838–2847

(221) De Silva, E. K.; Gehrke, A. R.; Olszewski, K.; León, I.; Chahal, J. S.; Bulyk, M. L.; Llinás, M. Specific DNA-Binding by Apicomplexan AP2 Transcription Factors. *Proc. Natl. Acad. Sci. U. S. A.* **2008**, *105* (24), 8393–8398.

(222) Wilson, N. C.; Choudhury, A.; Carstens, N.; Mavri-Damelin, D. Organic Cation Transporter 2 (OCT2/SLC22A2) Gene Variation in the South African Bantu-Speaking Population and Functional Promoter Variants. *Omi. A J. Integr. Biol.* **2017**, *21* (3), 169–176.

(223) Frame, I. J.; Deniskin, R.; Rinderspacher, A.; Katz, F.; Deng, S. X.; Moir, R. D.; Adjalley, S. H.; Coburn-Flynn, O.; Fidock, D. A.; Willis, I. M.; et al. Yeast-Based High-Throughput Screen Identifies *Plasmodium Falciparum* Equilibrative Nucleoside Transporter 1 Inhibitors That Kill Malaria Parasites. *ACS Chem. Biol.* **2015**, *10* (3), 775–783.

(224) Parker, M. D.; Hyde, R. J.; Yao, S. Y. M.; Mcrobert, L.; Cass, C. E.; Young, J. D.; Mcconkey, G. A.; Baldwin, S. A. Identification of a Nucleoside/Nucleobase Transporter from *Plasmodium Falciparum*, a Novel Target for Anti-Malarial Chemotherapy; *Biochem. J.* **2000**; *349* (1), 67–75.

(225) Frame, I. J.; Deniskin, R.; Arora, A.; Akabas, M. H. Purine Import into Malaria Parasites as a Target for Antimalarial Drug Development. *Ann. N. Y. Acad. Sci.* **2015**,

1342 (1), 19–28.

(226) Riegelhaupt, P. M.; Cassera, M. B.; Fröhlich, R. F. G.; Hazleton, K. Z.; Hefter, J. J.; Schramm, V. L.; Akabas, M. H. Transport of Purines and Purine Salvage Pathway Inhibitors by the *Plasmodium Falciparum* Equilibrative Nucleoside Transporter PfENT1. *Mol. Biochem. Parasitol.* **2010**, *169* (1), 40–49.

(227) Cassera, M. B.; Hazleton, K. Z.; Riegelhaupt, P. M.; Merino, E. F.; Luo, M.; Akabas, M. H.; Schramm, V. L. Erythrocytic Adenosine Monophosphate as an Alternative Purine Source in *Plasmodium Falciparum*. *J. Biol. Chem.* **2008**, *283* (47), 32889–32899.

(228) Sosa, Y.; Deniskin, R.; Frame, I. J.; Steiginga, M. S.; Bandyopadhyay, D.; Graybill, T. L.; Kallal, L. A.; Ouellette, M. T.; Pope, A. J.; Widdowson, K. L.; et al. Identification via a Parallel Hit Progression Strategy of Improved Small Molecule Inhibitors of the Malaria Purine Uptake Transporter That Inhibit *Plasmodium Falciparum* Parasite Proliferation. *ACS Infect. Dis.* **2019**, *5* (10), 1738–1753.

(229) Akabas, M.; Frame, I. J.; Landry, D. W.; Deniskin, R.; Deng, S. X.; Rinderspacher, A. WO2014/210319 Inhibitors of *Plasmodium Falciparum* Equilibrative Nucleoside Transporter Type 1 as Anti-Parasitic Compounds, **2014**.

(230) Helium for Excel. Ceiba Solutions, Inc. 2015.

(231) Nikolova, N.; Jaworska, J. Approaches to Measure Chemical Similarity - A Review. *QSAR Comb. Sci.* **2004**, *22* (9–10), 1008–1009.

(232) Bajusz, D.; Rácz, A.; Héberger, K. Why Is Tanimoto Index an Appropriate Choice for Fingerprint-Based Similarity Calculations? *J. Cheminform.* **2015**, *7* (1), 20.

(233) Deniskin, R.; Frame, I. J.; Sosa, Y.; Akabas, M. H. Targeting the *Plasmodium Vivax* Equilibrative Nucleoside Transporter 1 (PvENT1) for Antimalarial Drug Development. *Int. J. Parasitol. Drugs Drug Resist.* **2016**, *6* (1), 1–11.

(234) Staines, H. M.; Derbyshire, E. T.; Slavic, K.; Tattersall, A.; Vial, H.; Krishna, S. Exploiting the Therapeutic Potential of *Plasmodium Falciparum* Solute Transporters. *Trends Parasitol.* **2010**, *26* (6), 284–296.

(235) Noller, H. F. Evolution of Protein Synthesis from an RNAworld. *Cold Spring Harb. Perspect. Biol.* **2012**, *4* (4).

(236) Root-Bernstein, M.; Root-Bernstein, R. The Ribosome as a Missing Link in the Evolution of Life. *J. Theor. Biol.* **2015**, *367*, 130–158.

(237) Bréhélin, L.; Florent, I.; Gascuel, O.; Maréchal, É. Assessing Functional Annotation Transfers with Inter-Species Conserved Coexpression: Application to *Plasmodium Falciparum*. *BMC Genomics* **2010**, *11* (1), 35.

(238) Bottger, E. C. Visions & Reflections (Minireview) Antimicrobial Agents Targeting the Ribosome: The Issue of Selectivity and Toxicity - Lessons to Be Learned. *Cell. Moll. Life Sci.* **2007**, *64*, 791–795.

(239) Sidhu, A. B. S.; Sun, Q.; Nkrumah, L. J.; Dunne, M. W.; Sacchettini, J. C.; Fidock, D. A. In Vitro Efficacy, Resistance Selection, and Structural Modeling Studies Implicate the Malarial Parasite Apicoplast as the Target of Azithromycin. *J. Biol. Chem.* **2007**, *282* (4), 2494–2504.

(240) Lazaro, E.; San Felix, A.; van den Broek, L. A.; Ottenheijm, H. C.; Ballesta, J. P. Interaction of the Antibiotic Sparsomycin with the Ribosome. *Antimicrob. Agents Chemother.* **1991**, *35* (1), 10–13.

(241) Overington, J. P.; Al-Lazikani, B.; Hopkins, A. L. How Many Drug Targets Are There? *Nat. Rev. Drug Discov.* **2006**, *5* (12), 993–996.

(242) Shi, H.; Zhang, C. J.; Chen, G. Y. J.; Yao, S. Q. Cell-Based Proteome Profiling of Potential Dasatinib Targets by Use of Affinity-Based Probes. *J. Am. Chem. Soc.* **2012**, *134* (6), 3001–3014.

(243) Tindall, S. M.; Vallières, C.; Lakhani, D. H.; Islahudin, F.; Ting, K. N.; Avery, S. V. Heterologous Expression of a Novel Drug Transporter from the Malaria Parasite Alters Resistance to Quinoline Antimalarials. *Sci. Rep.* **2018**, *8* (1), 2464.

(244) Weiner, J.; Kooij, T. W. A. Phylogenetic Profiles of All Membrane Transport Proteins of the Malaria Parasite Highlight New Drug Targets. *Microb. Cell* **2016**, *3* (10), 511–521.

(245) Koenderink, J. B.; Kavishe, R. A.; Rijpma, S. R.; Russel, F. G. M. The ABCs of Multidrug Resistance in Malaria. *Trends in Parasitology*. **2010**, *26* (9), 440–446.

(246) Bissantz, C.; Kuhn, B.; Stahl, M. A Medicinal Chemist's Guide to Molecular Interactions. *J. Med. Chem.* **2010**, *53* (14), 5061–5084.

(247) Smith, A. J. T.; Zhang, X.; Leach, A. G.; Houk, K. N. Beyond Picomolar Affinities: Quantitative Aspects of Noncovalent and Covalent Binding of Drugs to Proteins. *Journal of Medicinal Chemistry*. **2009**, *52* (2), 225–233.

(248) Kuntz, I. D.; Chen, K.; Sharp, K. A.; Kollman, P. A. The Maximal Affinity of Ligands. *Proc. Natl. Acad. Sci. U. S. A.* **1999**, *96* (18), 9997–10002.

(249) De Cesco, S.; Kurian, J.; Dufresne, C.; Mittermaier, A. K.; Moitessier, N. Covalent Inhibitors Design and Discovery. *European Journal of Medicinal Chemistry*. **2017**, *138*, 96–114.

(250) Haffner, C. D.; Becherer, J. D.; Boros, E. E.; Cadilla, R.; Carpenter, T.; Cowan, D.; Deaton, D. N.; Guo, Y.; Harrington, W.; Henke, B. R.; et al. Discovery, Synthesis, and

Biological Evaluation of Thiazoloquin(Az)Olin(on)Es as Potent CD38 Inhibitors. *J. Med. Chem.* **2015**, *58* (8), 3548–3571.

(251) Glennon, R. A.; Hong, S.-S.; Bondarev, M.; Law, H.; Dukat, M.; Rakhit, S.; Power, P.; Fan, E.; Kinneau, D.; Kamboj, R.; et al. Binding of *O* -Alkyl Derivatives of Serotonin at Human 5-HT1Dβ Receptors. *J. Med. Chem.* **1996**, *39* (1), 314–322.

(252) Müller, S.; Webber, M. J.; List, B. The Catalytic Asymmetric Fischer Indolization. *J. Am. Chem. Soc.* **2011**, *133* (46), 18534–18537.

(253) L. V. H.; Keck, G. E. A New Construction of 2-Alkoxypyrans by an Acylation−Reductive Cyclization Sequence. **2007**, *9* (10), 1951–1954.

(254) Trager, W.; Jensen, J. B. Human Malaria Parasites in Continuous Culture. *Science* **1976**, *193* (4254), 673–675.

(255) Ponnudurai, T.; Leeuwenberg, A. D.; Meuwissen, J. H. Chloroquine Sensitivity of Isolates of *Plasmodium Falciparum* Adapted to *in vitro* Culture. *Trop. Geogr. Med.* **1981**, *33* (1), 50–54.

(256) Walliker, D.; Quakyi, I.; Wellems, T.; McCutchan, T.; Szarfman, A.; London, W.; Corcoran, L.; Burkot, T.; Carter, R. Genetic Analysis of the Human Malaria Parasite *Plasmodium Falciparum*. *Science* **1987**, *236* (4809), 1661–1666.

(257) Elliott, J. L.; Saliba, K. J.; Kirk, K. Transport of Lactate and Pyruvate in the Intraerythrocytic Malaria Parasite, *Plasmodium Falciparum*. *Biochem. J.* **2001**, *355* (3), 733–739.

(258) Cranmer, S. L.; Magowan, C.; Liang, J.; Coppel, R. L.; Cooke, B. M. An Alternative to Serum for Cultivation of *Plasmodium Falciparum in vitro*. *Trans. R. Soc. Trop. Med. Hyg.* **1997**, *91* (3), 363–365.

(259) Huertas, B.; Hermoso, A. GSK Unpublished Work. **2019**.

(260) Sanz, O. GSK Unpublished Work. **2018**.

(261) Linares, M.; Viera, S.; Crespo, B.; Franco, V.; Gómez-Lorenzo, M. G.; Jiménez-Díaz, M. B.; Angulo-Barturen, Í.; Sanz, L. M.; Gamo, F.-J. Identifying Rapidly Parasiticidal Anti-Malarial Drugs Using a Simple and Reliable in Vitro Parasite Viability Fast Assay. *Malar. J.* **2015**, *14* (1), 441.

(262) Sanz, O.; Alfonso Torres-Gomez, P. GSK Unpublished Work, **2019**.

(263) Baumann, E.; Stoya, G.; Völkner, A.; Richter, W.; Lemke, C.; Linss, W. Hemolysis of Human Erythrocytes with Saponin Affects the Membrane Structure. *Acta Histochem.* **2000**, *102* (1), 21–35.

(264) Burghaus, P. A.; Lingelbach, K. Luciferase, When Fused to an *N*-Terminal Signal Peptide, Is Secreted from Transfected *Plasmodium Falciparum* and Transported to the

Cytosol of Infected Erythrocytes. *J. Biol. Chem.* **2001**, *276* (29), 26838–26845.

(265) Llergo-Largo, J. L. GSK Unpublished Work. **2019**.

(266) Franken, H.; Mathieson, T.; Childs, D.; Sweetman, G. M. A.; Werner, T.; Tögel, I.; Doce, C.; Gade, S.; Bantscheff, M.; Drewes, G.; et al. Thermal Proteome Profiling for Unbiased Identification of Direct and Indirect Drug Targets Using Multiplexed Quantitative Mass Spectrometry. *Nat. Protoc.* **2015**, *10* (10), 1567–1593.

(267) Savitski, M. M.; Mathieson, T.; Zinn, N.; Sweetman, G.; Doce, C.; Becher, I.; Pachl, F.; Kuster, B.; Bantscheff, M. Measuring and Managing Ratio Compression for Accurate ITRAQ/TMT Quantification. *J. Proteome Res.* **2013**, *12* (8), 3586–3598.

(268) Savitski, M. M.; Sweetman, G.; Askenazi, M.; Marto, J. A.; Lang, M.; Zinn, N.; Bantscheff, M. Delayed Fragmentation and Optimized Isolation Width Settings for Improvement of Protein Identification and Accuracy of Isobaric Mass Tag Quantification on Orbitrap-Type Mass Spectrometers. *Anal. Chem.* **2011**, *83* (23), 8959–8967.

(269) Carrillo, B.; Yanofsky, C.; Laboissiere, S.; Nadon, R.; Kearney, R. E. Methods for Combining Peptide Intensities to Estimate Relative Protein Abundance. *Bioinformatics* **2009**, *26* (1), 98–103.